Expanding The Chemical Space of RiPPs in Rare Actinobacetria Employing a Tunable Metabologenomic Approach

Dissertation

der Mathematisch-Naturwissenschaftlichen Fakultät

der Eberhard Karls Universität Tübingen

zur Erlangung des Grades eines

Doktors der Naturwissenschaften

(Dr. rer. nat.)

vorgelegt von

Hamada Saad

aus Gharbeya/Ägypten

Tübingen

2021

Gedruckt mit Genehmigung der Mathematisch-Naturwissenschaftlichen Fakultät der Eberhard Karls Universität Tübingen.

Tag der mündlichen Prüfung:	17.08.2021
Dekan:	Prof. Dr. Thilo Stehle
1. Berichterstatter:	Prof. Dr. Harald Groß

DEDICATION

For always supporting me in my endeavors, I dedicate this thesis to my family. Thanks to all of you for your confidence and encouragement during my doctoral years. I emerge from this journey as a confident scientist who has not lost the passion you have instilled upon me. Thank you for all you have done in shaping who I am and enabling this achievement.

“Do not go gentle into that good night,
Old age should burn and rave at close of day;
Rage, rage against the dying of the light.”
Dylan Thomas, 1914-1953

Statement on The Originality of This Thesis

I hereby declare that I alone wrote the doctoral work submitted here under the title 'Expanding The Chemical Space of RiPPs in Rare Actinobacteria Employing a Tunable Metabologenomic Approach', that I only used the sources and materials cited in the work, and that all citations, whether word for word or paraphrased are given as such. I declare that I adhered to the guidelines set forth by the University of Tübingen to guarantee proper academic scholarship (Senate Resolution 25.05.2000). I declare that these statements are true and that I am concealing nothing. I understand that any false statements can be punished with a jail term of up to three years or a financial penalty.

…………………………… ……………………………..

Place, Date Signature

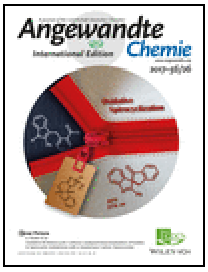

Thank you for your order!

Dear Mr. Hamada Saad,

Thank you for placing your order through Copyright Clearance Center's RightsLink® service.

Order Summary

Licensee:	Mr. Hamada Saad
Order Date:	Jun 18, 2021
Order Number:	5091790223041
Publication:	Angewandte Chemie International Edition
Title:	Nocathioamides, Uncovered by a Tunable Metabologenomic Approach, Define a Novel Class of Chimeric Lanthipeptides
Type of Use:	Dissertation/Thesis
Order Total:	0.00 EUR

View or print complete details of your order and the publisher's terms and conditions.

Sincerely,

Copyright Clearance Center

Tel: +1-855-239-3415 / +1-978-646-2777
customercare@copyright.com
https://myaccount.copyright.com

This message (including attachments) is confidential, unless marked otherwise. It is intended for the addressee(s) only. If you are not an intended recipient, please delete it without further distribution and reply to the sender that you have received the message in error.

Table of Contents

Table of Contents

Publications, Posters and Workshops

Publications

Michelle A. Schorn, Stefan Verhoeven,……., **Hamada Saad**, ………., Justin J. J. van der Hooft, A Community Resource for Paired Genomic and Metabolomic Data Mining, *Nature Chemical Biology*, 2021, 17, 363-368.

Hamada Saad, Saefuddin Aziz, Matthias Gehringer, Markus Kramer, Jan Straetener, Anne Berscheid, Heike Brötz-Oesterhelt, Harald Gross, Nocathioamides, Uncovered by a Tunable Metabologenomic Approach, Define a Novel Class of Chimeric Lanthipeptides, *Angewandte Chemie International Edition*, 2021, 60, 16472-16479.

Ira Handayani*, **Hamada Saad***, Shanti Ratnakomala, Puspita Lisdiyanti, Wien Kusharyoto, Janina Krause, Andreas Kulik, Wolfgang Wohlleben, Saefuddin Aziz, Harald Gross, Athina Gavriilidou, Nadine Ziemert, and Yvonne Mast, Mining Indonesian Microbial Biodiversity for Novel Compounds by a Combined Genome Mining and Molecular Networking Approach, *Marine Drugs*, 2021, 19, 316.

** Equal contribution*

Alicia Engelbrecht, **Hamada Saad**, Harald Gross, Leonard Kaysser, Natural Products from *Nocardia* and their Role in Pathogenicity. *Microbial Physiology*, 2021, DOI: 10.1159/000516864.

Posters

"Exploring the Molecular Basis of *Pseudomonas fluorescens* BBc6R8-*Laccaria bicolor* S238N Interactions Under Iron-Depleted Conditions", **Hamada Saad**, Jeannie Horak, Michael Läemmerhofer, Max Schnepf, Harald Gross, International Workshop of the VAAM-Section Biology of Natural Products Producing Bacteria, Tübingen, Germany, 27-29 September 2017.

"Mapping The Metabolomes of *Lythrum salicaria* Microbial Endophytes", **Hamada Saad**, Ghazaleh Jahanshah, Saefuddin Aziz, Harald Gross, Copenhagen Bioscience Conference - Natural Products - Discovery, Biosynthesis and Application, Favrholm Campus, Roskildevej, Hillerød, Denmark, 5-9 May 2019.

Workshops

3rd International Workshop: Genome-Mining for Natural Products, DTU Biosustain, The Novo Nordisk Foundation Center of Biosustainability, Denmark, 12-14 September 2018.

Training Course: Avance/TopSpin Basic Introduction to System Operation / Basic NMR Methods, Bruker BioSpin, Rheinstetten, Germany, 17-21 September 2018.

Training Course: Profiling and Identification Strategies for Metabolomics Using Metaboscape®, Bruker Daltonik GmbH, Fahrenheitstrasse 4, Bremen, Germany, 4 October 2018.

Contributions of Other Scientists to This Work

➢ Genome-Guided Discovery of Nocathioamides from *Nocardia terpenica* IFM 0406

The biological evaluations of the isolated nocathioamide A and B were conducted by the group of Prof. Heike Brötz-Oesterhelt (The Interfaculty Institute for Microbiology and Infection Medicine Tübingen (IMIT), University of Tübingen). Mr. Jan Straetener carried out the antibacterial and cytotoxicity assays whereas Dr. Anne Berscheid performed the antifungal tests.

The provision of the clinical *Candida* species was arranged by Prof. Silke Peter (Tübingen University Hospital (UKT), University of Tübingen).

Dr. Saefuddin Aziz (Department of Pharmaceutical Biology, Pharmaceutical Institute, University of Tübingen) aided in the preparation of the bacterial isolates (IFM 0407 and IFM 0706^{T}) to be genomically resequenced besides performing preliminary bioassays of nocathioamide A.

➢ Genome-Driven Discovery of Nocapeptins from *N. terpenica* IFM 0406 and Longipeptins from *Longimycelium tulufanense* CGMCC 4.5737

The isolation of nocapeptin A was performed by my colleagues M.Sc. Keshab Bhattarai and M.Sc. Thomas Majer (Department of Pharmaceutical Biology, Pharmaceutical Institute, University of Tübingen).

The preparation of cryo cultures of *Longimycelium tulufanense* was carried out by my colleague M.Sc. Patricia Arlt (Department of Pharmaceutical Biology, Pharmaceutical Institute, University of Tübingen) in addition to the currently ongoing antibacterial tests of nocapeptin A.

High-Resolution Nuclear Magnetic Resonance

The collection of the 700 MHz NMR datasets of nocathioamide A, nocathioamide B and nocapeptin A was supported by Dr. Markus Kramer (Institute of Organic Chemistry, University of Tübingen). Furthermore, the setup of special NMR experiments like ^{1}H-^{15}N HSQC-TOCSY and LR-HSQMBC was supervised by him.

High-Resolution Mass Spectrometry

HRMSMS measurements were obtained by Dr. Dorothee Wistuba (Institute of Organic Chemistry, University of Tübingen).

Abbreviations

µM	Micromolar
2D	Two dimensional
Abu	α-aminobutyric acid
Ala/A	Alanine
antiSMASH	Antibiotics & Secondary Metabolite Analysis SHell
Asn/N	Asparagine
Asp/D	Aspartic acid
ATP	Adenosine triphosphate
AviCys	*S*-[(*Z*)-2-aminovinyl]-D-cysteine
BAGEL	BActeriocin GEnome mining tooL
BGC	Biosynthetic Gene Cluster
BLAST	Basic Local Alignment Search Tool
C (domain)	Condensation domain
C (protein)	Lasso Peptide Macrocyclase
CID	Collison Induced Dossciation
CP	Core Peptide
CYP450	Cytochrome P450 enzyme
Cys/C	Cysteine
Da	Dalton
DAD	Diode Array Detector
DDA	Data Dependent Acquisition
Dha	2,3-dehydroalanine
DHAA	Dehydrated amino acid
Dhb	(*Z*)-2,3-dehydrobutyrine
DNA	Deoxyribonucleic acid
DSMZ	German collection of microorganisms and cell cultures
DTT	Dithiothreitol
E/B2	Leader Peptide Protease in Lasso Peptide Biosynthesis
E1-like	Partner Protein Potentiates the Cyclodehydratase Activity
ESI	Electron Spray Ionization
FBMN	Feature-Based Molecular Network
FMN	Flavin mononucleotide
Glu/E	Glutamic acid
Gly/G	Glycine
GTP	Guanosine triphosphate
HMBC	Heteronuclear Multiple Bond Correlation
HR	High Resolution
HSQC	Heteronuclear Single Quantum Coherence
IFM	Research Center for Pathogenic Fungi and Microbial Toxicoses, Chiba University, Japan
Lab	Labionin
Lac	Lactyl
Lal	Lysinoalanine

Lan	Lanthionine
LanA	Precursor Peptide of Lanthipeptide
LanB	Lanthipeptide Dehydratase
LanC	Lanthipeptide Cyclase
LanKC	Lanthipeptide Dehydratase and Cyclase of class III
LanL	Lanthipeptide Dehydratase and Cyclase of Class IV
LanM	Lanthipeptide Dehydratase and Cyclase of Class II
LAP	Linear Azoline Peptides
LC	Liquid Chromatography
Leu/L	Leucine
LP	Leader Peptide
M/Met	Methionine
m/z	mass/charge
MeLab	Methyllabionin
MeLan	3-methyllanthionine
mg	milligram
MHz	Megahertz
MIC	Minimum Inhibitory Concentration
MRSA	Methicillin-resistant *Staphylococcus aureus*
MS	Mass Spectrometry
MSMS(MS2)	Tandem Mass Spectrometry
NCBI	National Center for Biotechnology Information, U.S. National Library of Medicine
NMR	Nuclear Magnetic Resonance
NOESY	Nuclear Overhauser Effect Spectroscopy
NRPS	Non-Ribosomal Peptide Synthetase
Ocin-ThiF	Partner Protein Required for the Cyclodehydratase Activity
ORF	Open Reading Frame
OSMAC	One Strain MAny Compounds
PAD	Peptidyl Arginine Deiminase
PCP	Peptidyl Carrier Protein
Pfam	Protein Family
Phe/F	Phenylalanine
PK/PD	Pharmacokinetic/Pharmacodynamic
PKS	Polyketide Synthase
PRISM	PRediction Informatics for Secondary Metabolomes
Pro/P	Proline
PTM	Posttranslational modification
Pyr	2-oxopropionyl (Pyruvyl)
RiPP	Ribosomally Synthesized and Posttranslationally Modified Peptide
RiPPER	RiPP Precursor Peptide Enhanced Recognition
RODEO	Rapid ORF Description & Evaluation Online
RP	Reversed-Phase
RRE(B1)	RiPP Recognition Element (Lasso Peptides)

SagB	FMN-Dependent Dehydrogenase
SAM	S-adenosylmethionine
SAR	Structure-Activity Relationship
Ser/S	Serine
SSN	Sequence Similarity Network
T	Thiolation
TfuA-like	Partner Protein Required for the Backbone Thioamide Formation
Thr/T	Threonine
TOCSY	Total Correlation Spectroscopy
TOMMs	Thiazole/Oxazole Modified Microcins
Trp/W	Tryptophan
Tyr/Y	Tyrosine
VLC	Vaccum Liquid Chromatography
YcaO	Bacterial Protein Involved in the Catalysis of Different Structural Modifications
Δ	Difference
δ	NMR chemical shift (ppm)

Summary

The intrinsic driving force of finding new RiPP scaffolds is largely attributed to their appreciable biological/physiological functions, however the constantly growing interest in disclosing novel architectures currently extends beyond the classical needs. For example, RiPP-BGCs regularly provide a rich pool of enzymatic machineries that can install specific, in some cases rare, tailorings expanding the biobrick toolbox in synthetic biology and chemistry.

Although the analyses of different genome sequences of *Nocardia* spp. disclosed a huge cryptic biosynthetic potential waiting to be unearthed, the discovery of such genetically encoded entities is insurmountable. Thus, to partially overcome the typical limitations offered by the common silence of biosynthetic gene clusters (BGCs) and the inherited challenge to connect the genotype(s) with the chemotype(s), a tunable metabologenomic approach was developed within the frame of this work.

The application of the OSMAC concept in tandem with the configured analytical strategy in *Nocardia terpenica* IFM 0406, 0706^{T} and *Longimycelium tulufanense* CGMCC 4.5737 enabled to chart unprecedented chemical space belonging to RiPPs with three novel molecular families.

The first study case comprises a genome-oriented prioritization of a novel BGC associated with a new-to-nature combination of multiple post-translational enzymes in *N. terpenica* IFM 0406. It was hypothesized that the gene cluster will in turn assemble a novel chemical entity blending three different class-defining post-translational modifications (PTMs). Recruiting a synergism of bioinformatics, stable isotope labeling experiments and NMR spectroscopy facilitated the successful identification, isolation and structural characterization of three new RiPPs, named nocathioamides A-C. Aside from structurally featuring unprecedented PTM in the form of a macrocyclic imide bridge, they inaugurate the first-in-nature combinatorial tribrid RiPPs hovering over three different biosynthetic machineries of lanthipeptides, LAPs and thioamitides.

The second investigation deals with the deorphanization of an additional unique RiPP-BGC found in *N. terpenica* genomes. The bioinformatic annotation and prediction pinpoint to an unknown scaffold belonging to class II lasso peptide which is additionally decorated with a possible oxidative event(s). A quick bioinformatic survey revealed the presence of homologous BGCs coding for similar entities in other bacteria exemplified by *Longimycelium tulufanense*. Relying on the predicted core peptides in tandem with the tuned workflow, the encoded products were deciphered from both isolates, termed nocapeptins and longipeptins. Nocapeptins, from *N. terpenica,* and longipeptins, from *L. tulufanense*, symbolize the founders of a novel molecular family of lasso peptides in which a conserved regional PTM as a unique oxidative crosslink is structurally appended. Aside from the characteristic skeletal interlinkage embedded in longipeptin A, the structure could leverage the modification scope with further tailoring events like hydroxylation and methylation, delivering thereby the most tailored lasso architecture till now.

The discovery of nocathioamides and nocapeptins stretched with longipeptins portrays a proof of concept to the effectiveness of employing the technique of genome mining prioritization to unearth a new chemical space with uncharted biosynthetic enzymes from underexplored species.

Zusammenfassung

Die Suche nach neuen ribosomal gebildeten und post-translational modifizierten Peptiden (RiPPs) ist ein sehr aktives Feld und ist damit begründet, dass man auf völlig neuartige Moleküle trifft, die entweder biologisch hochaktiv sind oder interessante physiologische Funktionen aufweisen. Zudem sind die entsprechenden Biosynthesegencluster eine reichhaltige Quelle für neuartige Gene, deren Produkte spezifische und seltene Reaktionen katalysieren. Diese Gene stellen wiederum eine interessante Erweiterung der molekularbiologischen Werkzeuge („Biobricks“) im Bereich der synthetischen Biologie dar.

Die Genom-Analyse von verschiedenen *Nocardia* Spezies haben gezeigt, dass diese Bakterien ein enormes Potential aufweisen, Sekundärmetabolite zu produzieren. In den meisten Fällen handelt es sich jedoch um stille Biosynthesegencluster und es gelingt nicht die vorhergesagten Naturstoffe zu isolieren. Um dieses Problem teilweise zu überwinden wurde im Rahmen dieser Arbeit ein variabler metabolomischer Ansatz entwickelt, womit letztendlich dennoch die genetische mit der metabolomischen Ebene korreliert werden kann.

Die Anwendung des OSMAC-Konzepts in Verbindung mit einer angepassten analytischen Strategie auf *Nocardia terpenica* IFM 0406, 0706^T und *Longimycelium tulufanense* CGMCC 4.5737 ermöglichte es, den chemischen Raum dieser Bakterien zu erforschen und hinsichtlich drei neuer RiPP-Moleküle zu erweitern.

Die erste Fallstudie beinhaltet die Genom-gestützte Priorisierung eines neuartigen Biosynthesegenclusters im Genom von *N. terpenica*, welches durch eine ungewöhnlich hohe Anzahl an Genen auffiel, die für diverse posttranslationale Modifikationsenzyme kodierten. Es wurde vermutet, dass die resultierende Verbindung gleich drei verschiedene Strukturklassen-bestimmende post-translationale Modifikationen in sich vereint. Die Anwendung von bioinformatischen Methoden, Istopen-Markierungsexperimenten und NMR Spektroskopie führte schließlich in synergistischer Weise zur Findung, Isolation und Strukturaufklärung von drei neuen RiPPs, die Nocathioamid A-C genannt wurden. Diese fallen durch zwei Besonderheiten auf: Zum einen stellt die ungewöhnliche Imid-Brücke ein Novum hinsichtlich einer posttranslationalen Modifikationen dar und zum anderen vereint der Bioassemblierungsprozess eine Kombination der Maschinerien der Lanthipeptide, der Linearen Azol(in)-Peptide und der Thioamitide.

Die zweite Fallstudie handelt von der Entdeckung des Produkts eines weiteren einzigartigen RIPP-Biosynthesegenclusters aus *N. terpenica* Genomen. Die bioinformatische Annotation erlaubte die Vorhesage eines Klasse II Lasso-Peptids, welches durch oxidative Vorgänge weiter modifiert sein musste. In Rahmen von weiterführenden bioinformatischen Screeningansätzen wurde dieses Gencluster auch in anderen Bakterien gefunden, u.a. in dem Stamm *Longimycelium tulufanense*. Mittels der vorhergesagten Struktur und der oben beschriebenen analytischen Strategie konnten die entsprechenden Produkte der Gencluster (Nocapeptine und Longipeptine) in den jeweiligen Isolaten gefunden werden. Diese beiden Naturstoffe begründen eine neue strukturelle Klasse von Lasso-Peptiden die oxidativ quervernetzt sind. Im Vergleich zu Nocapeptin, weist Longipeptin noch zusätzliche posttranslationale Modifikationen auf, wie z.B. eine Hydroxylierung und eine Methylierung. Damit stellt Longipeptin eines der höchst-modifizierten Lasso-Peptide dar.

Die Entdeckung der Nocathioamide und der Nocapeptine bzw. Longipeptine stellen einen Machbarkeitsbnachweis dar und zeigen die Effektivität der gewählten genom-getriebenen Forschungsstrategie, die letztendlich die Erforschung von bisher unbekannten chemischen Räumen und biosynthetischen Enzymen erlaubte.

1. Introduction

1.1. Peptide-Derived Natural Products

Over the last few years, peptides have earned increasing traction as multifaceted-therapeutics by various pharmaceutical companies to fill the void between the morphed small molecules and protein drugs with hybrid advantages of both molecular entities. Such interest is unequivocally manifested by the currently approved ixazomib for multiple myeloma, the hormone insulin, the anti-diabetic semaglutide, and afamelanotide, an analog of α-melanocyte-stimulating hormone to prevent skin damage and pain.[1]

Nature, in its standard models as prokaryotic and eukaryotic systems, has evolved multiple routes to biosynthesize a plethora of small peptides with a vast spectrum of biological activities ranging from antibiotics, antifungal to antiviral agents in addition to being immunosuppressives.[2]

One of the biosynthetic strategies that bacteria and/or fungi can recall to deliver peptide-based products is the nonribosomal peptide synthetase (NRPS) assembly line. Supported by modular NRP assembly with a thio template minimally consisting of three main domains: adenylation (A), thiolation or peptide carrier protein (T or PCP), and condensation (C), the nascent nonribosomal peptides (NRPs) can be prepared. NRPs usually experience further enzymatic processing pre- and/or post-release, resulting in specific structural alterations crucial for their assumed molecular targets.[3]

The utility of NRPs as medical drugs is clearly indisputable through surveying the currently marketed drugs with approximately 30 NRP core scaffolds contributing substantially to the pharmaceutical industry. For instance, penicillin/cephalosporin, vancomycin and daptomycin are models of NRP-based antibiotics that are predominantly employed to treat systemic and topical bacterial infections in humans with diverse mechanisms of action, including disruptions of membrane integrity, cell wall biosynthesis, protein synthesis, DNA replication, RNA transcription, and fatty acid biosynthesis.[4-6]

1.2 Ribosomally Synthesized and Posttranslationally Modified Peptides

In parallel, a prevalent alternative route that microorganisms often recruit to biosynthesize peptides-derived secondary metabolites is by the ribosome. Since the resultant ribosomal products are subjected to additional structural changes during a post-translational transformation process, they have been termed ribosomally synthesized and post-translationally modified peptides (RiPPs).[7]

In contrast to NRP antibiotics, the analogous ribosomal ones are less acknowledged in terms of being approved antibiotics. Despite such pitfall as small-molecule medicines from an anthropocentric perspective, RiPPs are the fastest-growing superfamily of peptidic natural products furnished with a myriad of constantly expanding index of new chemical skeletons supported by multi profiles of biological potencies.[8]

Considering that RiPPs entities can mediate various biological purposes, the succeeding catalogs (Tables **1** and **2)** outline a brief overview regarding the multiple biological and physiological implications associated with some selected members belonging to various RiPPs classes.

Table 1. Representative microbial RiPPs belonging to different classes with described biological potency

RiPP class	Peptide	Organism(s)	Bioactivity/Mechanism of action
Lanthipeptides	Actagardine[9]	*Actinoplanes garbadinensis*	Antibacterial (Gram-positive)
	Cinnamycin[10]	*Streptomyces cinnamoneus* subsp. *cinnamone*us DSM 40005	Antibacterial (Gram-positive, permeabilize lysophosphatidylethanolamine lipids), Antiviral (HSV-1)
	Divamide A[11]	*Prochloron didemni*	Antiviral (HIV)
	Duramycin[12]	*Streptomyces cinnamoneus* ATCC 12686	Antibacterial (Gram-positive), Antiviral
	Labyrinthopeptins[13]	*Actinomadura namibiensis*	Antiviral (Broad spectrum of enveloped viruses HIV, ZikV, HSV, HCV, WNV, RSV)
	Microbisporicin[14]	*Microbispora corallina*	Antibacterial (Gram-positive)
	Nisin[15]	*Lactococcus lactis*	Antibacterial (Gram-positive), Food preservative
	Pinensins[16]	*Chitinophaga pinensis*	Antifungal (Filamentous fungi and yeasts)
Lassopeptides	Aborycin/RP 71955[17]	*Streptomyces griseoflavus* TÜ 4072	Antibacterial (Gram-positive), Antiviral (HIV)
	Actinokineosin[18]	*Actinokineospora spheciospongiae* DSM 45935T	Antibacterial (Gram-positive)
	Anantin[19]	*Streptomyces coerulescens* DSM 4777/4788	Atrial natriuretic peptide (ANP) antagonist
	BI-32169[20]	*Streptomyces* sp. DSM 14996	Glucagon receptor antagonist
	Capistruin[21]	*Burkholderia thailandensis* E264 DSM 13276	RNA polymerase inhibition (Gram-negative)
	Chaxapeptin[22]	*Streptomyces leeuwenhoekii* strain C58	Antibacterial (Gram-positive), Inhibition in cell invasion of lung cancer cell
	Humidimycin[23]	*Streptomyces humidus* F-100,629	Caspofungin activity potentiator
	Lariatins[24]	*Rhodococcus jostii* K01-B0171	Antimycobacterial
	Lassomycin[25]	*Lentzea kentuckyensis* sp.	Antimycobacterial (mycobacterial ClpC1 ATPase)
	Propeptin[26]	*Microbispora* sp. SNA-115	Antibacterial (Gram-positive), Prolyl endopeptidase inhibitor
	Microcin J25[27]	*Escherichia coli* AY25	RNA polymerase inhibition (Gram-negative)
	Siamycins[28]	*Streptomyces* sp. AA6532, *Streptomyces* sp. AA3891	Antiviral (HIV)
	Specialicin[29]	*Streptomyces specialis* JCM 16611T	Antibacterial (Gram-positive), Antiviral (HIV)
	Sungsanpin[30]	*Streptomyces* sp. SNJ013	Anti-invasive activity with the human lung cancer cell line
	Ulleungdin[31]	*Streptomyces* sp. KCB13F003	Inhibitory activities against cancer cell invasion and migration
Thiopeptides	Berninamycin[32]	*Streptomyces berniensis*	Antibacterial (Gram-positive)
	Cyclothiazomycin[33]	*Streptomyces hygroscopicus* 5008	RNA polymerase inhibitor, filamentous antifungal, renin inhibitor
	GE2270A[34]	*Planobispora rosea*	Antibacterial (Gram-positive, elongation factor Tu inhibitor)
	Kocurin[35]	*Kocuria palustris*	Antibacterial (Gram-positive)

	Micrococcin P1[36]	*Micrococcus* sp., *Staphylococcus equorum* WS2733	RNA polymerase inhibitor, filamentous antifungal, renin inhibitor
	Nocardithiocin[37]	*Nocardia pseudobrasiliensis* IFM 0757	Antibacterial (Gram-positive)
	Nocathiacins[38]	*Nocardia* sp. WW-12651 (ATCC 202099)	Antibacterial (Gram-positive)
	Nosiheptide[39]	*Streptomyces actuosus*	Antibacterial (Gram-positive)
	Siomycin A[40]	*Streptomyces sioyaensis*	Immunosuppressant
	Sulfomycin[41]	*Streptomyces viridochromogenes*	Antibacterial (Gram-positive)
	Thiomuracins[42]	*Nonomuraea* sp.	Antibacterial (Gram-positive, elongation factor Tu inhibitor)
	Thiostrepton[43]	*Streptomyces azureus*	Antibacterial (Gram-positive), antimalarial, Proteasome inhibition activity, apoptosis induction in human cancer cells
	TP-1161[44]	*Nocardiopsis* sp. TFS65-07	Antibacterial (Gram-positive)
Cyanobactins	Aerucyclamides[45]	*Microcystis aeruginosa* PCC 7806	Antimalarial potency against *Plasmodium faclciparum*
	Dolastatins[46]	*Dolabella auricularia*	Antineoplastic activity
	Patellamides[47]	*Prochloron* sp.	Anticancer activity against L1210 murine leukemia cells
	Trunkamide A1[48]	*Prochloron* sp.	Anticancer activity against HT-29 human colon carcinoma and MEL-28 human melanoma cell lines
	Ulithiacyclamide[49]	*Lissoclinum patella*	Anticancer activity against L1210 murine leukemia and KB cells
Thioamitides	Saalfelduracin[50]	*Amycolatopsis saalfeldensis* NRRL B-24474	Selective antibiotic activity
	Thioalbamide[51]	*Amycolatopsis alba* DSM44262	Selective antiproliferative activity
	Thioholgamides[52]	*Streptomycetes malaysiense* MUSC 136 57	Submicromolar activity against HCT-116 cancer cell lines
	Thiopeptin[50a]	*Micromonospora arboorensis* NRRL 8041	Selective antibiotic activity
	Thioviridamides[53]	*Streptomycetes olivoviridis* NA05001	Anticancer activity against several cancer cell lines
Amatoxins	α-Amanitin[54]	*Amanita phalloides*	Selective inhibitor of RNA polymerase II, toxin-component of antibody-drug conjugates (ADC)
Dikaritins	Phomopsins[55]	*Phomopsis leptostromiformis*	Antimitotic agent
	Ustiloxins[56]	*Ustilaginoidea virens*	Antimitotic agent, anticancer activity
Bottromycins	Bottromycin A2[57]	*Streptomyces bottropensis* DSM 40262	Antibacterial activity towards multidrug-resistant bacteria (Selective blocking of aminoacyl-tRNA binding to the A site of bacterial 50S ribosomes)
Proteusins	Polytheonamides[58]	*Theonella swinhoei*, uncultivated bacterial symbiont	Picomolar cytotoxic activity

Graspetides	Microviridins[59]	*Microcystis*, *Planktothrix agardhii*	Serine protease inhibitors such as trypsin, chymotrypsin, subtilase, elastase, and the 20S proteasome

Table 2. Exemplary microbial RiPPs with deciphered physiological and/or ecological function[60]

RiPP class	**Peptide**	**Organism(s)**	**Physiological/Ecological role**
Lanthipeptides	Cytolysins	*Enterococcus faecalis*	Autoinducing peptide; virulence factor
	Lacticin 3147 (LtnA1/LtnA2)	*Lactococcus lactis*	Interference competition
	Nisin	*Lactococcus lactis*	Autoinducing peptide
	Planosporicin	*Planomonospora alba*	Autoinducing peptide
	SapB/SapT	*Streptomycetes coelicolor*, *Streptomycetes tendae*	Morphological development in Streptomyces
	Sh-lantibiotics-α/β	*Streptomycetes hominis* A9	Interference competition
Lassopeptides	Microcin J25	*E. coli* AY25	Interference competition
Thiopeptides	Lactocillin	*Lactobacillus gasseri*	Interference competition
	Thiocillin	*Bacillus cereus* ATCC 14579	Stimulation of biofilm formation in *Bacillus*
	Thiostrepton	*Streptomycetes laurentii*	Morphological development in *Streptomyces*
LAPs	Goadsporin	*Streptomyces* sp.	Morphological development in *Streptomyces*
	Listeriolysin S	*Listeria monocytogenes*	Interference competition (virulence factor)
	Streptolysin S	*Streptococcus pyogenes*	Virulence factor (cytotoxin)
Sactipeptides	Ruminococcin C	*Ruminococcus gnavus* E1	Interference competition
	Sporulation killing factor	*Bacillus subtilis* 168	Cannibalism
	Streptosactin	*Streptococcus* spp.	Fratricidal agent
	Thuricin CD (Trnα/Trnβ)	*Bacillus thuringiensis* DPC6431	Interference competition
Streptides	Streptide	*Streptococcus thermophilus*	Quorum-sensing response
	Tryglsins	*Streptococcus mutans*, *Streptococcus ferus*	Quorum-sensing response, Interference competition
Miscellaneous	AIP	*Staphylococcus aureus*	Quorum-sensing signal
	ComX	*Bacillus subtilis*	Quorum-sensing signal
	Methanobactin	*Methylosinus trichosporium* OB3b	Metallophore (chalkophores)
	Mycofactocin	*Mycobacterium tuberculosis*	Redox enzyme cofactor
	Pyrroloquinoline quinone	*Klebsiella pneumoniae*	Redox enzyme cofactor
	RaxX	*Xanthomonas oryzae* pv. *oryzae* (Xoo)	Host-bacteria interaction

1.3 RiPPs Potential Applications

1.3.1 Thiopeptides

Given the fact of the broad spectrum of the intriguing and unique biological activities presented by several members of RiPPs, thiopeptides have always been earning more interest than any other classes with untapped potential scaffolds in terms of clinical needs. Despite their structural attractiveness, which is evident by their potent antibiotic behavior and different modes of action from the currently used drugs, their progression into the clinical trials has been hindered due to their challenging synthesis and inadequate pharmacological issues such as poor solubility, absorption and bioavailability.[61]

Nevertheless, two thiopeptides are currently commercialized for veterinary purposes. Thiostrepton, besides its utility as a molecular biology toolkit, is the first example of a commercially used thiopeptide for treating skin infections for both companion animals and livestock as topical ointment Animax®. The second marketed candidate is nosiheptide, whose addition at subtherapeutic concentrations in animal feeds can promote growth.[8b]

Structurally, the introduction of azol(in)e(s) heterocycles into peptides is assumed to evade the proteases susceptibility issue and to imply specific configurations to the scaffold facilitating its fine interaction with its proposed molecular target(s).[62] Exemplified by such perception, thiazole heterocycles units can be retrieved in some approved drugs arising from the hybrid polyketide synthase (PKS)/non-ribosomal peptide synthetases (NRPS) pathway, e.g. bleomycin, a PKS/NRPS product as an anticancer agent driving DNA intercalation. An additional anticancer thiazole-derived candidate is depicted as epothilone and its approved synthetic macrolactam variant, ixabepilone.[63]

Within the same context, azol(in)e-containing RiPPs usually offer tempting drug-lead archetypes that can be harnessed in various therapeutic needs of human diseases. For instance, LFF571, a semisynthetic derivative of GE2270A, underwent development by Novartis to overcome its solubility difficulty (12 mg/mL compared to <0.001 mg/mL). Strikingly, in a panel consisting of 50 strains of vancomycin-sensitive *Clostridium difficile*, LFF571 delivered an MIC_{90} of 0.25 mg/l, compared to 2.0 mg/l of vancomycin. More importantly, both antibiotics have distinct mechanisms of action, so possible cross-resistance would not be anticipated. As a result of this, LFF571 was nominated to a phase II clinical trial (NCT01232595), in which its comparable safety and efficacy in contrast to vancomycin for the treatment of *C. difficile* infections were found to be highly promising.[64]

In 2018, Novartis' antibacterial program, unfortunately, was suspended, halting the development of this thiopeptide despite its potential. However, dedicated improvements should be recalled to optimize the formulation and tune alterations to the framework amending the solubility and bioavailability limitations.[8a,8d]

A further illustration of the therapeutic potential of thiopeptides can be gleaned from the development of CB-06-01 (NAI-003), a chemical derivative of GE2270A, for the treatment of moderate to severe acne by Cassiopea, an Italian pharmaceutical company with an interest in developing dermatological agents. Interestingly, Donadio and his co-workers demonstrated that CB-06-01 exhibited weaker potency towards a broad spectrum of Gram-positive contrary to GE2270A. In the meantime promising low MIC values against *Propionibacterium acnes* were observed, proposing a selective and less disruptive advantage to the normal skin microflora.[65]

According to 2020 pipeline news of Cassiopea's, CB-06-01 successfully completed phase II clinical trials with a plan to optimize formulation and to execute a dose-ranging study.

Bearing in mind the highly potent chemical space that thiopeptides occupy, semi-synthesis was often consulted to morph their different skeletons to gain accession to structurally relevant analogs with improved pharmacokinetic and pharmacodynamic (PK/PD) properties and maintaining their potency profiles. Such efforts can be demonstrated by the trials to harness the multiple chemical handles of thiomuracin A to prepare a suite of substituted proline variants from the ILe epoxide motif. In a similar fashion, the replacement of its Phe with Gly afforded a more water-soluble derivative with a kept potency.[66]

The nocathiacin archetype similarly underwent various chemical modifications by a group at Bristol-Myers Squibb through the C-terminus as a free carboxylic acid handle for multiple derivatizations with more solubilizing groups. Considering its hydroxypyridine and indole moieties, mono- and bis-alkylated homologs were semi-synthesized with significantly improved solubility character and sustained activity.[67]

Analogously, an additional hybrid strategy combining mutasynthesis and precursor-directed diversification was adopted to fetch groups with exclusive and particular changes within the quinaldic acid motif of thiostrepton. Remarkably, such alterations markedly achieved a substantial effect on the solubility limitation besides enhancing the antibiotic profile.[43d,68]

1.3.2 Lasso peptides

A further RiPP molecular family displaying a fascinating array of biological activities with numerous potential candidates is formed by lasso peptides.[69] Such therapeutical scope can be gleaned, for example, from microcin J25 with its antimicrobial ability towards gram-negative bacteria by targeting RNA polymerase through blocking the entry of NTP substrates owing to its binding to the uptake channel. Moreover, microcin J25 was found to counteract endotoxins ETEC K88 without any noticeable toxicity raising the possibility to be envisioned as a preventative drug against intestinal damage and inflammatory response by pathogenic infections.[70]

A different instance of a promising biological significance is portrayed by lassomycin, which exhibited antimycobacterial activity against multidrug-resistant *Mycobacterium tuberculosis*. Its potency was delineated by stimulating ATP hydrolysis of ClpC1, whereas at the same time it uncouples the ATPase activity from the ClpP1P2- mediated proteolysis causing cell death. Deciphering the molecular basis of lassomycin can be harnessed as a template for the development of new possible therapies for tuberculosis.[25,71]

In an anti-infective context, the lack of cytotoxicity and the positive potentiation ability offered by humidimycin in combination with caspofungin present a possible setup for developing a synergistic cocktail for invasive fungal infections since the resistance issue is highly improbable due to its non-antifungal activity alone.[23,72]

As a result of the biosynthetic malleability and characteristic rigid topology inherited by lasso peptides, Marahiel, and his co-workers were able to non-conventionally repurpose them in new targeted biological matters via an epitope grafting approach. Such a strategy involves the possible amalgamation of a small peptide epitope, known for a particular biological profile, into a lasso peptide by the precursor gene mutation utilizing the highly stable conformation to deliver epitope in a defined, active format. The generation of a microcin J25 variant with an epitope of RGD peptide, a recognition sequence of integrin receptors, was an example of rebranding an antimicrobial lasso peptide entity as a binder with a high affinity and selectivity to the αvb3 integrin receptor, which is involved in angiogenesis and important for the growth of certain types of tumors.[73]

1.4 Selected Classes of Ribosomally Synthesized Peptides

1.4.1 Lanthipeptides

Ribosomally synthesized and posttranslationally modified peptides (RiPPs) as a superfamily of peptidic natural products encompass a rapidly growing group of diverse archetypes spanning over a vast chemical landscape. As one of the prominent RiPPs classes, lanthipeptides arise with the largest and most exhaustively mined entities which are known to structurally contain one or more intramolecular thioether cross-links between β-carbons of alanine residues, termed lanthionine (Lan) or methyllanthionine (MeLan) as class-defining modifications.[74]

Aside from Lan and MeLan motifs, further structural decorations are often appended within the mature peptide, endowing a bountiful array of posttranslational modifications (PTMs) ranging from dehydration, hydroxylation, methylation, oxidation, epimerization to glycosylation. Such PTMs assist in delivering highly morphed entities with proteolytic resistance rendering a broad profile of bioactivities and potential therapeutic functions.[8a,75]

Like all RiPPs, all the discovered bacterial lanthipeptides so far share a similar biosynthetic blueprint in which all the necessary genes contribute to their biogenesis, usually colocalized on the bacterial genome in the form of a biosynthetic gene cluster (BGC). Through a similar biosynthetic logic, lanthipeptides BGCs often harbor a structural gene encoding a ribosomally translated larger peptide defined as a precursor peptide LanA.[74a,76] Convergently, LanAs' translation products are typically fused elements of a N-terminal leader peptide (LP), which plays a role in orientating some of the PTM-modifying enzymes, and a C-terminal core peptide (CP), which will be eventually afforded as the mature lanthipeptide upon LP excision (Figure **1**).[77]

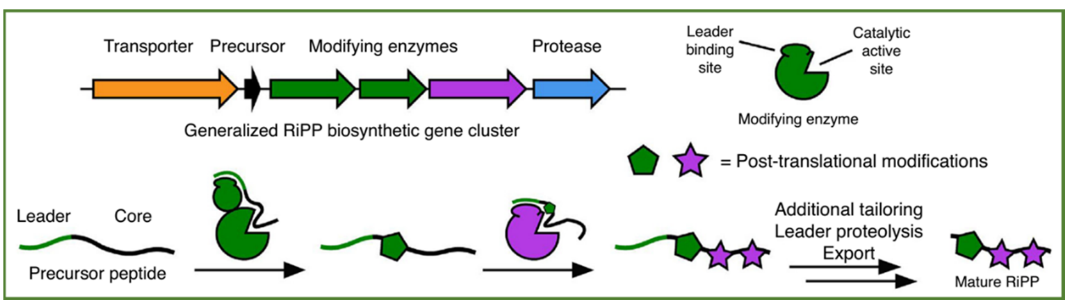

Figure **1**. Generalized RiPP biosynthesis and maturation

After that and guided by LP, the in-chain hydroxyl groups of serine (Ser) and/or threonine (Thr) residues in the CP of LanA will be dehydrated by Lan synthetases to deliver 2,3-dehydroalanine (Dha) and/or (*Z*)-2,3-dehydrobutyrine (Dhb) units, respectively. Following the dehydration, the unique thioether linkages are then installed by the intramolecular 1,4-conjugate addition of specific cysteine (Cys) residues onto the generated dehydro amino acids, in a regio- and stereoselective manner, providing specific patterns of thioether cross-links in the final product. The end product of the intramolecular addition of Cys thiols to the β-carbon of Dha/Dhb is governed by the generated enolate intermediate, which either would form a Lan/MeLan linkage through a protonated mechanism or adopts a further attack on a second Dha/Dhb motif to convey an α,α-disubstituted triamino acid labionin (Lab)/methyllabionin (MeLab) macrocycle (Figure **2**).[7,74a,78]

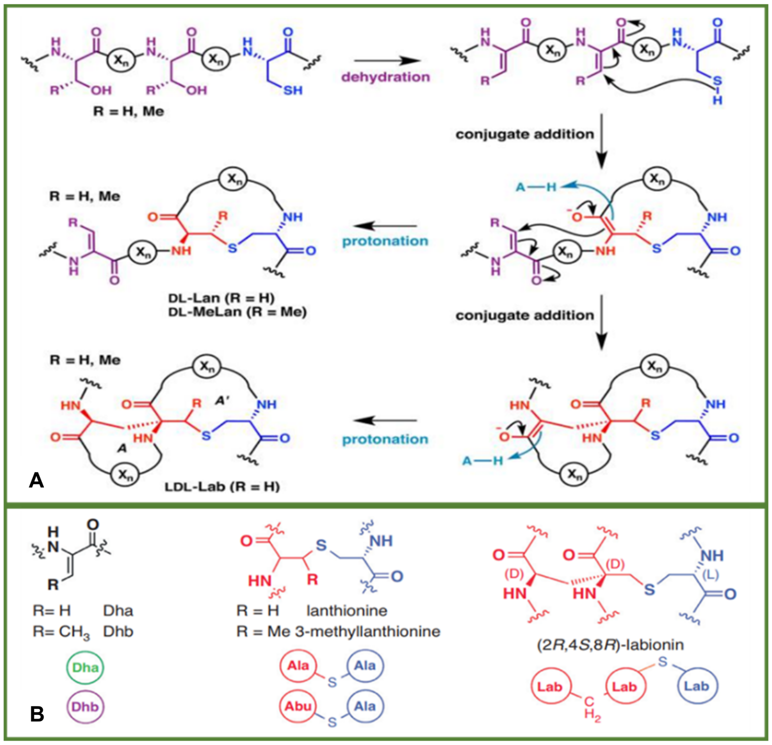

Figure **2**. A) Mechanistic reactions to install (Me)Lan or (Me)Lab cross-links
B) Class-defining PTMs of lanthipeptides

Since the underlying mechanism of lanthipeptides dehydration varies, the classification was recruited to untangle such implication, outlining four different classes taking into account the additional differences between the Lan synthetases as well (Figure **3**).[74a]

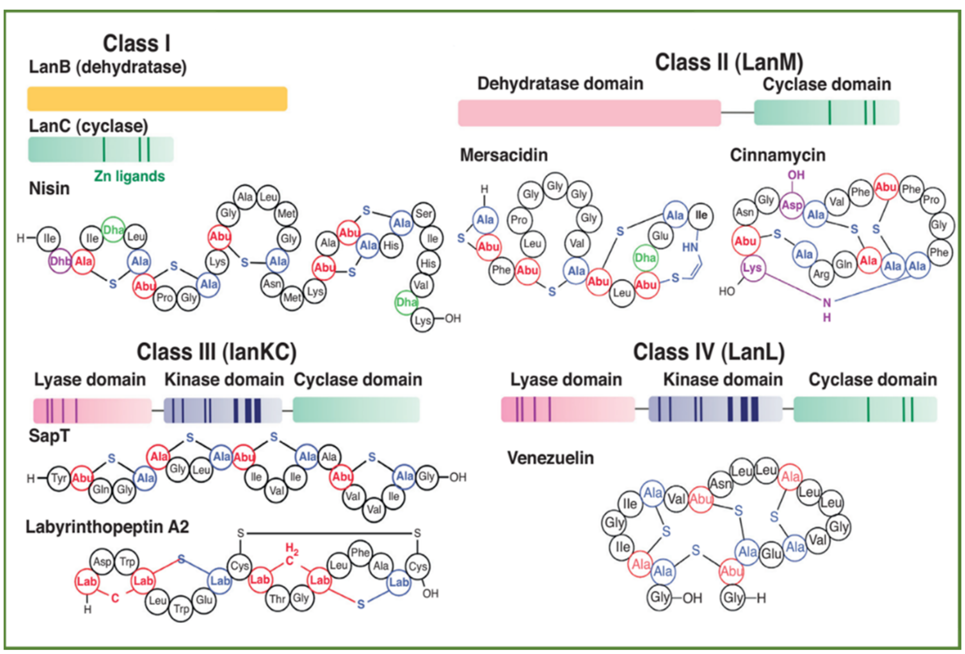

Figure **3**. Schematic representation of the four classes of lanthipeptides synthetases

1.4.1.1 Class I Lanthipeptides: Biosynthesis and Tailoring

In class I lanthipeptides, the formation of (Me)Lan is catalyzed by the cumulative roles of a dehydratase (LanB) and a cyclase (LanC) (Figure **3**). Despite the early detection of genes in charge of nisin and subtilin biosynthesis as representative members of class I, the mechanistic basis of LanB as a dehydratase was just laid out recently. The in vitro characterization experiments of LanB deciphered its function through two domains, one as a N-terminal glutamylator and another referred to as a C-terminal glutamate elimination domain. Counting on α-carboxylate glutamyl-tRNA as glutamate donor, the activation of the inert hydroxyl groups of the Ser/Thr residues, translated in the CP of LanA, is achieved through transesterification by the glutamylation domain.[79]

Afterwards, a β-elimination reaction is carried out on the formerly activated Ser/Thr side chains with the aid of the elimination domain to introduce the carbon-carbon double bond units formatted as Dha/Dhb. Eventually, regional and stereoselective Michael-type additions are facilitated by the cyclase enzyme LanC through the nucleophilic side chain of Cys residues and the electrophilic β-carbons of Dha/Dhb yielding (Me)Lan interlinks (Figure **2**).[80]

Crystal structure of NisC, nisin cyclase, exhibited a toroidal conformation containing a single zinc (Zn) ion catalytic site with a proposed mechanism of activating the thiol side chain of Cys residues towards the cyclization PTM.[81]

Aside from the characteristic thioether modifications, class I entities frequently provide additional ancillary alterations to finally morph the mature peptide against proteases and/or enhance the stability. For instance, the presence of lactyl (Lac) and pyruvyl (Pyr) groups at the N-termini was perceived in multiple class I members exemplified by epicidin 280, epilancin K7, and pinensins. Biosynthetically, such tailoring arises from a N-terminal Ser residue, which undergoes dehydration under the effect of LanB, giving N-teminal Dha1 that in turn tautomerizes into an unstable imine following spontaneous hydrolysis to generate a Lac or Pyr moiety (Figure **4**).[82]

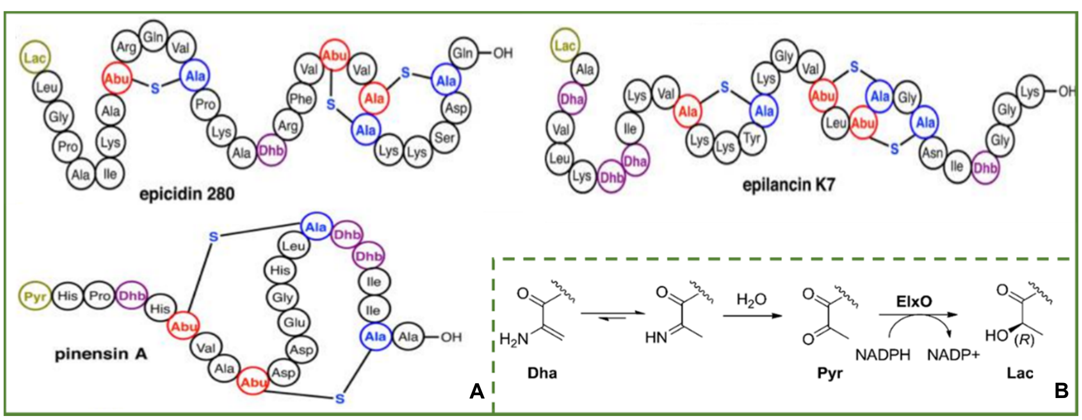

Figure **4**. A) Selected members of class I lanthipeptides featuring N-terminal Lac and Pyr motifs
B) Proposed mechanism of the formation of Lac and Pyr tailorings

S-[(*Z*)-2-aminovinyl]-D-cysteine (AviCys) installation was an additional unique RiPP structural refinement at the C-terminus, that can be found in a handful of class I candidates as epidermin, gallidermin, microbisporicin (NAI-107) and mutacin 1140 (Figure **5**). Such skeletal change was envisioned to be introduced through a 1,4-nucleophilic attack of an oxidatively decarboxylated Cys residue onto a Dha unit. In vitro reconstitution experiments aided in gleaning a plausible mechanism in which LanD enzyme supported with a flavin mononucleotide (FMN) catalyzes Cys decarboxylation followed by the 1,4- Michael addition by the in-situ generated thioenolate nucleophile (Figure **5**).[14,74a,83]

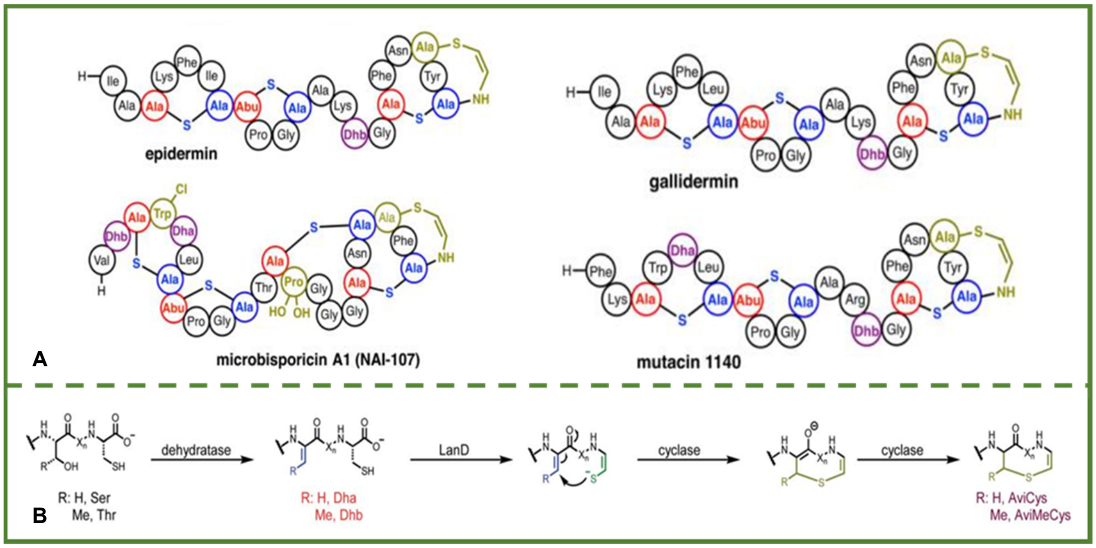

Figure **5**. A) Representative entities of class I lanthipeptides tailored with AviCys decoration B) Proposed mechanism of the formation of AviCys PTM

Despite the fact of the hydroxylation prevalence as a secondary PTM in other RiPP family e.g. thiopeptides, its occurrence within a lanthipeptide context is rather rare. Consistent with such observations, microbisporicin (NAI-107), produced by *Microbispora* sp. 107891, structurally frames two novel tailorings, defined as halogenation on Trp and dihydroxylation on Pro. Interestingly, the native version of microbisporicin with 5-chlorotryptophan (5-Cl-Trp) was found to be 2 to 32-fold more potent than the deschloro variant, considering the tested bacterial isolates panel. The halogenase encoded by *mibH* was proven to be responsible for catalyzing such unprecedented makeup with very high substrate specificity and more flexibility regrading the halogen nature.[84]

1.4.1.2 Class II Lanthipeptides: Biosynthesis and Tailoring

Unlike class I of having two standalone processing enzymes, LanBC, a full-length single enzyme, LanM, catalyzes both the dehydration step and the cyclization reaction equipped with its N-terminal dehydration and a C-terminal cyclization domain. An additional discriminative feature of class II is that LanMs recruit a different mechanism to activate the hydroxyl groups of Ser/Thr residues than LanB proteins in which ATP phosphorylation is recalled, followed by phosphate elimination to append the Dha/Dhb moiety (Figure **3**).[85]

In a similar fashion to class I and expectedly considering the sequence similarity, the cyclase domain of LanM shares a resemblance to the previously reported one of class I (LanC) in terms of the role of Zn to facilitate the activation of the Cys motifs for the cyclization (Figure **3**).[74a,86]

Along the same tailoring lines of class I, class II conveys as well further modifications beside the typical (Me)Lan linkages. The first architectural change that can be enlisted is their ability to encode D-configured amino acids within the mature peptide backbone either as D-Ala and/or D-aminobutyric acid (D-Abu) (Figure **6**). The utility of such installation is to improve the product stability against proteolysis. Lactocin S was the first characterized lanthipeptide II to harbor D-Ala residues, which inferred genetically and biosynthetically to be installed via the conversion of L-

Ser to D-Ala in the CP in a stereospecific reductive manner of Dha catalyzed by a LanJ dehydrogenase. Further examples retrieving such an epimerization tailoring were witnessed in lacticin 3147 (Figure **6**) and more recently in carnolysins.[87]

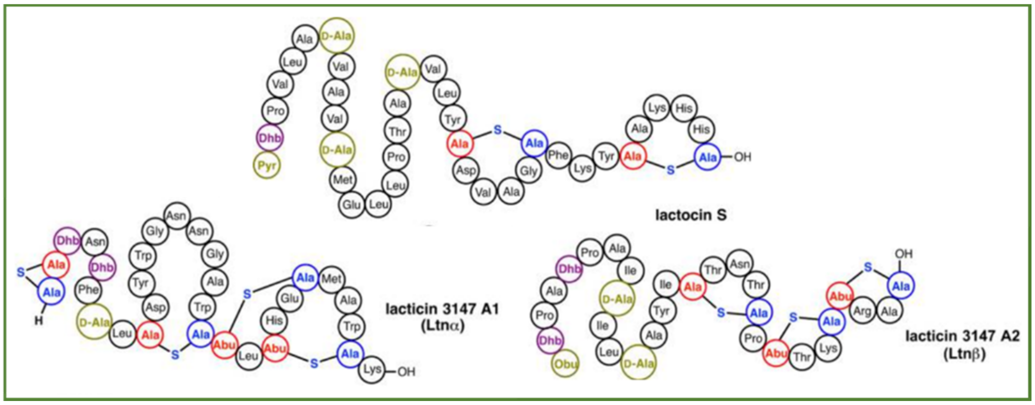

Figure **6**. Representative entities of class I lanthipeptides tailored with AviCys decoration

Comparably to NAI-107 as a hydroxylated member of class I, duramycins portray the analogous hydroxylated scaffold of class II carrying such PTM as *erythro*-3-hydroxy-L-aspartic acid for their antimicrobial activity (Figure **7**). An extra appealing C-N cross-link was exclusively featured in duramycins and cinnamycins molecular families in the form of the lysinoalanine (Lal) macrocycle installed by an aza-Michael-type addition between the 3-amine of the C-terminal Lys19 to a dehydrated Ser6 (Dha) residues. The mechanistic facilitator for appending such structural alteration was genetically proposed to be carried out by the protein DurN through positioning Dha6 and Lys19 residues in adjacent proximity enabling the macrocycle generation (Figure **7**).[12b,88]

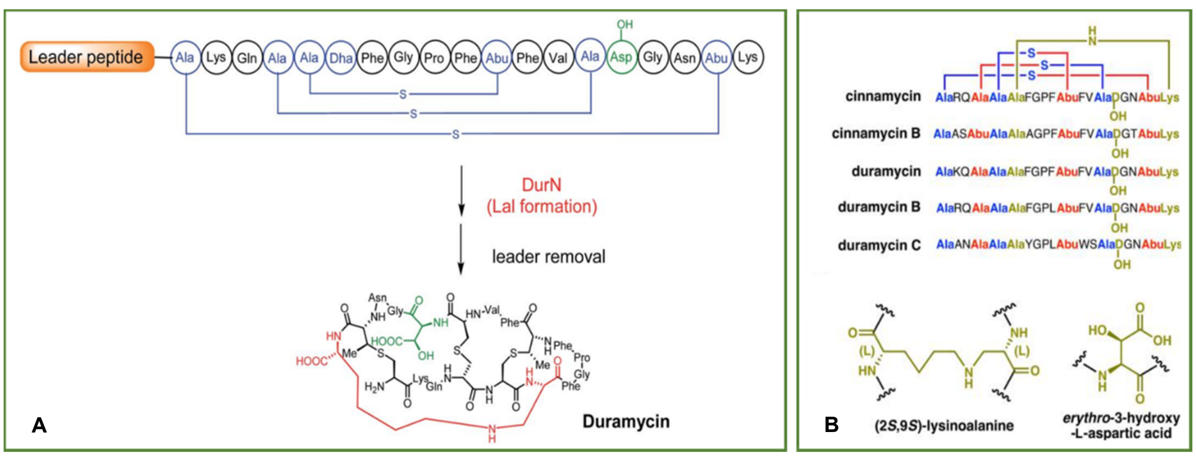

Figure **7**. A) Schematic architecture of duramycin
B) Shared identical tailorings across cinnamycins and duramycins members

1.4.1.3 Class III and IV Lanthipeptides: Biosynthesis and Tailoring

In contrast to class I and similar to II, class III and IV possess a single enzyme that is responsible for the dehydration and cyclization events within their members. Differently to LanM as a di-modular Lan synthetase, classes III and IV recruit trimodular Lan synthetases, called LanKC and LanL respectively, to phosphorylate, dephosphorylate and cyclize their respective substrates (Figure **3**).[74a,78]

The previous in vitro investigations discerned that the dehydration reaction is carried out by utilizing two separate active sites of LanKC and LanL where the phosphorylation is achieved via the central Ser/Thr kinase domain and phosphate elimination takes place in the N-terminal pSer/pThr lyase domain. In a distinctive fashion to the ATP phosphorylation mechanism accepted by LanM or LanL, the N-terminal kinase domain of LabKC fulfills the activation of the inert in-chain groups of Ser/Thr by consuming a GTP substrate.[89]

Additionally, the C-termini of LanM and LanL proteins exhibit an analogous LanC-like domain containing a Zn^{2+} site, whereas LanKC lacks the signature of the catalytic residues and such zinc ligands (Figure **3**).[85c,90]

The most noticeable structural modification of class III lanthipeptides is their ability to frame either (Me)Lan or Lab residues through a remarkable tandem cross-linking event.[91] A Lab as class defining decoration of class III enables the installation of two cross-links into the mature peptide, where the carbacyclic ring is N-terminal, and the thioether ring closure points towards the C-terminus. While the majority of the characterized Lab containing structures of class III lanthipeptides are modeled with a SX_2SX_3C motif, variable sequences of the thioether ring were found to be tolerated in Lab resulting in a contracted ring size as given in catenulipeptin or in an expanded version exemplified by labyrinthopeptin and NAI-112 (Figure **8**).[74a,92]

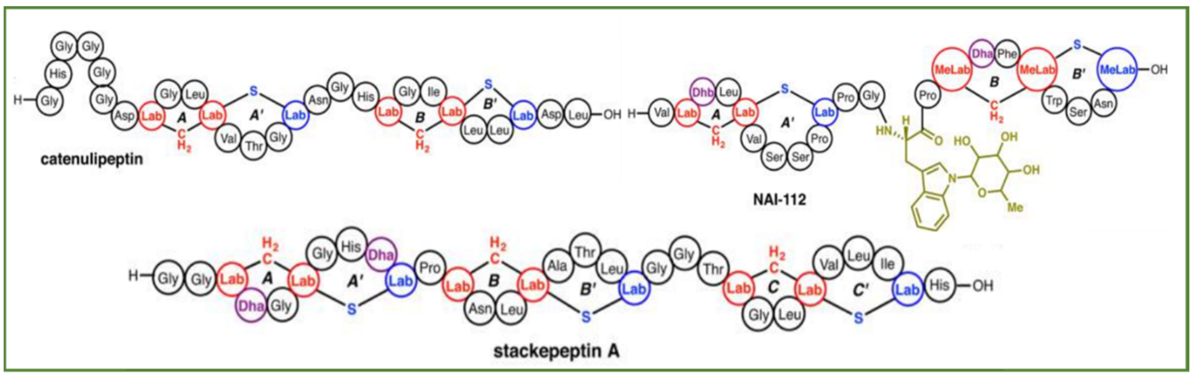

Figure **8**. Selected archetypes of class III lanthipeptides framing Lab modifications

The frequent occurrence of different PTMs in classes III and IV is not as rich and diverse as in classes I and II which might be partly attributed to the less characterized members belonging to both categories.

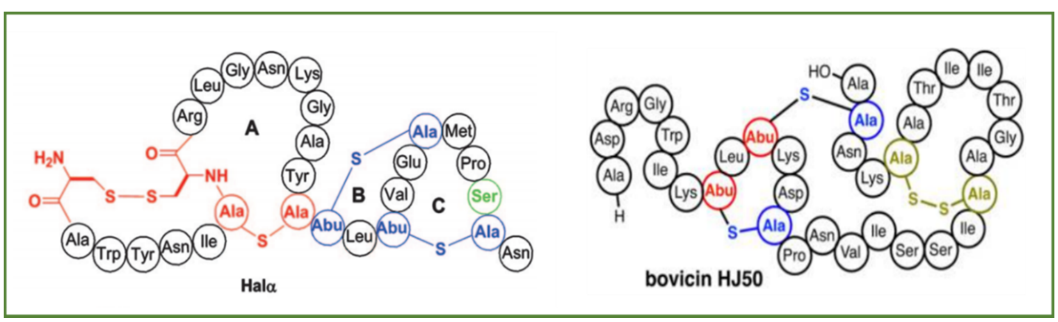

Figure **9**. Exemplary architectures of class II lanthipeptides scaffolds embedded with a disulfide linkage

The first observed tailoring in class III was installed in its prototype member, labyrinthopeptin A2 and its related scaffolds labyrinthopeptin A1/A3, in the form of a disulfide linkage made between Cys9-Cys18 in case of A2 and Cys9-Cys20 in A1/A3 (Figure **3**). Additionally, some class II candidates, haloduracin α and bovicin HJ50, structurally append such disulfide decoration (Figure **9**). Although the disulfides proved to be essential for the bioactivity in bovicin related lanthipeptides, it was found to be marginal in the α component of haloduracin.[75,93] The second modification was illustrated as N-glycosylated lanthipeptide in NAI-112 produced by *Actinoplanes* sp. DSM 24059. Analyzing the putative BGC encoding NAI-112 revealed a glycosyltransferase (GTF) which was hypothesized to introduce this PTM (Figure **8**).[92c]

1.4.2 Linear Azoline Peptides

Further common structural elements that ribosomally-made peptides known to feature within their architectures are thiazoles and oxazoles units. Such imprinted skeletal modifications are encoded in a vast space of bacterial RiPPs, defined as thiazole/oxazole modified microcins (TOMMs).[7,94] As a result of their high abundance and wide distribution across multitudes of RiPPs families in tandem with other unique structural alterations, more precise subclassification was adopted to accurately subdivide them into a variety of molecular classes, including linear azol(in)e-containing peptides (LAPs), thiopeptides (pyritides) and cyanobactins.[95]

Convergently, the biosynthetic basis to install (methyl)azol(in)es is highly analogous in the three classes via a heterotrimeric enzyme complex (Figure **10**), referred as YcaO, administering the heterocyclization of Ser/Thr and Cys residues to frame (methyl)azolines residues which would be subsequently oxidized into (methyl)azoles catalyzed by a flavin mononucleotide (FMN)-dependent dehydrogenase, termed SagB.[7,95d]

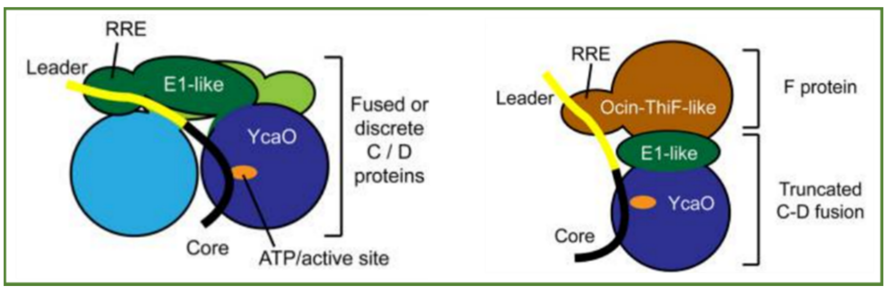

Figure **10**. Cartoon models of the E1-like (left) and F-dependent (right) cyclodehydratase

Mechanistically, the structural framing of (methyl)azol(in)es blocks into the CP backbone by YcaO protein is achieved by an ATP-dependent cyclodehydration event in which the in-chain β-hydroxyl group of Ser/Thr and/or thiol group of Cys residues execute a nucleophilic attack onto the former amide bond to yield a hemiorthoamide species. Upon cyclization, ATP-oriented O-phosphorylation occurs followed by N-deprotonation facilitating the loss of a phosphate moiety to deliver the final (methyl)azoline heterocycle (Figure **11**).[95d,96] Despite the similar processing action exerted by azoline-forming YcaO enzymes across the different RiPP classes, the utilized accessory domains to potentiate such cyclodehydration activity vary significantly across these biosynthetic routes.[96b,96c]

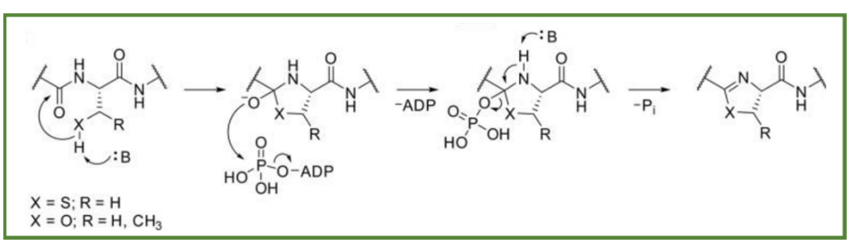

Figure **11**. ATP-dependent mechanism for the cyclodehydration process

The majority of the so far reported LAP BGCs were found to contain an E1-ubiquitin (E1-like) activating protein as a cognate protein paired with the main YcaO enzyme. The in vitro biochemical characterization demonstrated that in the absence of the partner E1-like proteins the majority of the cyclodehydratase activity of YcaO proteins is minimal. The current state of structural biology data illustrates that the E1-like domain binds with the precursor substrate via its leader peptide specifically through a conserved domain, called RiPP recognition element (RRE), to conformationally enforce the propeptide to be in close vicinity to the catalytic center of the YcaO for cyclodehydration.[96d,97]

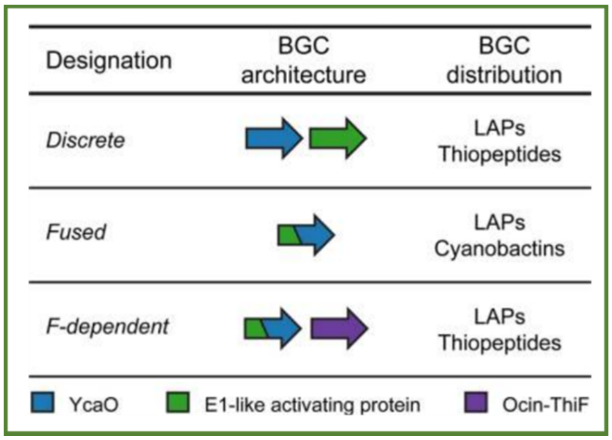

Figure **12**. Schematic representatives of different RiPP cyclodehydratases

Unlike most LAP YcaOs, thiopeptide BGCs commonly share a shortened N-terminal E1-like activating domain fused with a YcaO protein, which is further accompanied by a discrete “Ocin-ThiF-like” protein, termed as F-dependent YcaO (Figure **12**).[95d,96c,98]

Upon cyclodehydration and to enhance the chemical stability of such installed tailorings in the mature peptide, a further and common modification is exerted through a selective dehydrogenation of (methyl)azolines into azoles. Such skeletal mofication is found to be catalyzed by a member of FMN-dependent dehydrogenases by deprotonating the Cα of the (methyl)azoline followed by the Cβ hydride transfer of the (methyl)azoline to yield the oxidized (methyl)azole.[95d,99]

An additional architectural alteration frequently coupled with the introduction of azol(in)e residues into LAPs and mostly in thiopeptides, is the formation of the dehydrated amino acids Dha and/or Dhb. In a complete analogous dehydrating mechanism of lanthipeptides class I, the installation of Dha/Dhb motifs in the CP is facilitated by a homologous of lantibiotic-type dehydratases (LanB). Differently to the typical class I full-length LanB, LAPs and thiopeptides recruit two split-proteins to convey such PTM. Mechanistically, the glutamylation domain, recognized by its sequence similarity, mediates the tRNA-dependent glutamylation reaction, while the subsequent elimination is catalyzed by the other protein as a glutamate eliminator considering the homology.[42,79,80,98a,100]

1.4.2.1 Microcin B17

The first discovered example of LAPs is microcin B17 (MccB17) from *Escherichia coli* as a narrow-spectrum growth-suppressive metabolite targeting DNA gyrase and enabling their producers to compete within its niche (Figure **13**).[101] Similarly to the most defined microcins in terms of their selective activities, MccB17-specificity against other Enterobacteriaceae and some *Pseudomonas* species was mainly attributed to the selective cellular uptake machinery of the cells.[102] The discovery of the MccB17-BGC and its precursor peptide McbA proved to match the structural characterization efforts regarding the posttranslationally modified residues in which the scaffold is architecturally morphed with a pair of four thiazole and oxazole motifs arising from Cys and Ser residues under the effect of a trimeric synthetase comprised of McbB, McbC, and McbD (E1-like, dehydrogenase, and YcaO proteins, respectively) (Figure**13**).[95a,97,103]

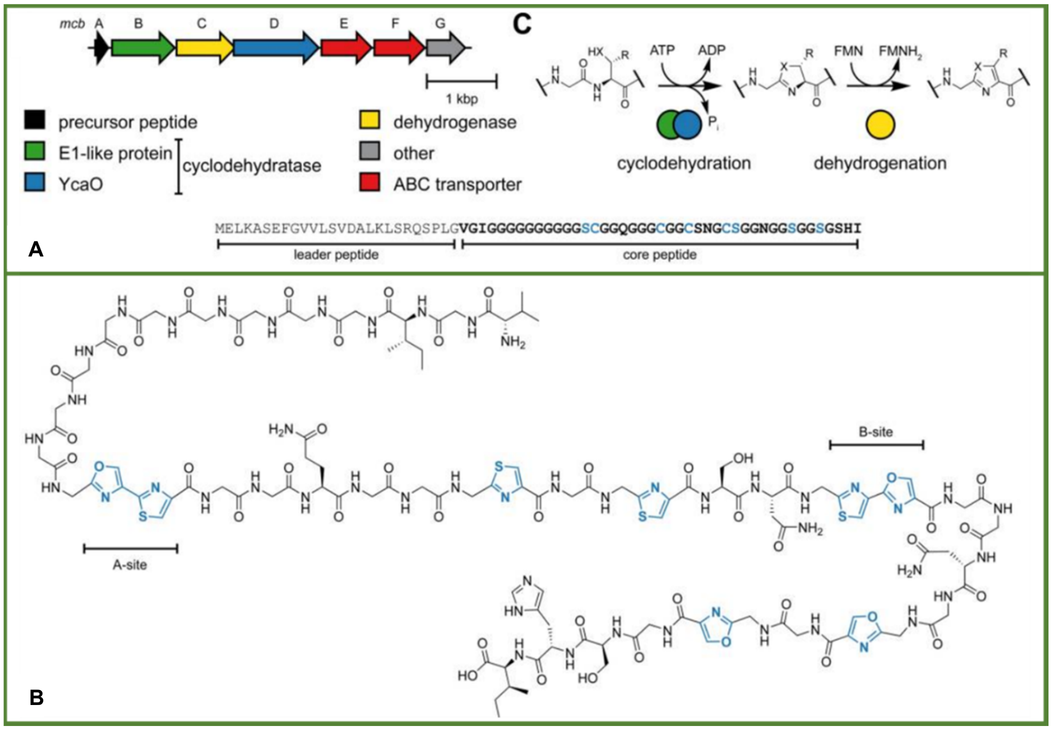

Figure **13**. Microcin B17 BGC (A) and structure (B)

The site-directed mutagenesis investigations verified that the thiazole and oxazole heterocycles are undoubtedly critical for the observed activity and the defined antibacterial effect counts on the heterocycles number encoded in the peptide. The generation of MccB17 variants by deleting and/or altering C-terminal residues delivered a library of analogs with retained in vitro inhibitory profile of DNA replication but less potency against living bacteria. Interestingly, the chimeric entity resulted from the Gly3 introduction of *P. syringae* MccB17 into *E. coli* McbA displayed a broad index of potency highlighting that the sequence residues manipulation at different segments offers a general possible route to tune the activity profiles of other microcins.[101a,104]

1.4.2.2 Plantazolicins

Plantazolicin (PZN) is an additional example of LAPs possessing an ultra-specific bactericidal antibiotic property against *Bacillus anthracis*, the causative agent of anthrax (Figure **14**). Unlike the traditional bioactivity scheme of MccB1, PZN discovery from *Bacillus velezensis* FZB42 (formerly *Bacillus amyloliquefaciens*) was assisted by the genomics paradigm in which the putative gene cluster and biosynthetic logic of azoline-forming YcaOs orient the discovery as well as the structural elucidation efforts.[105]

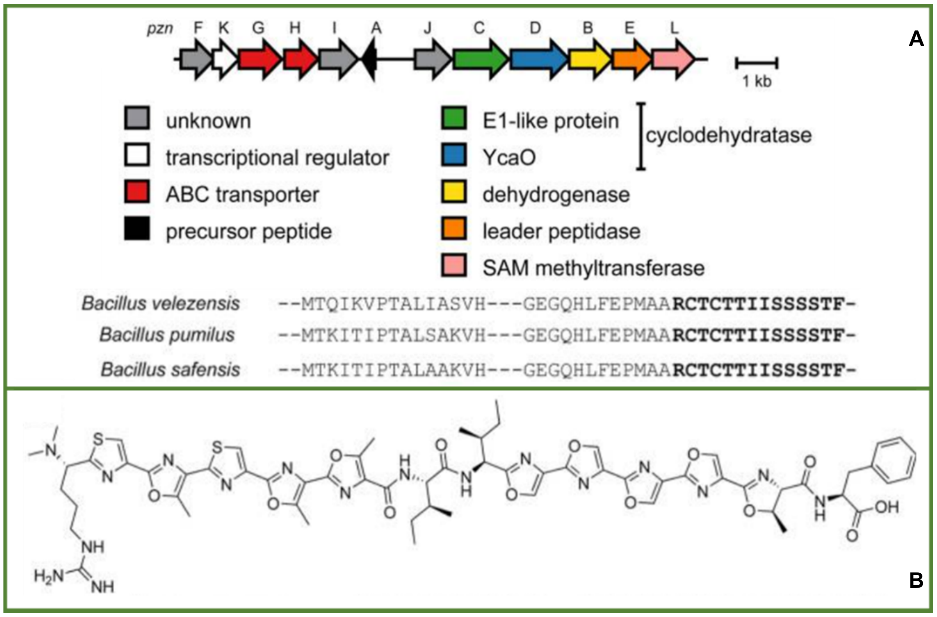

Figure **14**. Plantazolicin BGC (A) and structure (B)

As a standard for LAP BGCs, PZN biosynthetic cluster comprises BamA (PZN precursor peptide), and a (methyl)azol(in)e installing machinery (cyclodehydratase/dehydrogenase, BamBCD) which was found to process all Cys, Ser, and Thr residues into decazol(in)es product. Notably, the existence a S-adenosylmethionine (SAM)-dependent methyltransferase (BamL) within the BGC was structurally translated into double N-terminus methylation (Figure **14**).[105b]

The continuous proliferation of available genome sequences in combination with homology-based motifs similarity could expand the PZN molecular family with 14 further BGCs. The first PZN variant, badiazolicin (BZN), was confirmed via its characterization from the native producer, *Bacillus badius*, with an expected potency against *B. anthracis*. An additional PZN-related entity, coryneazolicin (CZN), was deciphered through successful in vitro reconstitution of the azole synthetase (CurBCD) delivering ten azoles on CurA followed by leader peptide removal and final N-terminal dimethylation by chemical means.[105b,106]

Driven by the highly specific activity profile of PZN scaffolds, several studies were conducted to untangle their mode of action and to define structure-activity relationships (SAR) for their selective potency. Supported with PZN resistance mutants and fluorescently labeled architectures, the possible mode of action was hypothesized in the frame of PZN interaction with specific regions of the *B. anthracis* membrane associated with cardiolipin, a diphosphatidylglycerol lipid, suggesting the destabilization of cardiolipin synthetase to lyse the cell membrane.[107]

To reveal the hidden SAR of PZN, methyltransferase disruption in tandem with precursor peptide mutagenesis laid the fact of the crucial necessity and importance of the dimethylation in addition to the full heterocyclization in the potency index. The mutagenesis experiments also revealed that only a few PZN analogs were possible to be generated through the alteration of certain residues without losing activity against *B. anthracis*.[105b,108]

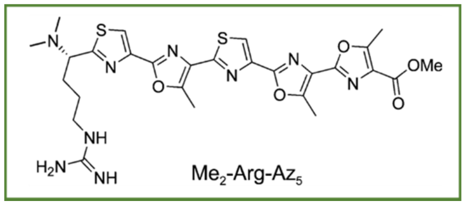

Figure **15**. Synthetic Me_2-Arg-Az_5 variant of PZN

Along the same line by total synthesis means, the shortened pentazole variant was yielded with retained behavior of antibiosis against *B. anthracis*. Unexpectedly, interesting biological leverage with a high profile towards *Staphylococcus aureus* was observed shedding light on the N-terminal end of PZN as the bioactive portion while the C-terminal chunk orients the selectivity (Figure **15**).[109]

1.4.2.3 Azolemycins

Azolemycin shapes an exceptional LAP whose architecture encodes a rare oxime moiety with modest efficacy against mammalian cancer cell lines. Despite the framing of such an unusual decoration in only a handful of some natural products, for example, caerulomycin A, althiomycin, and nocardicins A and B, azolemycin represents the sole RiPP example to append such ancillary modification which possibly plays a role against proteolysis (Figure **16**).[110]

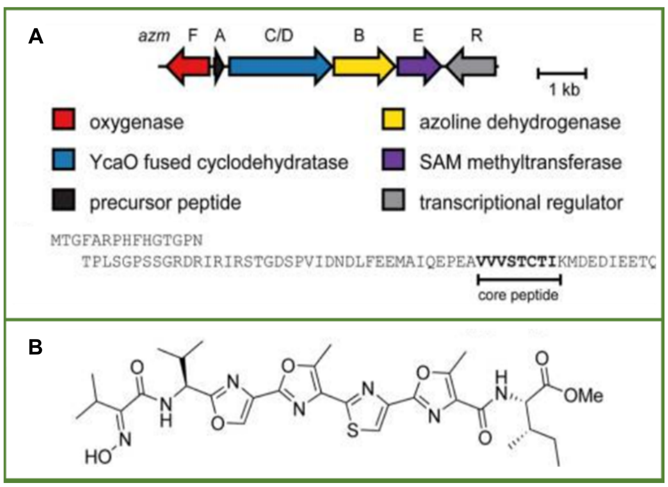

Figure **16**. Azolemycin BGC (A) and structure (B)

Mining the genomic data of the producer *Streptomyces* sp. FXJ1.264 revealed a putative BGC with a precursor peptide (AzmA) that could be responsible for the azolemycins production (Figure **16**). In addition to AzmA, additional processing genes were co-localized such as a fused cyclodehydratase (AzmC/D) and a discrete dehydrogenase (AzmB) to set up the four (methyl)azole units. Interestingly, the BGC of azolemycin disclosed a further protein, AzmF, with homology to flavin-dependent monooxygenases that can account for the oxime decoration, proven by *azmF* knockout product.[111] In alignment with the methylated structure of azolemycin, AzmE as a SAM-dependent methyltransferase was also validated to be in charge of such PTM.[111]

1.4.2.4 Goadsporin

Inspired by the fact that microorganisms live in multilayered complex communities and develop their chemical language to communicate, the discovery of goadsporin from *Streptomyces* sp. TP-A0584 was achieved through a co-culture screening campaign of hundreds of actinomycete broths to induce the actinorhodin production from *Streptomyces lividans* TK23. Interestingly, more physiological characterization unveiled that goadsporin can promote the secondary metabolism and sporulation across various streptomycetes at a concentration of 1 µM while higher doses (>1 µM) deliver an inhibitory profile.[112]

The structural elucidation of such an entity culminated in an unusual LAP consisting of 19 amino acids morphed with six (methyl)azole motifs, two dehydrated alanine residues (Dha), and N terminal acetylation (Figure **17**).[100a]

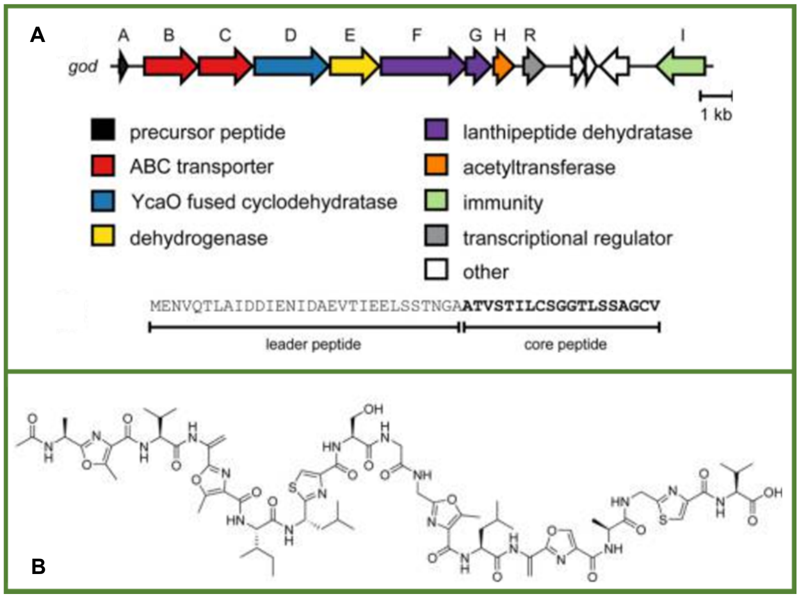

Figure **17**. Goadsporin BGC (A) and structure (B)

The detection of the goadsporin BGC in tandem with systematic experiments of genetic deletion rationalized the biosynthetic pathway in which the azoles introduction into the CP backbone is carried out firstly by the fused cyclodehydratase (GodD) and dehydrogenase (GodE). Afterward, the installation of Dha residues is catalyzed by homologous proteins being involved in lanthipeptide biosynthesis, termed a split LanB dehydratase (GodG for glutamylation followed by GodF for elimination) (Figure **17**). Furthermore, a candidate protein for the N-acetylation was also retrieved as N-acetyltransferase (GodH).[100b,113] Biological evaluations of the different installed structural features verified that Dha groups are indeed crucial for its observed bioactivity.[100b]

1.4.3 Thioamitides

In complementation to the YcaOs-mediating azoline, further categories of this protein family were spotted in multiple genomic contexts, uniquely installing specific structural alterations than the well-characterized azoline type. Candidates of such a distinct subfamily of YcaO proteins seem to be neither fused (E1-like) nor co-occur with partner proteins (ThiF-like), referred to as standalone YcaO, exemplified by the one involved in bottromycins to frame amidine units (Figure **18**).[95d,114]

A further skeletal transformation mediated by specific YcaO proteins is the rare thioamidation tailoring in which the amidic oxygen of the backbone is replaced with sulfur affording thioamitides. Besides the expanded scope of the unique structural modifications catalyzed by such protein family, in nearly all thioamide-containing RiPPs, YcaO is encoded adjacent to a ‘TfuA-like’ protein, as responsible pair for installing the class-defining thioamide(s) in the backbone (Figure **18**).[77,115]

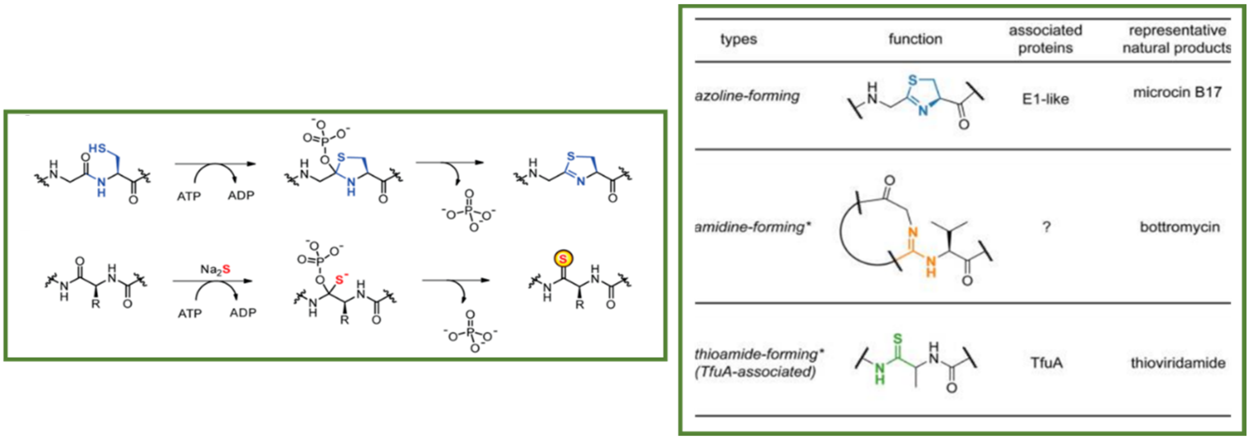

Figure **18**. Comparative proposed mechanisms catalyzed by different YcaO members (left) and selected PTMs overview mediated by some YcaO members (right)

Aside from the proposed classification by the RiPPs community as an independent class termed thioamitides, thioamidated RiPPs are exceptionally rare and catalyzing such compelling PTM in the CP has profound impacts on the mature peptide in terms of the hydrogen bonding, protease resistance and bioactivity index.[115]

Historically, thioviridamide, from *Streptomyces olivoviridis* NA05001, is considered the representative entity of this molecular family characterized by an apoptosis induction profile (Figure **19**). In addition to the five thioamide groups that thioviridamide carries, an additional set of posttranslational decorations are structurally embedded within the CP encompassing a β-hydroxy-*N1*,*N3*-dimethylhistidinium, AviCys, and an N-terminal pyruvyl motif.[116]

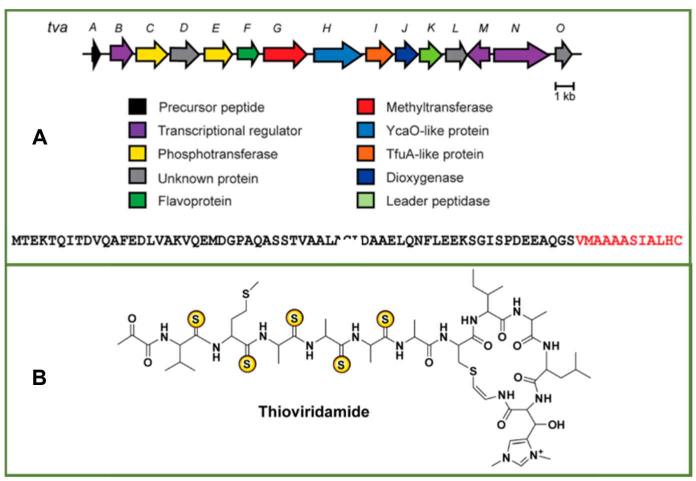

Figure **19**. Thioviridamide BGC (A) and structure (B)

The allocation of the BGC of thioviridamide and the function assignment for each gene eased and accelerated the genome mining trails to leverage such a potent chemical space. The successful discovery of multiple thioviridamide-like compounds with enhanced inhibitory behavior against the growth of various cancer cell lines was demonstrative of these targeted efforts exemplified by three analogs of thioalbamide (from *Amycolatopsis alba* DSM 44262) in addition to thioholgamides A/B (*Streptomyces malaysiense*) (Figure **20**).[52,53a,117]

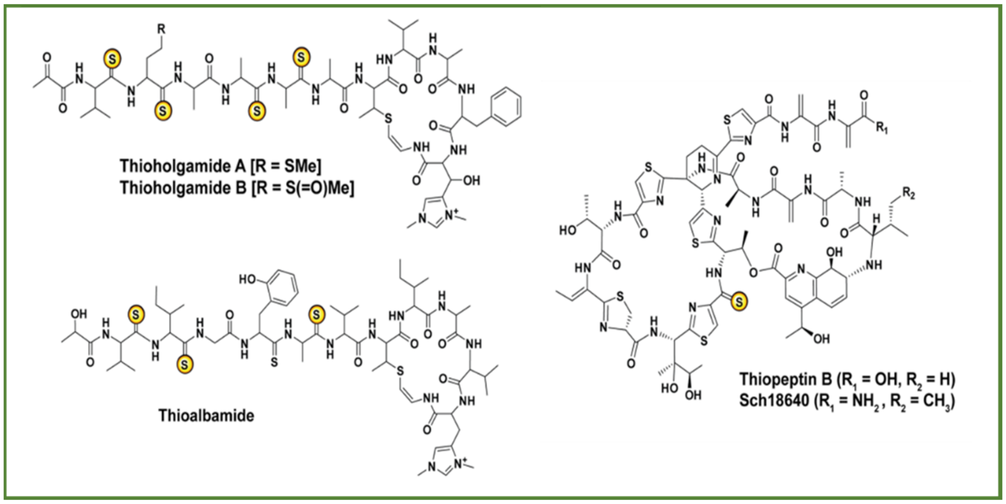

Figure **20**. Thioviridamide-related structures

Despite no biochemical characterization was recruited to study the thioviridamide pathway, genetic disruption experiments of thiovarsolins and the thiostreptamide S4 variant proved the requirement of YcaO and TfuA proteins for the backbone thioamidation. It was early hypothesized that TvaH, a YcaO homolog, is the in-charge protein to feature the class-defining thioamide transformations during the biosynthesis. Moreover, TvaI, a TfuA-like protein, was additionally envisioned to contribute to the thioamidation step as a supportive partner protein existent in all thioviridamide similar BGCs.[51a,118]

Extra evidence about the responsibility of the YcaO/TfuA pair in RiPP thioamidation was gleaned from capitalizing the bioinformatic expansion of the thiopeptide family that can harbor thioamidated members. Such a bioinformatic-driven approach afforded a novel thiopeptide framing a solo thioamide residue, designated as saalfelduracin besides similar entities like Sch 18640 and thiopeptin (Figure **20**). The BGC identification was enabled by sequencing the native producers in which YcaO–TfuA proteins are encoded adjacent to each other. Further indisputable proof about the dependency of thioamidation on YcaO and TfuA proteins was derived from the chromosomal insertion of the corresponding genes couple from Sch 18640 (*Streptomyces tateyamensis*) as a thioamide producer into a non-thioamide producer of thiostrepton (*Streptomyces laurentii*) uncovered an identical metabolite to Sch 18640.[50a]

1.4.4 Lasso Peptides

A further peptidic group with an expeditious growing nature affiliated with the superfamily RiPPs is the subgroup of lasso peptides in which their archetypes share specific class-defining architecture achieved by lariat knot-like threading (Figure **21**).[69a,77,119]

Historically until 2008, the biological needs mainly directed the chemical investigations as the main paradigm that enabled the discovery of several lasso peptides. Recently, the remarkable advances in sequencing technologies in synergy with the publicly shared genomic datasets empowered the genome mining strategy to be broadly adopted as the ideal tool to unearth diverse scaffolds of lasso peptide.[120]

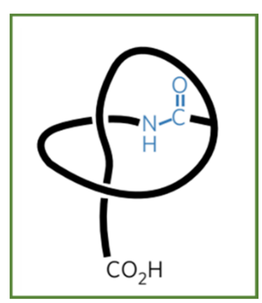

Figure **21**. Threading depiction of lasso peptides

1.4.4.1 Topology, Classification and Stability

Structurally, lasso peptides feature at the scaffold level an N-terminal macrolactam ring connected to a linear C-terminal tail in such a way that the tail is threaded through the ring yielding a complex and unique topology that resembles a lasso. Such macrolactam rings are formed as a result of a characteristic isopeptide bonding between the free N-terminus and the carboxylic acid side chain of an Asp or Glu located at positions 7, 8, or 9. The insertion of the tail within the ring creating a fold is topologically sustained by steric plugs in the form of bulky amino acids situated above and below the ring. Further introduced crosslinks between the Cys residues as disulfide crosslink(s) contribute to the stabilization of such an interlocked molecular frame (Figure **22**).[120c,121]

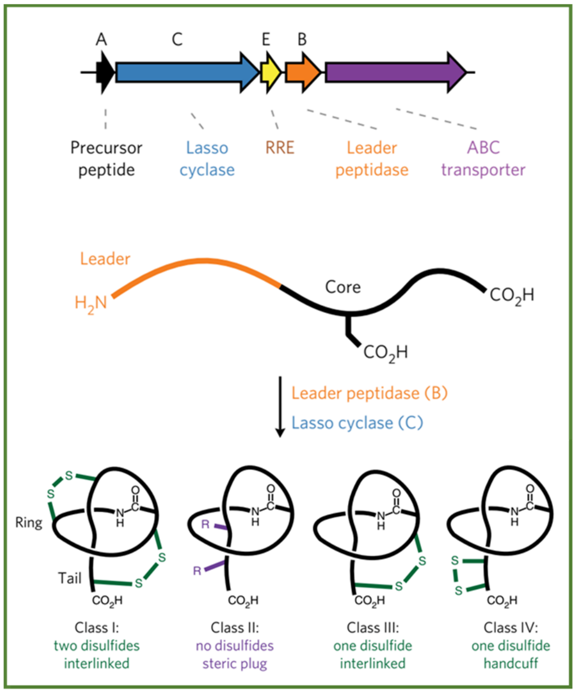

Figure **22**. Schematic representation of lasso peptides BGC and the possible architectures

Considering the presence, absence and localization of the disulfide crosslinks, lasso peptides are categorized into four different classes. Class II lasso peptides are renowned for the absence of disulfide interlinks. Their topologies are solely kept by steric dependence. However, two disulfide bonds are featured in class I entities while, class III and IV models harbor a single interlinkage (Figure **22**).[119b] In class I, one of the disulfide bridges is accomplished between the N-terminal Cys residue of the ring and the one located at the loop region. In addition, another disulfide linkage is recruited between a further Cys motif of the macrolactam ring with an additional one enoded at the lower region of the threaded tail. In contrast to class I, members of class III, and IV are chemically characterized by one connection of a disulfide PTM. The location of the involved Cys residues can discriminate between both. In class III, the bond formation occurs between a Cys unit from the ring with a Cys placed in the C-terminal tail, while the single connectivity between the two Cys residues of the C-terminal tail delivers class IV (Figure **22**).[20b,119a,120c]

From a structural point of view and aside from the biological significance, the tailoring with disulfide bridge(s) is supposed to promote the stability of the exceptional chemical fold that lasso peptides inherit but even in class II lacking such a decoration, substantial stability was iteratively proven for the lasso conformation. Previous thermal stability studies showed that multiple lasso peptides are able to tolerate prolonged exposure to higher temperatures e.g. 95 °C and autoclaving at 120 °C.[121,122] Nevertheless, at elevated thermal conditions, some heat-sensitive lasso peptides were converted into branched-cyclic peptides through unthreading the C-terminal tail out of the ring exhibiting a retention time drift in liquid chromatography (LC).[27,123]

Upon several investigations about the thermal steadiness of multiple lasso peptides, it was deciphered that both ring and steric plug residues sizes are the skeletal determinants of their thermal resistance. For example, site-directed mutagenesis of the CP of xanthomonin II, a lasso peptide isolated from *Xanthomonas gardneri* with a seven-membered macrolactam ring (Gly1-Glu7), revealed that all steric residues larger than Ser retained the topology in the thermal denaturation protocol.[121,123a,123c] On the contrary, capistruin, from *Burkholderia thailandensis* with a nine-membered isopeptide linkage (Gly1-Asp9) morphed by Arg15 as a bulky lower plug, was liable to thermal degradation upon replacing Arg15 and Phe16 as a next candidate bulky residue with Ala. Despite that the Phe18 unit was expected to act as the final lower plug, the longer sequence offered by the Phe18 position relative to the ring threading conveys a flexible un-lassoed tail under elevated temperatures.[124]

An additional instance describing the impact and utility of the size replacement of the steric unit on upgrading the thermal resistance properties of the heat-sensitive lasso peptides can be outlined with the bulky residues substitutions at the tails of caulosegnin I (Gly1-Glu8 ring, Glu16 as plug residue) and astexin-1 (Gly1-Asp9, Phe15 as plug residue) with Trp resulting in heat-stable scaffolds.[123a,123c,125]

In complementary to the thermal stability, the lasso topology also brings resistance against proteases pictured in numerous study cases. Commonly, carboxypeptidases Y, as a typically employed peptidase in most lasso reports to infer their enzymatic stability, continuously degrade the C-terminal residues out of the tail until the shielding effect of the macrolactam ring is called.[120b,121,123a]

1.4.4.2 Lasso Peptide Biosynthesis

The biogenesis of lasso peptides as a member of the RiPP superfamily is initiated with the precursor peptide synthesis by the ribosome, yielding a typical precursor peptide consisting of the N-terminal leader required for the enzymatic processing and a C-terminal core sequence translated into the mature lasso peptide. Minimally to biosynthesize a lasso peptide, the candidate BGC should harbor at least three biosynthetic genes, a precursor peptide (A), a cysteine leader protease (B) sharing homology to transglutaminases, and an asparagine synthetases homolog defined as ATP-dependent lasso macrocyclase (C) (Figure **22**).[69a,119,126]

The proteolysis stage in the biosynthesis of lasso peptides counts on protein (B) which can be either expressed as a fused di-modular catalyst or discrete fragmented proteins encompassing a RiPP Recognition Element (RRE/B1) and a discrete protease (E/B2) with the catalytic domains (Figures **22,23**).[120b,120c,127]

The mechanistic scheme of lasso peptides obeys the same route in both cases where the translated propeptide recognition is achieved by the RRE which in turn guides the subsequent processing events. Mediated by the RRE binding, the proteolytic leader cleavage is catalyzed by the protease (E/B2) to deliver the core peptide as a substrate undergoing the class-defining isopeptide tailoring (C) between the released N-terminal α-amine and the Asp or Glu side chain by the macrocyclase in an ATP dependent manner (Figure 23).[96d,119b,128]

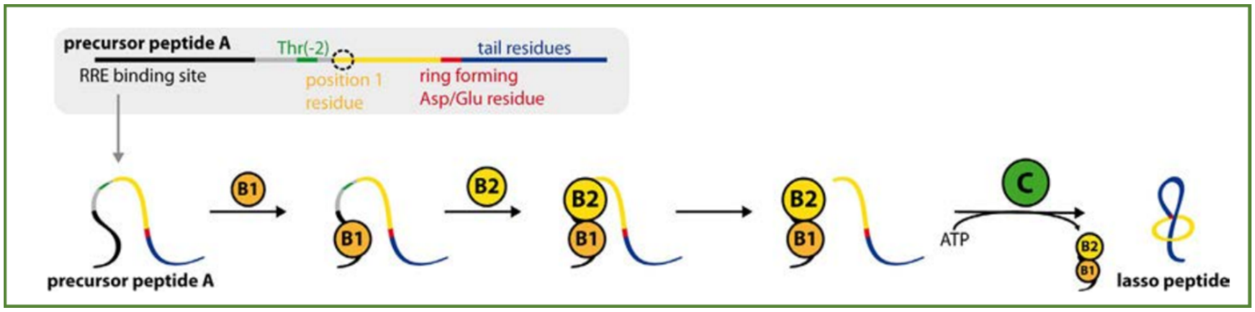

Figure **23**. Generic mechanistic depiction of the lasso peptide biosynthesis

Several and recent in vitro studies proved that the prefolding adjustment of the CP is recruited before the macrocyclization step potentiated by C protein (Figure **23**). Furthermore, the unique steric nature, afforded by the lasso architecture and maintained by the rotaxane-like topology, additionally prevents the C- terminal tail from threading upon the installation of the macrolactam ring.[129]

Within the course of the in vitro biochemical characterization of the microcin J25 processing enzymes McjB and McjC, an interdependency relation was interestingly found for both enzymes where no individual activity could be detected in the performed assays. Together, the catalytic activities were restored thereby deciphering the necessity of the close proximity of both protease and macrocyclase active sites to overcome the short-fate burden of the in vivo linear biosynthetic intermediate of the lasso peptide.[130]

A further noticeable biosynthetic feature lasso peptides inherit for enzymatic tailoring is the common existence of conserved residues embedded within the precursor peptide in both leader and core regions. The first universal residue (Thr) is located in the leader peptide at the penultimate position Thr(-2) (Figure **23**).[121,122a] Multiple mutagenesis studies showed that the replacement of this residue impaired the lasso peptide production and in some cases halted the proteolytic turnover. More insights about the role of this conserved motif were gleaned by conducting in vitro assays to demonstrate the proteolytic maturation machinery of paeninodin, a lasso peptide from *Paenibacillus dendritiformis* C454, decoding that Thr(-2) is crucial for the leader recognition by the peptidase PadeB2.[123d,129b,131]

A second maintained aspect of the lasso maturation enzymes is their strict affinity of engaging Asp or Glu residues in the macrolactam modification to produce entities with 7,8 and 9 membered ring systems. Repeatedly, the lasso macrocyclase C has confirmed its high stringent specificity to such macrocycle sizes, while shifting these residues in their respective precursor variants are not processed enzymatically.[121,129a,130]

As a deviating instance of such a conserved feature, the C protein encoded in caulosegnins I-III BGC from *Caulobacter segnis* is an exceptional model from the common lasso macrocyclase with efficient flexibility to cyclize variable ring sizes in different precursor peptides. This was exemplified by Gly1-Glu8 in caulosegnin I besides Gly1-Glu9 in caulosegnins II and III (Figure **24**).[125] Along the same line, fusilassin macrolactam-forming enzyme FusC, naturally cyclize a 9-mer Trp1-Glu9 macrolactam, exhibits via in vitro reconstitution experiments a compelling tolerance in the threaded ring size to be not only 7-9 but also 10 residues as new-to-nature tailoring (Figure **25**).[129a]

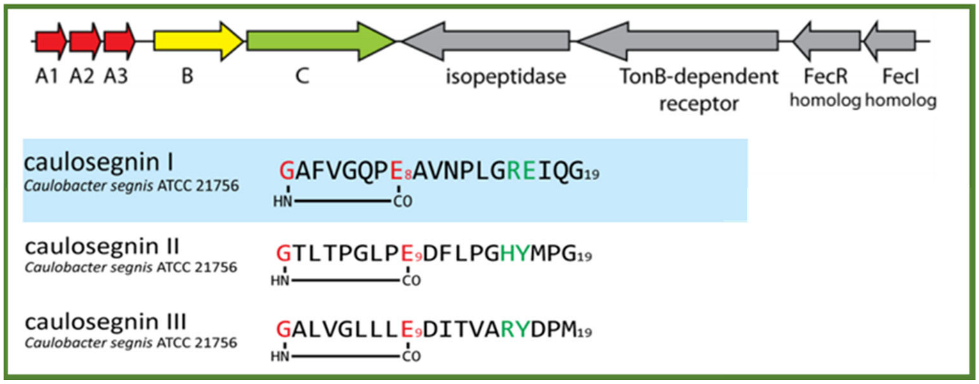

Figure **24**. Caulosegnins BGC and their simplified structures

A third feature that most lasso peptides universally share across their biosynthetic machineries is their biogenetic preference for a Gly residue at position 1 of the CP whereas its substitution usually impacts the lasso production negatively. The early exception of such enzymatic affinity was exemplified by the fusilassin archetype (Trp1-Glu9), whose precursor peptide homologs at position 1 were tolerant towards all amino acids replacements except Pro residue (Figure **25**).

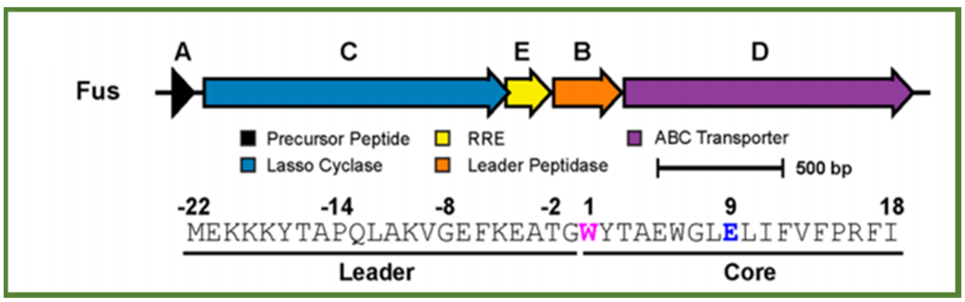

Figure **25**. Fusilassin BGC and its precursor peptide

Despite the accumulated knowledge regarding the strong biosynthetic bias towards Gly1 unit in classes II and III, recent genome mining-guided schemes leveraged the panel in this regard with Ala1, Ser1, Leu1, Asp1, Tyr1 and the previously described Trp1.[119b,127b,129a,132] Additionally, large-scale bioinformatic charting of BGCs encoding putative lasso peptides expanded the variation scope at position 1 with all canonical amino acids except for Pro.[120c]

An additional conserved motif uncovered by genome mining is the YxxP (or sometimes WxxP) sequence situated in the leader region of the precursor lasso, exclusively retrieved in the biosynthetic loci encoding discrete RRE proteins and leader peptidases. Site-derived mutagenesis investigations concluded that the residues Tyr and Pro are crucial for the lasso recognition and the maturation steps whereas their substitutions compromised the binding affinity with the RRE protein.[120c,129a,129b,133]

1.4.4.3 Lasso Peptide Tailoring

Aside from the isopeptide defining motif that lasso peptides architecturally feature, a suite of variable functional groups were found to be appended into their skeletons upon the maturation process catalyzed by the tailoring enzymes. The scope of such skeletal decorations witnessed for lasso scaffolds is spanning from phosphorylation,[123d,134] over acetylation,[127a] methylation,[25] hydroxylation,[135] deimination[120c] to epimerization (Figure **26**).[29,136]

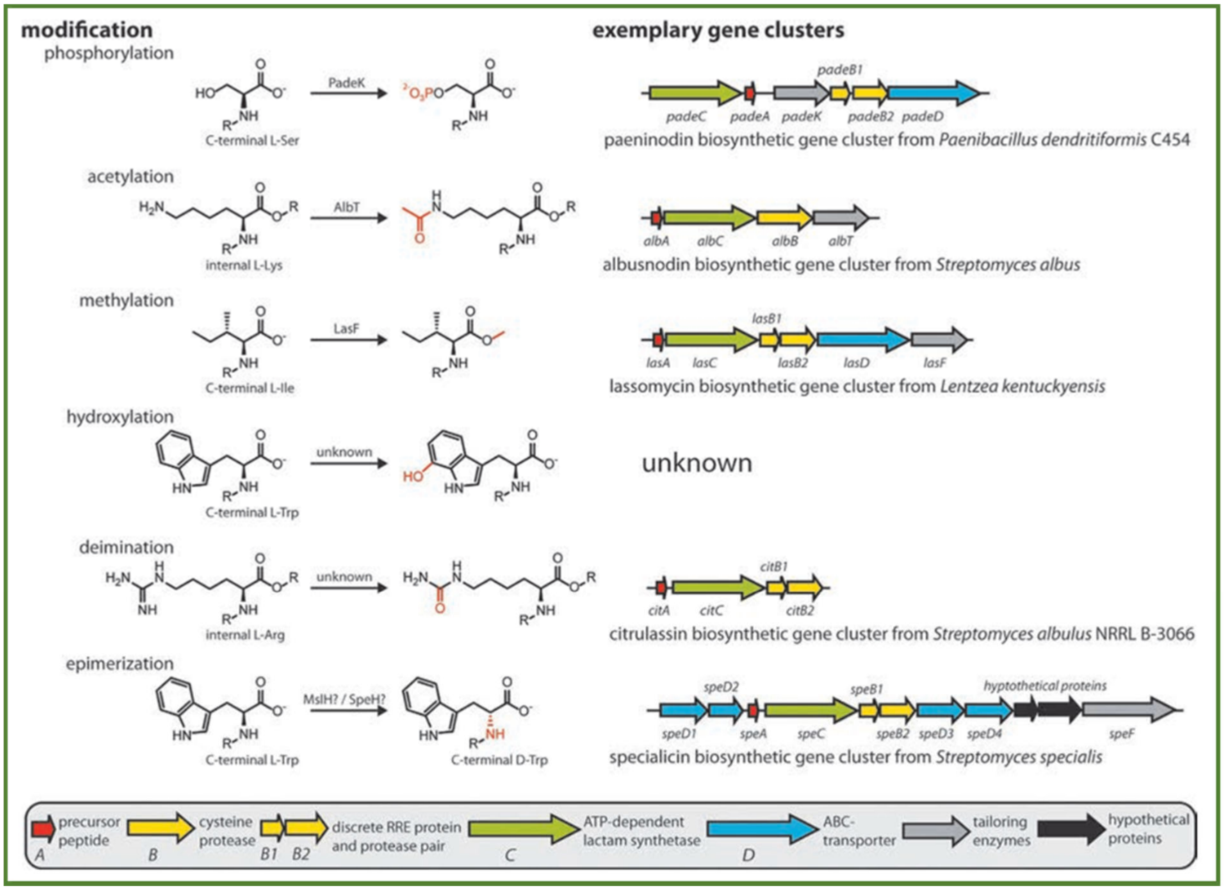

Figure **26**. Overview of the PTMs scope across various tailored lasso peptide

The possible genetic elements responsible for carrying out such modifications were usually identified from their putative encoding BGCs. For example, a putative acetyltransferase was envisioned to execute the acetylation of Lys10 in albusnodin, and a presumed O-methyltransferase methylates the C-terminus of lassomycin (Figure **26**).[25,127a] Although the biochemical validation to corroborate the roles of the putative epimerase SpeH in specialicin biosynthesis is missing till now, the in vivo and in vitro functional characterization of MslH in MS-271 verified its catalytic function to conduct the epimerizations of the C-terminal Trp residues.[29,136b,137]

The in vitro studies of the kinase homolog (PadeK), involved in the C-terminal phosphorylation of the Ser residue in paeninodin, exhibit its ability to tailor the linear precursor peptide and not the mature lasso version. This was mechanistically rationalized as a result of the steric hindrance presented by the macrolactam ring topology. Additionally, the promiscuity and regioselectivity of PadeK were shown with the C-terminal Ser and other residues as well.[123d]

Citrulassin A, a characterized lasso peptide from *Streptomyces albulus* NRRL B-3066, carries an unprecedented deimination illustrating of the unusual modification that lasso peptides can deliver (Figure **26**). The framing of the nonproteinogenic citrullline residue at position 9 instead of the genetically encoded Arg was enzymatically hypothesized to be catalyzed by a peptidyl arginine deiminase (PAD).[120c,138]

1.5 Bioinformatics/Metabolomics-Guided The Leverage of RiPPs Chemical Space

The affordability of whole-genome sequencing compounded with various bioinformatic platforms has empowered the introduction of a parallel frontier, denoted as genome mining, in the natural products pipeline to prioritize the discovery efforts. The genome mining-oriented approach is a process in which the putative BGC(s) is identified in the context of their corresponding biosynthetic products. In the meantime, the exponential growth of genomic data impelled numerous bioinformatic tools to adopt a high throughput computational format to expedite the exploration of novel natural products.[139]

Since the majority of various RiPPs classes are commonly known to feature a short precursor peptide in close vicinity to a unique set of post-translational modifying enzyme(s) differentiating one from another, the bioinformatic usage of such characteristic biosynthetic hallmarks as genetic signatures unveiled a hidden plethora of different RiPP BGCs.[139]

Constrained by the formerly selected and represented RiPP classes, below we highlight some exemplary schemes of genome mining frequently recruited to disclose new RiPP entities belonging to these different families.

1.5.1 Mining BGCs by Searching Both PTM Enzymes and Precursors

The first and early genome mining trials were based on the sequences of the precursor peptides, the substrates of the ribosomal biosynthetic machinery, and/or the processing enzymes as an input to retrieve structurally related entities sharing analogous skeletal alterations. Despite the inherited RiPP limitations that the multipurpose genome mining tools like antiSMASH, and PRISM possess in terms of accuracy, the implementation of exclusively designed RiPP algorithms e.g. BAGEL, RODEO, RiPPMiner, DeepRiPP, and RiPPER improve the comprehensive detection and prediction of RiPP BGCs in addition to their respective precursors' anticipation.[51a,120c,140]

1.5.2 BGC Comparison and Clustering by Similarity Network

Aside from the classical homology-based querying of either the precursor peptide and/or the conserved modifying enzymes, a comparative BGC workflow was lately introduced to discriminate between the known and novel PTM enzymes. Utilizing a sequence similarity score in the form of sequence similarity networks (SSNs) offers a quick prioritization of novel RiPP BGCs with new PTM. Similarly but with a broader context, Medema and his co-workers developed the BiG-SCAPE platform that can align and correlate single, multiple ORFs or a complete BGC against the already discovered and deposited RiPP families from the MIBiG database in a high throughput manner speeding up the large-scale genomic data mining.[120c,141]

1.5.3 Metabologenomics

As a result of the exquisite scope of the bioinformatically-predicted motifs that RiPPs can encode gleaned from the genomic data. These chemical features can be exploited as handles in a reactivity setting to facilitate the linkage between the assay hits and putative BGCs offering a rapid shortcut to different RiPP entities of interest.[142]

Mitchell's group utilized this inherited chemical property within different RiPP classes to selectively label them chemically via their specific functional groups enabling their detection and dereplication. The common occurrence of dehydrated amino acid (DHAA) moieties in the form of Dha and/or Dhb units within different classes like lanthipeptides, LAPs, thiopeptides, and linaridins enabled Cox *et al*., to streamline the identification of such reactive posttranslationally modified features. Using dithiothreitol (DTT) as a soft nucleophile with the MS measurements of the treated extracts, indicative mass shifts could define the number of the labeled groups (Figure **27**).[143]

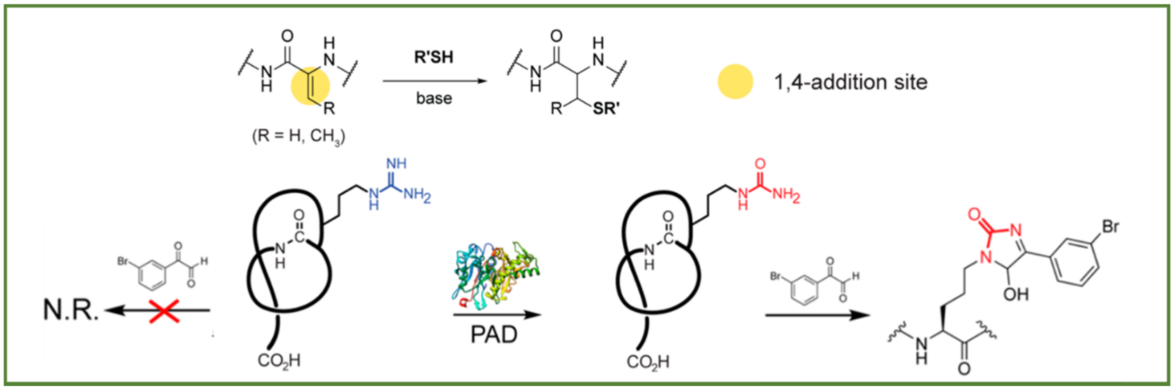

Figure **27**. Chemoselective tagging of defined PTMs in different RiPPs classes

A further example of the selective chemical labeling was presented with lasso peptides in which a chemical probe, 3-bromophenylglyoxal, was validated to specifically tailor the primary ureido functional groups encoded within citrulline lasso peptides (Figure **27**). The employment of such selective chemical tags presents a noticeable acceleration in the identification and characterization of the targeted RiPPs especially in conjunction with sensitive MS-based measurements.[138]

Exploiting the sensitivity and high throughput setup offered by the MS technique, a RiPPquest tool was developed by Dorrestein's team to automate the early connection between the RiPP BGCs and their cognate chemotypes from the metabolomic datasets. This is achieved by allocating the PTM genes and their small precursor peptide from the genomic data followed by generating a list of in-silico MSMS spectra of the predicted CPs. Final cross matching between the calculated masses and experimental ones is automated to deconvolute the candidate hits from the bacterial extracts.[144]

1.6 The Genus *Nocardia*: Pathogenicity and Biosynthetic Capacity

The genus *Nocardia*, which belongs to the aerobic actinomycetes and can be ubiquitously recovered from soil and water, comprises a group of clinical pathogens that contribute to severe infections associated with high morbidity to humans and animals. The health implication initiated by *Nocardia* usually impacts the immunocompromised patients and sometimes impairs the immunocompetent individuals aside. The nocardial infections, which are often attained by inhalation as a result of their environmental abundance, target the skin and lung as primary sites triggering severe pulmonary or central nervous system illnesses that can be developed into life-threatening scenarios in the immunocompromised ones.[145,146]

Although numerous studies were conducted on *Nocardia* spp. for a long time, the driving force and ramifications of such investigations were mainly poured on their isolation, taxonomic classification, clinical diagnosis in conjunction with understanding their host pathophysiology. Driven by such a medical interest, several whole-genome sequencing projects were executed on several *Nocardia* isolates within the last ten years. Markedly, an extraordinary capacity for the assembly of diverse secondary metabolites was disclosed upon these sequencing initiatives for the majority of *Nocardia* species, surpassing even some genera known for their prolific biosynthetic potential such as *Amycolatopsis*.[147]

Even though bacterial pathogens have always gained more traction for many decades to understand their inherited pathogenicities and virulent factors, in the meantime they are also deemed to be rich reservoirs of specialized bioactive metabolites. *Nocardia* genome mining studies in tandem with bioinformatic approaches revealed considerably that they do not only produce enabling metabolites for their virulent behaviour but also novel druggable molecules that can be harnessed in different biological needs e.g. immunosuppressive, antimicrobial, cytotoxic or antifungal aspects.[148]

1.6.1 *Nocardia terpenica*, a Promising Source of Exceptional RiPPs

Nocardia terpenica species, including IFM 0406 (formerly known as *N. brasiliensis*) and 0706^T isolated from patients with lung nocardiosis, are classified as clinical gram-positive isolates. They share the same primary feature of forming colorless to beige mycelia that can shatter into rod to coccoid-shaped bacteroid non-motile elements during growth. Similar to other *Nocardia* members, their cell walls are equipped with an unusual envelope consisting of mycolic acids as characteristic components of the cell wall differentiating them from other bacteria.[148d,144]

Recently, the comparative genome sequence alignment of both isolates reflected their phylogenetic relatedness and enormous biosynthetic talent in terms of secondary metabolites with around thirty-eight BGCs predicted by antiSMASH v5.1. Expectedly, the antiSMASH results revealed a large number of BGCs translating various polyketide synthases (PKS) and non-ribosomal peptide synthetases (NRPS) in accordance with the previous analysis of multiple *Nocardia* spp. genome sequences.[147c]

Nocardia was previously described within a limited number of studies to be able to assemble RiPPs (Figure **28**). Taking into account the mainly deduced in vitro potency of these ribosomal entities, it was hypothesized that they are more likely involved in their producers' natural habitats for competition and survival purposes.[149]

Besides the highly diverse pool of unknown PKS and NRPS products, the BGCs coding for the antifungal brasilinolides, the immunosuppressant brasilicardins and the terpenibactins were seamlessly detected as well. In complementation to PKS and NRPS machineries, minimal five BGCs encode for different and unique RiPPs were additionally identified in both isolates' genomes.[150, 151]

The first ribosomally biosynthesized features isolated from *Nocardia* spp. were thiopeptides, termed nocathiacins and nocardithiocin. They exhibited an interesting bioactivity index against a broad panel of some clinical pathogens (Figure **28**).

Nocathiacins, from *Nocardia* sp. ATCC 202099, structurally frame, besides the class-characteristic six-membered nitrogenous ring of thiopeptides, an additional nosiheptide-indolic skeleton decorated with a unique glycosylation tailoring of rare sugar enhancing their solubility (Figure **28**). A further thiocillin-similar thiopeptide, nocardithiocin, was discovered in a bioactivity-guided scheme from *N. pseudobrasiliensis* IFM 0757 with promising minimal inhibitory concentration (MIC) values towards rifampicin-resistant and -sensitive *Mycobacterium tuberculosis* strains.[37,38a,38b]

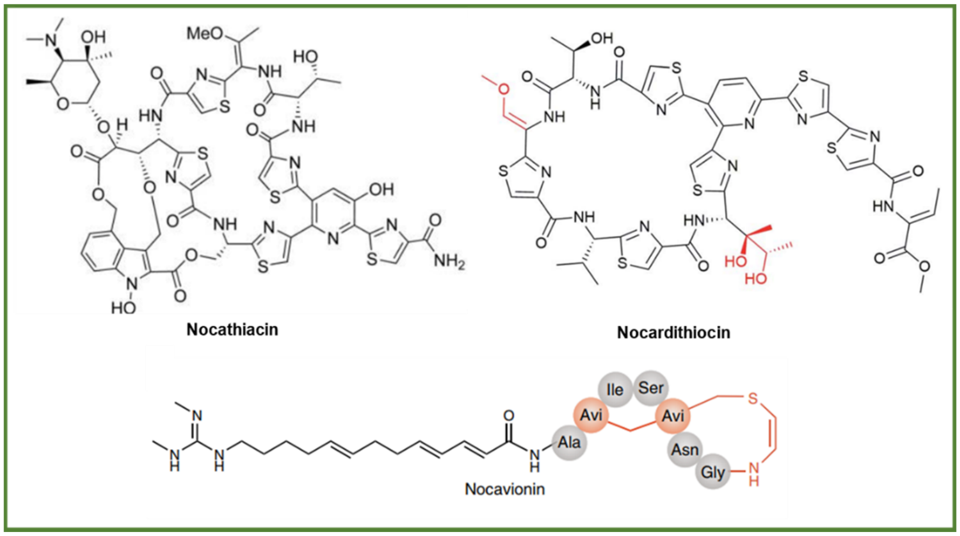

Figure **28**. Isolated RiPPs from *Nocardia*

Recuriting the classical bioactivity–guided isolation with genome mining approach, the discovery of nocavionin from the extracts of *N. terpenica* IFM 0406 was achieved. Nocavionin, as a hybrid lipidated lanthipeptide termed lipolanthine, charts the first example of a ribosomally synthesized peptide framing an unprecedented decarboxylated avionin motif in addition to a lipidatation character (Figure **28**). Despite the non-availability of the antibacterial assessments for nocavionin, its structural analog microvionin, from *Microbacterium arborescens*, showed notable antibacterial profiles against Methicillin-resistant *Staphylococcus aureus* (MRSA) and *Streptococcus pneumoniae*.[152]

2. Aims of The Present Study

As has been discussed formerly, the value of RiPPs investigation is well appreciated in terms of their versatile biological significance that can be repurposed in numerous human and/or animal-related therapeutic needs. In addition, the myriad ecological and physiological roles associated with some RiPP archetypes can assist in understanding microbial ecosystems and interactions.

Driven by such promises and the less characterized RiPP entities from the genus *Nocardia*, this study has been fundamentally focused on expanding the chemical space of RiPPs from *N. terpenica* IFM 0406 and 0706^T.

The genome analysis of *N. terpenica* IFM 0406 clearly exhibited five different RiPP gene clusters (1 x lanthipeptide, 1 x linaridin, 2 x lasso peptides and 1 x hybrid RiPP) that can possibly assemble unknown RiPP scaffolds (Figure 29). Among these clusters, two BGCs were prioritized to be surveyed within the scope of the current study considering their novel constituting biosynthetic elements.

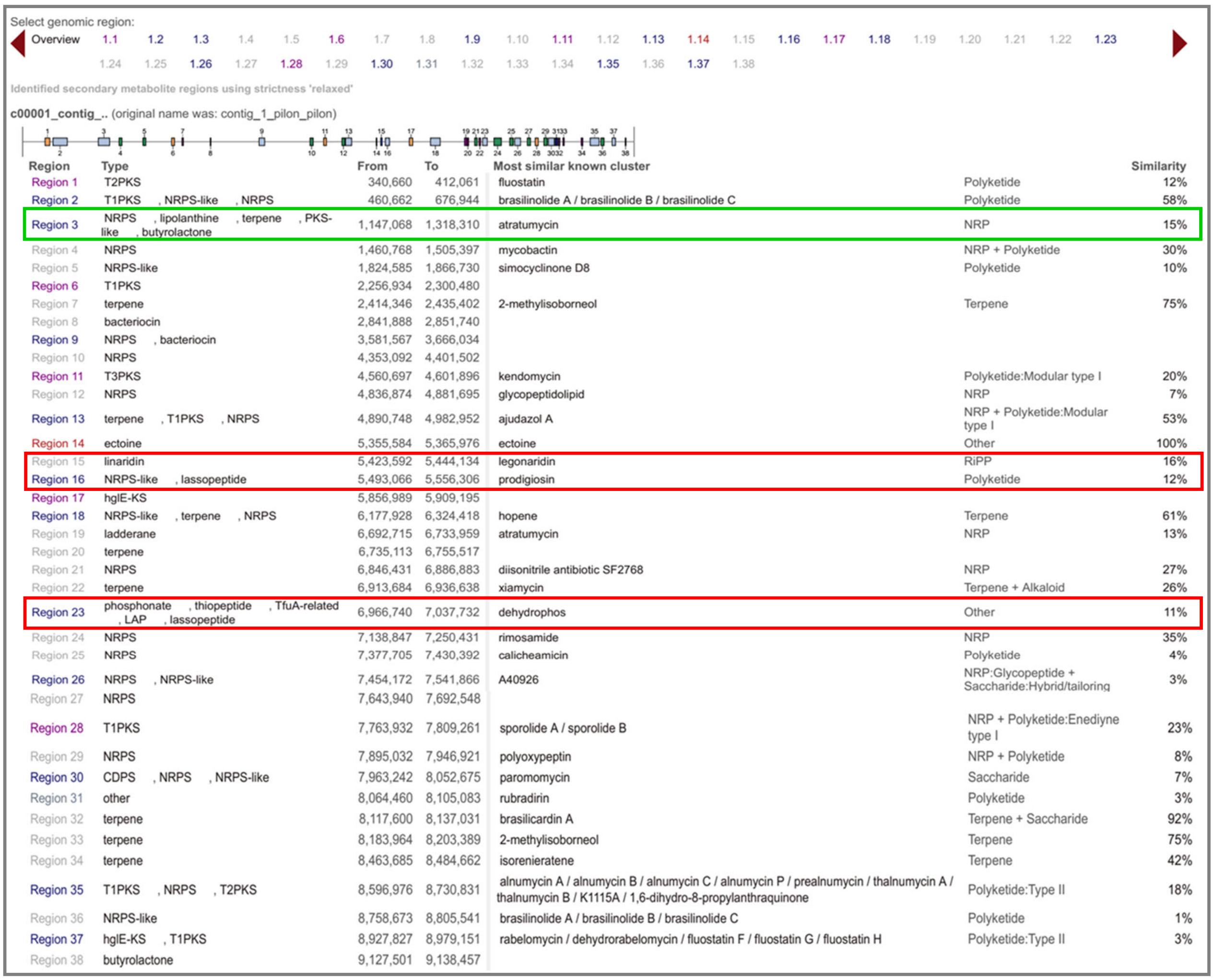

Select genomic region:
Overview 1.1 1.2 1.3 1.4 1.5 1.6 1.7 1.8 1.9 1.10 1.11 1.12 1.13 1.14 1.15 1.16 1.17 1.18 1.19 1.20 1.21 1.22 1.23
1.24 1.25 1.26 1.27 1.28 1.29 1.30 1.31 1.32 1.33 1.34 1.35 1.36 1.37 1.38

Identified secondary metabolite regions using strictness 'relaxed'

c00001_contig_.. (original name was: contig_1_pilon_pilon)

Region	Type	From	To	Most similar known cluster		Similarity
Region 1	T2PKS	340,660	412,061	fluostatin	Polyketide	12%
Region 2	T1PKS, NRPS-like, NRPS	460,662	676,944	brasilinolide A / brasilinolide B / brasilinolide C	Polyketide	58%
Region 3	NRPS, lipolanthine, terpene, PKS-like, butyrolactone	1,147,068	1,318,310	atratumycin	NRP	15%
Region 4	NRPS	1,460,768	1,505,397	mycobactin	NRP + Polyketide	30%
Region 5	NRPS-like	1,824,585	1,866,730	simocyclinone D8	Polyketide	10%
Region 6	T1PKS	2,256,934	2,300,480			
Region 7	terpene	2,414,346	2,435,402	2-methylisoborneol	Terpene	75%
Region 8	bacteriocin	2,841,888	2,851,740			
Region 9	NRPS, bacteriocin	3,581,567	3,666,034			
Region 10	NRPS	4,353,092	4,401,502			
Region 11	T3PKS	4,560,697	4,601,896	kendomycin	Polyketide:Modular type I	20%
Region 12	NRPS	4,836,874	4,881,695	glycopeptidolipid	NRP	7%
Region 13	terpene, T1PKS, NRPS	4,890,748	4,982,952	ajudazol A	NRP + Polyketide:Modular type I	53%
Region 14	ectoine	5,355,584	5,365,976	ectoine	Other	100%
Region 15	linaridin	5,423,592	5,444,134	legonaridin	RiPP	16%
Region 16	NRPS-like, lassopeptide	5,493,066	5,556,306	prodigiosin	Polyketide	12%
Region 17	hglE-KS	5,856,989	5,909,195			
Region 18	NRPS-like, terpene, NRPS	6,177,928	6,324,418	hopene	Terpene	61%
Region 19	ladderane	6,692,715	6,733,959	atratumycin	NRP	13%
Region 20	terpene	6,735,113	6,755,517			
Region 21	NRPS	6,846,431	6,886,883	diisonitrile antibiotic SF2768	NRP	27%
Region 22	terpene	6,913,684	6,936,638	xiamycin	Terpene + Alkaloid	26%
Region 23	phosphonate, thiopeptide, TfuA-related, LAP, lassopeptide	6,966,740	7,037,732	dehydrophos	Other	11%
Region 24	NRPS	7,138,847	7,250,431	rimosamide	NRP	35%
Region 25	NRPS	7,377,705	7,430,392	calicheamicin	Polyketide	4%
Region 26	NRPS, NRPS-like	7,454,172	7,541,866	A40926	NRP:Glycopeptide + Saccharide:Hybrid/tailoring	3%
Region 27	NRPS	7,643,940	7,692,548			
Region 28	T1PKS	7,763,932	7,809,261	sporolide A / sporolide B	NRP + Polyketide:Enediyne type I	23%
Region 29	NRPS	7,895,032	7,946,921	polyoxypeptin	NRP + Polyketide	8%
Region 30	CDPS, NRPS, NRPS-like	7,963,242	8,052,675	paromomycin	Saccharide	7%
Region 31	other	8,064,460	8,105,083	rubradirin	Polyketide	3%
Region 32	terpene	8,117,600	8,137,031	brasilicardin A	Terpene + Saccharide	92%
Region 33	terpene	8,183,964	8,203,389	2-methylisoborneol	Terpene	75%
Region 34	terpene	8,463,685	8,484,662	isorenieratene	Terpene	42%
Region 35	T1PKS, NRPS, T2PKS	8,596,976	8,730,831	alnumycin A / alnumycin B / alnumycin C / alnumycin P / prealnumycin / thalnumycin A / thalnumycin B / K1115A / 1,6-dihydro-8-propylanthraquinone	Polyketide:Type II	18%
Region 36	NRPS-like	8,758,673	8,805,541	brasilinolide A / brasilinolide B / brasilinolide C	Polyketide	1%
Region 37	hglE-KS, T1PKS	8,927,827	8,979,151	rabelomycin / dehydrorabelomycin / fluostatin F / fluostatin G / fluostatin H	Polyketide:Type II	3%
Region 38	butyrolactone	9,127,501	9,138,457			

Figure 29. Secondary metabolite BGCs within the genome of *N. terpenica* IFM 0406 identified by antiSMASH 5.1.2; The boxes highlight BGCs coding for four different unknown RiPPs (Red) and the known lipolanthine nocavionin (Green).

2.1 Genome-Guided Discovery of Nocathioamides From *Nocardia terpenica* IFM 0406

A putative lanthipeptide BGC (*nta*) was prioritized and annotated, showing a unique combination of post-translational enzymes that have not been observed so far for any lanthipeptides. Based on this finding and taking into account the unprecedented peptide sequence of the core peptide, it was intended to deorphanize the cognate product(s) of the *nta* BGC.

2.2 Genome-Driven Discovery of Nocapeptins From *N. terpenica* IFM 0406 and Longipeptins From *Longimycelium tulufanense* CGMCC 4.5737

Adjacent to the *nta* BGC, a further prioritized RiPP locus belonging to class II lasso peptides was detected in the genome of *N. terpenica* and termed *nop* BGC. The in silico annotation of its biosynthetic genes depicted a putative unknown architecture with possible oxidative tailoring. The homology-based query using NCBI BlastP uncovered analogous BGCs assembling similar unknown entities of lasso peptides exemplified by the *lop* BGC in *L. tulufanense*.

Armed with the predicted scaffolds, this project aimed at deciphering the *nop* and *lop* products from *N. terpenica* and *L. tulufanense*, respectively.

3. Materials and Methods

3.1 Catalog of The Chemicals and Stationary Phases

Table 3: List of solvents, chemicals and stationary phases used in the study

Category	Chemical	Manufacturer
HPLC solvents	Methanol (MeOH)	Sigma-Aldrich
	Acetonitrile (ACN)	Sigma-Aldrich
	Formic acid (HCO_2H)	Sigma-Aldrich
	Trifluoroacetic acid (TFA)	Sigma-Aldrich
Extraction solvents	*n*-Butanol (*n*-BuOH)	Fischer Scientific
MS solvents	MeOH	Sigma-Aldrich
	Acetonitrile	Sigma-Aldrich
NMR solvents	d_4-CH_3OH	Sigma-Aldrich
	d_3-CH_3OH	Sigma-Aldrich
	d_6-DMSO (Dimethylsulfoxide)	Sigma-Aldrich
Labeled substrates	$(^{15}NH_4)_2SO_4$, 98%	Sigma-Aldrich
	[$^2H_{10}$] L-leucine, 97-98%	Cambridge Isotope Laboratories
	[$^2H_7$] L-proline, 97-98%	Cambridge Isotope Laboratories
	[$^2H_4$] L-alanine, 97-98%	Cambridge Isotope Laboratories
	[$^2H_3$] L-cysteine, 97-98%	Cambridge Isotope Laboratories
	[$^2H_2$] L-glycine, 97-98%	Cambridge Isotope Laboratories
	[$^2H_7$] L-tyrosine, 97-98%	Cambridge Isotope Laboratories
	[$^2H_8$] L-tryptophan, 97-98%	Cambridge Isotope Laboratories
Stationary phases	Polygoprep 50-60, Reversed-Phase (RP) C18 silica gel	Macherey-Nagel
	Sephadex LH-20	GE Healthcare

3.2 Media Recipes for Bacterial Cultivation

The following set of media were prepared using milliQ-H_2O, where the pH value was adjusted with 1 M HCl / 1 M NaOH to be 7.0 ± 0.2. Media were sterilized at 121 °C for 20 min and the salts solutions via sterile-filtered prior usage.

Table 4: List of media used in OSMAC studies

Medium	Ingredients	Amount (g/l)	Supplier
Brain heart infusion (BHI)[153]	Agar (for agar plates)	20	Sigma-Aldrich
	BHI broth	37	Sigma-Aldrich
Ikeda's seed medium[154]	Soluble starch	10	Roth
	Glucose	5	Sigma-Aldrich
	NZ-case	3	Sigma-Aldrich

	Yeast extract	2	DB
	Tryptone	5	DB
	K_2HPO_4	1	Sigma-Aldrich
	$MgSO_4•7H_2O$	0.5	Sigma-Aldrich
	$CaCO_3$	3	ChemSolute
Ikeda's production medium[154]	Glucose	5	Sigma-Aldrich
	Glycerol	20	Roth
	Soluble starch	20	Roth
	Pharma media	15	
	Yeast extract	3	DB
Czapek-Dox medium	Saccharose	30	Difco
	Sodium nitrate	3	Difco
	Dipotassium phosphate	1	Difco
	Magnesium sulfate	0.5	Difco
	Potassium chloride	0.5	Difco
	Ferrous sulfate	0.01	Difco
Peptidolipins medium[155]	Soluble starch	20	Roth
	Glucose	10	Sigma-Aldrich
	Peptone	5	DB
	Yeast extract	5	DB
	$CaCO_3$	5	ChemSolute
PC-766B medium[156]	Glycerol	50	Roth
	Soybean flour	30	Sigma-Aldrich
	$CaCO_3$	4	ChemSolute
Caniferolides medium[157]	Glucose	50	Sigma-Aldrich
	Soluble starch	12	Roth
	Soybean flour	30	Sigma-Aldrich
	$CoCl_2•6H_2O$	0.002	Fluka
	$CaCO_3$	7	ChemSolute
Brasilinolides medium[148b,149a]	Glycerol	20	Roth
	Polypepton	10	DB
	Meat extract	5	Sigma-Aldrich
Nocavionin medium[152]	Peptone	10	DB
	Yeast extract	5	DB
	Glucose	1	Sigma-Aldrich
	4-Morpholinopropanesulfonic acid (MOPS)	150 mmol	Sigma-Aldrich
GYM medium	Glucose	4	Sigma-Aldrich
	Yeast extract	4	DB
	Malt extract	10	DB

ISP2 medium	Yeast extract	4	DB
	Malt extract	10	Oxoid
	Dextrose	4	Sigma-Aldrich
ISP4 medium	Soluble starch	10	Roth
	$(NH_4)_2SO_4$	1	Merck
	$CaCO_3$	1	ChemSolute
	$FeSO_4$•$7H_2O$	1	Sigma-Aldrich
	$MgSO_4$•$7H_2O$	2	Sigma-Aldrich
	K_2HPO_4	2	Sigma-Aldrich
	NaCl	0.001	Sigma-Aldrich
	$ZnSO_4$•$7H_2O$	0.001	MP
	$MnCl_2$•$2H_2O$	0.001	Roth
ISP5 medium	L-asparagin	1	Sigma-Aldrich
	K_2HPO_4	1	Sigma-Aldrich
	$FeSO_4$•$7H_2O$	0.001	Sigma-Aldrich
	$MnCl_2$•$4H_2O$	0.001	Sigma-Aldrich
	$ZnSO_4$•$7H_2O$	0.001	MP
	Glycerol	10	Roth
AGS	Arginine HCl	1	Sigma-Aldrich
	Glycerol	12.5	Roth
	K_2HPO_4	1	Sigma-Aldrich
	NaCl	1	Sigma-Aldrich
	$MgSO_4$•$7H_2O$	0.5	Sigma-Aldrich
	$Fe_2(SO_4)_3$•$7H_2O$	0.01	Sigma-Aldrich
	$CuSO_4$•$5H_2O$	0.001	Sigma-Aldrich
	$MnSO_4$•H_2O	0.001	Sigma-Aldrich
	$ZnSO_4$•$7H_2O$	0.001	MP
Modified R4 medium	Glucose	5	Sigma-Aldrich
	Yeast extract	1	DB
	$MgCl_2$•$6H_2O$	5	Sigma-Aldrich
	$CaCl_2$•$2H_2O$	2	Roth
	K_2SO_4	1	Sigma-Aldrich
	Casminoacid	0.5	MP
	L-proline	0.7	Sigma-Aldrich
	L-valine	1.18	Sigma-Aldrich
	TES (N-Tris(hydroxymethyl)methyl-2-aminoethanesulfonic acid)	2.8	Roth
	Trace elements solution	1	-----------
Trace elements solution	$ZnCl_2$	0.04	MP
	$FeCl_3$•$6H_2O$	0.02	Sigma-Aldrich
	$CuCl_2$•$2H_2O$	0.01	Sigma-Aldrich

	$MnCl_2 \cdot 4H_2O$	0.01	Roth
	$Na_2B_4O_7 \cdot 10H_2O$	0.01	Merck
	$(NH_4)_6Mo_7O_{24} \cdot 4H_2O$	0.01	Sigma-Aldrich

3.3 Bacterial Strains

Nocardia terpenica IFM 0406 was attained from the Medical Mycology Research Center (MMRC) culture collection, Chiba University, Chiba, Japan, while *N. terpenica* IFM 0706 (DSM 44935) and *Longimycelium tulufanense* (DSM 46696) were purchased from the DSMZ (German collection of microorganisms and cell cultures).

Table 5: List of the bacterial and fungal isolates used in the current studies

Strain	Genotype	Source
For secondary metabolites investigation		
N. terpenica IFM 0406	wild type	Medical Mycology Research Center (MMRC) culture collection, Chiba University, Chiba, Japan
N. terpenica IFM 0706	wild type	DSMZ (German collection of microorganisms and cell cultures)
Longimycelium tulufanense	wild type	DSMZ (German collection of microorganisms and cell cultures)
For antibacterial assay		
Enterococcus faecium BM4147-1	wild type	Group of Brötz-Oesterhelt, IMIT, University of Tübingen
Staphylococcus aureus ATCC 29213	wild type	Group of Brötz-Oesterhelt, IMIT, University of Tübingen
Klebsiella pneumoniae ATCC 12657	wild type	Group of Brötz-Oesterhelt, IMIT, University of Tübingen
Acinetobacter baumannii 09987	wild type	Group of Brötz-Oesterhelt, IMIT, University of Tübingen
Pseudomonas aeruginosa ATCC 27853	wild type	Group of Brötz-Oesterhelt, IMIT, University of Tübingen
Enterobacter aerogenes ATCC 13048	wild type	Group of Brötz-Oesterhelt, IMIT, University of Tübingen
Escherichia coli ATCC 25922	wild type	Group of Brötz-Oesterhelt, IMIT, University of Tübingen
Bacillus subtilis 168	wild type	Group of Brötz-Oesterhelt, IMIT, University of Tübingen
Staphylococcus aureus NCTC 8325	wild type	Group of Brötz-Oesterhelt, IMIT, University of Tübingen
Mycobacterium smegmatis mc2 155	wild type	Group of Brötz-Oesterhelt, IMIT, University of Tübingen
For antifungal assay		
Candida albicans TüC01	wild type	Prof. Silke Peter, UKT, University of Tübingen
Candida albicans TüC02	wild type	Prof. Silke Peter, UKT, University of Tübingen
Candida albicans TüC03	wild type	Prof. Silke Peter, UKT, University of Tübingen
Candida glabrata TüC04	wild type	Prof. Silke Peter, UKT, University of Tübingen
Candida tropicalis TüC05	wild type	Prof. Silke Peter, UKT, University of Tübingen

3.4 Culture Conditions of The OSMAC Approach and The Extraction Procedures

Over Brain Heart Infusion (BHI) broth agar plates, *N. terpenica* IFM 0406, 0706 were revived by their incubation at 37 °C for three days monitored by their colonies growth. Triplicates of seed cultures, BHI broth (80 ml) in 250 ml baffled Erlenmeyer flasks containing metal coils, were inoculated with fresh spores of IFM 0406 and grown under 37 °C with 150 rpm for four days using an orbital shaker.

0.4 ml of the BHI preculture was added into 100 ml of the production media in a 300 ml Erlenmeyer baffled flask shaken with 150 rpm at 37 °C for 6-7 days in triplicate format.

The cell-free supernatants, prepared by centrifugation, were extracted twice with 80 ml of *n*-BuOH. The organic layers were dried *in vacuo* affording n-Bu extracts, which were dissolved in MeOH and prepared for the subsequent analytical procedures, including either HPLC profiling and/or mass spectrometry (MS).

3.5 HPLC Profiling and Liquid Chromatography/High-resolution Electron Spray Ionization Mass Spectrometry (LC/HRESI-MSMS)

HPLC profiles of OSMAC trials were generated via a system consisting of a Waters 1525 Binary Pump with a 7725i Rheodyne injection port, a Kromega Solvent Degasser, a Waters 2998 Photodiode Array Detector, connected with a Luna Omega polar C18 column (5 µm, 250 × 4.6 mm, Phenomenex). ACN (solvent A) and H_2O + 0.1% TFA (solvent B) were used for the gradual elution of the analytes with a steady flow rate of 0.5 ml/min and an injection volume of 7 µl as follow:

Table 6: HPLC gradient used for universal profiling

Time (min)	Flow (ml/min)	A	B
0	0.50	10	90
3	0.50	10	90
10	0.50	30	70
20	0.50	35	65
32	0.50	50	50
42	0.50	100	0
50	0.50	100	0
57	0.50	10	90
60	0.50	10	90

Liquid Chromatography/High-resolution Electron Spray Ionization Mass Spectrometry (LC/HRESI-MSMS) measurements were carried out using a system consisting of an Ultimate 3000 HPLC (Thermo Fisher Scientific) united with MaXis-4G instrument (Bruker Daltonics, Bremen, Germany). The adopted HPLC-method was (0.1% FA in H_2O as solvent A and either MeOH or ACN as solvent B), a gradient of 10% B to 100% B in 40 min holding an isocratic elution of 100% B for an additional 15 min, with a flow rate of 0.3 ml/min, 5 µl injection volume and UV detector (UV/VIS) wavelength monitoring at 210, 254, 280 and 360 nm.

The separation was achieved on a Phenomenex Luna Omega polar C18 (3 µm, 150 x 3 mm) column with MS acquisition range of *m/z* 50-1800. A capillary voltage of 4500 V, nebulizer gas pressure (nitrogen) of 2 (1.6) bar, ion source temperature of 200 °C, the dry gas flow of 9 l/min source temperature, and spectral rates of 3 Hz for MS^1 and 10 Hz for MS^2 were recruited. To trigger MS/MS fragmentation in a data-dependent manner (DDA), the 10 most intense ions per MS1 were prioritized for collision-induced dissociation (CID) with the recommended stepped CID energies.[158]

3.6 Isotopic Labeling Experiments

As formerly described, 49.5 ml of the modified R4 production medium, in triplicates, were inoculated with 0.5 ml of the grown BHI seed culture, in a 250 ml Erlenmeyer baffled flask at 37 °C with 150 rpm for 5-6 days with a final concentration of 2-3 mM of the supplemented labeled amino acids. After 5-6 days, the supernatants were freed from cells by centrifugation and extracted twice with 50 ml of n-BuOH. The organic phases were combined, dried *in vacuo*, dissolved in MeOH and submitted to LC/HRESI-MSMS.

3.7 Large Scale Fermentation, Extraction Scheme, and Vaccum Liquid Chromatography (VLC)

Counting on the OSMAC-MS readings, *Nocardia terpenica* IFM 0406 was cultivated considering Ikeda's *et al*. recipe and Chen's *et al*. culturing parameters up to twenty-two liters for nocathioamides.[154,159] For nocapeptins production, twenty liters of modified R4 nutrients were prepared as a production medium employing the same cultivation parameters of nocathioamides.

Upon large scale cultivations, cultures were centrifuged twice in a Thermo Scientific Heraeus Multifuge 4KR centrifuge at 4000 g at 4 °C for 30 min to discard the cells. Subsequently, the butanol extracts of cell-free supernatants were attained by the twice extraction using n-BuOH (1:1). The evaporation under reduced pressure afforded the crude extracts (Bu SN extracts), which were dissolved in methanol followed by centrifugation to eliminate debris before the LC/MS analysis, HPLC profilings, and VLC. Fractionation of the Bu SN extracts was accomplished using a VLC system operated with a controllable vacuum pump running a stepwise elution of solvents mixture consisting of H_2O and methanol (MeOH) with a decreased polarity gradient, shifting from 100% H_2O to pure methanol in ten fractions (750 ml per each) (Figure A17 Left).

3.8 (Sub)Fractionation, HPLC Isolation, and Purification

In the case of nocathioamides, the prioritized VLC fraction (70% MeOH VLC) was redissolved in a mixture of MeOH:H_2O (40:60) to be further sub-fractionated over a Sephadex LH-20 open column. With a gradual elution starting with 100% H_2O and ending with 100% MeOH, eight subfractions were delivered where subfractions A, and B were tracked down in terms of isolation and purification (Figure A17 Right).

Aided with a polar gradient for 23 minutes using the formerly described HPLC setup equipped with a Phenomenex Kinetex EVO C18 column (5 µm, 4.6 × 250 mm); 1 ml/min flow rate, and UV monitoring at 211, 250 and 280 nm, nocathioamides A and B were isolated. An additional round of purification was completed with a shorter run time, which resulted in pure nocathioamide A (**1**) (25 mg) and nocathioamide B (**2**) (12 mg) (Figures A18 and A19).

Table 7: HPLC gradients used for nocathioamides isolation and purification

Time (min)	Flow (ml/min)	A	B
Isolation			
0	1	20	80
3	1	20	80
8	1	25	75
15	1	25	75
18	1	30	70
20	1	20	80
23	1	20	80

Time (min)	Flow (ml/min)	A	B
Purification			
0	1	23	77
2	1	23	77
3	1	24	76
5	1	24	76
9	1	25	75
10	1	23	77
11	1	23	77

Regrading nocapeptin A (**5**), the nominated VLC fraction (60% MeOH VLC) directly proceeded into HPLC isolation and purification without any further subfractionation steps.

Integrating a Phenomenex Kinetex PFP column (5 µm, 4.6 × 250 mm) to the previously defined HPLC system running with 1 ml/min flow rate, and UV monitoring at 211, 250 and 280 nm, with a polar gradient for 28 minutes enabled the isolation of pure lasso peptide (17 mg) (Figure A60).

Table 8: HPLC gradient used for nocapeptin A (**5**) isolation

Time (min)	Flow (ml/min)	A	B
0	1	10	90
5	1	20	80
8	1	25	75
20	1	30	70
21	1	100	0
25	1	100	0
26	1	10	90
28	1	10	90

3.9 NMR Spectroscopy

1D and 2D NMR spectra were measured on a Bruker Avance III HD spectrometer (400, 100 and 40.6 MHz for ^{1}H, ^{13}C and ^{15}N NMR, respectively) at 297 K using a 5 mm SMART probe head. The NMR spectra were collected in d_4-CH_3OH, d_3-CH_3OH in addition to d_6-DMSO and processed with TopSpin 3.5 besides MestReNova 12.0.4. Before the analysis, spectra were calibrated to the corresponding residual solvent signals ($\delta_{H/C}$ 3.31/49.15 => d_4-CH_3OH, d_3-CH_3OH & $\delta_{H/C}$ 2.50/39.51=> d_6-DMSO). Mixing times were 80 ms for TOCSY and 300 ms for NOESY experiments. Band-Selective constant time HMBC spectra were recorded to dissect the peptide carbonyl region.

Further d_3-CH_3OH datasets were attained from Bruker Avance III HDX spectrometer (700, 176 and 71 MHz for ^{1}H, ^{13}C and ^{15}N NMR, respectively) equipped with a 5 mm Prodigy TCI CryoProbe head. Mixing times were 80 ms for TOCSY and 300, 500 ms for NOESY spectra. For both spectrometers, ^{15}N unreferenced chemical shifts were reported in ppm (spectrometer default values).

3.10 Infrared (IR) Spectroscopy

IR spectrometry was performed with a Jasco FT/IR-4200 series spectrometer, comprising a ZnSe optical window and processed with the software Spectra Manager 2.10.01.

3.11 Ultraviolet/Visible (UV/VIS) Spectroscopy

UV measurements were performed on a Perkin-Elmer 25 UV/VIS spectrometer, using 1 cm quartz cells and dissolving samples either in ddH_2O or LCMS-grade MeOH. UV scans were recorded over the range from 780 to 190 nm.

3.12 MS-Based Molecular Networking

Mass spectral data were analyzed using Compass Data Analysis 4.4 (Bruker Daltonik), while MetaboScape 3.0 (Bruker Daltonik) was consulted for molecular features selection. Raw data files were imported into MetaboScape 3.0 for the entire data treatment and pre-processing in which T-ReX 3D (Time aligned Region Complete eXtraction) algorithm is integrated for retention time alignment with an automatic detection to decompose fragments, isotopes, and adducts intrinsic to the same compound into one single feature. All the harvested ions were categorized as a bucket table with their corresponding retention times, measured *m/z*, molecular weights, detected ions, and their intensity within the sample. The bucket table was prepared with an intensity threshold ($1e^4$) for the positive measurement with a minimum peak length 3 for the retention time range of interest from 15 to 30 min possessing a mass range *m/z* 150-1600 Da.

Metaboscape bucketing parameters were chosen as follow:

Intensity threshold [counts]	10000.0
Minimum peak length [spectra]	3
Minimum peak length (recursive) [spectra]	1
Minimum # Features for Extraction	1
Presence of features in minimum # of analyses	1
Lock mass calibration	false
Mass calibration	true
Primary Ion	$[M+H]^+$
Seed Ions	$[M+Na]^+$, $[2M+H]^+$, $[2M+Na]^+$, $[M+2H]^{2+}$, $[M+H+Na]^{2+}$
Common Ions	$[M-H_2O+H]^+$, $[M+H_2O+H]^+$, $[2M+H_2O+H]^+$, $[2M-H_2O+H]^+$
EIC correlation	0.8
Mass range: Start [*m/z*]	150.0
Mass range: End [*m/z*]	1600.0
Retention time range: Start [min]	15.0
Retention time range: End [min]	30.0
Perform MS/MS import	true
Group by collision energy	true
MS/MS import method	average

The features list of the pre-processed retention time range was exported from MetaboScape as a single MGF file which was in turn uploaded to the GNPS online platform where Feature-Based Molecular Network (FBMN) was created. The precursor ion mass tolerance was set to 0.03 Da and an MS/MS fragment ion tolerance of 0.03 Da. A network was then created where edges were filtered to have a cosine score above 0.70 and more than 5 matched peaks. Further, edges between two nodes were kept in the network if and only if each of the nodes appeared in each other's respective top 10 most similar nodes. Finally, the maximum size of a molecular family was set to 100, and the lowest-scoring edges were removed from molecular families until the molecular family size was below this threshold. Cytoscape 3.5.1 was used for molecular network visualization.[160]

GNPS job URL:
https://gnps.ucsd.edu/ProteoSAFe/status.jsp?task=450f6e9825bd4accb5fe353d4e4ebe42

3.13 Bioinformatics

The usage of different bioinformatic tools *e.g.* antiSMASH 5.1[140a] and RODEO 2.0[120c] enabled the detection of the putative biosynthetic gene clusters (BGCs) of nocathioamides, nocapeptins, and longipeptins. Chiefly relying on RODEO annotation, the assignment of the possible functions of each biosynthetic gene from IFM 0406, IFM 0706, and *L. tulufanense* was conceivable.[150a,150b,161]

The exclusive integration of the RiPPMiner tool[140d] was called to assist in predicting the probable proteolytic site in nocathioamides CP whereas the RRE protein in nocathioamides BGC was deciphered by Antismash 6.0 implemented with the RRE algorithm.[162]

To corroborate the putative function of nocathioamides biosynthetic genes suggested by the automated RODEO output, a manual BlastP query was conducted against the NCBI GenBank repository. In addition, the retrieval of further homologous nocapeptins was also facilitated by a BlastP search of the nocapeptin precursor peptide in synergy with the antiSMASH algorithm.

3.14 Biological Assays

The antibacterial assays and the determination of the cytotoxicity were performed as previously described.[159] For MIC testing of *Mycobacterium smegmatis*, instead of cation adjusted Müller Hinton medium, Middlebrook 7H9 broth was used.

The minimal inhibitory concentration (MIC) of nocathioamide (**1**) and nocathioamide (**2**) against different *Candida* clinical isolates was determined by broth microdilution using the direct colony suspension method with an inoculum of 0.5-2.5 x 10^5 CFU/ml, according to the recommendations of the European Committee on Antimicrobial Susceptibility Testing (EUCAST).

Caspofungin was used as a reference antifungal agent. MIC testing was performed in sterile 96-well microdilution plates using MOPS-buffered RPMI 1640 medium supplemented with glucose to a final concentration of 2%, pH 7.0. MICs were read after incubation of the microplates at 37°C for 24-48 h.[163]

4. Results and Discussion

Within the course of our genome-driven investigations of *Nocardia* strains, we noted that the highly similar genomes of *Nocardia terpenica* IFM 0406 and 0706^{T} both contain, beside nocavionin[152], a further RiPP BGC which codes for a core ribosomal peptide co-localized with a unique combination of post-translational enzymes that have not been observed for lanthipeptides.

Here, we report a genome-guided identification, isolation and characterization of three structurally novel RiPPs, designated as nocathioamides A-C, from these strains, which represent the first members of a new class of chimeric lanthipeptides.

The upcoming results and discussion sections of nocathioamides part were taken from the published manuscript permitted by the copyrights clearance with the journal, Angewandte Chemie International Edition and publisher, Wiley-VCH GmbH.[164]

4.1 Genome Mining of The Nocathioamide Biosynthetic Gene Cluster in *N. terpenica* IFM 0406 and 0706^{T}

Mining the genomes of *N. terpenica* IFM 0406 and 0706, employing the bioinformatic tools antiSMASH 5.1 and RODEO readily revealed the presence of a putative lanthipeptide BGC.[140a,120c] The comparatively large *nta* gene cluster (17.1 kb) consists of 14 open reading frames (ORFs), annotated as *ntaA-ntaN*. The genetic set of *ntaA-ntaJ* is transcribed in one direction, while *ntaK-ntaN* is translated in the opposite orientation (Figure 30).

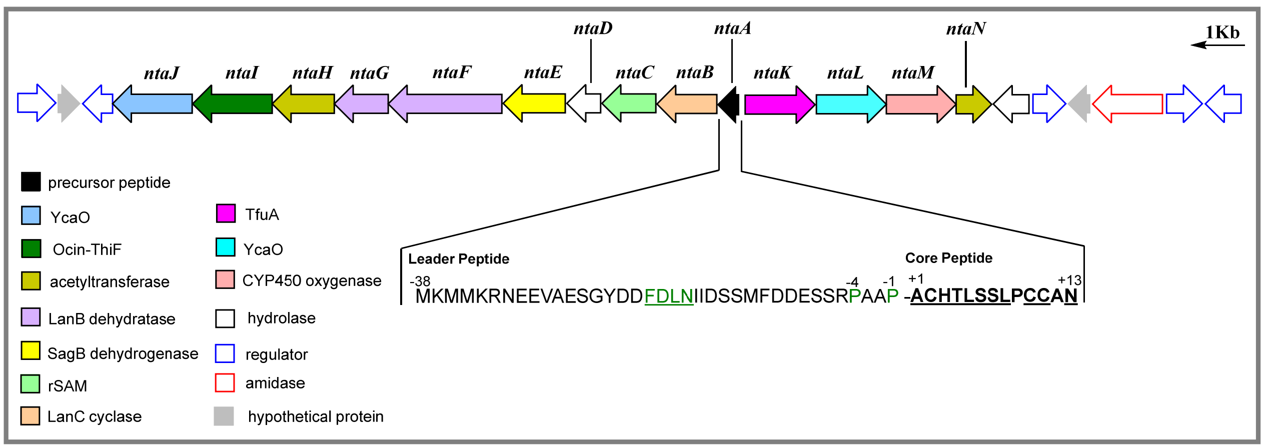

Figure 30. Biosynthetic gene cluster (BGC) coding for nocathioamides A-C

The gene *ntaA* encodes a 51-aa precursor peptide which showed no sequence similarity to any known RiPPs. The leader peptide possessed the conserved FDLN motif and towards its C-terminal end two proline residues, which typically occur in propeptides of class I lantibiotics and suggest, with P commonly located at position -2, two putative cleavage sites.[165]

To complicate matters further, NtaA contains, in addition, one characteristic tandem alanine "AA" and two "PA" cleavage sites which give rise to multiple possibilities for dividing the precursor peptide into an N-terminal leader peptide and a C-terminal core peptide.[152,166]

The application of the automated web-based tool RIPPMiner corroborated these findings and predicted the formation of a 12 or 14mer. At this stage of the study, we assumed that the cleavage site is located within the "PAAPAC" sequence (residues -4 to +2) of the NtaA precursor peptide, which culminates in 12 to 15mer.[140d]

We additionally expected that the dehydratases (NtaF, Protein family PF04738) and (NtaG, PF14028) catalyze up to three dehydrations (on Thr4, Ser6 and Ser7), enabling thereby, in conjunction with the LanC-like enzyme NtaB, the formation of up to three (methyl)lanthionine bridges (with Cys2, Cys10 and Cys11).[74a]

Moreover, the *nta* cluster contained two YcaO-encoding genes (*ntaJ* and *ntaL*) which would lead, depending on their type and partner protein, either to (methyl)azoline(s) formation or conversion of an amide(s) into a thioamide bond(s).[95d] The partner proteins were readily identified employing the RODEO algorithm[120c] (Table 9): *ntaK*/*ntaL* was predicted to code for a pair of TfuA/YcaO proteins (PF07812 / PF02624), and *ntaI*/*ntaJ* to encode the tandem Ocin-ThiF/YcaO (TIGR03693 / PF02624).

Thus, we hypothesized that at the resultant RiPP would be thioamidated by NtaK/NtaL and that at least one Ser/Thr/Cys residue is converted into a (methyl)azoline catalyzed by NtaI/NtaJ. Notably, the application of RRE-Finder implemented in antiSMASH 6.0 unveiled that the RiPP recognition element (RRE), which binds specifically to the precursor peptide (NtaA) guiding the post-translationally modifying enzymes to their substrates, is fused to the F-dependent cyclodehydratase, NtaI (Table 9).[96d,154]

Taking into account the presence of a SagB-dehydrogenase-encoding gene (*ntaE*, PF00881), it is conceivable that (methyl)azoline would be oxidized to (methyl)azole during the maturation of the RiPP.[95d] Notably, the presence of a (methyl)azole ring system reduces, in turn, the maximum number of possible (methyl)lanthionine-bridges from three to two. The analysis of the remaining ORFs of the *nta* BGC revealed genes for two GNAT-N-acetyltransferases (NtaH, PF13527 and NtaN, PF00583), a CYP450 oxygenase (NtaM, PF00067), a hydrolase (NtaD, PF01738) and a methyltransferase (NtaC, PF01135).

Consequently, we anticipated that the final peptide to be twice N-acetylated and harbors an additional hydroxyl or keto-group. Since methyltransferases catalyze a diverse spectrum of chemical reactions ranging from actual methyl transfer over epimerization to C-C crosslinking reactions, no reliable prediction can be currently performed.

In summary, the bioinformatic analysis suggested the production of a RiPP, formed by 12-15 amino acids featuring one to two (methyl)lanthionine bridges, thioamide bond(s), (methyl)azole ring(s) and possibly oxygenated and acetylated amino acid residues. Due to the unprecedented peptide sequence and the predicted modifications of the resultant peptide, we embarked on the screening for the product(s) of the *nta* BGC.

Table 9. Putative functions of proteins from the *nta* BGC based on the web-based tool RODEO and a manual BlastP search.

	Automated RODEO Analysis						Manual BlastP Analysis	
Protein	Nucleotide Accession Nr. IFM 0706[a] IFM 0406[b]	Protein Accession Nr. IFM 0706 IFM 0406	Length [aa]	PFAM hits (TIGRFam hits)	Description	E-value	Protein hits (Protein ID)	Identity/ Similarity [% / %]
Orf-1	HPY32_RS36330 AWN90_28350	NQE92403.1 KZM72695.1	231 210	PF00440	Bacterial regulatory proteins, tetR family	3.20E-17	TetR/AcrR family transcriptional regulator (WP_139175378.1) TetR/AcrR family transcriptional regulator (WP_068369163.1) TetR family transcriptional regulator (WP_162141431.1)	37/52 34/54 40/63
NtaJ	HPY32_RS36335 AWN90_28345	NQE92404.1 KZM72694.1	614 592	PF02624 (TIGR03604, TIGR03882)	YcaO cyclodehydratase, ATP-ad Mg^{2+}-binding	6.10E-73	TOMM precursor leader peptide-binding protein (WP_189056215.1) TOMM precursor leader peptide-binding protein (WP_090933850.1) TOMM precursor leader peptide-binding protein (WP_071803308.1)	48/62 42/54 37/51
NatI	HPY32_RS36340 AWN90_28340	NQE92405.1 KZM72693.1	617 630	TIGR03693	Ocin_ThiF_like: putative thiazole-containing bacteriocin maturation protein	3.30E-23	hypothetical protein (WP_189056217.1) hypothetical protein (WP_100559871.1) hypothetical protein (WP_107412486.1)	37/52 31/43 31/44
		The RRE domain, fused to NtaI, is indicated in green (AA 9-91 of NatI) MDRDHKLDLRRPVLRAGVRATPTPEGIALEGPSELRITLQGPEVRDVLVWLVSQFDGVTGANEIMGRLDED RRSLAERIIVALDRYGIIRDRARDRSHSLTAHELDCHAGEIAQIARHRESPEQRFDDFRSTPMVLIGSVHAVSP VVRLALDSGLRRLRVLVPGGMSCEPGDLARCADVRIIDAGAPGIETIRPLLAEFPVVVHVCTAHSADLLRRLD RLCWEERKYLVPAVVLGDQAWIGPVGLPGHEWTRWAAFWQRHRTTVPEQPRHSDPTLVQLELVANHLLLL WFRRITGIEQARAPDVVHLEFGELRSRKRTVAPHPHGLPRSPETSTEVAAKIGALSDAEPLIEHDFYRSIRRYI DERVGIFADIRAARTDPLPLQVAEVVVTDPLKSYRAQHVPVIVRGAGPDMLRARLDALRRACELYAYLVVDP QRLHTADGTPAFLEFMPDEWAAGRLWGMSLGTGQPCTVRAGDAFPHLVSGPTATTPVGVASGNTFCEAV ERALIDQCASHAITSAETEQSPLDLWSLELRGIGSHYRNLLRLSGETVHAVRFTHELAPPVVRLSNSTVGDLY STGRSLGEAIGHGIEQLLLHRQCQRLSPPESPCPPVGHRIGQPAPGPRTSGASTLGRRLVDRLTRRGLHPV AVTLDHDPVLSRLHPFVVRVLVLPDAAEGPGTCW						
NatH	HPY32_RS36345 AWN90_28335	NQE92406.1 KZM72692.1	424 424	PF13527 PF13530 PF17668	Acetyltransferase (GNAT) domain Sterol carrier protein domain Acetyltransferase (GNAT) domain	2.80E-23 1.10E-19 3.80E-13	GNAT family N-acetyltransferase (WP_189056219.1) GNAT family N-acetyltransferase (PZN46310.1) GNAT family N-acetyltransferase (WP_124440951.1)	55/68 43/54 42/56
NatG	HPY32_RS36350 AWN90_28330	NQE92407.1 KZM72691.1	286 286	PF14028	Lantibiotic biosynthesis dehydratase C-terminus	4.30E-30	thiopeptide-type bacteriocin biosynthesis protein (WP_189056204.1) thiopeptide-type bacteriocin biosynthesis protein (WP_131736176.1) thiopeptide-type bacteriocin biosynthesis protein (WP_099929903.1)	70/80 49/58 48/55
NtaF	HPY32_RS36355 AWN90_28325	NQE92408.1 KZM72690.1	830 796	PF04738	Lantibiotic dehydratase, N-terminus	5.30E-19	lantibiotic dehydratase (WP_189056202.1) hypothetical protein GCM10012275_19850 (GGM48992.1) lantibiotic dehydratase (WP_189056221.1)	66/76 49/59 49/59
NtaE	HPY32_RS36360 AWN90_28320	NQE92409.1 KZM72689.1	512 512	PF00881 (TIGR03605)	SagB: SagB-type dehydrogenase domain	5.00E-41	SagB family peptide dehydrogenase (WP_189056200.1) SagB-type dehydrogenase domain (KPI02545.1) SagB family peptide dehydrogenase (WP_020665156.1)	60/70 44/57 44/56
NtaD	HPY32_RS36365 AWN90_28315	NQE92410.1 KZM72688.1	193 193	PF01738 PF12697	Dienelactone hydrolase family Alpha/beta hydrolase family	2.60E-12 2.40E-07	α/β fold hydrolase (WP_189056198.1) hypothetical protein GCM10012275_19730 (GGM48884.1) dienelactone hydrolase family protein (WP_131968989.1)	72/80 72/80 48/60
NtaC	HPY32_RS36370 AWN90_28310	NQE92411.1 KZM72687.1	377 365	PF01135 (TIGR04188, TIGR04364)	Methyltransferase	3.20E-38	hypothetical protein (WP_189056196.1) methyltransferase domain-containing protein (WP_189060694.1) methyltransferase domain-containing protein (WP_102918215.1)	62/77 38/52 37/49
NtaB	HPY32_RS36375 AWN90_28305	NQE92412.1 KZM72686.1	421 414	PF05147	Lanthionine synthetase C-like protein	1.90E-51	hypothetical protein (WP_189056194.1) lanthionine synthetase C family protein (RLU79699.1) lanthionine synthetase C family protein (WP_189782898.1)	62/74 35/47 35/48
NtaA	HPY32_RS36380 not annotated	NQE92413.1 not annotated	51		---------------------	---------	hypothetical protein (WP_189056192.1)	78/86

NtaK	HPY32_RS36385 AWN90_28300	NQE92414.1 KZM72685.1	426 394	PF07812	TfuA-like protein	2.80E-32	hypothetical protein (WP_189056190.1) hypothetical protein GCM10012275_19690 (GGM48852.1) hypothetical protein (WP_063274436.1)	66/76 66/76 48/63
NtaL	HPY32_RS36390 AWN90_28295	NQE92415.1 KZM72684.1	391 391	PF02624 (TIGR00702)	YcaO cyclodehydratase, ATP-ad Mg^{2}+-binding	7.90E-58	YcaO-like family protein (WP_189056188.1) YcaO-like family protein (WP_063274437.1) hypothetical protein (MQT02134.1)	70/83 52/70 54/67
NtaM	HPY32_RS36395 AWN90_28290	NQE92416.1 KZM72683.1	394 368	PF00067	cytochrome P450	5.20E-37	cytochrome P450 (WP_189056186.1) cytochrome P450 (GGM48838.1) cytochrome P450 (WP_189060646.1)	69/78 70/79 53/65
NtaN	HPY32_RS36400 AWN90_28285	NQE92417.1 KZM73943.1	155 155	PF00583 PF13508 PF13673	Acetyltransferase (GNAT) family Acetyltransferase (GNAT) domain Acetyltransferase (GNAT) domain	2.00E-10 2.10E-07 1.30E-05	GNAT family N-acetyltransferase (WP_150404808.1) GNAT family N-acetyltransferase (WP_067538111.1) GNAT family N-acetyltransferase (WP_169813135.1)	75/84 78/83 69/83
Orf+1	HPY32_RS36405 AWN90_28280	NQE92418.1 KZM72682.1	230 230	PF13419 PF00702 PF13242	Haloacid dehalogenase-like hydrolase haloacid dehalogenase-like hydrolase HAD-hyrolase-like	2.20E-08 3.40E-08 2.80E-05	haloacid dehalogenase type II (WP_165257141.1) haloacid dehalogenase type II (WP_201875758.1) haloacid dehalogenase type II (WP_190052985.1)	83/91 81/87 81/87
Orf+2	HPY32_RS36410 AWN90_28275	NQE92419.1 KZM72681.1	190 190	PF07336 PF11706	Putative stress-induced transcription regulator CGNR zinc finger	4.70E-17 4.20E-16	ABATE domain-containing protein (WP_165257307.1) ABATE domain-containing protein (WP_042153133.1) ABATE domain-containing protein (WP_027942564.1)	90/92 88/91 85/90
Orf+3	HPY32_RS36415 AWN90_28270	Not annotated KZM72680.1	29 64	PF00248	Aldo/keto reductase family	5.60E-06	aldo/keto reductase (WP_185941606.1) aldo/keto reductase (WP_192776860.1) aldo/keto reductase (GFE07022.1)	100/100 100/100 97/100
Orf+4	HPY32_RS36420 AWN90_28265	NQE92420.1 KZM72679.1	465 465	PF01425	Amidase	6.50E-105	amidase (WP_173868031.1) amidase (WP_073766127.1) amidase (NEW71157.1)	66/74 65/72 67/76
Orf+5	HPY32_RS36425 AWN90_28260	NQE92421.1 KZM72678.1	192 192	PF16859 PF00440	Tetracyclin repressor-like, C-terminal domain Bacterial regulatory proteins, tetR family	1.70E-14 5.20E-09	TetR/AcrR family transcriptional regulator (WP_092550168.1) TetR/AcrR family transcriptional regulator (WP_188675544.1) TetR family transcriptional regulator (GGF20957.1)	58/76 57/73 57/73
Orf+6	HPY32_RS36430 AWN90_28255	NQE92422.1 KZM72677.1	284 284	PF00126 PF03466	Bacterial regulatory helix-turn-helix protein, lysR family LysR substrate binding domain	2.20E-20 9.20E-18	transcriptional regulator, LysR family (CDR16212.1) LysR family transcriptional regulator (WP_020873917.1) LysR family transcriptional regulator (WP_040020027.1)	87/91 87/91 84/90

a) The *nta* BGC of strain IFM 0706 is located on contig 5 of the genome (Accession: NZ_JABMCZ010000005.1).
b) The *nta* BGC of strain IFM 0406 is located on contig 15 of the genome (Accession: LWGR01000007.1).

Protein homology analysis found in the nocathioamide biosynthetic gene cluster (*nta* BGC) employing the web-based tool RODEO and a manual BlastP search.
The manual BlastP search was limited to records that exclude the species ´*Nocardia terpenica* (taxid:455432)´; listed are the top 1-3 hits. The protein hits, which represent the products of the *nta* BGC in the bacterium *Longimycelium tulufanense* CGMCC 4.5737 are indicated in orange.

4.2 Targeted Identification and Isolation of Nocathioamides Using a Configured Metabologenomic Approach

Counting on the bioinformatically predicted structural features and the limitation of formulating only a very broad mass range of the mature peptide, a three-layered metabolomic workflow was designed to track down the resultant RiPP using OSMAC-mass spectrometry (OSMAC-MS), stable isotope labeling and ^{1}H-^{13}C HMBC NMR (Figure 31).

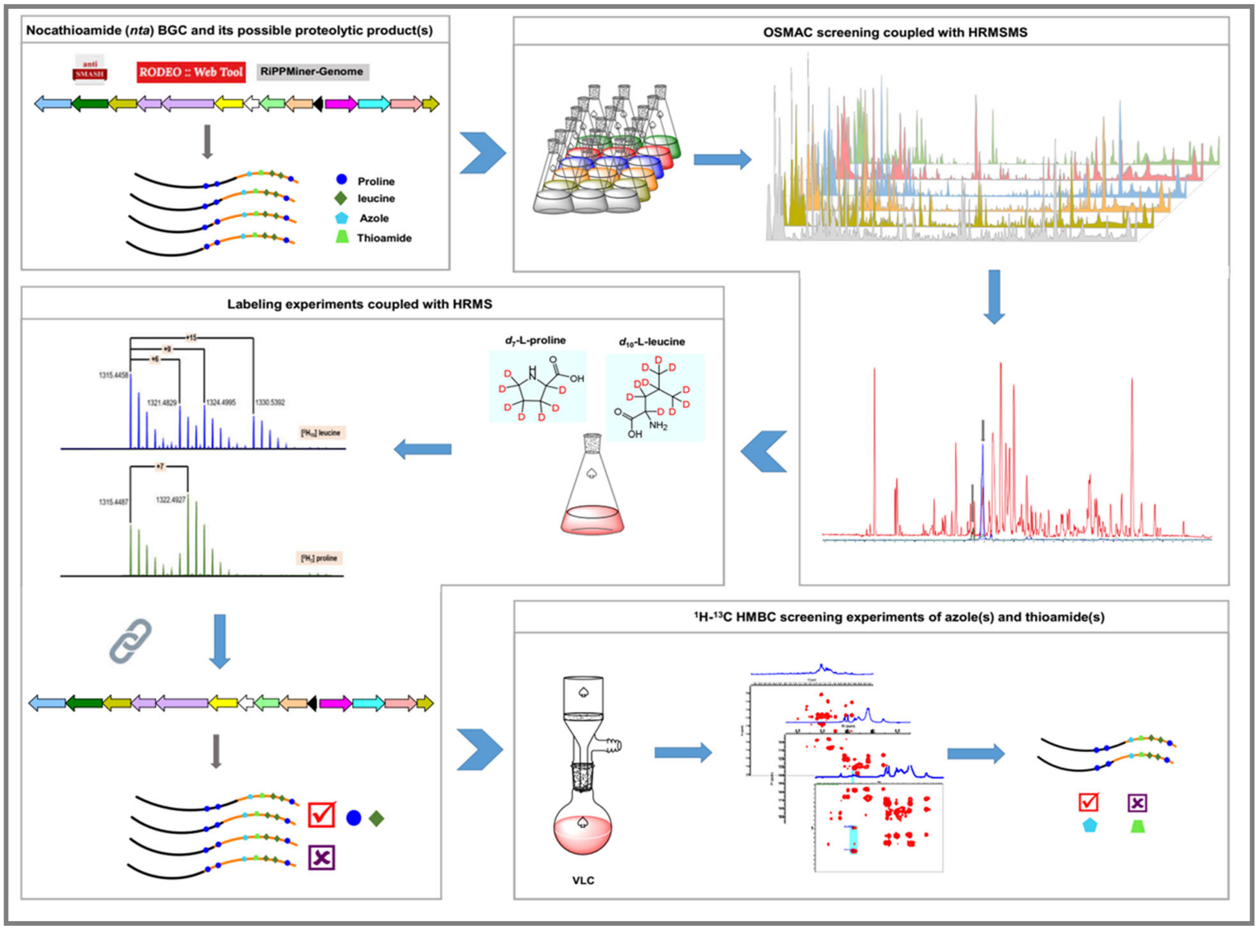

Figure 31. The adopted metabologenomic strategy for the discovery of nocathioamides

A panel of extracts, prepared under different culture conditions (30 different culture recipes, while temperature and fermentation periods were kept constant), was screened by liquid chromatography-high resolution (LC-HR)MS/MS with particular attention given to nitrogen-containing metabolites with a mass higher than 1000 Da. The pharma media-based extracts offered a reproducible candidate set of structurally related ions (*m/z* 1315, 1331 and 1347) with a peptidic nature inferred via their molecular formula predictions, the intense formation of doubly charged species and their very similar MS^2 spectra (Figures 32 and 33). Initial attempts to interpret the peptides sequence using the MS/MS technique were not successful, which were attributed by then to the processing degree of the substrates under investigation.

To corroborate the candidate compounds, three feeding experiments, employing isotopically labeled $(^{15}NH_4)_2SO_4$, [$^{2}H_{10}$] Leucine and [$^{2}H_{7}$] L- proline, respectively, were carried out on a small scale with strain IFM 0406.

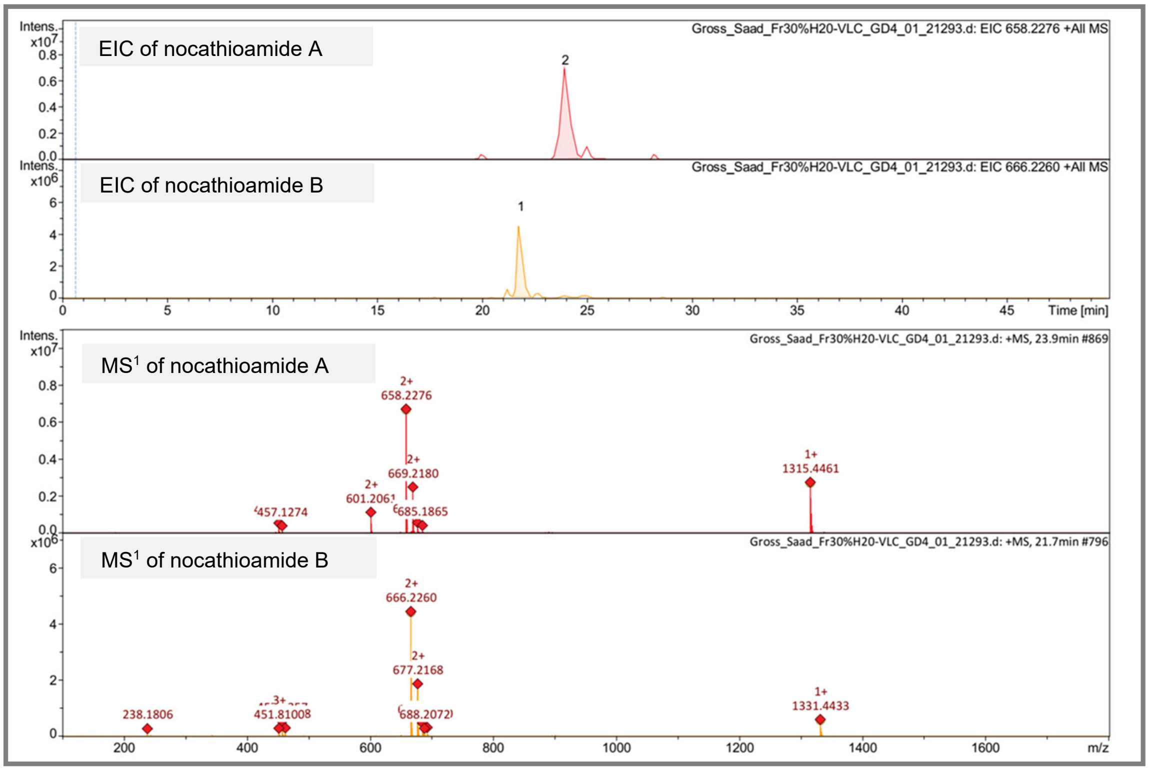

Figure 32. Extracted ion chromatograms (EICs) and MS¹ of nocathioamide A (**1**) (1315 Da $[M+H]^+$) and B (**2**) (1331 Da $[M+H]^+$)

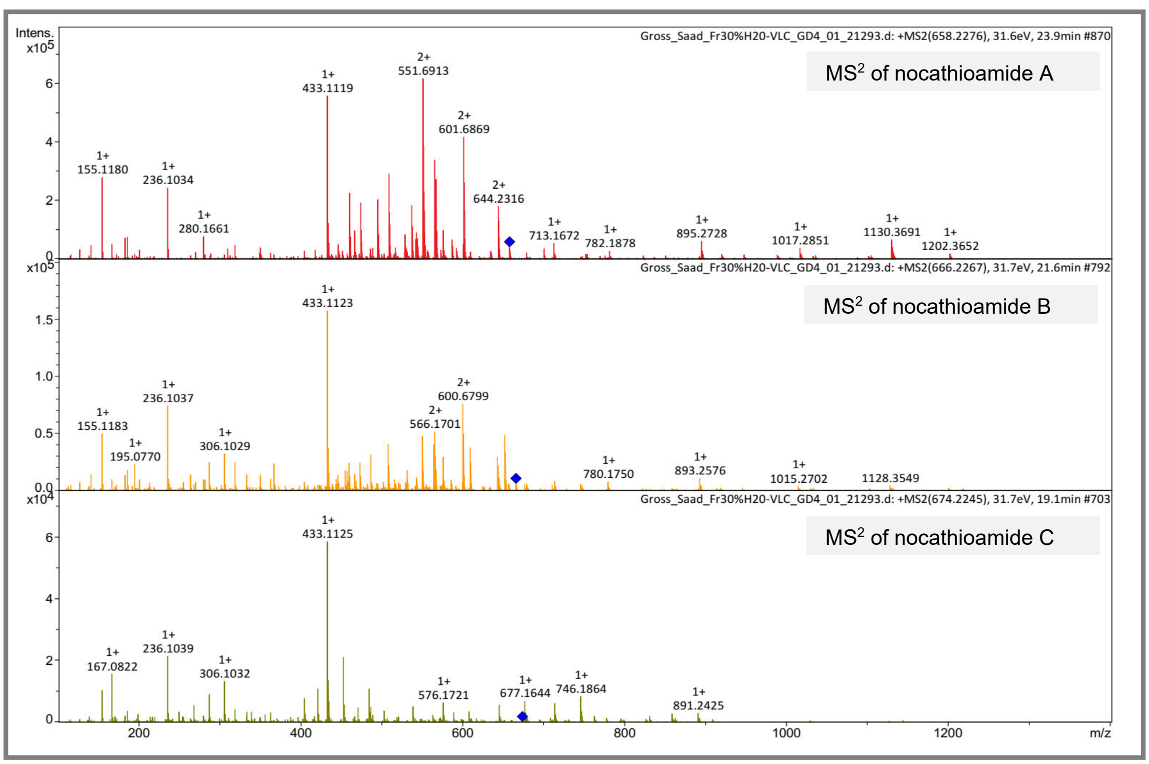

Figure 33. Comparative $[M+2H]^{2+}$ MS² of nocathioamide A, B, and C (**1**-**3**) (658, 666, and 674 Da)

As postulated, the ^{15}N-labeling experiment led to uniformly ^{15}N-labeled peptides. In agreement with our hypothesis, each of the three candidate compounds showed in their corresponding LC/MS spectra a characteristic ^{15}N-isotope-envelope pattern that pointed to the presence of 12 to 13mer (Figures 34 and 35). In order to prove that the targeted peptides are indeed the product of the *nta* gene cluster, [$^{2}H_{10}$] L-leucine was fed, which was expected to be incorporated twice and to produce a +9/10 and a +18/19/20 Da pattern.

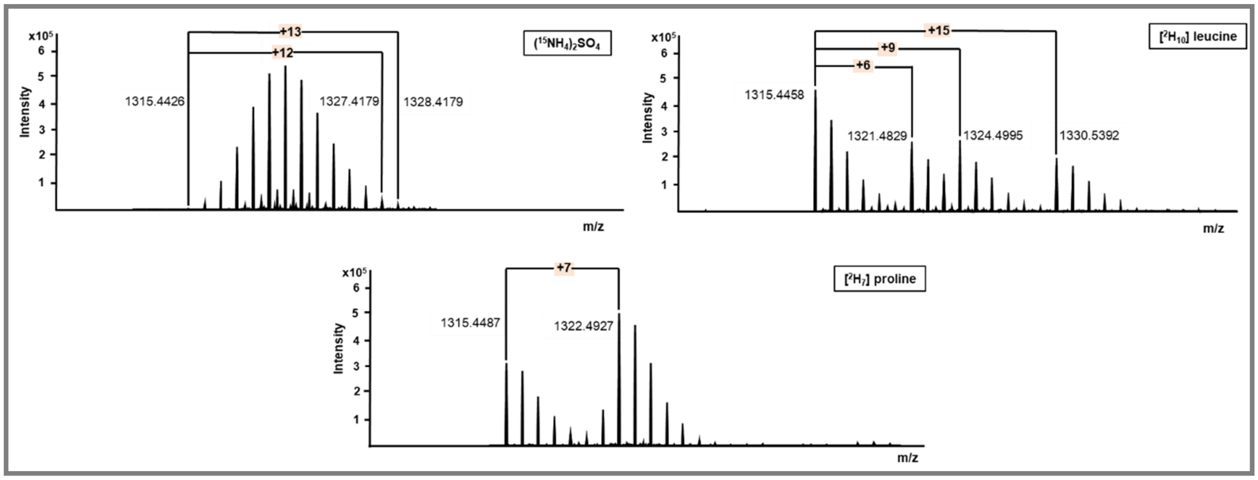

Figure 34. Labeling experiments of nocathioamide A (**1**)

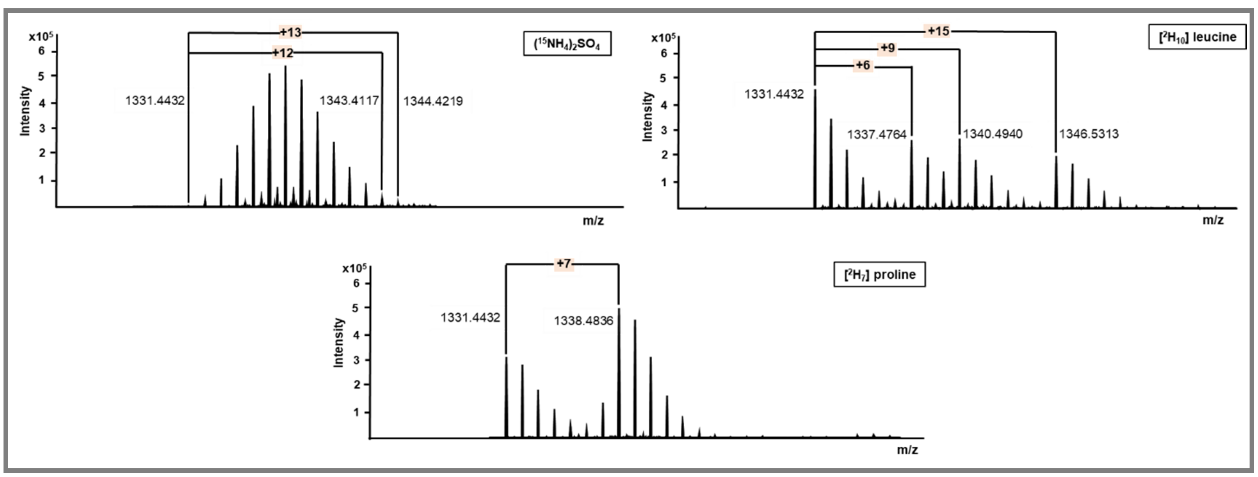

Figure 35. Labeling experiments of nocathioamide B (**2**)

Strikingly, mass shifts of +6, +9, and +15 Da were observed for all candidate compounds' pseudomolecular ions (Figures 34 and 35), which readily hinted on the crude level prior to any isolation steps that one Leu residue must have undergone an unusual modification. Within the same context and driven by the numerous predicted possible cleavage sites, the labeled substrate [$^{2}H_7$] L-proline was supplemented into IFM 0406 cultures to validate more the features in question and the probable hydrolytic site within the prepeptide. Notably, the proline experiment exhibited an extra 7 Da as a clear indication of a single encoded proline residue within the peptides under investigation (Figures 34 and 35), which on the one hand validated that we are tracking down the products of interest and on the other hand automatically shrank the cleavage position from the “PAAPAC” to the “AC” sequence (residues +1 to +2) which corroborates, in turn, the formation of a 12 to 13mer.

At this point and motivated by the suggested molecular formula which showed no fit with any known compound derived from a natural resource using SciFinder (Figures A13-A15), IFM 0406 was fermented on a large scale (22 L). Upon C18-vacuum liquid chromatography (RP-VLC), we took advantage of the in silico predicted rare thioamide and common (methyl)azole moieties, which produce distinctive downfield resonances in NMR spectra (Figure 31).

Guided by LC-MS of RP-VLC fractions, a series of ^{1}H-^{13}C HMBC NMR experiments were complementarily executed on the (sub)fractions exhibiting masses > *m/z* 1300. Cross correlations, typical for oxazole and/or thiazole entities ($\delta_{H/C}$ 8.18/148.32 and $\delta_{H/C}$ 8.18 /174.91) were exclusively observed in the VLC-fraction, eluting with 70% MeOH which was, beside the known secondary metabolite brasilicardin A, mainly enriched with the unknown peptides in pursuit (Figure 36).

In contrast, pronounced downfield ^{1}H-^{13}C HMBC cross-peaks (δ_C > 200 ppm) were not detectable at all in any fractions, thusly crippling the envisioned thioamide-based NMR screening scheme. However, upon further purification and having this molecular family in hand, the thioamide motif was found to reveal weaker resonances under the applied standard NMR conditions. Using Sephadex LH-20 column chromatography, and followed by sequential rounds of RP-HPLC (Figures A17-A19), pure nocathioamides A (**1**), B (**2**) and traces of C (**3**) were obtained.

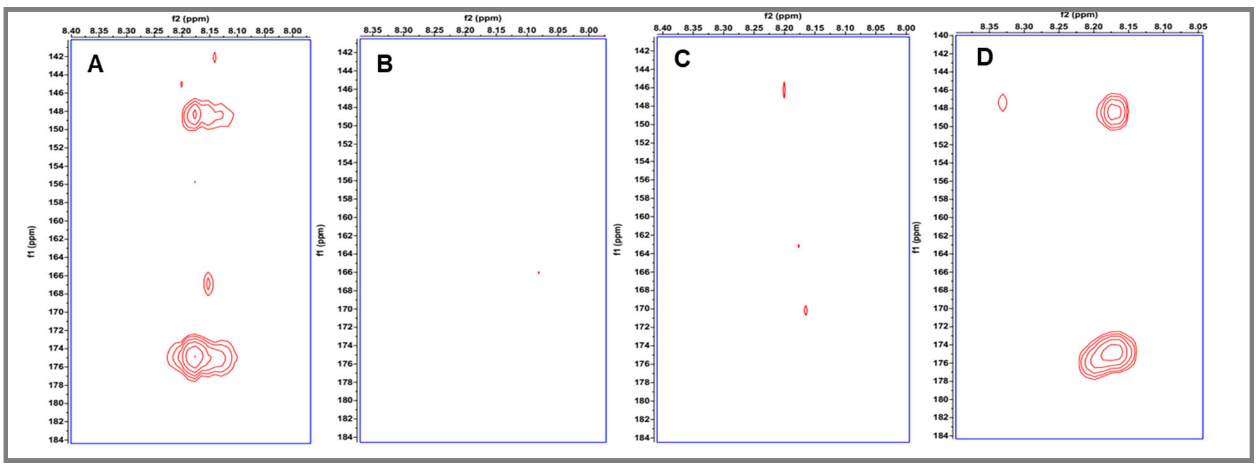

Figure 36. ^{1}H-^{13}C HMBC spectra of fractions 70% (panel A), 80% (panel B), 90% (panel C), and B LH20_70% (panel D) MeOH (d_4-CH_3OH, 400 MHz)

4.3 Structure Elucidation of Nocathioamides A-C

In combination with extensive NMR analyses, the suggested elemental compositions of nocathioamide A (**1**) possessing *m/z* 1315 $[M+H]^+$ and 658 $[M+2H]^{2+}$ was expected to be $C_{54}H_{74}N_{16}O_{15}S_4$ with 26 degrees of unsaturation (RDB) with no matched hits to any known naturally occurring compound from any natural resource.

Expectedly, ^{13}C-NMR spectra in the differently used solvents (d_4-, d_3-CH_3OH) exhibited a greater number of signals due to the inseparable minor conformer(s), which were also observed in the LC/MS (Figure 32) and HPLC (Figure A19) profiles. Additionally, careful inspection of the 1D and 2D NMR data unveiled a pairing phenomenon of almost all signals emphasizing a mixture of conformers (Figures A20 and A25). The observation of multiple doubly charged species as 658 $[M+2H]^{2+}$, 669 $[M+H+Na]^{2+}$, 677 $[M+H+K]^{2+}$ (Figure 32) with a large number of exchangeable amide NH protons (δ_H 6.5-10.5) and carbonyl carbons (δ_C 160-185) from 1D NMR (Figures A25) aligned with the postulated peptide nature.

Analyzing various 2D (^{1}H-^{1}H, ^{1}H-^{13}C and ^{1}H-^{15}N) NMR experiments (COSY, TOCSY, NOESY, HSQC, HSQC-TOCSY, HMBC) instantly resulted in the assignment of four proteogenic amino acid residues encompassing leucine (Leu-8), proline (Pro-9), alanine (Ala-12), and asparagine/aspartic acid (Asn-13/Asp-13 due to the initial inabilities to allocate the δ_H of either -CONH$_2$ or –CO$_2$H, respectively). Exploiting HMBC and NOESY correlations, the connectivity between these readily discovered spin systems was directly established, offering a pair of fragments (I, and II), each consisting of two-stitched residues (Figure 37).

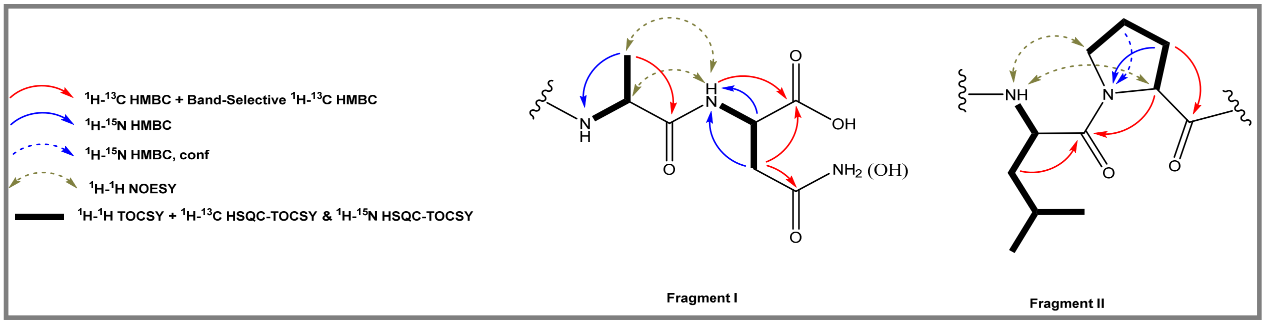

Figure 37. Structural fragments I, and II

The distinctive olefinic CH$_2$ [$\delta_{H/C}$ 5.35/111.63 ppm in d_3-CH$_3$OH (700/176 MHz)] and its characteristic downfield NH$_2$ signal [$\delta_{H/N}$ 10.05/127.35 ppm in d_3-CH$_3$OH (700/71 MHz)] in tandem with the correlations from HMBC and NOESY experiments could unequivocally outline extended fragment II with an extra unit in the form of 2,3-didehydroalanine (Dha-7) (Figure 38).

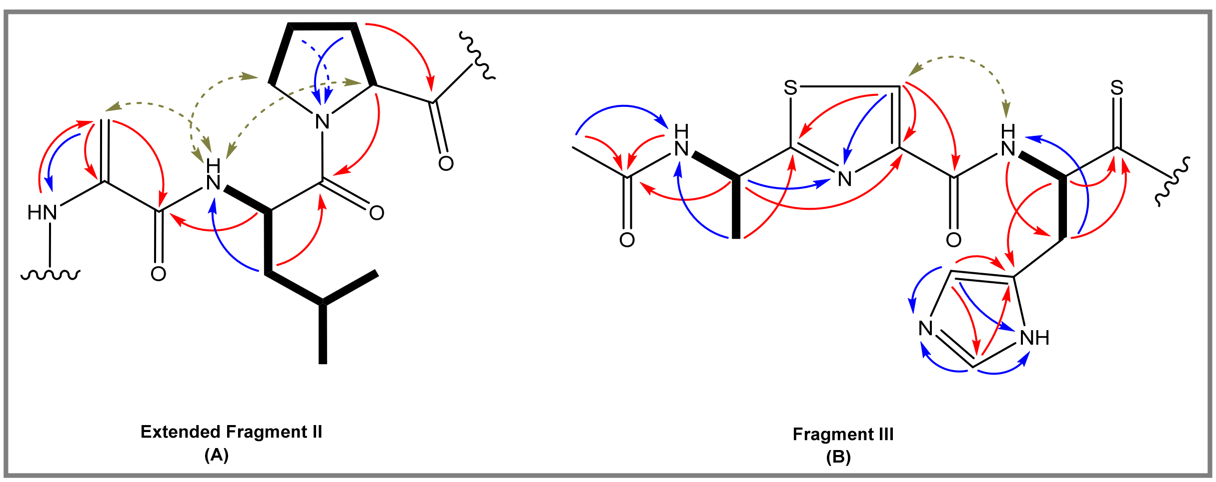

Figure 38. Structural fragments extended II, and III

The clearly found singlets and their conformers in the aliphatic and aromatic regions [δ_H (2.02–2.04 & 7.30–8.90) ppm in d_4-CH$_3$OH (400 MHz)] aided in constructing fragment III with the help of the derived data mostly from ^{1}H-^{13}C and ^{1}H-^{15}N HMBC experiments. It started with a terminal acetyl group (Ac) linked to an alanine residue (Ala-1) which was in turn found to be connected to the thiazole moiety (Thz). Guided by the unique Thz resonances of 3-CH ($\delta_{H/C}$ 8.16/126.66 ppm in d_4-CH$_3$OH), and –N= (δ_N 305.60 ppm in d_3-CH$_3$OH) in joint with the ^{1}H-^{13}C and ^{1}H-^{15}N HMBC couplings, Thz unit was completely assigned to be in in a direct fusion with Ala-1 (Figure 38).

Analogously, histidine (His) was deciphered from its characteristic imidazole signals ($\delta_{5H/C}$ 7.48/119.05, $\delta_{6H/C}$ 8.86/135.23, δ_{5N} 175.04, and δ_{6N} 191.59 ppm in d_4-CH_3OH). The inter-residue NOESY proved its occurrence to be in a direct linkage with Thz unit. Moreover, the ^{1}H-^{13}C HMBC exhibited several cross-peaks around δ_C 206 - 209 ppm corresponding to an intensely relaxed signal in the 1D ^{13}C-NMR spectrum, which were identified as couplings between the 2-CH (αH), and 3-CH_2 (βH) of His-3 with the genetically expected thioamide tailoring that typically resonates around 200–210 ppm (Figure 39). Thus, His was selectively post-translationally modified into thio-histidine portraying fragment III (Figure 38).

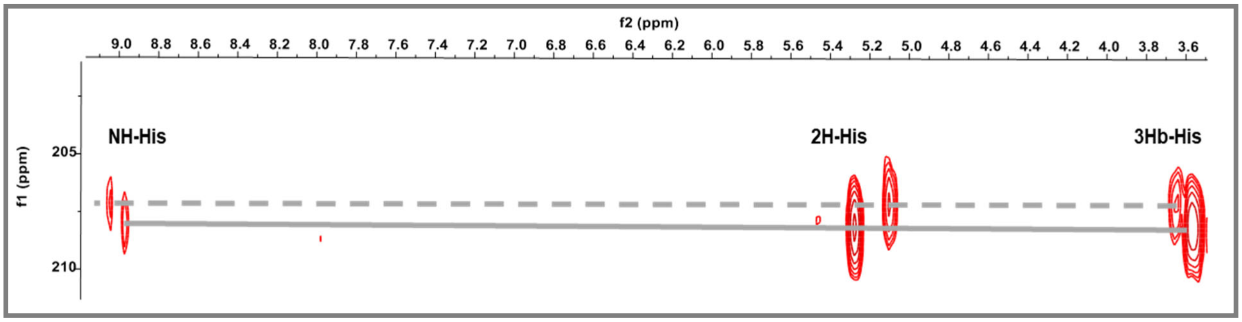

Figure 39. ^{1}H-^{13}C HMBC cross-peaks between C=S and 2H, 3Hb and the amidic hydrogen of His

The assembly of the highly morphed fragment IV (Figure 40) was initiated by the guidance of ^{1}H-^{1}H TOCSY, ^{1}H-^{13}C HSQC-TOCSY, and ^{1}H-^{1}H NOESY experiments, which enabled the decoding of a common post-translationally tailored motif as α-aminobutyrate (Abu), biosynthetically originating from threonine. Tracing up this spin system (Abu) with ^{1}H-^{13}C HMBC, and NOESY correlations uncovered three additional transformed amino acid residues (AlaS-6, AlaS-10, and AlaS-11), comprising typical methyllanthionine (MeLan = Abu + AlaS-10), and lanthionine (Lan = AlaS-6 + AlaS-11) bridges, besides an exceptionally δ-oxidized leucine in the form of 4-methylglutamate (4-Meglu) (Figure 40).

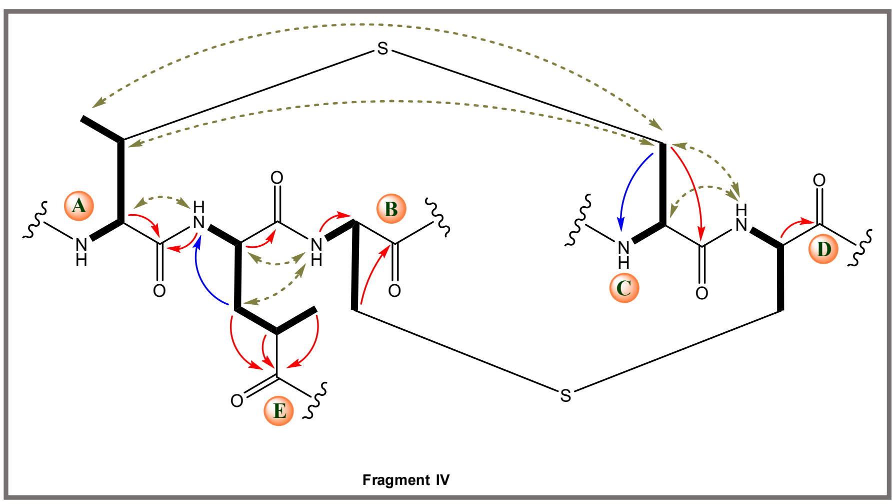

Figure 40. Structural fragment IV

As a result of the highly similar (almost identical) chemical shifts of α-protons of AlaS-6 and AlaS-11 across the different datasets (Tables 10, 12 and 14), the NOESY analysis did not result in any convincing correlations using neither the β-, or α- protons of the Lan residues to validate the crosslink. Mainly supervised by the homonuclear correlations arising from NOESY data, MeLan and Lan blocks were found to be directly bonded to each other on one side whilst being disjointed on the Abu flank by 4-Meglu (Figure 40).

Taking into account the deduced skeletons of fragments (I–IV), it was clear that fragment I portrayed the C-terminus of the peptide while the amino-terminus was represented as fragment III, N-capped with an acetyl group. Besides the heteronuclear connections of αH and βH-His to ^{13}C=S, an extra set of aligned couplings ($\delta_{2H/C}$, major 5.48/65.74, $\delta_{2H/C}$, minor 5.37/65.74 in d_4-CH_3OH) was identified signifying the αH of the Abu motif.

The confirmatory observation of ^{1}H-^{15}N HMBC couplings between αH-His and NH of the Abu offered further unambiguous proof of fitting fragment III together with component IV/A (Figure 41). Notably, the uniquely deshielded NH signals of the Abu spin system [$\delta_{H/N}$ 9.77/ 155.59 ppm in d_3-CH_3OH (700/71 MHz)] were also in alignment with its straight association with the thiocarbonyl group (Figure 41). The additional attachment of fragment I to IV/D was basically gleaned from both ^{1}H-^{13}C HMBC along with ^{1}H-^{1}H NOESY data (Figure 41).

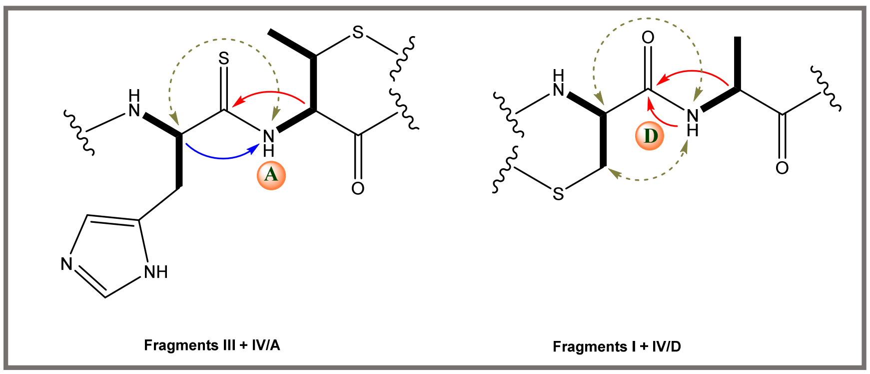

Figure 41. Structural fragments III+IV/A, and I+IV/D

Finally, the extended fragment II was found to be architecturally inserted within IV using solely NOE connections which placed the Dha structural brick in association with AlaS-6 feature (IV/B), whereas Pro-9 was attached to the AlaS-10 system (IV/C) (Figure 42).

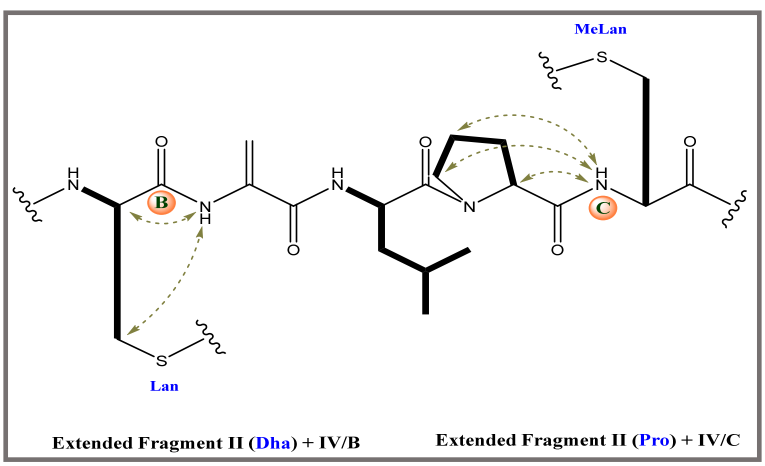

Figure 42. Structural fragments extended II (Dha) + IV/B, and extended II (Pro) + IV/D

Although fragment IV possessed five possible attachment sites (A – E), only four (A – D) could be structurally ruled out. Unfortunately, meticulous investigation of the different NMR datasets (d_4-CH_3OH, and d_3-CH_3OH) did not infer any valuable couplings that could sort out any structural connection with the last remaining decoration E. However, bearing in mind the anticipated molecular formula besides its RDB, one final macrocyclization has to be recruited. Driven by the inability to assign δ_H of neither the in-chain NH_2 nor C-terminus CO_2H of Asn-13 of fragment I, two possible crosslinks have been suggested either as an imide or anhydride macrocyclization, respectively (Figure 43).

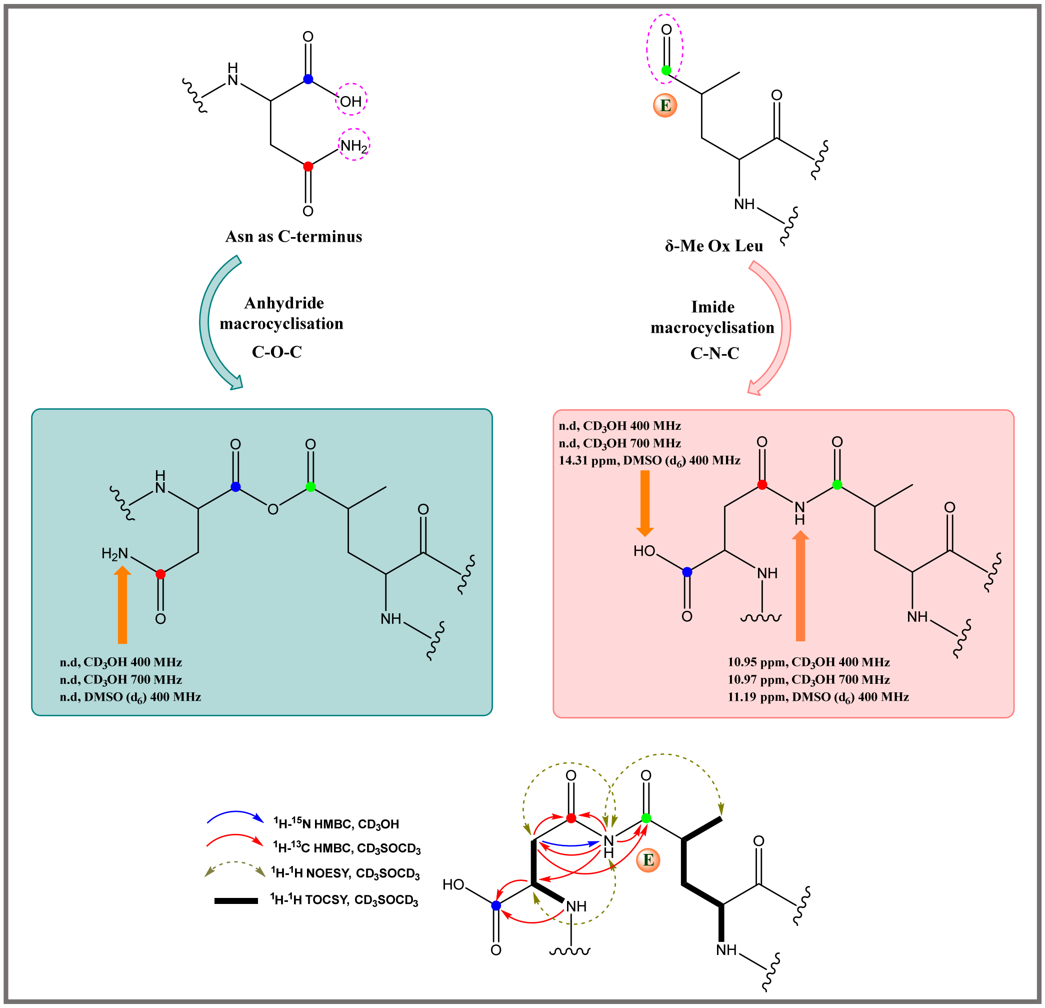

Figure 43. Possible crosslinks between fragment I-Asn and fragment IV/E (Top) and macrocylic imide PTM connected by NMR through NOESY and HMBC correlations (Bottom)

The possibility of having a macrocyclic anhydride makeup was apparently in strong contradiction with **1** in terms of the given chemical stability observed during the extraction, separation, purification and storage as well.

Luckily, the ^1H-^{15}N HMBC spectrum of **1** in the CD_3OH/700 MHz dataset, in an unintentional partial sweep width (partial SW) experiment, disclosed a so far non-interpreted pair of two unfamiliar cross-peaks ($\delta_{3Ha/Asn}$ 2.64/ δ_N 172.80, $\delta_{3Hb/Asn}$ 2.99/ δ_N 172.80 ppm) (Figure 44C) which were consistent with the reported ^{15}N values of imides.[167]

Additionally, ^1H-^{15}N HSQC of NH glutarimide, an imide-containing standard, ($\delta_{H/N}$ 10.33/172.25 in d_3-CH_3OH) supported such a range of chemical shifts (Figure A58) and corroborated the imide linkage hypothesis.

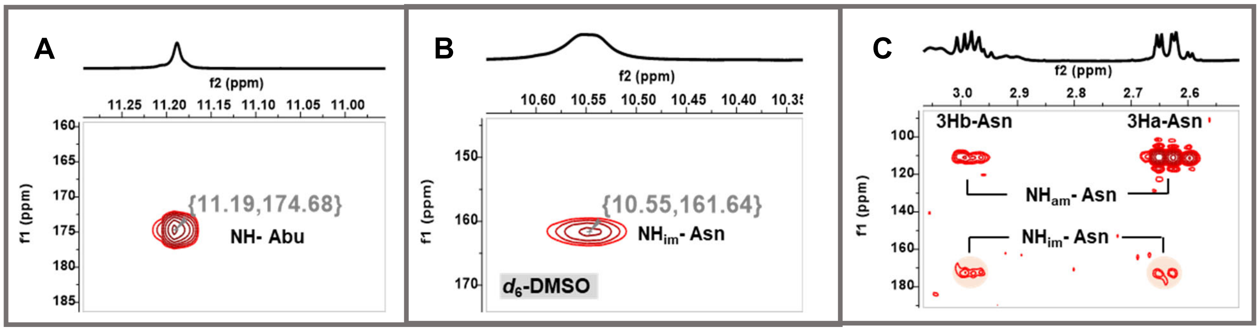

Figure 44. A) ^{1}H-^{15}N HSQC NMR spectra highlighting the chemical shifts of the NH of Abu connected to C=S, B) the macrocyclic imide NH of Asn and C) ^{1}H-^{15}N HMBC NMR spectrum showing the key cross-peaks between 3Ha, and 3Hb of Asn with the amidic and imidic NH of Asn

Within the course of our preliminary NMR trials recording in various solvents, d_6-DMSO was tested even though the data quality was not good enough to fully elucidate the structure of **1**. Unexpectedly, the ^{1}H-^{15}N HSQC spectrum showed two characteristic downfield correlations ($\delta_{H/N}$ 10.55/161.63, and $\delta_{H/N}$ 11.19/174.72 ppm) (Figures 44A and 44B), which were tracked down by ^{1}H-^{1}H TOCSY, ^{1}H-^{1}H NOESY, and ^{1}H-^{13}C HMBC correlations. The $\delta_{H/N}$ 10.55/161.63 ppm coupling was assigned to define the thioamide –NH– of Abu entity, whereas the sharp singlet $\delta_{H/N}$ 11.19/174.72 ppm was found to be in an equivocal consistency with the presumed imide crosslink evidenced by a multitude of connectivities (Figures 43 and 45).

Regardless of the unsatisfactory NMR data quality in d_6-DMSO compared to d_3- and d_4-CH_3OH, the dataset could still successfully and efficiently fill the remaining gap regarding the last unprecedented structural ornament and complete the 2D structure of nocathioamide A (**1**) (Figure 45).

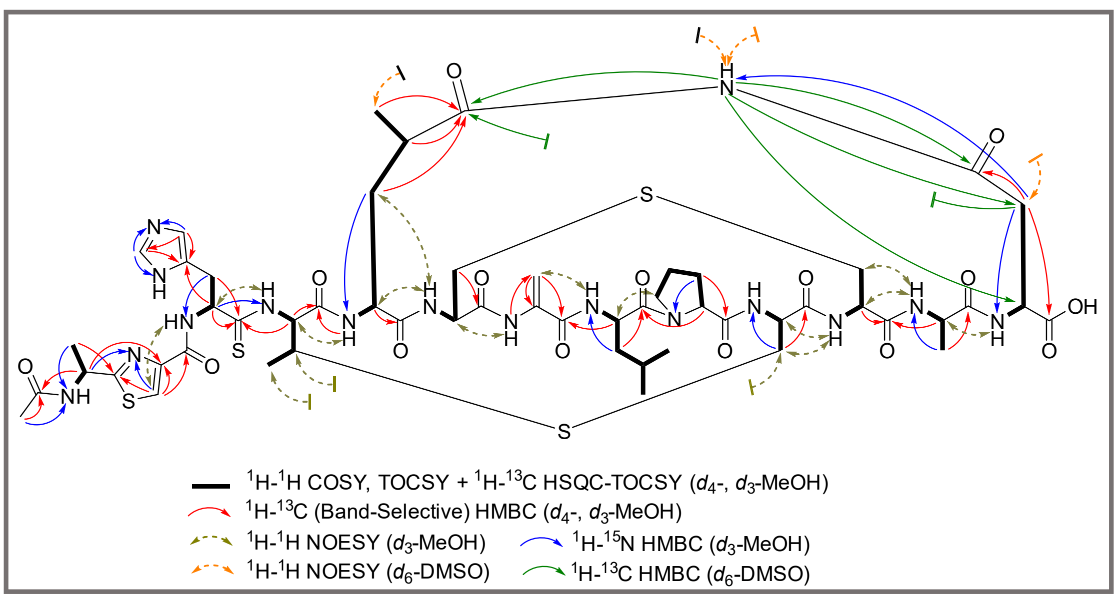

Figure 45. NMR key correlations of nocathioamide A (**1**)

Taking into account the suggested molecular formula of the additional isolated feature, $C_{54}H_{74}N_{16}O_{16}S_4$, it was envisioned that nocathioamide B (**2**) encode an extra oxygen atom within its architecture relative to **1** (Figure A14).

Expectedly, **2** exhibited almost identical NMR spectra of **1** except with a lower degree of signals overlap besides a significant drift in the β-carbons chemical shifts of AlaSO-6 and AlaSO-11. The attained ^1H-^{13}C HSQC spectra in d_3- and d_4-CH_3OH datasets all share that the Lan bridge forming residues (AlaSO-6, AlaSO-11) inherited an upfield shift with their α-carbons (δ_C AlaS6 55.49 => δ_C AlaSO6 51.50 & δ_C AlaS11 53.60 => δ_C AlaSO11 49.46, d_3-CH_3OH, 176 MHz) whilst the β-carbons resonated strongly downfield (δ_C AlaS6 34.18 => δ_C AlaSO6 55.52 & δ_C AlaS11 35.43/35.52 => δ_C AlaSO11 59.73, d_3-CH_3OH, 176 MHz).[74a]

In addition, the Lan crosslink motifs in **2**, unlike **1**, were found to exhibit more resolved NOESY correlations proving the bridge formation between AlaSO-6, and AlaSO-11 (Figures 46).[168]

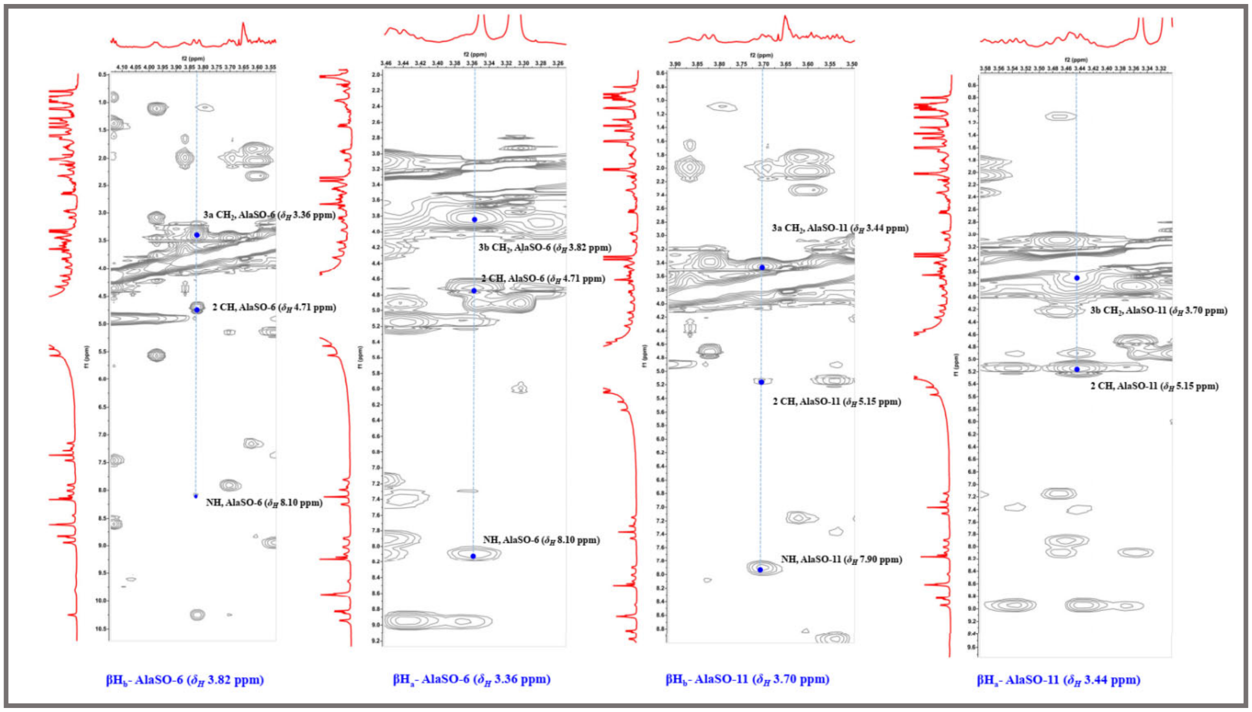

Figure 46. ^1H-^1H NOESY spectrum of the sulfoxide-Lan bridge of nocathioamide B (**2**)

Considering such a change in the chemical shifts that typically occur upon diagnostic oxidation of the thioether functionality, **2** was deduced to be the S-monooxidized congener of **1** (Figure 47).

In contrast to **1** and **2**, nocathiamide C (**3**) was solely analyzed by HR-ESI-MS for $C_{54}H_{74}N_{16}O_{17}S_4$ (Figures 33 and A15) exhibiting 32 additional Da (2 x O) in comparison with **1**. Thus, this difference could be readily accounted for two S-oxide groups instead of the typical thioether bridges featured in **1** (Figure 47).

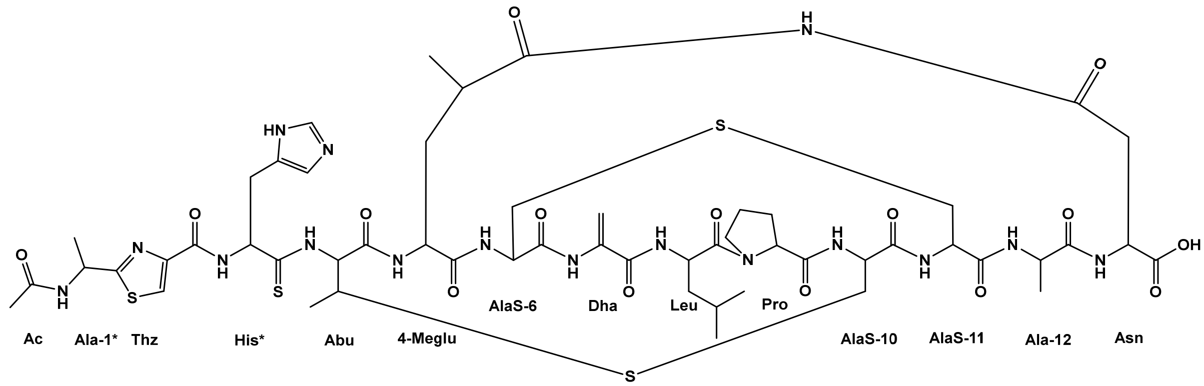

1

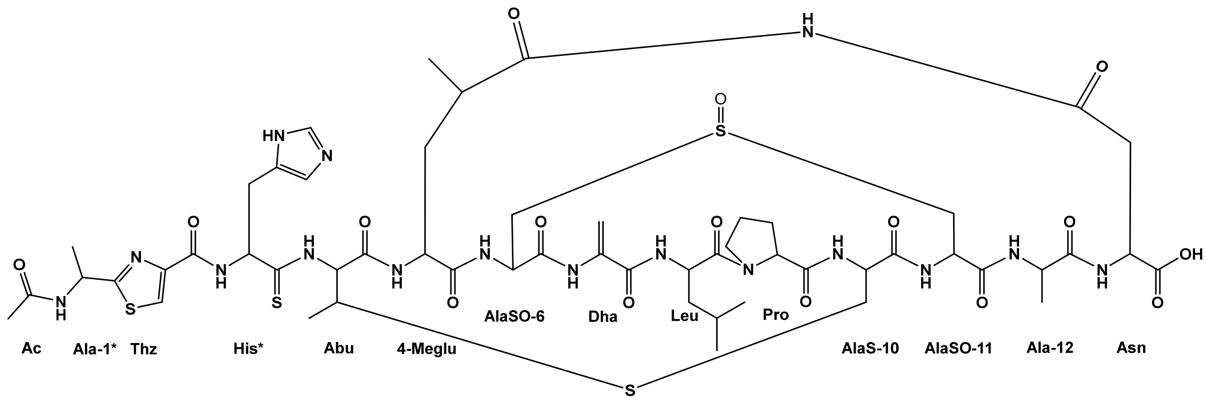

2

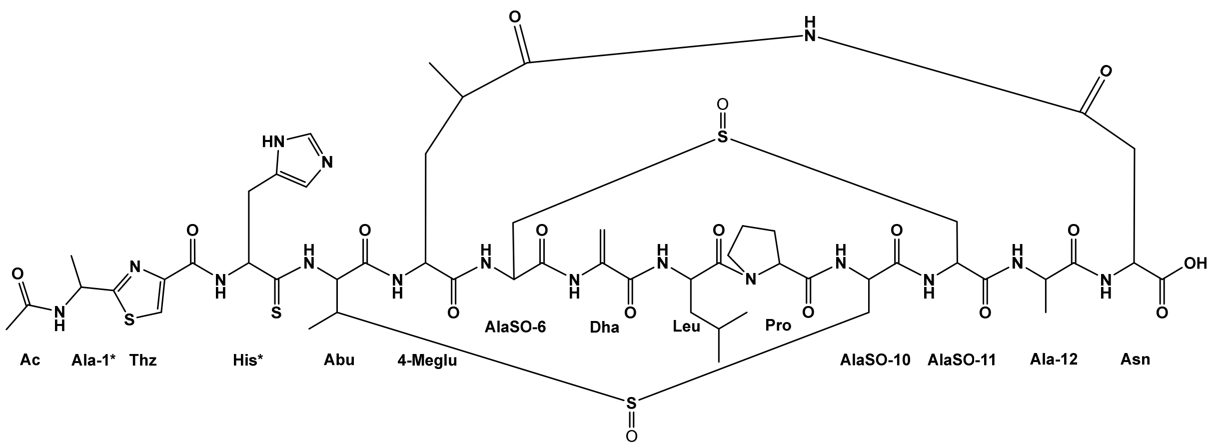

3

Figure 47. Chemical structures of the nocathioamides molecular family [A (**1**), B (**2**), and C (**3**)]

Table 10. ^{1}H, ^{13}C and ^{15}N-NMR data of nocathioamide A (**1**) (d_3-CH_3OH; 400 MHz; major conformer)

Residue	Position	δ_C / δ_N	δ_H, mult (*J* in Hz)	Residue	Position	δ_C / δ_N	δ_H, mult (*J* in Hz)
Ac	1	173.05, C	--------	**Dha**	1	166.77, C	--------
	2	22.64, CH_3	2.02, s		2	138.27, C	--------
Ala-1 *	1	48.92 [b], CH	5.30, p (7.0)		3	107.87, CH_2	5.36, brs
	2	20.98, CH_3	1.60, d (7.0)		-NH-	126.95	10.00, brs
	-NH-	132.2	8.79, d (7.5)	**Leu**	1	173.96, C	--------
Thz	1	163.69, C	--------		2	51.02, CH	4.86, m
	2	149.74, C	--------		3	41.67, CH_2	1.46, m + 1.82, m
	3	126.45, CH	8.15, s		4	26.19, CH	1.70, m
	4	176.73, C	--------		5	22.19, CH_3	0.91, d (6.7)
	=N-	305.66	--------		6	23.75, CH_3	0.97, d (6.6)
His *	1	207.98 [d], C	--------		-NH-	120.49	8.66, d (8.1)
	2	60.64, CH	5.27, m	**Pro**	1	174.72, C	--------
	3	30.69, CH_2	3.44 dd (14.7, 6.9) + 3.56, m		2	62.87, CH	4.68 [b]
	4	130.78, C	--------		3	33.09, CH_2	2.28, m + 2.37, m
	5	119.02, CH	7.46, s		4	22.94, CH_2	1.85, m + 2.07, m
	=N-	184.38	--------		5	47.97, CH_2	3.64, m
	6	135.31, CH	8.80, s		=N-	129.45	--------
	=NH	174.74	--------	**AlaS-10**	1	172.85/172.55 [c], C	--------
	-NH-	123.55	8.97, d (5.8)		2	58.93 [d], CH	4.27, m
Abu	1	170.58, C	--------		3	35.60, CH_2	3.13, m + 3.72, m
	2	65.78, CH	5.47, brs		-NH-	117.43	7.20, brs
	3	44.79, CH	3.93, m	**AlaS-11**	1	171.72, C	--------
	4	20.23, CH_3	1.14, d (7.3)		2	53.39; CH	4.52, m
	-NH-	156.00	9.84, d (5.8)		3	35.61/35.64 [c], CH_2	3.11, m + 3.36, m
4-Meglu	1	172.61, C	--------		-NH-	115.11	8.03 [a], br
	2	53.38, CH	4.64, m	**Ala-12**	1	174.90, C	--------
	3	35.73 [a], CH_2	1.46, m + 2.20, m		2	50.91, CH	4.16, m
	4	36.71, CH	2.45, m		3	18.18, CH_3	1.29, d (7.0)
	5	179.39, C	--------		-NH-	119.65	7.57, brs
	6	18.65, CH_3	0.83 [a], d (6.7)	**Asn**	1	178.95, C	--------
	-NH-	120.33	8.04 [a]		2	51.55, CH	4.54, m
AlaS-6	1	169.60, C	--------		3	37.27, CH_2	2.64, dd (17.7, 5.6) + 2.99, dd (17.7, 9.2)
	2	55.48, CH	4.52, m		4	178.22, C	--------
	3	34.22, CH_2	3.06, m + 3.31, m		-NH-	110.92	8.43, d (7.6)
	-NH-	114.16	7.68, brs		-CONHCO-	n.d	10.96, brs

[*] AA with modified CO within the backbone**,** [a] Overlapped, [b] Masked by water/solvent ^{1}H/^{13}C-NMR signals, [c] Interchangeable, [d] Weak, [n.d] not determined

Table 11. ^{1}H, ^{13}C, and ^{15}N-NMR data of nocathioamide A (**1**) (d_3-CH_3OH; 400 MHz; minor conformer)

Residue	**Position**	δ_C / δ_N	δ_H, **mult (*J* in Hz)**	**Residue**	**Position**	δ_C / δ_N	δ_H, **mult (*J* in Hz)**
Ac	1	173.13, C	--------	**Dha**	1	166.70, C	--------
	2	22.67, CH_3	2.04, s		2	138.09, C	--------
Ala-1 *	1	48.95 [b], CH	5.26 [a], m		3	111.69, CH_2	5.43 [a] + 5.50 [a]
	2	20.68, CH_3	1.60, d (7.0)		-NH-	129.92	10.20, s
	-NH-	132.20	8.82, d (7.5)	**Leu**	1	174.12, C	--------
Thz	1	163.87, C	--------		2	57.82, CH	4.31, m
	2	149.85, C	--------		3	38.45, CH_2	1.62, m + 1.88, m
	3	126.42, CH	8.14, s		4	26.37, CH	1.79, m
	4	176.94, C	--------		5	22.16, CH_3	0.93, d (6.5)
	=N-	n.d	n.d		6	23.18, CH_3	1.00, d (6.5)
His *	1	207.03 [d], C	--------		-NH-	135.57	9.01 [a], brs
	2	60.99, CH	5.10, m	**Pro**	1	n.d	--------
	3	30.39, CH_2	n.d + 3.65, m		2	64.87, CH	4.35, m
	4	131.01, C	--------		3	30.39, CH_2	2.07, m + 2.36, m
	5	118.88, C	7.36, s		4	27.08, CH_2	1.98, m + 2.13, m
	=N-	188.01	--------		5	48.88 [b], CH_2	3.73, m + 3.86, m
	6	n.d	8.76 [a], s		=N-	n.d	--------
	=NH	174.08	--------	**AlaS-10**	1	n.d	--------
	-NH-	122.30	9.05, d (5.8)		2	56.16, CH	4.96 [b]
Abu	1	171.24, C	--------		3	38.88, CH_2	3.15 [a], m + 3.59 [a], m
	2	65.70, CH	5.36 [a], m		-NH-	106.11	6.66, d (9.0)
	3	45.27, CH	3.90, m	**AlaS-11**	1	n.d	n.d
	4	n.d	1.13 [a]		2	n.d	n.d
	-NH-	155.1	9.51, brs		3	n.d	n.d
4-Meglu	1	172.03, C	--------		-NH-	n.d	n.d
	2	54.06, CH	4.47 [b]	**Ala-12**	1	175.08, C	--------
	3	35.73, CH_2	1.42 [a], m + 2.19 [a], m		2	51.27, CH	4.31, m
	4	36.71, CH	2.40 [a], m		3	17.71, CH_3	1.42, d (6.7)
	5	179.39 [a], C	--------		-NH-	120.17	7.88, d (6.7)
	6	18.52, CH_3	0.72, d (7.0)	**Asn**	1	178.91, C	--------
	-NH-	119.50	7.92, d (8.0)		2	51.41, CH	4.60, m
AlaS-6	1	169.75, C	--------		3	37.34, CH_2	2.60, m + 2.94, m
	2	55.79, CH	4.64, m		4	n.d	--------
	3	34.38, CH_2	2.94, m + 3.20, m		-NH-	111.15	8.30, d (7.7)
	-NH-	113.86	7.32 [a], m		-CO<u>NH</u>CO-	n.d	n.d

[*] AA with modified CO within the backbone**,** [a] Overlapped, [b] Masked by water/solvent ^{1}H/^{13}C-NMR signals, [c] Interchangeable, [d] Weak, [n.d] not determined

Table 12. [1]H, [13]C, and [15]N-NMR data of nocathioamide A (**1**) (d_3-CH_3OH; 700 MHz; major conformer)

Residue	Position	δ_C / δ_N	δ_H, mult (*J* in Hz)	Residue	Position	δ_C / δ_N	δ_H, mult (*J* in Hz)
Ac	1	173.07, C	--------	**Dha**	1	166.70, C	--------
	2	22.64, CH_3	2.02, s		2	138.33, C	--------
Ala-1 *	1	48.89 [b], CH	5.30, p (7.0)		3	111.63, CH_2	5.35, brs
	2	20.94, CH_3	1.60, d (7.0)		-NH-	127.35	10.05, brs
	-NH-	132.3	8.81, d (7.4)	**Leu**	1	174.00, C	--------
Thz	1	163.68, C	--------		2	50.94, CH	4.86 [b]
	2	149.73, C	--------		3	41.66, CH_2	1.45, m + 1.82, m
	3	126.43, CH	8.16, s		4	26.19, CH	1.70, m
	4	176.64, C	--------		5	22.17, CH_3	0.91, d (6.5)
	=N-	305.80	--------		6	23.75, CH_3	0.97, d (6.5)
His *	1	208.21 [d], C	--------		-NH-	120.58	8.68 [a]
	2	60.94, CH	5.23, m	**Pro**	1	174.85, C	--------
	3	30.89; CH_2	3.43, m + 3.54, m		2	62.89, CH	4.67, m
	4	131.22, C	--------		3	33.15, CH_2	2.27, m + 2.36, m
	5	118.95, CH	7.40, s		4	22.93, CH_2	1.84, m + 2.05, m
	=N-	189.63	--------		5	47.98, CH_2	3.63, m
	6	135.57, CH	8.67, s		=N-	129.27	--------
	=NH	175.21	--------	**AlaS-10**	1	172.84/172.59 [c], C	--------
	-NH-	123.78	8.94, d (5.1)		2	59.21, CH	4.26, brs
Abu	1	170.70, C	--------		3	35.43/35.52 [c], CH_2	3.13, m + 3.69, m
	2	65.62, CH	5.48, brs		-NH-	117.55	7.23, very brs
	3	44.77, CH	3.96, m	**AlaS-11**	1	171.77, C	--------
	4	20.24, CH_3	1.12, d (7.1)		2	53.60, CH	4.51 [a], m
	-NH-	155.59	9.77, brs		3	35.52/35.43 [c], CH_2	3.11, m + 3.35, m
4-Meglu	1	172.63 [a], C	--------		-NH-	114.99	8.02, brs
	2	53.41, CH	4.63, m	**Ala-12**	1	174.94, C	--------
	3	35.70, CH_2	1.48, m + 2.18, m		2	50.94, CH	4.15, m
	4	36.75, CH	2.44, m		3	18.17, CH_3	1.30, d (5.7)
	5	179.54, C	--------		-NH-	119.70	7.56, brs
	6	18.65, CH_3	0.83, brs	**Asn**	1	179.00, C	--------
	-NH-	120.30	8.09, brs		2	51.56, CH	4.54, m
AlaS-6	1	169.62, C	--------		3	37.26, CH_2	2.64, dd (18.0, 5.6) + 2.99, dd (18.0, 9.3)
	2	55.49, CH	4.51 [a], m		4	178.27, C	--------
	3	34.18, CH_2	3.05, m + 3.29, m		-NH-	110.93	8.44, d (7.3)
	-NH-	114.08	7.66, very brs		-CONHCO-	172.80 [d]	10.94, very brs

[*] AA with modified CO within the backbone**,** [a] Overlapped, [b] Masked by water/solvent [1]H/[13]C-NMR signals, [c] Interchangeable, [d] Weak, [n.d] not determined

Table 13. [1]H, [13]C, and [15]N-NMR data of nocathioamide A (**1**) (*d_3*-CH_3OH; 700/176/71 MHz; minor conformer)

Residue	**Position**	**δ_C / δ_N**	**δ_H, mult (*J* in Hz)**	**Residue**	**Position**	**δ_C / δ_N**	**δ_H, mult (*J* in Hz)**
Ac	1	173.14, C	--------	**Dha**	1	166.80, C	--------
	2	22.65, CH_3	2.03, s		2	138.09, C	--------
Ala-1 *	1	48.97 [b], CH	5.26 [a], m		3	111.61, CH_2	5.42 + 5.49, brs
	2	20.96, CH_3	1.59, d		-NH-	129.08	10.22, brs
	-NH-	132.3	8.84, d (7.4)	**Leu**	1	174.15, C	--------
Thz	1	163.87, C	--------		2	57.86, CH	4.31, m
	2	149.85, C	--------		3	38.43, CH_2	1.62, m + 1.87, m
	3	126.40, CH	8.14, s		4	26.36, CH	1.78, m
	4	176.87, C	--------		5	22.15, CH_3	0.93, d (6.5)
	=N-	305.8	--------		6	23.18, CH_3	1.00, d (6.5)
His *	1	207.30 [d], C	--------		-NH-	135.70	9.04 [a]
	2	61.30, CH	5.07 [b]	**Pro**	1	n.d	--------
	3	30.72, CH_2	3.41, m + 3.61, m		2	64.90, CH	4.34, t (8.1)
	4	131.56, C	--------		3	30.40, CH_2	2.06, m + 2.35, m
	5	118.68, CH	7.29, s		4	27.09, CH_2	1.97, m + 2.13, m
	=N-	191.86	--------		5	48.95 [b], CH_2	3.73, m + 3.86, m
	6	135.52, CH	8.62, s		=N-	130.18	--------
	=NH	174.32	--------	**AlaS-10**	1	n.d	--------
	-NH-	122.62	9.03, d (5.0)		2	56.13, CH	4.96, m
Abu	1	171.33, C	--------		3	38.81, CH_2	3.15, m + 3.58, m
	2	65.62 [a], CH	5.35 [a]		-NH-	106.32	6.68, brs
	3	45.19, CH	3.89, m	**AlaS-11**	1	n.d	n.d
	4	20.65, CH_3	1.09, d (7.1)		2	n.d	n.d
	-NH-	154.69	9.45, brs		3	n.d	n.d
4-Meglu	1	172.58/172.84 [c], C	--------		-NH-	n.d	n.d
	2	53.41 & 54.05, CH	4.62 [a] & 4.47 [b], m	**Ala-12**	1	175.12, C	--------
	3	35.70 [a], CH_2	1.45 + 2.17, m & 1.54 + 2.19, m		2	51.27, CH	4.31, m
	4	36.75 [a], CH	2.43 [a] & 2.47 [a]		3	17.69, CH_3	1.42, d (7.2)
	5	n.d	--------		-NH-	120.38	7.91, d (6.4)
	6	18.65, CH_3	0.74, d (7.2) & 0.82 [a]	**Asn**	1	178.95, C	--------
	-NH-	119.70	7.97 [a] & 7.99 [a]		2	51.42, CH	4.60, m
AlaS-6	1	169.78, C	--------		3	37.33, CH_2	2.61 [a] + 2.77 [a], dd
	2	55.82, CH	4.64, m		4	178.26, C	--------
	3	34.35, CH_2	2.91 + 3.18, m		-NH-	111.15	8.32, d (7.8)
	-NH-	113.90	7.32, brs		-CONHCO-	n.d	n.d

[*] AA with modified CO within the backbone**,** [a] Overlapped, [b] Masked by water/solvent [1]H/[13]C-NMR signals, [c] Interchangeable, [d] Weak, [n.d] not determined

Table 14. ^{1}H, and ^{13}C-NMR data of nocathioamide A (**1**) (d_4-CH_3OH; 400 MHz; major conformer)

Residue	Position	δ_C / δ_N	δ_H, mult (*J* in Hz)	Residue	Position	δ_C / δ_N	δ_H, mult (*J* in Hz)
Ac	1	173.15, C	--------	**Dha**	1	166.76, C	--------
	2	22.70, CH_3	2.02, s		2	138.21, C	--------
Ala-1 *	1	48.97 [b], CH	5.31, m (7.0)		3	108.13, CH_2	5.37, brs
	2	21.04, CH_3	1.61, d (7.0)		-NH-	--------	--------
	-NH-	--------	--------	**Leu**	1	174.19, C	--------
Thz	1	163.84, C	--------		2	51.11, CH	4.87, m
	2	149.79, C	--------		3	41.71, CH_2	1.47, m + 1.84, m
	3	126.66, CH	8.16, s		4	26.34, CH	1.72, m
	4	177.08, C	--------		5	22.30, CH_3	0.92, d (6.2)
	=N-	--------	--------		6	23.86, CH_3	0.98, d (6.5)
His *	1	207.99 [d], C	--------		-NH-	--------	--------
	2	60.71, CH	5.25, t (7.5)	**Pro**	1	174.83, C	--------
	3	30.52, CH_2	3.47, dd (14.7, 7.5) + 3.59, dd (14.7, 7.5)		2	63.01, CH	4.69, m
	4	130.69, C	--------		3	33.23, CH_2	2.28, m + 2.37, m
	5	119.05, CH	7.48, s		4	23.06, CH_2	1.87, m + 2.08, m
	=N-	--------	--------		5	48.13, CH_2	3.66, m
	6	135.23, CH	8.86, s		=N-	--------	--------
	=NH	--------	--------	**AlaS-10**	1	172.93/172.64 [c], C	--------
	-NH-	--------	--------		2	65.74, CH	5.48, brs
Abu	1	170.68, C	--------		3	44.76, CH_2	3.98, m
	2	65.74, CH	5.48, brs		-NH-	--------	--------
	3	44.76, CH	3.98, m	**AlaS-11**	1	171.82, C	--------
	4	20.24, CH_3	1.15, d (6.8)		2	53.37, CH	4.52 [a]
	-NH-	--------	--------		3	35.49/35.67 [c], CH_2	3.12 [a] + 3.36 [a]
4-Meglu	1	172.64 [a], C	--------		-NH-	--------	--------
	2	53.37, CH	4.65, m	**Ala-12**	1	174.99, C	--------
	3	35.79, CH_2	1.47, m + 2.19, m		2	50.92, CH	4.17 [a]
	4	36.79, CH	2.46, m		3	18.25, CH_3	1.31, d (6.9)
	5	179.48, C	--------		-NH-	--------	--------
	6	18.73, CH_3	0.85 [a]	**Asn**	1	178.99, C	--------
	-NH-	--------	--------		2	51.58, CH	4.56 [a]
AlaS-16	1	169.70, C	--------		3	37.34, CH_2	2.65, dd (17.7, 5.5) + 3.00, dd (17.7, 9.3)
	2	55.53, CH	4.53 [a]		4	178.28, C	--------
	3	34.32, CH_2	3.06 [a] + 3.32 [a]		-NH-	--------	--------
	-NH-	--------	--------		-CONHCO-	--------	--------

[*] AA with modified CO within the backbone**,** [a] Overlapped, [b] Masked by water/solvent ^{1}H/^{13}C-NMR signals, [c] Interchangeable, [d] Weak, [n.d] not determined

Table 15. ^{1}H, and ^{13}C-NMR data of nocathioamide A (**1**) (d_4-CH_3OH; 400 MHz; minor conformer)

Residue	Position	δ_C / δ_N	δ_H, mult (*J* in Hz)	Residue	Position	δ_C / δ_N	δ_H, mult (*J* in Hz)
Ac	1	173.23, C	--------	**Dha**	1	166.76, C	--------
	2	22.73, CH_3	2.04, s		2	138.04, C	--------
Ala-1 *	1	49.00 [b], CH	5.25 [a], m		3	111.63, CH_2	5.42 [a] + 5.49 [a]
	2	21.02 [a], CH_3	1.61, d (7.0)		-NH-	--------	--------
	-NH-	--------	--------	**Leu**	1	174.28, C	--------
Thz	1	163.99, C	--------		2	57.83, CH	4.32, m
	2	149.93, C	--------		3	38.50, CH_2	1.62, m + 1.90, m
	3	126.60, CH	8.14, s		4	26.50, CH	1.79, m
	4	177.08, C	--------		5	22.26, CH_3	0.93 [a]
	=N-	--------	--------		6	23.30, CH_3	1.01, d (6.5)
His *	1	206.90 [d], C	--------		-NH-	--------	--------
	2	60.91, CH	5.09, t (7.5)	**Pro**	1	n.d	--------
	3	30.32, CH_2	n.d + 3.68 [a]		2	65.00, CH	4.36 [a]
	4	130.92, C	--------		3	30.53 [a], CH_2	2.08 [a] + 2.36 [a]
	5	118.88, CH	7.37, s		4	27.21, CH_2	1.99 [a] + 2.14 [a]
	=N-	--------	--------		5	49.00, CH_2	3.72 [a] + 3.88 [a]
	6	135.17; CH	8.82, s		=N-	--------	--------
	=NH	--------	--------	**AlaS-10**	1	n.d	--------
	-NH-	--------	--------		2	56.20, CH	4.97 [b]
Abu	1	171.40, C	--------		3	38.97, CH_2	3.16 [a] + 3.61 [a]
	2	65.74 [a], CH	5.37, brs		-NH-	--------	--------
	3	45.40, CH	3.92, m	**AlaS-11**	1	n.d	n.d
	4	n.d	1.14 [a]		2	n.d	n.d
	-NH-	--------	--------		3	n.d	n.d
4-Meglu	1	n.d	--------		-NH-	--------	--------
	2	n.d	4.62 [a]	**Ala-12**	1	175.18, C	--------
	3	35.79 [a], CH_2	1.44 [a] + 2.18 [a]		2	51.29, CH	4.32 a
	4	36.79 [a], CH	2.43, m		3	17.79, CH_3	1.43, d (7.0)
	5	n.d	--------		-NH-	--------	--------
	6	18.62, CH_3	0.74, d (7.2)	**Asn**	1	178.93, C	--------
	-NH-	--------	--------		2	51.42, CH	4.62 [a]
AlaS-6	1	n.d	--------		3	37.41, CH_2	2.62 [a], m+ 2.96 [a], m
	2	55.82, CH	4.60, m		4	n.d	--------
	3	n.d	n.d		-NH-	--------	--------
	-NH-	--------	--------		-CONHCO-	--------	--------

[*] AA with modified CO within the backbone**,** [a] Overlapped, [b] Masked by water/solvent ^{1}H/^{13}C-NMR signals, [c] Interchangeable, [d] Weak, [n.d] not determined

Table 16. ^{1}H and ^{13}C-NMR data of nocathioamide B (**2**) (d_3-CH_3OH; 400 MHz; major conformer)

Residue	**Position**	δ_C / δ_N	δ_H, **mult (*J* in Hz)**	**Residue**	**Position**	δ_C / δ_N	δ_H, **mult (*J* in Hz)**
Ac	1	173.15, C	--------	**Dha**	1	166.44, C	--------
	2	22.59, CH_3	2.01, s		2	138.79, C	--------
Ala-1 *	1	48.97 [b], CH	5.30, m		3	109.33, CH_2	5.25 + 5.32, brs
	2	20.95, CH_3	1.60, d (7.0)		-NH-	--------	10.20, s
	-NH-	--------	8.81, d (7.7)	**Leu**	1	173.77, C	--------
Thz	1	163.87, C	--------		2	50.63, CH	4.84 [a]
	2	149.77, C	--------		3	42.12, CH_2	1.44, m + 1.80, m
	3	126.38, CH	8.17, s		4	26.12, CH	1.66, m
	4	176.81, C	--------		5	21.97, CH_3	0.91, d (6.5)
	=N-	--------	--------		6	23.70, CH_3	0.96, d (6.6)
His *	1	208.53 [d], C	--------		-NH-	--------	8.59, d (7.7)
	2	61.00, CH	5.16 [b]	**Pro**	1	175.10, C	--------
	3	30.49, CH_2	3.46, m + 3.55, m		2	62.90, CH	4.57 [a]
	4	130.87, C	--------		3	33.16, CH_2	2.33, m
	5	119.04, CH	7.44, s		4	23.04, CH_2	1.83, m + 2.05, m
	=N-	--------	--------		5	48.16, CH_2	3.62, m
	6	135.44, CH	8.79, s		=N-	--------	--------
	=NH	--------	--------	**AlaS-10**	1	172.14, C	--------
	-NH-	--------	9.00, d (5.5)		2	58.82, CH	4.23, m
Abu	1	170.55, C	--------		3	34.68, CH_2	3.09, m + 3.48, m
	2	65.73, CH	5.56, brs		-NH-	--------	7.07, brs
	3	44.66, CH	3.97, m	**AlaSO-11**	1	171.06, C	--------
	4	20.08, CH_3	1.13, d (6.97)		2	49.47, CH	5.13 [b]
	-NH-	--------	9.87, brs		3	59.74, CH_2	3.44, m + 3.68, m
4-Meglu	1	172.70, C	--------		-NH-	--------	7.90 [a]
	2	53.36, CH	4.67 [b]	**Ala-12**	1	175.22, C	--------
	3	35.52, CH_2	1.51, m + 2.21, m		2	51.27, CH	4.14, m
	4	36.75, CH	2.39, m		3	18.14, CH_3	1.37, d (7.1)
	5	179.60, C	--------		-NH-	--------	7.48, d (5.8)
	6	18.50, CH_3	0.80, d (7.0)	**Asn**	1	179.04, C	--------
	-NH-	--------	7.94 [a]		2	51.58, CH	4.52, m
AlaSO-6	1	167.62, C	--------		3	37.20, CH_2	2.64, dd (17.8, 5.5) + 2.97, dd (17.8, 9.4)
	2	51.52, CH	4.70 [a]		4	178.24, C	--------
	3	55.52, CH_2	3.35, m + 3.83, m		-NH-	--------	8.58, d (7.9)
	-NH-	--------	8.09 [a], brs		-CONHCO-	--------	11.00, brs

[*] AA with modified CO within the backbone**,** [a] Overlapped, [b] Masked by water/solvent ^{1}H/^{13}C-NMR signals, [c] Interchangeable, [d] Weak, [nd] not determined

Table 17. [1]H and [13]C-NMR data of nocathioamide B (**2**) (d_3-CH_3OH; 400 MHz; minor conformer)

Residue	Position	δ_C / δ_N	δ_H, mult (*J* in Hz)	Residue	Position	δ_C / δ_N	δ_H, mult (*J* in Hz)
Ac	1	nd	--------	**Dha**	1	nd	--------
	2	22.62, CH_3	2.03, s		2	nd	--------
Ala-1 *	1	49.03 [b], CH	5.26 [a]		3	nd	nd
	2	20.92, CH_3	1.60 [a]		-NH-	--------	nd
	-NH-	--------	8.84 [a]	**Leu**	1	nd	--------
Thz	1	nd	--------		2	nd	4.48 [b]
	2	149.84, C	--------		3	nd	nd
	3	126.00, CH	8.13, s		4	26.33, CH	1.75 [a]
	4	176.85, C	--------		5	nd	0.93 d (6.6)
	=N-	--------	--------		6	nd	0.99, d (6.6)
His *	1	nd	--------		-NH-	--------	nd
	2	nd	nd	**Pro**	1	nd	--------
	3	30.16, CH_2	3.46, [a] + 3.55, [a]		2	64.74, CH	4.32, m
	4	131.12, C	--------		3	30.15, CH_2	1.99, m + 2.35, m
	5	118.84, CH	7.34, s		4	26.90, CH_2	2.00, m + 2.13, m
	=N-	--------	--------		5	49.10, CH_2	3.69, m + 3.86, m
	6	135.32, CH	8.75, s		=N-	--------	--------
	=NH	--------	--------	**AlaS-10**	1	nd	--------
	-NH-	--------	nd		2	nd	nd
Abu	1	nd	--------		3	nd	nd
	2	nd	nd		-NH-	--------	nd
	3	nd	nd	**AlaSO-11**	1	nd	--------
	4	nd	nd		2	nd	nd
	-NH-	--------	9.62, brs		3	nd	nd
4-Meglu	1	nd	--------		-NH-	--------	nd
	2	nd	nd	**Ala-12**	1	175.33, C	--------
	3	nd	nd		2	51.36, CH	4.33, m
	4	nd	nd		3	17.65, CH_3	1.45, d (7.0)
	5	nd	--------		-NH-	--------	8.14 [a]
	6	nd	nd	**Asn**	1	179.11, C	--------
	-NH-	--------	nd		2	51.41, CH	4.57, m
AlaSO-6	1	nd	--------		3	37.20 [a], CH_2	2.64 [a], m + 2.97 [a], m
	2	nd	nd		4	nd	--------
	3	nd	nd		-NH-	--------	8.43, d (6.8)
	-NH-	-------	nd		-CONHCO-	--------	nd

[*] AA with modified CO within the backbone**,** [a] Overlapped, [b] Masked by water/solvent [1]H/[13]C-NMR signals, [c] Interchangeable, [d] Weak, [nd] not determined

Table 18. ^{1}H, and ^{13}C-NMR data of nocathioamide B (**2**) (d_3-CH_3OH; 700 MHz; major conformer)

Residue	**Position**	**δ_C / δ_N**	**δ_H, mult (*J* in Hz)**	**Residue**	**Position**	**δ_C / δ_N**	**δ_H, mult (*J* in Hz)**
Ac	1	173.15, C	--------	**Dha**	1	166.41, C	--------
	2	22.60, CH_3	2.01, s		2	138.82, C	--------
Ala-1 *	1	48.94 [b], CH	5.31, m		3	109.30, CH_2	5.24 + 5.32, brs
	2	20.88, CH_3	1.60, d (6.9)		-NH-	--------	10.25, s
	-NH-	--------	8.83, d (7.4)	**Leu**	1	173.71, C	--------
Thz	1	163.81, C	--------		2	50.57, CH	4.85 [b]
	2	149.76, C	--------		3	42.15; CH_2	1.43, m + 1.80, m
	3	126.31, CH	8.16, s		4	26.10, CH	1.65, m
	4	176.67, C	--------		5	21.97, CH_3	0.91, d (6.5)
	=N-	--------	--------		6	23.70, CH_3	0.96, d (6.5)
His *	1	208.75 [d], C	--------		-NH-	--------	8.62 [a]
	2	61.29, CH	5.15 [b]	**Pro**	1	175.12, C	--------
	3	30.97, CH_2	3.44, m + 3.54, m		2	62.89, CH	4.57, m
	4	131.60, C	--------		3	33.23, CH_2	2.32, m
	5	118.87, CH	7.37, s		4	23.04, CH_2	1.82, m + 2.05, m
	=N-	--------	--------		5	48.17, CH_2	3.60, m
	6	135.81, CH	8.62, s		=N-	--------	--------
	=NH	--------	--------	**AlaS-10**	1	172.16, C	--------
	-NH-	--------	8.94, d (5.1)		2	59.03, CH	4.23, m
Abu	1	170.67, C	--------		3	34.59, CH_2	3.08, m + 3.47, m
	2	65.62, CH	5.57, brs		-NH-	--------	7.15, brs
	3	44.68, CH	3.97, m	**AlaSO-11**	1	171.07, C	--------
	4	20.04, CH_3	1.11, d (6.4)		2	49.46, CH	5.14/5.15 [a], m
	-NH-	--------	9.80, very brs		3	59.73, CH_2	3.44, m + 3.70, m
4-Meglu	1	172.73, C	--------		-NH-	--------	7.90, d (9.0)
	2	53.44, CH	4.68, m	**Ala-12**	1	175.20, C	--------
	3	35.56, CH_2	1.52, m + 2.21, m		2	51.30, CH	4.13, p (6.7)
	4	36.84, CH	2.41, m		3	18.13, CH_3	1.38, d (7.1)
	5	179.72, C	--------		-NH-	--------	7.46, d (4.7)
	6	18.54, CH_3	0.80, d (6.9)	**Asn**	1	179.06, C	--------
	-NH-	--------	8.01, d (7.6)		2	51.57, CH	4.53, m
AlaSO-6	1	167.61, C	--------		3	37.19, CH_2	2.64, dd (17.8, 5.5) + 2.97, dd (17.8, 9.5)
	2	51.52/51.50 [c]	4.71 [b]		4	178.25, C	--------
	3	55.52	3.36, m + 3.82, m		-NH-	--------	8.60 [a]
	-NH-	--------	8.10, brs		-CO<u>NH</u>CO-	--------	11.00, very brs

[*] AA with modified CO within the backbone**,** [a] Overlapped, [b] Masked by water/solvent $^{1}H/^{13}C$-NMR signals, [c] Interchangeable, [d] Weak, [nd] not determined

Table 19. ^{1}H, and ^{13}C-NMR data of nocathioamide B (**2**) (d_3-CH_3OH; 700 MHz; minor conformer)

Residue	Position	δ_C / δ_N	δ_H, mult (*J* in Hz)	Residue	Position	δ_C / δ_N	δ_H, mult (*J* in Hz)
Ac	1	173.20, C	--------	**Dha**	1	nd	--------
	2	22.62, CH_3	2.03, s		2	137.71, C	--------
Ala-1 *	1	49.05 [b], CH	5.27 [a]		3	nd	nd
	2	20.92, CH_3	1.59 [a]		-NH-	--------	nd
	-NH-	--------	8.85, d (7.2)	**Leu**	1	nd	--------
Thz	1	nd	--------		2	nd	4.44 [b]
	2	149.86, C	--------		3	nd	nd
	3	126.16, CH	8.14, s		4	26.33, CH	1.75 [a]
	4	176.77, C	--------		5	nd	0.94, d (6.4)
	=N-	--------	--------		6	nd	0.99, d (6.4)
His *	1	nd	--------		-NH-	--------	nd
	2	61.21, CH	5.15 [b]	**Pro**	1	nd	--------
	3	30.75, CH_2	3.44, [a] + 3.54, [a]		2	64.81, CH	4.32, m
	4	131.75, C	--------		3	30.13, CH_2	1.96, m + 2.35, m
	5	118.64, CH	7.28, s		4	26.96, CH_2	1.99, m+ 2.14, m
	=N-	--------	--------		5	49.14, CH_2	3.68, m + 3.86, m
	6	135.56, CH	8.60, s		=N-	--------	--------
	=NH	--------	--------	**AlaS-10**	1	nd	--------
	-NH-	--------	--------		2	nd	nd
Abu	1	nd	--------		3	nd	nd
	2	nd	nd		-NH-	--------	nd
	3	nd	nd	**AlaSO-11**	1	nd	--------
	4	nd	nd		2	nd	nd
	-NH-	--------	9.55, very brs		3	nd	nd
4-Meglu	1	nd	--------		-NH-	--------	nd
	2	nd	nd	**Ala-12**	1	175.40, C	--------
	3	nd	nd		2	51.35, CH	4.32, m
	4	nd	nd		3	17.64, CH_3	1.45, d (7.1)
	5	nd	--------		-NH-	--------	8.18 [a]
	6	18.63, CH_3	nd	**Asn**	1	179.13, C	--------
	-NH-	--------	nd		2	51.50/51.52 [c], CH	4.57, m
AlaSO-6	1	nd	--------		3	37.24, CH_2	2.64 [a] + 2.97 [a]
	2	nd	nd		4	nd	--------
	3	nd	nd		-NH-	--------	8.45, brs
	-NH-	-------	nd		-CONHCO-	--------	n.d

[*] AA with modified CO within the backbone**,** [a] Overlapped, [b] Masked by water/solvent ^{1}H/^{13}C-NMR signals, [c] Interchangeable, [d] Weak, [nd] not determined

Table 20. ^{1}H, and ^{13}C-NMR data of nocathioamide B (**2**) (d_4-CH_3OH; 400 MHz; major conformer)

Residue	**Position**	δ_C / δ_N	**δ_H, mult (*J* in Hz)**	**Residue**	**Position**	δ_C / δ_N	**δ_H, mult (*J* in Hz)**
Ac	1	173.21, C	--------	**Dha**	1	166.48, C	--------
	2	22.67, CH_3	2.02, s		2	138.74, C	--------
Ala-1 *	1	49.09 [b], CH	5.31, m		3	109.46, CH_2	5.26 + 5.33, brs
	2	21.05, CH_3	1.61, d (7.1)		-NH-	--------	--------
	-NH-	--------	--------	**Leu**	1	173.88, C	--------
Thz	1	163.95, C	--------		2	50.69, CH	4.87 [b]
	2	149.87, C	--------		3	42.20, CH_2	1.45, m + 1.81, m
	3	126.55, CH	8.18, s		4	26.26, CH	1.67, m
	4	176.97, C	--------		5	22.10, CH_3	0.93, d (6.7)
	=N-	--------	--------		6	23.82, CH_3	0.97, d (6.7)
His *	1	208.43 [d], C	--------		-NH-	--------	--------
	2	60.90, CH	5.18, t (7.6)	**Pro**	1	175.14, C	--------
	3	30.45, CH_2	3.48, m + 3.58, m		2	63.01, CH	4.59, m
	4	130.75, C	--------		3	33.26, CH_2	2.34, m
	5	119.06, CH	7.47, s		4	23.17, CH_2	1.84, m + 2.06, m
	=N-	--------	--------		5	48.30, CH_2	3.64, m
	6	135.30, CH	8.86, s		=N-	--------	--------
	=NH	--------	--------	**AlaS-10**	1	172.15, C	--------
	-NH-	--------	--------		2	58.79, CH	3.10 dd (13.4, 4.2) + 3.50 [a]
Abu	1	170.59, C	--------		3	34.78, CH_2	4.24, dd (13.4, 4.0)
	2	65.85, CH	5.55, brs		-NH-	--------	--------
	3	44.77, CH	3.97, m	**AlaSO-11**	1	171.11, C	--------
	4	20.21, CH_3	1.13, d (7.0)		2	49.52, CH	5.14, m
	-NH-	--------	--------		3	59.84, CH_2	3.45, m + 3.68, m
4-Meglu	1	172.74, C	--------		-NH-	--------	--------
	2	53.34, CH	4.68, m	**Ala-12**	1	175.24, C	--------
	3	35.58, CH_2	1.52, m + 2.22, m		2	51.27, CH	4.16, m
	4	36.81, CH	2.40, m		3	18.21, CH_3	1.38, d (7.2)
	5	179.51, C	--------		-NH-	--------	--------
	6	18.60, CH_3	0.81, d (7.0)	**Asn**	1	179.02, C	--------
	-NH-	--------	--------		2	51.58, CH	4.52, dd (9.1, 5.7)
AlaSO-6	1	167.64, C	--------		3	37.28, CH_2	2.65, dd (17.8, 5.7) + 2.98, dd (17.8, 9.1)
	2	51.54, CH	4.71, m		4	178.23, C	--------
	3	55.63, CH_2	3.37, m + 3.83, m		-NH-	--------	--------
	-NH-	--------	--------		-CONHCO-	--------	--------

[*] AA with modified CO within the backbone**,** [a] Overlapped, [b] Masked by water/solvent ^{1}H/^{13}C-NMR signals, [c] Interchangeable, [d] Weak, [nd] not determined

Table 21. ^{1}H, and ^{13}C-NMR data of nocathioamide B (**2**) (d_4-CH_3OH; 400 MHz; minor conformer)

Residue	**Position**	δ_C / δ_N	δ_H, **mult (*J* in Hz)**	**Residue**	**Position**	δ_C / δ_N	δ_H, **mult (*J* in Hz)**
Ac	1	nd	--------	**Dha**	1	nd	--------
	2	21.01, CH_3	2.04, s		2	nd	--------
Ala-1 *	1	49.09 [b], CH	5.26 [a]		3	nd	nd
	2	21.05, CH_3	1.61 [a]		-NH-	-------	--------
	-NH-	--------	--------	**Leu**	1	nd	--------
Thz	1	nd	--------		2	nd	4.50
	2	149.95, C	--------		3	nd	nd
	3	126.38, CH	8.14, s		4	26.47, CH	1.77
	4	177.00, C	--------		5	nd	0.95 [a]
	=N-	--------	--------		6	nd	1.00, d (6.6)
His *	1	nd	--------		-NH-	-------	--------
	2	nd	5.15, m	**Pro**	1	n.d	--------
	3	30.30, CH_2	3.48 [a] + 3.58 [a]		2	64.87, CH	4.33, m
	4	131.03, C	--------		3	30.29, CH_2	2.00, m + 2.36, m
	5	118.88, CH	7.37, s		4	27.07, CH_2	2.00, m + 3.14, m
	=N-	--------	--------		5	49.28, CH_2	3.68, m + 3.88, m
	6	135.20, CH	8.81, s		=N-	-------	--------
	=NH	--------	--------	**AlaS-10**	1	nd	--------
	-NH-	--------	--------		2	nd	nd
Melan	1	nd	--------		3	nd	nd
	2	nd	nd		-NH-	-------	--------
	3	nd	nd	**AlaSO-11**	1	nd	--------
	4	nd	nd		2	nd	nd
	-NH-	--------	--------		3	nd	nd
4-Meglu	1	nd	--------		-NH-	-------	--------
	2	nd	nd	**Ala-12**	1	175.34, C	--------
	3	nd	nd		2	51.36, CH	4.33, m
	4	nd	nd		3	17.73, CH_3	1.46, d (7.0)
	5	nd	--------		-NH-	-------	--------
	6	nd	nd	**Asn**	1	179.10, C	--------
	-NH-	--------	--------		2	nd	4.57, m
AlaSO-6	1	nd	--------		3	37.32, CH_2	2.65 [a] + 2.98 [a]
	2	nd	nd		4	nd	--------
	3	nd	nd		-NH-	-------	--------
	-NH-	-------	--------		-CONHCO-	-------	--------

[*] AA with modified CO within the backbone**,** [a] Overlapped, [b] Masked by water/solvent ^{1}H/^{13}C-NMR signals, [c] Interchangeable, [d] Weak, [nd] not determined

4.4 Deciphering The Absolute Configuration of Nocathioamides Using Stable Isotope Labeling

The employment of different isotopically labeled amino acids within the currently developed metabologenomic approach enabled swiftly the determination of the stereochemistry of these amino acids via their observed mass shifts. The L- configuration delivers the intact mass shift while the D- version is observed with less 1 Da drift as a result of the stereochemistry flip at the α- position of the amino acid of interest.[169] Thus, the [$^2H_{10}$] L-Leu, and [$^2H_7$] L-Pro addition into IFM 0406 cultures in combination with their LCMS profiles indicated that Leu-5 (4-Meglu) and Leu-8 possess D- configuration whereas Pro-9 is architectured in L-format (Figures 34 and 35).

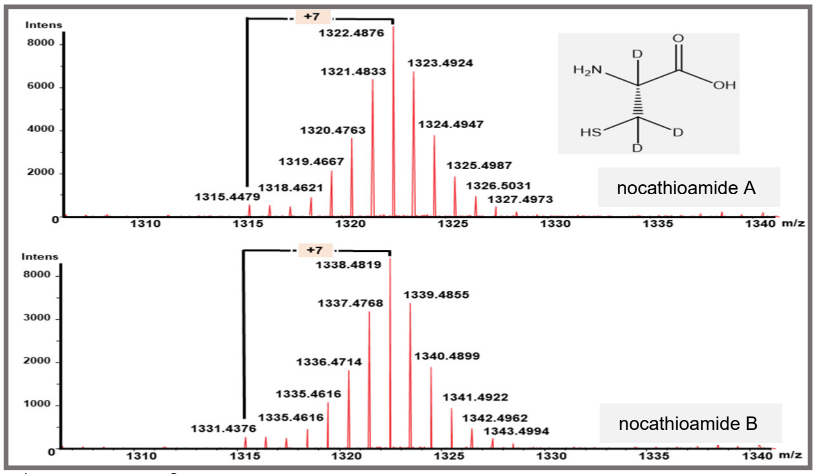

Figure 48. MS^1 spectra of [$^2H_3$] L-cysteine labeling experiment of nocathioamide A (**1**) and B (**2**)

Similarly, the supplementation of [$^2H_3$] L-cysteine decoded that Cys-10 (AlaS-10) and Cys-11 (AlaS-11 & AlaSO-11) are L-configured (Figure 48) in nocathioamides A (**1**) and B (**2**). Within the same context but in a different feeding fashion, the pulsed addition of [$^2H_4$] L-alanine after 3 and 4 successive days from the initial inoculation revealed in the MS profiles a mass shift of +8 Da (Figure 49) which was traced up at the MS^2 level concluding the L-stereochemistry of Ala-1 and Ala-12 residues (Figures 50, 51 and 52) in nocathioamides (Figure 53).

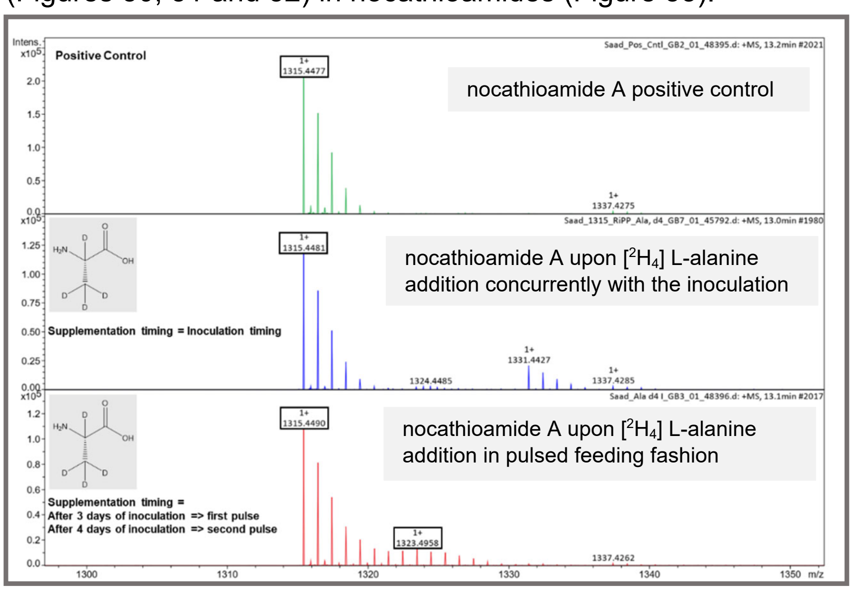

Figure 49. MS^1 spectra of nocathioamide A (**1**) and its [$^2H_4$] L-alanine labeled version

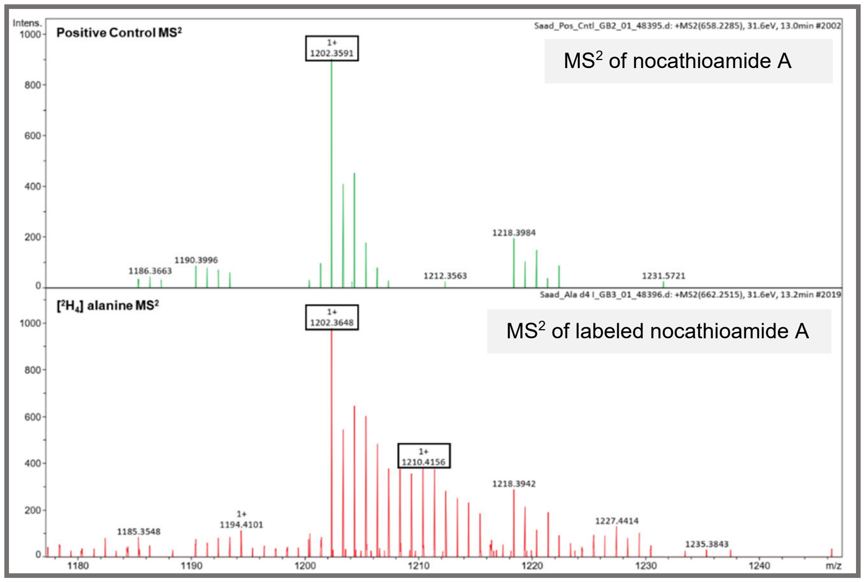

Figure 50. MS^2 spectra of nocathioamide A (**1**) and its [$^2H_4$] L-alanine labeled version

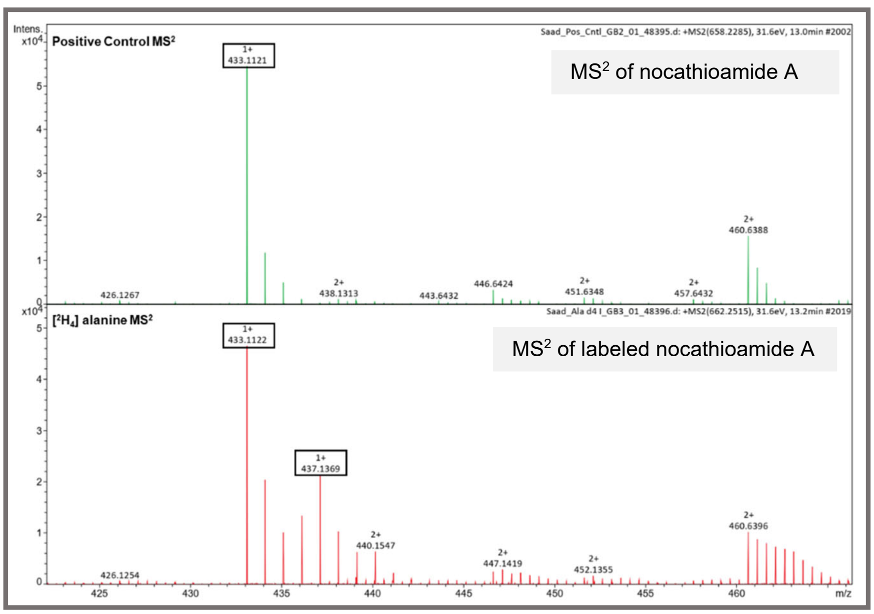

Figure 51. MS^2 spectra of nocathioamide A (**1**) and its [$^2H_4$] L-alanine labeled version

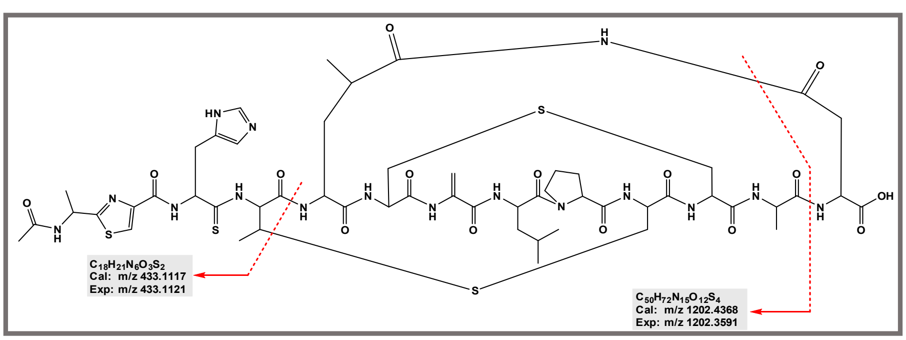

Figure 52. Schematic fragmentation of the key MS^2 fragments of nocathioamide A (**1**) highlighting the [$^2H_4$] L-Ala labeling

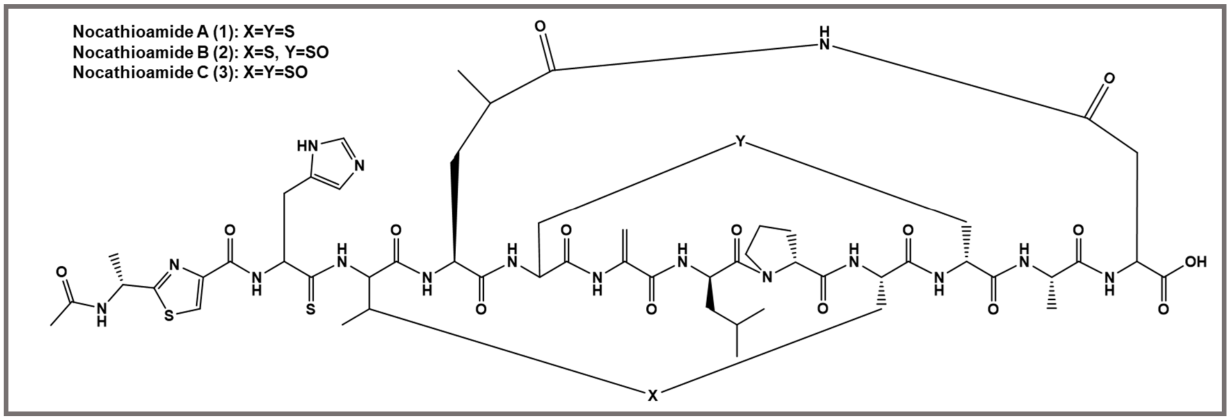

Figure 53. The elucidated chiral centers of the nocathioamides molecular family

4.5 Molecular Network Leveraging The Nocathioamides Molecular Family

To expedite further the molecular family, the recruitment of a Feature-Based Molecular Networking (FBMN) analysis seamlessly unveiled an additional suite of nocathioamide variants (Figure 54 and Table 22).[160]

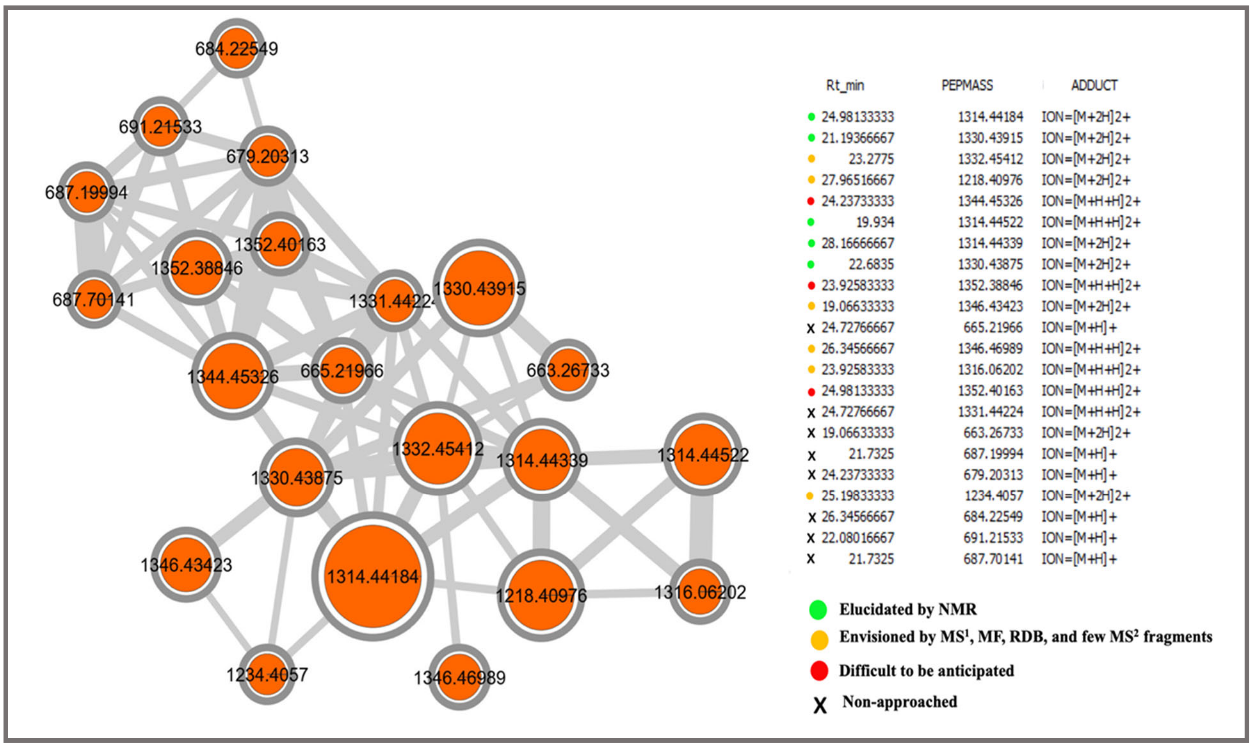

Figure 54. Molecular network of the nocathioamides molecular family

One of the noticeable ion was M= 1218.40976 Da, accounting for $C_{50}H_{70}N_{14}O_{14}S_4$ with 23 RDB, which was annotated as nocathioamide D (**4**) based on the few interpreted MS^2 fragments. Its architecture was dereplicated with a characteristic structural loss of Asn-13 residue and hence the breakage of the macrocyclic imide bridge (Figures 55 and Table 22).[16]

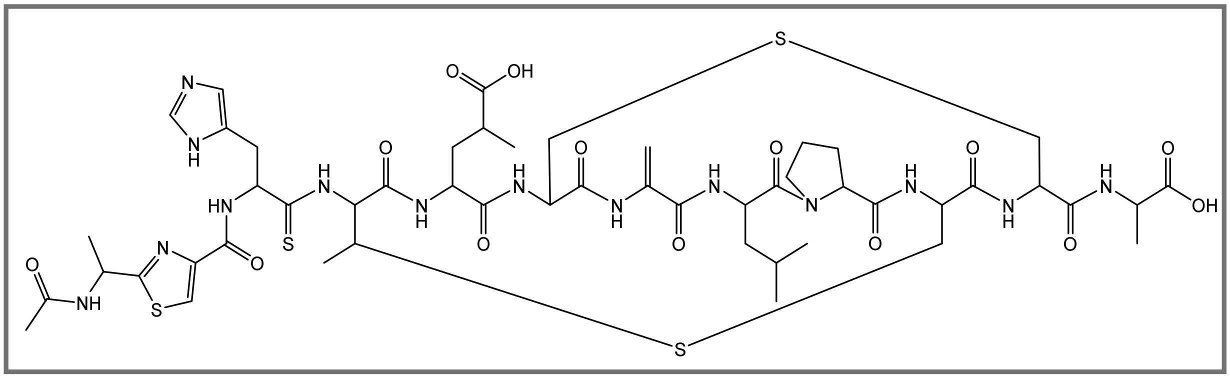

Figure 55. Putative chemical structure of nocathioamide D (**4**)

Table 22. Annotated members of the nocathioamides molecular family

[M]	Adduct	Rt (min)	Calculated Formula	Error (ppm)	RDB	(Tentative) structural modification(s) relative to nocathioamide A (1)
1314.44118	$[M+2H]^{2+}$, $[M+H]^{+}$	24.98	$C_{54}H_{74}N_{16}O_{15}S_4$	0.3	26	Nocathioamide A (**1**)
1330.43915	$[M+2H]^{2+}$, $[M+H]^{+}$	21.19	$C_{54}H_{74}N_{16}O_{16}S_4$	1.7	26	Nocathioamide B (**2**) (monosulfoxidation of Lan)
1346.43423	$[M+2H]^{2+}$, $[M+H]^{+}$	19.06	$C_{54}H_{74}N_{16}O_{17}S_4$	3.2	26	Nocathioamide C (**3**) (disulfoxidation of Lan , and MeLan)
1346.46989	$[M+2H]^{2+}$, $[M+H]^{+}$	26.34	$C_{55}H_{78}N_{16}O_{16}S_4$	2.6	25	Monosulfoxidation of (Me)Lan + 1 less RDB (possibly Dha => Ala)[16] + an extra CH_2
1332.45412	$[M+2H]^{2+}$, $[M+H]^{+}$	23.28	$C_{54}H_{76}N_{16}O_{16}S_4$	2.8	25	Monosulfoxidation of (Me)Lan + 1 less RDB (possibly Dha => Ala)[16]
1218.40976	$[M+2H]^{2+}$, $[M+H]^{+}$	27.97	$C_{50}H_{70}N_{14}O_{14}S_4$	2.5	23	Nocathioamide D (**4**) [17]
1234.4057	$[M+2H]^{2+}$, $[M+H]^{+}$	25.19	$C_{50}H_{70}N_{14}O_{15}S_4$	2.3	23	Nocathioamide D [17]+ monosulfoxidation of Me(Lan)
1344.45326	$[M+2H]^{2+}$, $[M+H+Na]^{2+}$	24.24	$C_{55}H_{76}N_{16}O_{16}S_4$	1.8	26	????
1352.38846	$[M+2H]^{2+}$, $[M+H]^{+}$	23.92	$C_{53}H_{72}N_{14}O_{20}S_4$ $C_{56}H_{68}N_{14}O_{20}S_3$ $C_{55}H_{68}N_{16}O_{17}S_4$	3.4//14.3 1.4//15.0 3.9//18.8	25 30 30	????
1314.44522	$[M+2H]^{2+}$, $[M+H]^{+}$	19.93	$C_{54}H_{74}N_{16}O_{15}S_4$, Conformer 1	3.8	26	Conformer I of nocathioamide A
1314.44339	$[M+2H]^{2+}$, $[M+H]^{+}$	28.16	$C_{54}H_{74}N_{16}O_{15}S_4$, Conformer 2	2.6	26	Conformer II of nocathioamide A
1330.43875	$[M+2H]^{2+}$, $[M+H]^{+}$	22.68	$C_{54}H_{74}N_{16}O_{16}S_4$, Conformer	2.9	26	Conformer of nocathioamide B

4.6 Evaluations of The Biological Activity

In guideline-conform determinations of the minimal inhibitory activity (MIC) by broth microdilution, nocathioamide A (**1**) and B (**2**) were inactive against an ESKAPE strain panel (of all eponymous species a representative strain was tested) as well as *Bacillus subtilis* and *Mycobacterium smegmatis* up to the highest concentration tested (MIC > 32 µg/ml, Table 23). Lack of antifungal activity was also noted against *Candida albicans*, *C. glabrata* and *C. tropicalis* (MIC > 32 µg/ml) and the metabolic activity of the HeLa cell line was not affected at 64 µg/ml (Table 23). Since **1** and **2** did not exhibit the classic biological activity of RiPPs, we assume that nocathioamides might possess an ecological or physiological function.

Table 23. Bioassay results. The letters indicated in red refer to the ESKAPE panel, an acronym comprising the scientific names of six highly virulent and resistant bacterial pathogens.

Antibacterial Assay			
	MIC in µg/ml		
	Nocathioamide A (1)	**Nocathioamide B (2)**	
***Enterococcus faecium* BM4147-1**	>32	>32	
***Staphylococcus aureus* ATCC 29213**	>32	>32	
***Klebsiella pneumoniae* ATCC 12657**	>32	>32	
***Acinetobacter baumannii* 09987**	>32	>32	
***Pseudomonas aeruginosa* ATCC 27853**	>32	>32	
***Enterobacter aerogenes* ATCC 13048**	>32	>32	
***Escherichia coli* ATCC 25922**	>32	>32	
***Bacillus subtilis* 168**	>32	>32	
***Staphylococcus aureus* NCTC 8325**	>32	>32	
***Mycobacterium smegmatis* mc^2 155 ATCC 700084**	>32	>32	
Antifungal Assay			
	MIC in µg/ml		
	Nocathioamide A (1)	**Nocathioamide B (2)**	**Caspofungin**
***Candida albicans* TüC01**	>32	>32	0.125
***Candida albicans* TüC02**	>32	>32	0.06
***Candida albicans* TüC03**	>32	>32	0.06
***Candida glabrata* TüC04**	>32	>32	0.125
***Candida tropicalis* TüC05**	>32	>32	0.25
Cytotoxicity Assay			
	IC_{50} in µg/ml		
	Nocathioamide A (1)	**Nocathioamide B (2)**	
HeLa cell line	>64	>64	

4.7 Biosynthetic Considerations and Classification of Nocathioamides

The performed bioinformatic prediction of the final product was largely correct but was, owing to the novelty of the involved genes cocktail, not able to predict a) the exact cleavage site, and therefore the length of the peptide, b) the imide ring closure, c) the catalytic activity of the methyltransferase NtaC and d) that only one acetylation reaction will take place despite the presence of two acetyltransferase encoding genes (*ntaH* and *ntaN*).

Regarding the latter issue, apparently only one acetyltransferase is contributing to the acetylation. We hypothesize that NtaH is the decisive enzyme for the N-acetylation of the Ala-1 residue due to the analysis of the very recently sequenced genome of *Longimycelium tulufanense* CGMCC 4.5737 (NZ_BMMK01000000)[161] which also contained the *nta* cluster (Table 9). Strikingly, all annotated *nta* genes exhibited a high identity and similarity score, except for NtaN which showed no significant similarity with all proteins of strain CGMCC 4.5737.

Since the nocathioamides A-C (**1-3**) bear no C- or N-methylated groups, but instead carries two D-configured leucine residues, the methyltransferase, NtaC, was hypothesized to be involved in the amino acid epimerization process, which is well established in the RiPP members of proteusin in which the rSAM epimerase is the responsible enzyme of carrying out such a PTM.[171]

From a PTM point of view, nocathioamides represent hypermodified RiPPs. 11 out of its 13 residues underwent different and specific enzymatic modifications to deliver unique chemical alterations [(Me)Lan, thioamidation, azole formation, N-acetylation, (C and S) oxidation, dehydration, epimerisation, and macroimidation].

Most intriguing is the unusual oxidation of the δ-carbon atom of Leu-5 (4-Meglu) residue, possibly mediated by the action of the cytochrome P450 enzyme (CYP450) NtaM, which prepares the molecule for a macrocylic imide ring closure. To the best of our knowledge, such a regio-specific CYP450-based oxidation reaction of Leu-5 was formerly reported so far for only seven NRPS-derived natural products, such as echinocandins, nostopeptolide, polyoxypeptin B, griselimycin, perthamide C, monamycin D and ilamycin, but never in a RiPP context (Figure 56).[172]

Moreover, the involved oxidative reactions never led to an imide macrocyclization, but rather to acyclic 4-methylglutamate or five and six-membered heterocycles such as 4-methylproline or cyclic hemiaminal substructures, respectively (Figure 56). Imide moieties themselves exist in several secondary metabolites, however either as succinimide or glutarimide units but not as a key element for ring closures of macrocycles, highlighting the uniqueness of nocathioamides again.

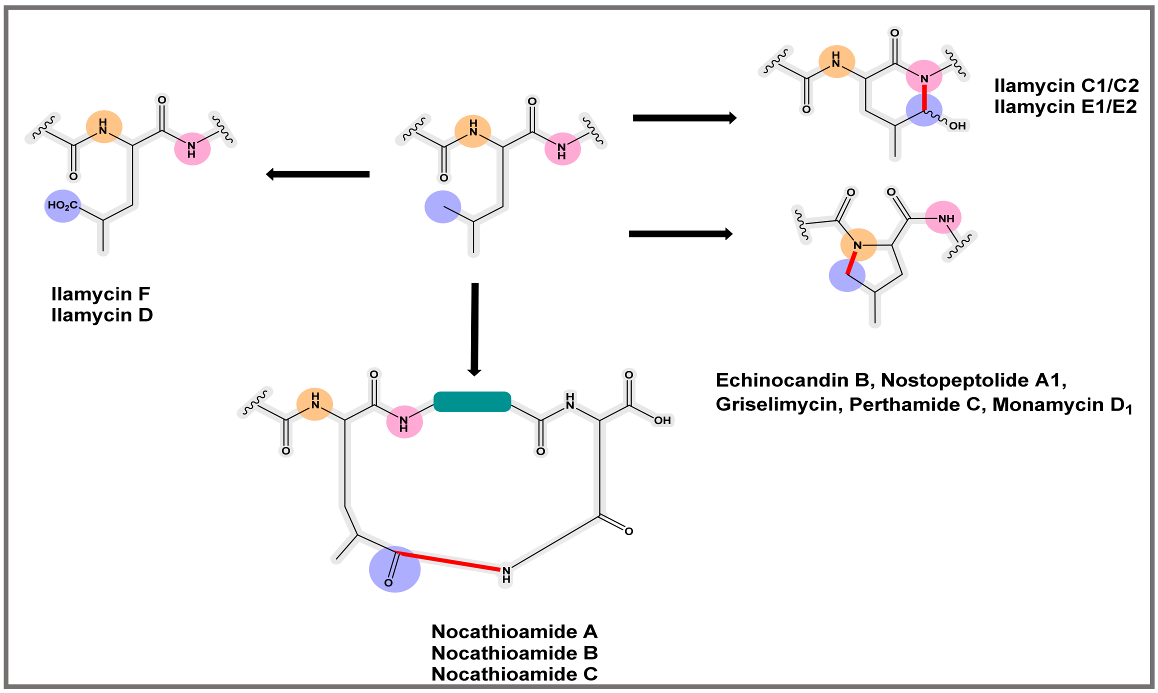

Figure 56. Different fates of oxidized δ-Methyl leucine (4-methylglutamate)

Another feature of the nocathioamide family is the single and double sulfoxidation of Lan and MeLan bridges. Remarkably, such unique oxidation was described in only a few RiPPs, such as the lanthipeptides actagardines, NAI-107 B1/B2 and NAI-802 (Figure 57).[84a,173]

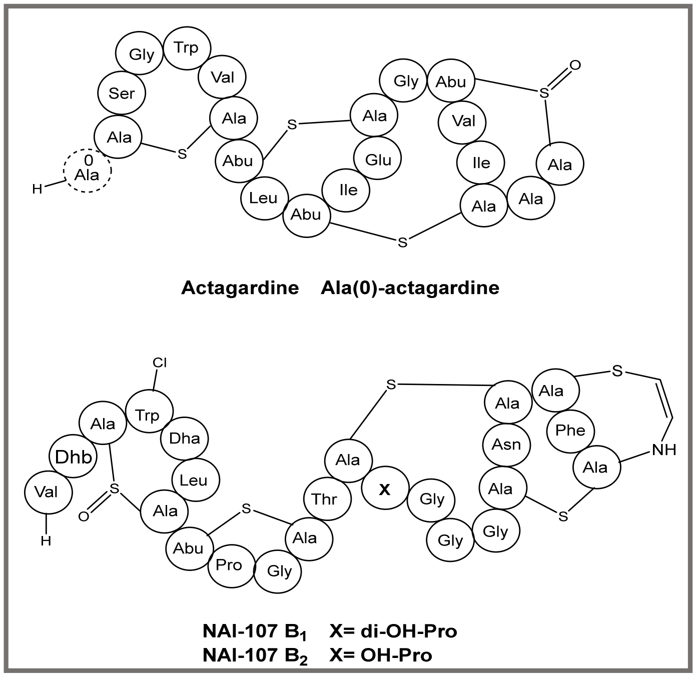

Figure 57. Exemplary RiPPs scaffolds framing a sulfoxide feature

However, in comparison to these molecules nocathioamide congener B (**2**) represents, besides NAI-107 B1/B2, the second example of a monosulfoxidized class I lanthipeptide, and C (**3**) expanded the scope of this novel modification to be carried out simultaneously on Lan and MeLan moieties as a disulfoxide for the first time. In addition, the process of sulfoxidation has been suggested either to be enzymatically controlled by a clustered monooxygenase or occur spontaneously under alkaline conditions.

To classify nocathioamides according to the rules of the RiPP community,[77] we consulted the *nta* BGC. Concerning the precursor peptide we found a hitherto unknown new AP cleavage site. Furthermore, we observed the presence of a split lanB-like dehydratase (*ntaF*/*ntaG*) beside a lanC like cyclase (*ntaB*), which clearly categorized the nocathioamides as a member of class I lanthipeptides. Notably, the co-occurrence of a split lanB with lanC was singly reported for class I lantibiotics of the antifungal pinensins despite its frequent existence in LAPs and thiopeptides.[16,74a,95d]

It is also noteworthy to mention the thioamidation, which exclusively occurs at the His residue. In contrast to the few so far discovered thioamide containing RIPPs, recent genome mining efforts commenced to leverage and expand this chemical space with new thioamidated candidates either as thioviridamide-similar entities or as thiopeptides, exemplified by saalfelduracin and thiopeptin.[50a,53a,53b]

Interestingly, the associations of lanthionine synthetases with either F-dependent and/or TfuA-paired YcaOs were bioinformatically projected before by the teams of Mitchell and van der Donk to chart novel multi-biosynthetic systems which were followed up by their engineering efforts through combinatorial biosynthesis to mix and match new-to-nature hybrid RiPPs as thiazolinyl–lanthipeptides (I, II).[76,174] Along the same lines, the nocathioamide family elegantly symbolises the first-in-nature combinatorial tribrid RiPPs hovering over three different class-defining biosynthetic machineries of lanthipeptides, LAPs and thioamitides, decorated with an additional unique PTM.

4.8 Genome Mining of The Nocapeptin Biosynthetic Gene Cluster in *Nocardia terpenica* IFM 0406 and 0706^{T}

In the adjacent vicinity to the nocathioamide locus, an additional set of RiPP genetic elements were grouped as a new RiPP-BGC encoding an unknown lasso peptide, entitled nocapeptin (Figure 58).[150a,150b]

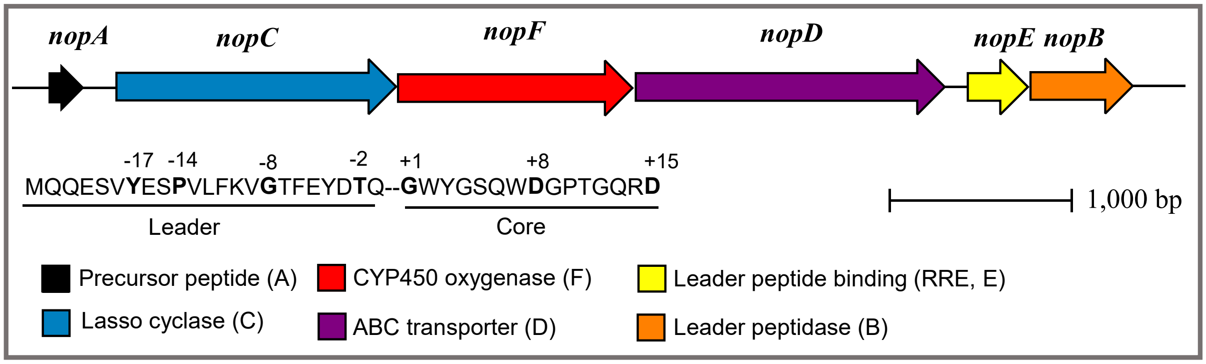

Figure 58. Putative biosynthetic gene cluster (BGC) of nocapeptin

The antiSMASH and RODEO results disclosed a new member of class II lasso peptides counting on the sequence of the precursor peptide*, nopA*. Classically, the annotation of the neighboring ORFs completed the necessary genetic suite for biosynthesizing the nocapeptin scaffold where the lasso cyclase (*nopC*, PF00733), as an asparagine synthetase homolog, was co-localized with a transglutaminase-like enzyme, termed leader peptidase (*nopB*, PF13471) (Table 24, Figure 58).[120c]

Notably, the RRE was found to be encoded as a standalone protein (NopE, PF05402)[96d,162] in conjunction with the expected ABC transporter-encoding gene (*nopD*, TIGR02204/PF00005). Interestingly and as a foundational motive for the current investigation, the nocapeptin BGC was found to additionally frame a cytochrome P450 gene (*nopF*, PF00067) (Table 24).

Table 24. Putative functions of proteins from the *nop* BGC using RODEO

	Automated RODEO Analysis				
Protein	Accession Nr.	Length [aa]	PFAM (TIGRFam) hits	Description	E-value
NopA	WP_195116738.1	43	--------------------	----------------	----------
NopC	WP_171983240.1	547	PF00733	Asparagine synthase	$4.20E^{-36}$
NopF	WP_156674500.1	404	TIGR04515 / TIGR04538	Cytochrome P450	$4.00E^{-50}$
NopD	WP_171983239.1	575	TIGR02204	ABC transporter	$9.40E^{-96}$
NopE	WP_067588831.1	86	PF05402	Stand alone lasso RRE	$2.10E^{-27}$
NopB	WP_082871451.1	157	PF13471	Transglutaminase	$7.60E^{-24}$

Taking into account the former bioinformatic annotations, we expected a mature lasso peptide consisting of a 15 AA sequence where the predictable proteolytic site is occurring at Gly+1 and Thr-2 catalyzed by the dual effects of NopE and NopB proteins (Figure 58). The cleaved CP shall be threaded to afford the lasso framework through the typical formation of an isopeptide bond between Gly+1 and Asp+8 residues (Figures 58 and 59) employing an ATP-mediated mechanism by NopC. Subsequently, the extracellular export of the final product is achieved via the transporter, NopD.[69a,119b]
In addition, the existence of CYP450 monooxygenase within *nop* BGC suggested that extra tailoring(s) is probably expected in the predicted peptide through either an oxidative and/or reductive event(s) which cannot be speculated bioinformatically.

Driven by the unmatched precursor peptide sequence in tandem with the unprecedented co-occurrence of cytochrome enzyme within lasso peptides BGCs in general, we commenced a media screening with IFM 0406 to deorphanize the *nop* gene cluster.

4.9 Targeted Identification of Nocapeptin(s) Using Metabologenomics

Similar to the nocathioamides discovery line and the ability to formulate a definitive *m/z* value(s) considering the bioinformatic analysis (Figure 59), an LCMS-guided campaign was recruited for the media screening of IFM 0406. In the light of the possible oxidative events that can be induced by NopF, hydroxylated variants and/or oxidized products were regarded during the inspection of the MS screening data.

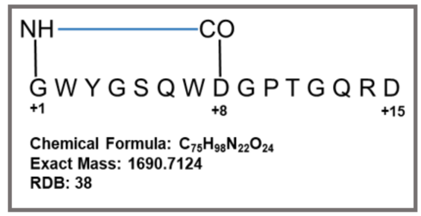

Figure 59. The predicted structure of nocapeptin

Out of almost 30 different cultivating recipes, the LCMS profiles of the modified R4 medium exclusively afforded a candidate with *m/z* values 845.356 and 563.9068 Da as $[M+2H]^{2+}$, $[M+3H]^{3+}$ features, respectively (Figure 60). Interestingly, the molecular formula prediction using the HRMS measurements was in an excellent agreement with the predicted CP sequence tailored with the macrolactam modification except for less 2 Da translated into – 2H in the form of an extra RDB within the lasso scaffold (Table 25).

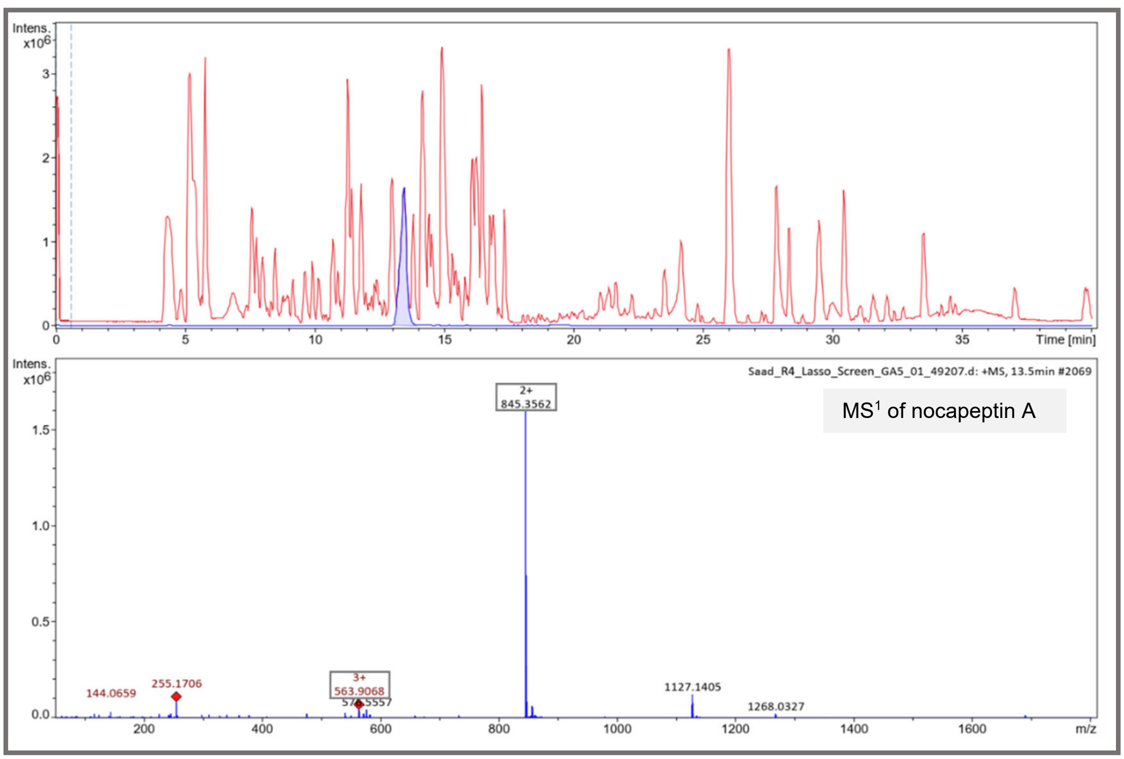

Figure 60. LCMS profile of R4 medium highlighting the nocapeptin A (**5**) production

Table 25. Molecular formula prediction of nocapeptin A (**5**)

Meas. *m/z*	Ion Formula	Calc. *m/z*	Error [ppm]	RDB	mSigma
563.907016	$C_{75}H_{99}N_{22}O_{24}$	563.906204	1.4	39	4.9
845.356216	$C_{75}H_{98}N_{22}O_{24}$	845.355667	0.9	39	3.3

To certify the feature of interest, the MS² fragments were studied to validate the *de novo* sequence of the peptide and hence fortify the connection between the questionable chemical entities and the lasso peptide BGC under investigation (Figures 61 and 62).

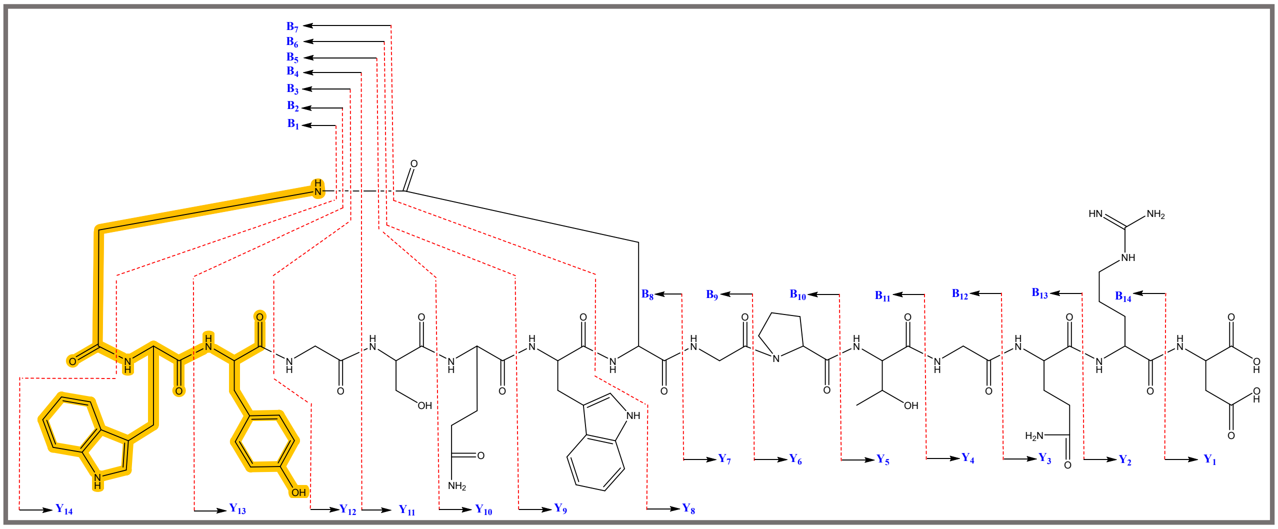

Figure 61. Schematic fragmentation of nocapeptins highlighting the localization of the crosslink

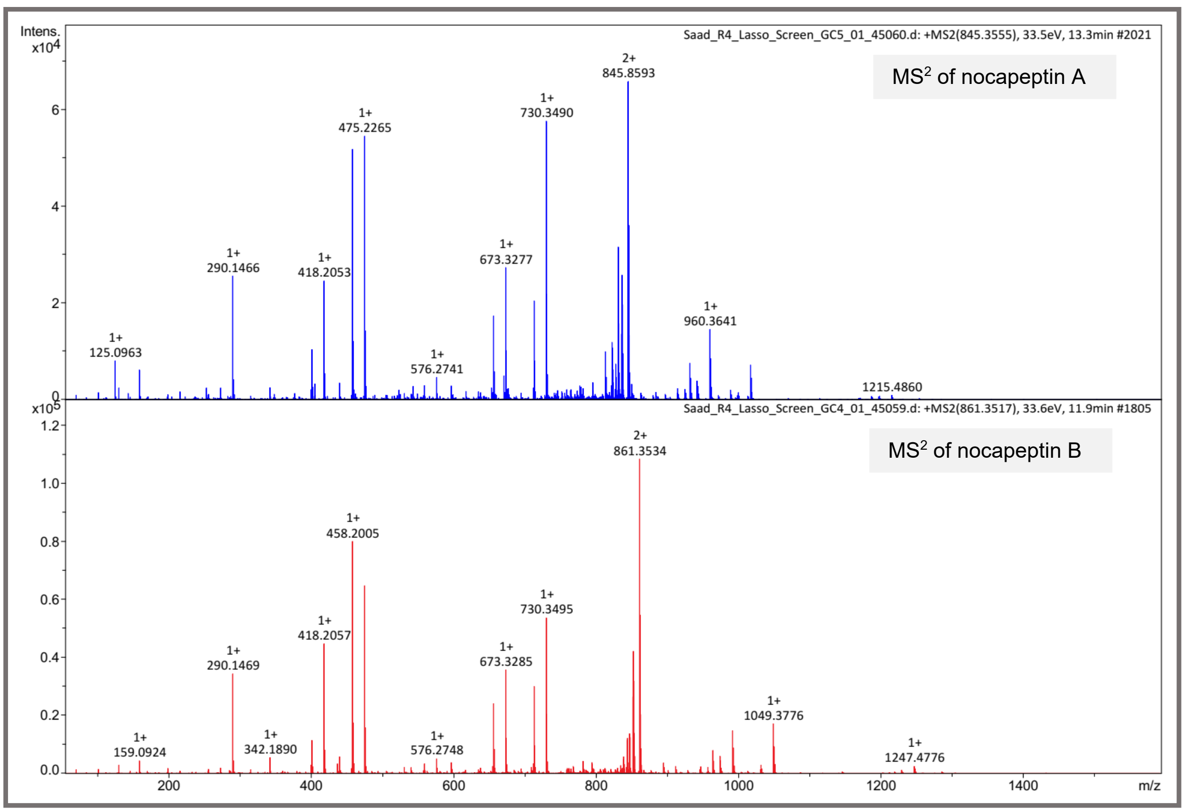

Figure 62. Comparative MS² profiles of nocapeptin A (**5**) and B (**6**)

The collisional-induced dissociation (CID) fragments of the $[M+2H]^{2+}$ feature of nocapeptin A (**5**) expectedly delivered a series of *y* ions that unequivocally proved the tail sequence. Despite the less probability to observe *y* ions arising from the ring breakage, a set of low intense fragments (y_9, y_{10}, and y_{12}) was spotted thereby presenting a further alignment with the predicted CP (Table

26). Moreover, an array of *b* ions was deconvoluted from the MS^2 spectrum confirming the order of the amino acids constituting the nocapeptin A ring and hence corroborating the BGC linkage (Figure 63, Table 26).

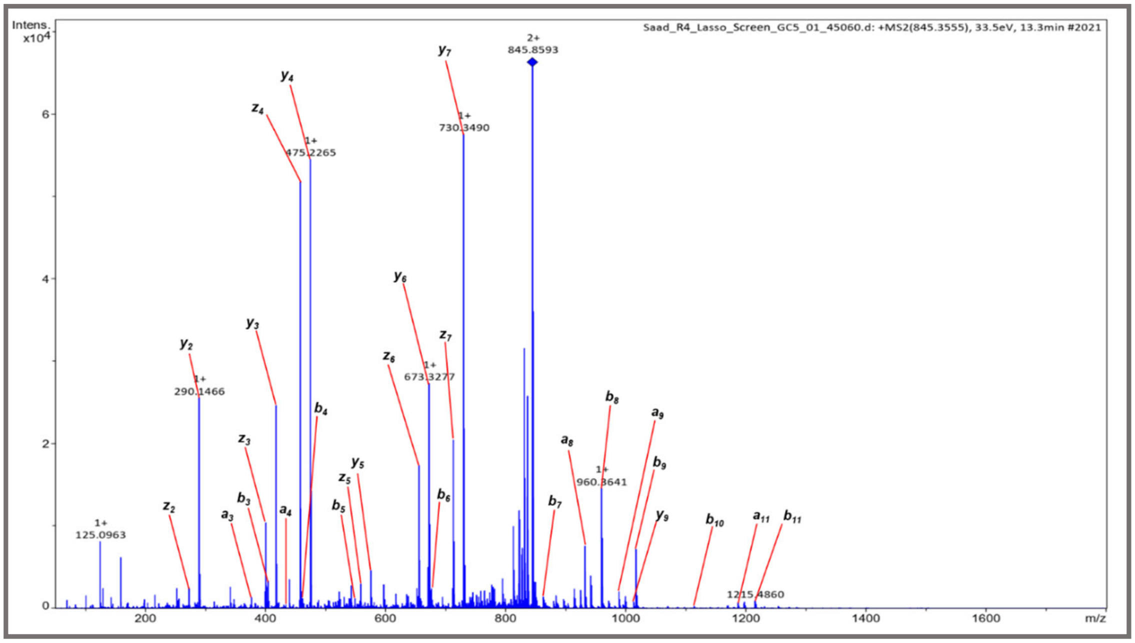

Figure 63. The annotated MS^2 spectrum of nocapeptin A (**5**)

Interestingly, the constant mass drift of 2 Da loss in the observed *b* ions series compared to the calculated ones and the absence of *m/z* values of b_1 / y_{14} and b_2 / y_{13} fragments facilitated the allocation of the extra crosslink morph to be specifically introduced into the first three N-terminal residues of the lasso ring, Gly+1, Trp+2, and Tyr+3 (Table 26).

Table 26. The assigned fragments of nocapeptin A (**5**)

Fragment	Ion Formula	RDB	Calc. *m/z*	Meas. *m/z*	Δ in ppm
y_1	$C_4H_8NO_4$	2	134.0453	134.0450	2.24
y_2	$C_{10}H_{20}N_5O_5$	4	290.1464	290.1466	0.69
z_2	$C_{10}H_{17}N_4O_5$	5	273.1199	273.1198	0.37
y_3	$C_{15}H_{28}N_7O_7$	6	418.2050	418.2053	0.72
z_3	$C_{15}H_{25}N_6O_7$	7	401.1785	401.1784	0.25
y_4	$C_{17}H_{31}N_8O_8$	7	475.2265	475.2265	0.00
z_4	$C_{17}H_{28}N_7O_8$	8	458.1999	458.2002	0.65
y_5	$C_{21}H_{38}N_9O_{10}$	8	576.2742	576.2741	0.17
z_5	$C_{21}H_{35}N_8O_{10}$	9	559.2476	559.2482	1.07
y_6	$C_{26}H_{45}N_{10}O_{11}$	10	673.3269	673.3277	1.19
z_6	$C_{26}H_{42}N_9O_{11}$	11	656.3004	656.3009	0.76
y_7	$C_{28}H_{48}N_{11}O_{12}$	11	730.3484	730.3490	0.82
z_7	$C_{28}H_{45}N_{10}O_{12}$	12	713.3218	713.3223	0.70
y_8	$C_{32}H_{51}N_{12}O_{14}$	14	827.3648	---------	---------
y_9	$C_{43}H_{61}N_{14}O_{15}$	21	1013.4441	1013.4434	0.69
z_9	$C_{43}H_{58}N_{13}O_{15}$	22	996.4175	996.4169	0.60
y_{10}	$C_{48}H_{69}N_{16}O_{17}$	23	1141.5027	1141.5036	0.79
y_{11}	$C_{51}H_{74}N_{17}O_{19}$	24	1228.5347	---------	---------

y_{12}	$C_{53}H_{77}N_{18}O_{20}$	25	1285.5562	1285.5639	5.98
z_{12}	$C_{53}H_{74}N_{17}O_{20}$	26	1268.5296	1268.5147	11.74
y_{13}	---------	---------	---------	---------	---------
y_{14}	---------	---------	---------	---------	---------
b_1	---------	---------	---------	---------	---------
b_2	---------	---------	---------	---------	---------
b_3	$C_{22}H_{21}N_4O_4$	15	405.1563	405.1562	0.25
a_3	$C_{21}H_{21}N_4O_3$	14	377.1614	377.1610	1.06
b_4	$C_{24}H_{24}N_5O_5$	16	462.1777	462.1778	0.22
a_4	$C_{23}H_{24}N_5O_4$	15	434.1828	434.1842	3.22
b_5	$C_{27}H_{29}N_6O_7$	17	549.2098	549.2099	0.18
a_5	$C_{26}H_{29}N_6O_6$	16	521.2149	521.2142	1.34
b_6	$C_{32}H_{37}N_8O_9$	19	677.2683	677.2675	1.18
a_6	$C_{31}H_{37}N_8O_8$	18	649.2734	649.2746	1.84
b_7	$C_{43}H_{47}N_{10}O_{10}$	26	863.3477	863.3494	1.97
b_8	$C_{47}H_{50}N_{11}O_{12}$	29	960.3640	960.3641	0.10
a_8	$C_{46}H_{50}N_{11}O_{11}$	28	932.3691	932.3705	1.50
b_9	$C_{49}H_{53}N_{12}O_{13}$	30	1017.3855	1017.3865	0.98
a_9	$C_{48}H_{53}N_{12}O_{12}$	29	989.3906	989.3904	0.20
b_{10}	$C_{54}H_{60}N_{13}O_{14}$	32	1114.4383	1114.4405	1.97
a_{10}	$C_{53}H_{60}N_{13}O_{13}$	31	1086.4434	1086.4480	4.23
b_{11}	$C_{58}H_{67}N_{14}O_{16}$	33	1215.4859	1215.4860	0.08
a_{11}	$C_{57}H_{67}N_{14}O_{15}$	32	1187.4910	1187.4883	2.27
b_{12}	$C_{60}H_{70}N_{15}O_{17}$	34	1272.5074	1272.5056	1.41
a_{12}	$C_{59}H_{70}N_{15}O_{16}$	33	1244.5125	1244.5106	1.53
b_{13}	$C_{65}H_{78}N_{17}O_{19}$	36	1400.5660	1400.5628	2.28
a_{13}	$C_{64}H_{78}N_{17}O_{18}$	35	1372.5711	1372.5808	7.07
b_{14}	$C_{71}H_{90}N_{21}O_{20}$	38	1556.6671	---------	---------

During our preliminary analysis of the LCMS data of the R4 medium extracts, a relevant minor feature (*m/z* 861.3517, $[M+2H]^{2+}$) was dereplicated to be structurally related to the nocapeptin A entity with a suggested ion formula of $C_{75}H_{98}N_{22}O_{26}$ and 39 RDB deciphering an additional tailoring with two oxygen atoms into the lasso architecture defining nocapeptin B (**6**) (Figure 62).
In a similar fashion to nocapeptin A, the MS^2 ions series of nocapeptin B (mainly *y* and *b* fragments) validated as well the sequence in terms of amino acid identities and order (Figure 64, Table 27). Expectedly, the further inter-linkage was found to be well kept within the ring sequence of the first three residues, Gly+1--Trp+2--Tyr3+ (Table 27). Moreover, the comparative CID-MS^2 fragments (b_n) of nocapeptin B against the annotated major entity eased the allocation of the additional oxidative reactions to be structurally located at the same sequence of residues chunk in the form of double hydroxylations (Table 27).

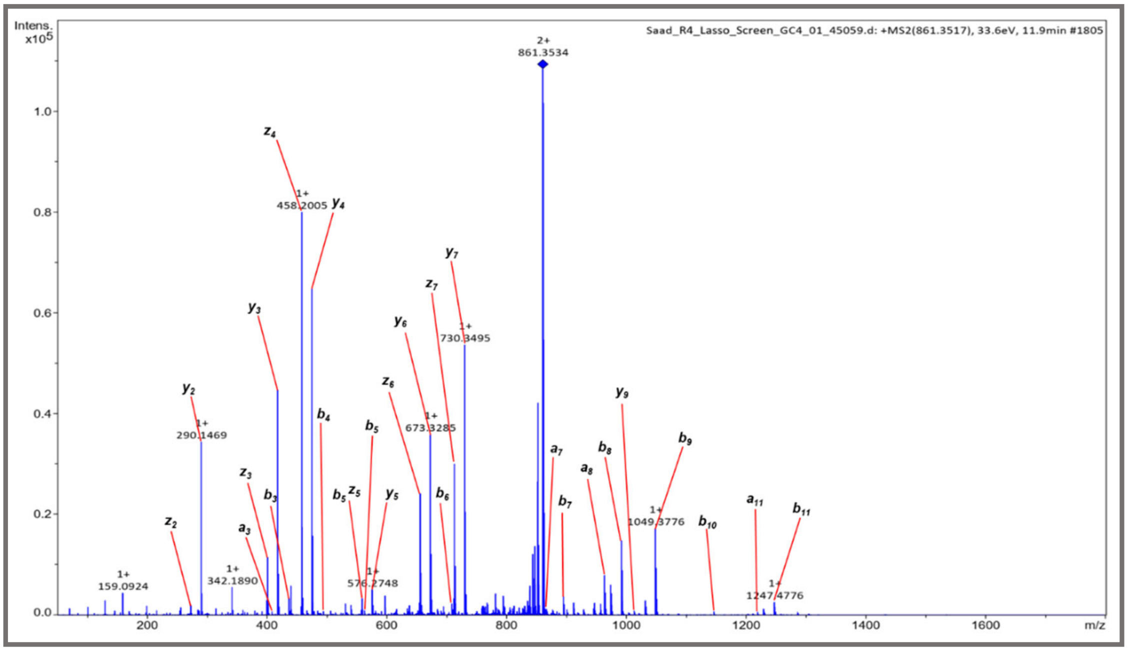

Figure 64. The annotated MS^2 spectrum of nocapeptin B (**6**)

Table 27. The assigned fragments of nocapeptin B (**6**)

Fragment	Ion Formula	RDB	Calc. *m/z*	Meas. *m/z*	Δ in ppm
y_1	$C_{10}H_{20}N_5O_5$	2	134.0453	134.0450	2.24
y_2	$C_{10}H_{20}N_5O_5$	4	290.1464	290.1469	1.72
z_2	$C_{10}H_{17}N_4O_5$	5	273.1199	273.1207	2.93
y_3	$C_{15}H_{28}N_7O_7$	6	418.2050	418.2057	1.67
z_3	$C_{15}H_{25}N_6O_7$	7	401.1785	401.1795	2.49
y_4	$C_{17}H_{31}N_8O_8$	7	475.2265	475.2273	1.68
z_4	$C_{17}H_{28}N_7O_8$	8	458.1999	458.2005	1.31
y_5	$C_{21}H_{38}N_9O_{10}$	8	576.2742	576.2748	1.04
z_5	$C_{21}H_{35}N_8O_{10}$	9	559.2476	559.2488	2.15
y_6	$C_{26}H_{45}N_{10}O_{11}$	10	673.3269	673.3285	2.38
z_6	$C_{26}H_{42}N_9O_{11}$	11	656.3004	656.3018	2.13
y_7	$C_{28}H_{48}N_{11}O_{12}$	11	730.3484	730.3495	1.50
z_7	$C_{28}H_{45}N_{10}O_{12}$	12	713.3218	713.3232	1.96
y_8	$C_{32}H_{51}N_{12}O_{14}$	14	827.3648	827.3652	0.48
y_9	$C_{43}H_{61}N_{14}O_{15}$	21	1013.4441	1013.4437	0.39
z_9	$C_{43}H_{58}N_{13}O_{15}$	22	996.4175	996.4167	0.80
y_{10}	$C_{48}H_{69}N_{16}O_{17}$	23	1141.5027	1141.4966	5.34
y_{11}	$C_{51}H_{74}N_{17}O_{19}$	24	1228.5347	---------	---------
y_{12}	$C_{53}H_{77}N_{18}O_{20}$	25	1285.5562	1285.5593	2.41
y_{13}	---------	---------	---------	---------	---------
y_{14}	---------	---------	---------	---------	---------
b_1	---------	---------	---------	---------	---------
b_2	---------	---------	---------	---------	---------
b_3	$C_{22}H_{21}N_4O_6$	15	437.1461	437.1465	0.92
a_3	$C_{21}H_{21}N_4O_5$	14	409.1512	409.1508	0.98
b_4	$C_{24}H_{24}N_5O_7$	16	494.1676	494.1684	1.62

b$_5$	$C_{27}H_{29}N_6O_9$	17	581.1996	581.2012	2.75
a$_5$	$C_{26}H_{29}N_6O_8$	16	553.2047	553.2033	2.53
b$_6$	$C_{32}H_{37}N_8O_{11}$	19	709.2582	709.2588	0.85
a$_6$	$C_{31}H_{37}N_8O_{10}$	18	681.2633	681.2683	7.34
b$_7$	$C_{43}H_{47}N_{10}O_{12}$	26	895.3375	895.3382	0.78
a$_7$	$C_{42}H_{47}N_{10}O_{11}$	25	867.3426	867.3448	2.54
b$_8$	$C_{47}H_{50}N_{11}O_{14}$	29	992.3539	992.3546	0.71
a$_8$	$C_{46}H_{50}N_{11}O_{13}$	28	964.3590	964.3606	1.66
b$_9$	$C_{49}H_{53}N_{12}O_{15}$	30	1049.3753	1049.3776	2.19
a$_9$	$C_{48}H_{53}N_{12}O_{14}$	29	1021.3804	1021.3828	2.35
b$_{10}$	$C_{54}H_{60}N_{13}O_{16}$	32	1146.4281	1146.4279	0.17
a$_{10}$	$C_{53}H_{60}N_{13}O_{15}$	31	1118.4332	1118.4271	5.45
b$_{11}$	$C_{58}H_{67}N_{14}O_{18}$	33	1247.4758	1247.4776	1.44
a$_{11}$	$C_{57}H_{67}N_{14}O_{17}$	32	1219.4809	1219.4809	0.00
b$_{12}$	$C_{60}H_{70}N_{15}O_{19}$	34	1304.4972	1304.4935	2.84
a$_{12}$	$C_{59}H_{70}N_{15}O_{18}$	33	1276.5023	1276.4985	2.98
b$_{13}$	$C_{65}H_{78}N_{17}O_{21}$	36	1432.5558	1432.5660	7.12
b$_{14}$	$C_{71}H_{90}N_{21}O_{22}$	38	1588.6569	---------	---------

As a result of the possible assignment of the crosslink locality within the nocapeptins CP by MS^2 fragments, labeling experiments were conducted using [$^2H_7$] L-tyrosine and [$^2H_8$] L-tryptophane in the same fashion with nocathioamides to strengthen the connectivity between the suspected chemotypes and the BGC in question besides probing the exact contributing residues to this PTM. Unsurprisingly, the LCMS profiles of [$^2H_7$] L-Tyr experiment in duplicates clearly showed the incorporation of +6 Da with an equivocal proof of Tyr+3 involvement in the interlink reaction (Figure 65).

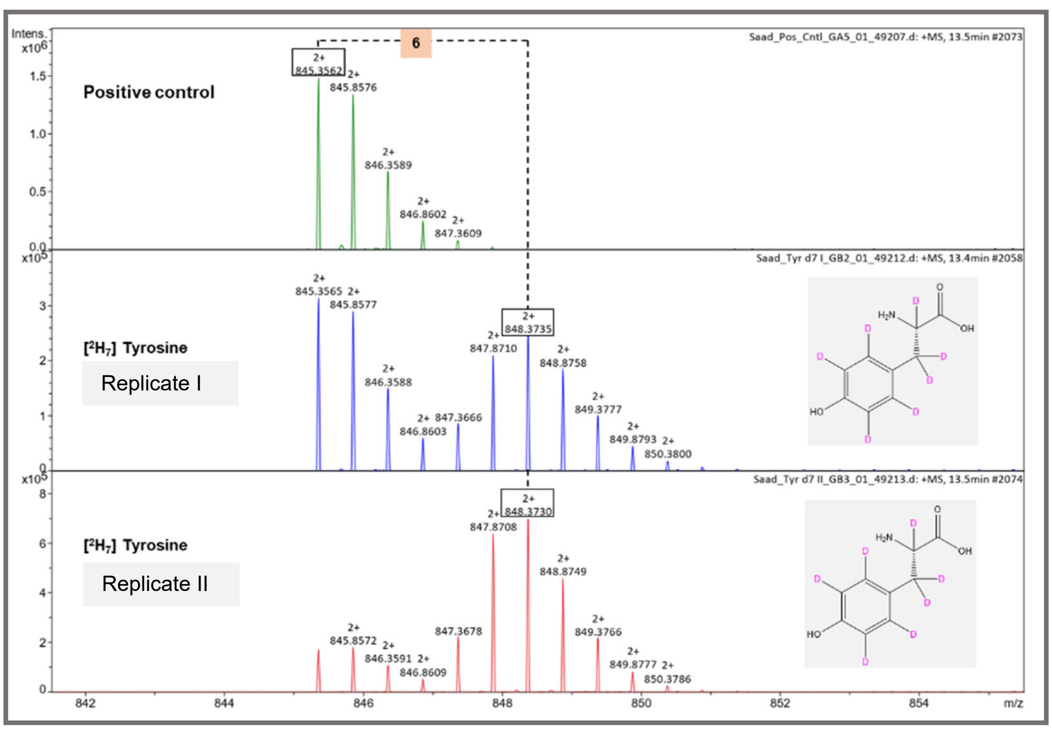

Figure 65. Comparative MS^1 of nocapeptin A (**5**) and its [$^2H_7$] L-tyrosine-based version

Within the same context and taking into account the predicted CP sequence of nocapeptins that codes for two Trp residues (+2 and +7), the supplementation of [$^2H_8$] L-Trp into IFM 0406 cultures resulted in a +16 Da mass drift which again added a further piece of evidence regarding tracking the right chemotypes (Figure 66).

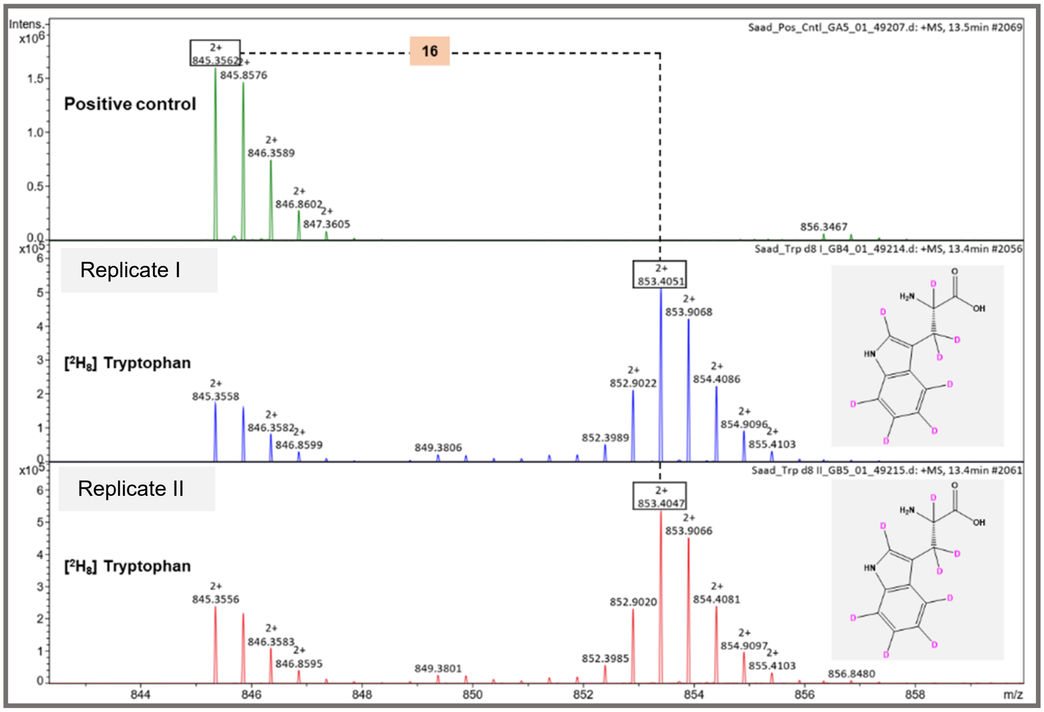

Figure 66. Comparative MS[1] of nocapeptin A (**5**) and its [$^2H_8$] L-tryptophan-based version

Aside from untangling the PTM of the crosslink, the observed mass shifts under the studied labeling conditions assisted to glean as well the L-stereochemistry of the Trp+2 and +7 in addition to Tyr+3 residues (Figures 65 and 66).

4.10 Genome Mining of CYP450-mediated C-X Crosslink Containing Lasso Peptides

In an attempt to retrieve further homologs of nocapeptin BGC featuring such unprecedented PTM within the lasso peptide context, *nopA* was used as an input query in alignment searches against the NCBI database. The sequence results conveyed a limited number of hits and on top of them *N. terpenica* NBRC 100888 and *Longimycelium tulufanense* CGMCC 4.5737 arose.

The antiSMASH output of both isolates indeed revealed the presence of nocapeptin-similar BGCs (Figure 67). In the case of *N. terpenica* NBRC 100888, the architecture of the putative gene cluster exhibited an identical organization to the IFM0406. In addition, the precursor gene (*A*) sequence which encodes the CP of the lasso scaffold was highly similar to the IFM 0406 except for S+5 and Q+6 motifs which were exchanged with Q+5 and H+6 residues, respectively.

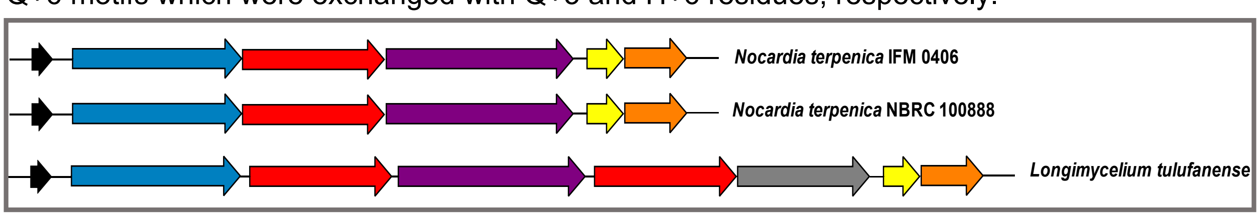

Figure 67. Putative homologous BGCs of nocapeptin

In contrast to the highly similar variant offered by NBRC 100888 gene cluster, the *L. tulufanense* hit comprised stark differences regarding its BGC and proposed chemical structure as well (Figure 67). At first glance, the putative BGC was found to harbor an additional cytochrome P450 (*lopG*, TIGR04515 / TIGR04538) beside a *lopH* that encodes a hypothetical protein (Figure 68, Table 28). In complementation with *lopG* and *lopH*, the remaining ORFs completed the genetic suite for assembling an unknown lasso peptide, termed longipeptin (Table 28).[120c]

Furthermore, the sequence analysis of the precursor gene, *lopA*, indicated that the predicted lasso CP is different from the IFM0406 by five residues (W+3, A+5, N+6, S+11 and M+13) considering the amino acid identities (Figure 68). Since NopF was proposed to catalyze a crosslink in nocapeptins architecture and governed by the order of the genes, the homologous LopF was assumed in turn to mediate a similar event in the predicted product of *L. tulufanense*.

Keeping in mind the numerous catalytic modifications that can be induced by CYP450 enzymes, LopG protein was anticipated to apply further PTM(s) in the longipeptin scaffold (Figure 68).

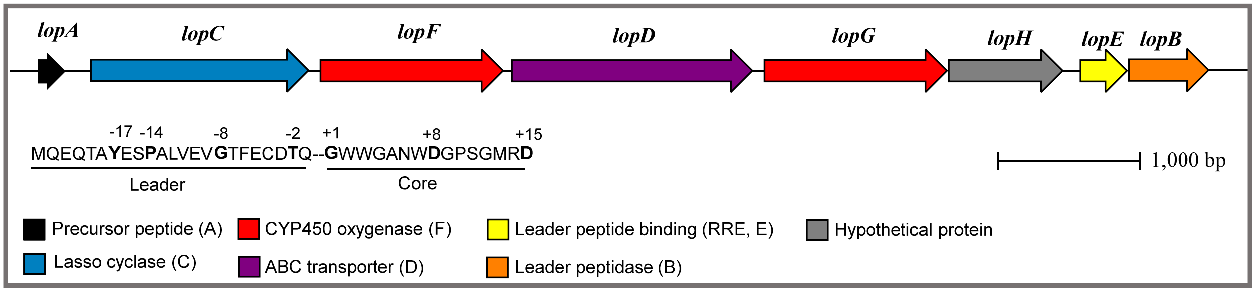

Figure 68. Biosynthetic gene cluster (BGC) of longipeptin

Table 28. Putative function of proteins from the *lop* BGC using RODEO

	Automated RODEO Analysis				
Protein	Accession Nr.	Length [aa]	PFAM (TIGRFam) hits	Description	E-value
LopA	WP_189061731.1	38	-----------------	-----------------	---------
LopC	WP_194500064.1	536	PF00733	Asparagine synthase	1.40E^{-38}
LopF	WP_189061729.1	404	TIGR04515 / TIGR04538	Cytochrome P450	1.10E^{-50}
LopD	WP_189061728.1	596	TIGR02204	ABC transporter	1.20E^{-94}
LopG	WP_189061727.1	406	TIGR04515 / TIGR04538	Cytochrome P450	1.00E^{-46}
LopH	WP_189061726.1	191	----------------	-----------------	---------
LopE	WP_189061725.1	85	PF05402	Stand alone lasso RRE	3.50E^{-27}
LopB	WP_189061724.1	137	PF13471	Transglutaminase	1.80E^{-26}

4.11 Targeted Identification of Longipeptin Using Metabologenomics

Armed with the compelling combination of two candidates of P450 cytochrome (*lopF* and *lopG*) within the longipeptin BGC and the unprecedented sequence of the *lopA* product, *L. tulufanense* was screened to uncover such a novel family of lasso peptide(s).

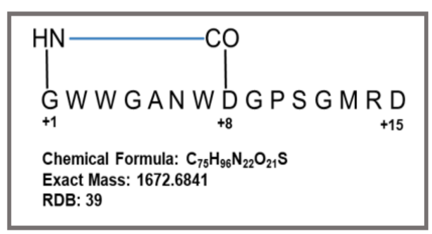

Figure 69. The predicted architecture of longipeptin

The R4 medium-based cultivation of *L. tulufanense* processed by the same cultivation and extraction protocols of nocapeptin yielded in triplicates a set of ions (*m/z* 851, 843, and 844 as $[M+2H]^{2+}$) falling in the mass range of interest formulated by the predicted cleaved CP (Figures

69 and 70). Using the HRMS measurements, the predicted molecular formula and RDB of such ions reflected indeed their relevance to the expected product, longipeptin (Table 29, Figure 69).

Considering the comparative difference between the theoretical and observed *m/z* values in terms of MF variations, the longipeptins scaffold was found to be morphed with additional ancillary PTMs aside from the typical class-defining isopeptide modification and the extra crosslink tailoring of interest.

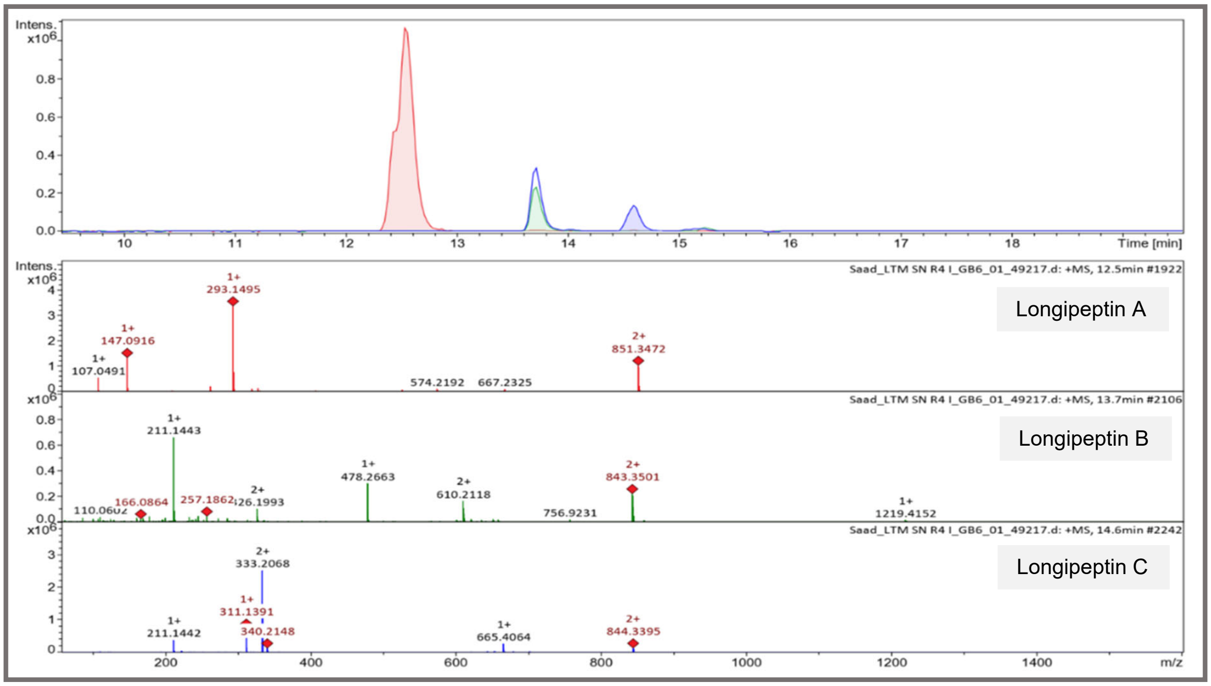

Figure 70. LCMS profile of R4 medium showing the production of longipeptins

Table 29. Molecular formula prediction of longipeptins

Meas. *m/z*	Ion Formula	Calc. *m/z*	Error [ppm]	RDB	mSigma
851.3472, Longipeptin A (**7**)	$C_{76}H_{98}N_{22}O_{22}S$	851.3461	0.4	40	4.6
843.3501, Longipeptin B (**8**)	$C_{76}H_{98}N_{22}O_{21}S$	843.3493	0.7	39	10.0
844.3395, Longipeptin C (**9**)	$C_{75}H_{96}N_{22}O_{22}S$	844.3390	0.6	40	11.2

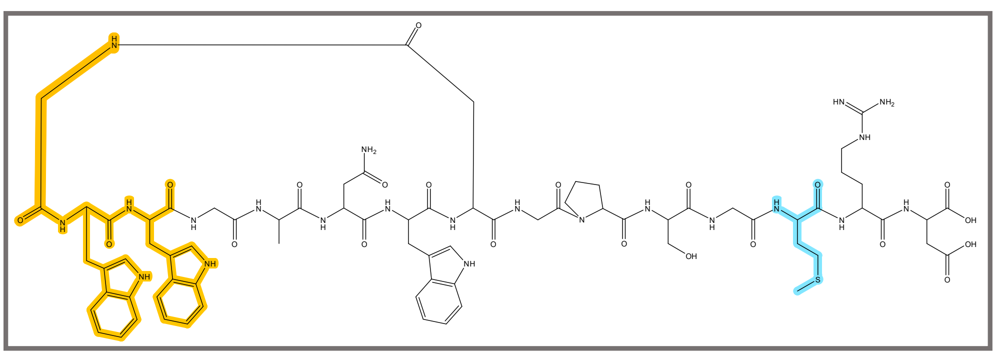

Figure 71. Schematic scaffold of longipeptins, highlighting the localization of the crosslink and the extra oxidative events

The inspection of the CID-MS^2 of the abundant feature *m/z* 851, longipeptin A (**7**), clearly presented a less informative spectrum in comparison to nocapeptins halting the complete *de novo* sequencing of the peptide (Figure 72). In light of the elemental deviations between the observed molecular formula and the predicted one, it was hinted that further cross-linkage, hydroxylation and methylation modifications were appended into the longipeptins framework. The successful deconvolution of *b* series assisted to localize both the extra crosslink tailoring and the hydroxylation event coupled with the class-defining macrolactam alteration (Figure 73, Table 30).

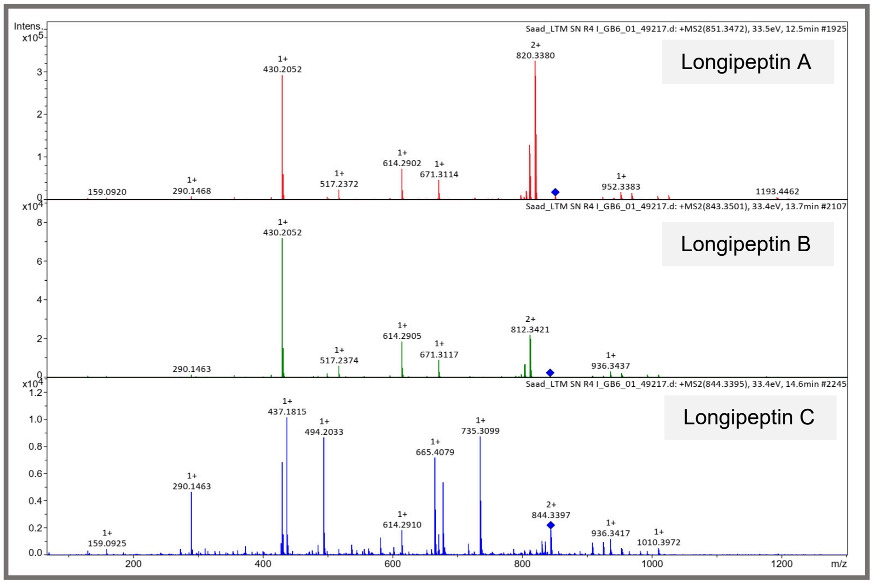

Figure 72. Comparative MS^2 profiles of longipeptins A (**7**), B (**8**) and C (**9**)

Likewise in nocapeptins, the absence of b_1 and b_2 fragments in addition to the constant additive mass shifts monitored with the sequential *b* ions could uncover the position of the crosslink and oxidation events to be specifically located at the N-terminal first three residues of the lasso ring in longipeptin A, Gly+1--Trp+2--Trp3+ (Table 30, and Figure 73).

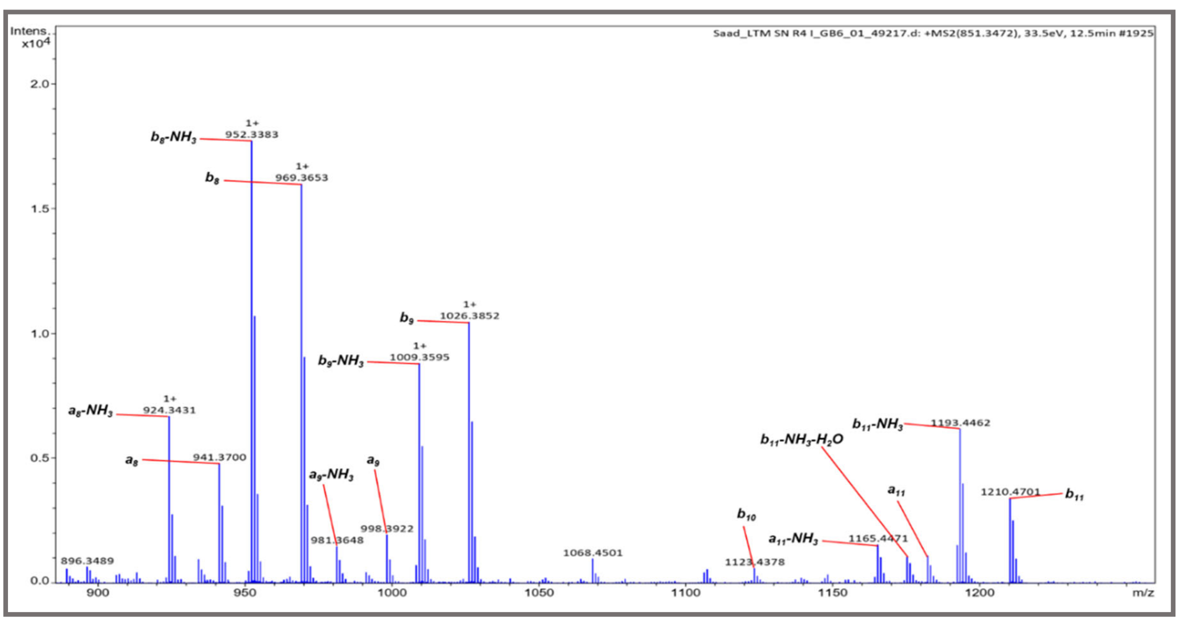

Figure 73. The annotated MS^2 spectrum of longipeptin A (**7**)

Table 30. The assigned fragments of longipeptin A (**7**)

Fragment	Ion Formula	RDB	Calc. *m/z*	Meas. *m/z*	Δ in ppm
b_1	---------	---------	---------	---------	---------
b_2	---------	---------	---------	---------	---------
b_3	$C_{24}H_{22}N_5O_4$	17	444.1672	444.1681	2.03
a_3	$C_{23}H_{22}N_5O_3$	16	416.1723	416.1728	1.20
b_4	$C_{26}H_{25}N_6O_5$	18	501.1886	501.1892	1.20
a_4	$C_{25}H_{25}N_6O_4$	17	473.1937	473.1945	1.70
b_5	$C_{29}H_{30}N_7O_6$	19	572.2258	572.2252	1.05
a_5	$C_{28}H_{30}N_7O_5$	18	544.2308	544.2306	0.37
b_6	$C_{33}H_{36}N_9O_8$	21	686.2687	686.2701	2.04
b_6-NH_3	$C_{33}H_{33}N_8O_8$	22	669.2421	669.2424	0.45
a_6	$C_{32}H_{36}N_9O_7$	20	658.2738	658.2715	3.50
a_6-NH_3	$C_{32}H_{33}N_8O_7$	21	641.2472	641.2470	0.31
b_7	$C_{44}H_{46}N_{11}O_9$	28	872.3480	872.3483	0.34
b_8	$C_{48}H_{49}N_{12}O_{11}$	31	969.3644	969.3653	0.93
b_8-NH_3	$C_{48}H_{46}N_{11}O_{11}$	32	952.3378	952.3383	0.53
a_8	$C_{47}H_{49}N_{12}O_{10}$	30	941.3695	941.3700	0.53
a_8-NH_3	$C_{47}H_{46}N_{11}O_{10}$	31	924.3429	924.3431	0.22
b_9	$C_{50}H_{52}N_{13}O_{12}$	32	1026.3858	1026.3852	0.58
b_9-NH_3	$C_{50}H_{49}N_{12}O_{12}$	33	1009.3593	1009.3595	0.20
a_9	$C_{49}H_{52}N_{13}O_{11}$	31	998.3909	998.3922	1.30
a_9-NH_3	$C_{49}H_{49}N_{12}O_{11}$	32	981.3644	981.3648	0.41
b_{10}	$C_{55}H_{59}N_{14}O_{13}$	34	1123.4386	1123.4378	0.71
b_{11}	$C_{58}H_{64}N_{15}O_{15}$	35	1210.4706	1210.4701	0.41
b_{11}-NH_3	$C_{58}H_{61}N_{14}O_{15}$	36	1193.4441	1193.4462	1.76
b_{11}-NH_3-H_2O	$C_{58}H_{59}N_{14}O_{14}$	37	1175.4335	1175.4315	1.70
a_{11}	$C_{57}H_{64}N_{15}O_{14}$	34	1182.4757	1182.4743	1.18
a_{11}-NH_3	$C_{57}H_{61}N_{14}O_{14}$	35	1165.4492	1165.4471	1.80
b_{12}	$C_{60}H_{67}N_{16}O_{16}$	36	1267.4921	1267.5161	18.94
a_{12}	$C_{59}H_{67}N_{16}O_{15}$	35	1239.4972	1239.5103	10.56

Despite the MS^2 spectral similarity between *m/z* 851 and 843 (Figure 72), the minor non-hydroxylated variant of longipeptin, B congener (**8**), afforded fewer *b* ions upon its CID fragmentation compared to the abundant representative (Figure 74). The observation of b_7, b_8 and b_9 fragments in combination with the a_8 and a_9 series secured the characteristic isopeptide formation along with the unique crosslink alteration within the ring of the lasso scaffold (Figure 74, Table 31).

Table 31. The assigned fragments of longipeptin B (**8**)

Fragment	Ion Formula	RDB	Calc. *m/z*	Meas. *m/z*	Δ in ppm
b_7	$C_{44}H_{46}N_{11}O_8$	28	856.3531	856.3499	3.73
b_8	$C_{48}H_{49}N_{12}O_{10}$	31	953.3695	953.3684	1.15
b_8-NH_3	$C_{48}H_{46}N_{11}O_{10}$	32	936.3429	936.3437	0.85
a_8	$C_{47}H_{49}N_{12}O_9$	30	925.3745	925.3723	2.38
a_8-NH_3	$C_{47}H_{46}N_{11}O_9$	31	908.3480	908.3486	0.67
b_9	$C_{50}H_{52}N_{13}O_{11}$	32	1010.3909	1010.3880	2.87
b_9-NH_3	$C_{50}H_{49}N_{12}O_{11}$	33	993.3644	993.3659	1.51

a_9	$C_{49}H_{52}N_{13}O_{10}$	31	982.3960	982.4099	14.15
a_9-NH_3	$C_{49}H_{49}N_{12}O_{10}$	32	965.3695	965.3748	5.49
b_{10}	$C_{55}H_{59}N_{14}O_{12}$	34	1107.4437	1107.4352	7.68
b_{11}	$C_{58}H_{64}N_{15}O_{14}$	35	1194.4757	1194.4710	3.93
b_{11}-NH_3	$C_{58}H_{61}N_{14}O_{14}$	36	1177.4492	1177.4526	2.89
b_{11}-NH_3-H_2O	$C_{58}H_{59}N_{14}O_{13}$	37	1159.4386	1159.4420	2.93
a_{11}	$C_{57}H_{64}N_{15}O_{13}$	34	1166.4808	1166.4720	7.54
a_{11}-NH_3	$C_{57}H_{61}N_{14}O_{13}$	35	1149.4543	1149.4795	21.92
b_{12}	$C_{60}H_{67}N_{16}O_{15}$	36	1251.4972	1251.4874	7.83

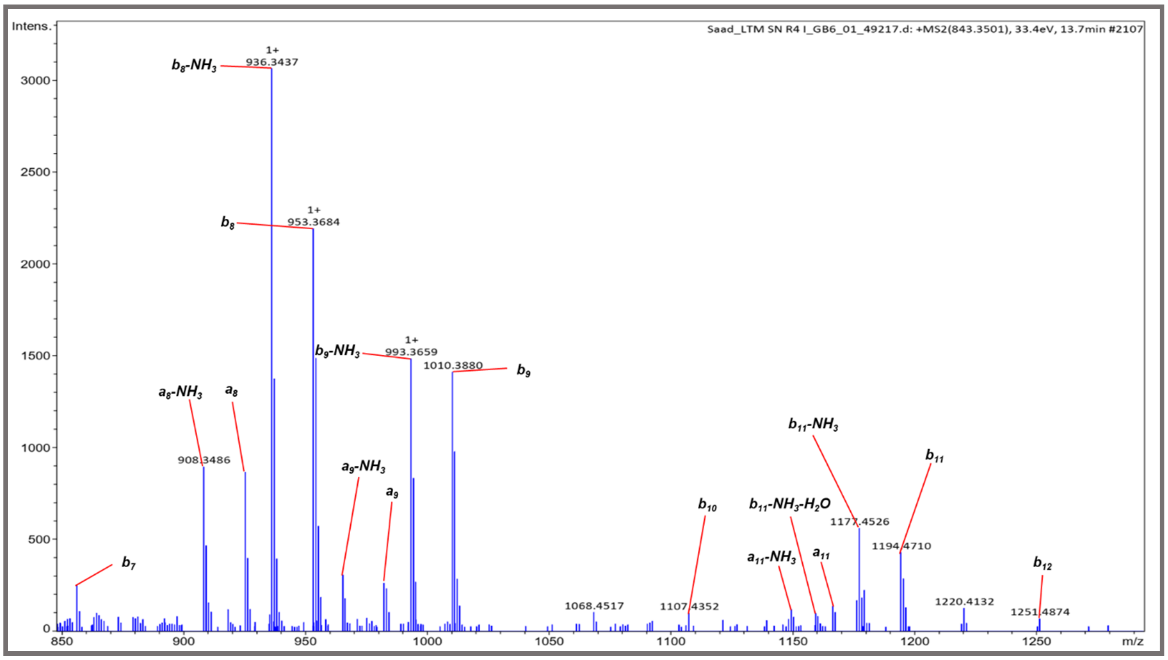

Figure 74. The annotated MS[2] spectrum of longipeptin B (**8**)

In contrast to *m/z* 851 and 843, the traces of the non-methylated congener, longipeptin C (**9**), revealed very descriptive fragments upon its CID fragmentation spectrum enabling the complete sequencing of the peptide (Figures 72 and 75). In an analogous fashion to nocapeptins, the absence of b_1 and b_2 *m/z* values with their corresponding y_{13} and y_{14} ions pinpointed the localization of the conserved interlink which was further validated by the annotation of more ions of the *b* series (Figure 75, Table 32). Furthermore, the *y* ions particularly the y_3 fragment and the constant H_2O loss of *y* features could unveil the position of the hydroxylation modification to occur at Met+13 residue in longipeptin C (Table 32, Figure 71).

Table 32. The assigned fragments of longipeptin C (**9**)

Fragment	Ion Formula	RDB	Calc. *m/z*	Meas. *m/z*	Δ in ppm
y_1	$C_4H_8NO_4$	2	134.0453	---------	---------
y_2	$C_{10}H_{20}N_5O_5$	4	290.1464	290.1467	1.03
y_3	$C_{15}H_{29}N_6O_7S$	5	437.1818	437.1821	0.69
y_3-H_2O	$C_{15}H_{27}N_6O_6S$	6	419.1713	419.1716	0.72
y_4	$C_{17}H_{32}N_7O_8S$	6	494.2033	494.2035	0.40
y_4-H_2O	$C_{17}H_{30}N_7O_7S$	7	476.1927	476.1940	2.73
y_5	$C_{20}H_{37}N_8O_{10}S$	7	581.2353	581.2343	1.72

y_{5}-H_2O	$C_{20}H_{35}N_{8}O_{9}S$	8	563.2248	563.2198	8.88
y_{6}	$C_{25}H_{44}N_{9}O_{11}S$	9	678.2881	678.2881	0.00
y_{6}-H_2O	$C_{25}H_{42}N_{9}O_{10}S$	10	660.2775	660.2750	3.79
y_{7}	$C_{27}H_{47}N_{10}O_{12}S$	10	735.3096	735.3101	0.68
y_{7}-H_2O	$C_{27}H_{45}N_{10}O_{11}S$	11	717.2990	717.2998	1.12
y_{8}	$C_{31}H_{50}N_{11}O_{14}S$	13	832.3259	---------	---------
y_{9}	$C_{42}H_{60}N_{13}O_{15}S$	20	1018.4053	1018.4202	14.63
y_{10}	$C_{46}H_{66}N_{15}O_{17}S$	22	1132.4482	1132.4597	10.15
y_{11}	$C_{49}H_{71}N_{16}O_{18}S$	23	1203.4853	---------	---------
y_{12}	$C_{51}H_{74}N_{17}O_{19}S$	24	1260.5068	1260.5104	2.86
y_{13}	---------	---------	---------	---------	---------
y_{14}	---------	---------	---------	---------	---------
b_{1}	---------	---------	---------	---------	---------
b_{2}	---------	---------	---------	---------	---------
b_{3}	$C_{24}H_{22}N_{5}O_{3}$	17	428.1723	428.1705	4.20
a_{3}	$C_{23}H_{22}N_{5}O_{2}$	16	400.1773	400.1789	3.99
b_{4}	$C_{26}H_{25}N_{6}O_{4}$	18	485.1937	485.1940	0.62
a_{4}	$C_{25}H_{25}N_{6}O_{3}$	17	457.1988	457.2015	5.90
b_{5}	$C_{29}H_{30}N_{7}O_{5}$	19	556.2308	556.2310	0.36
a_{5}	$C_{28}H_{30}N_{7}O_{4}$	18	528.2359	528.2394	6.63
b_{6}	$C_{33}H_{36}N_{9}O_{7}$	21	670.2738	670.2711	4.03
a_{6}	$C_{32}H_{36}N_{9}O_{6}$	20	642.2789	642.2817	4.36
b_{7}	$C_{44}H_{46}N_{11}O_{8}$	28	856.3531	856.3567	4.20
b_{8}	$C_{48}H_{49}N_{12}O_{10}$	31	953.3695	953.3685	1.05
b_{8}-NH_3	$C_{48}H_{46}N_{11}O_{10}$	32	936.3429	936.3435	0.64
a_{8}	$C_{47}H_{49}N_{12}O_{9}$	30	925.3745	925.3772	2.92
a_{8}-NH_3	$C_{47}H_{46}N_{11}O_{9}$	31	908.3480	908.3467	1.43
b_{9}	$C_{50}H_{52}N_{13}O_{11}$	32	1010.3909	1010.3935	2.57
b_{9}-NH_3	$C_{50}H_{49}N_{12}O_{11}$	33	993.3644	993.3627	1.71
a_{9}	$C_{49}H_{52}N_{13}O_{10}$	31	982.3960	982.3964	0.41
a_{9}-NH_3	$C_{49}H_{49}N_{12}O_{10}$	32	965.3695	965.3679	1.66

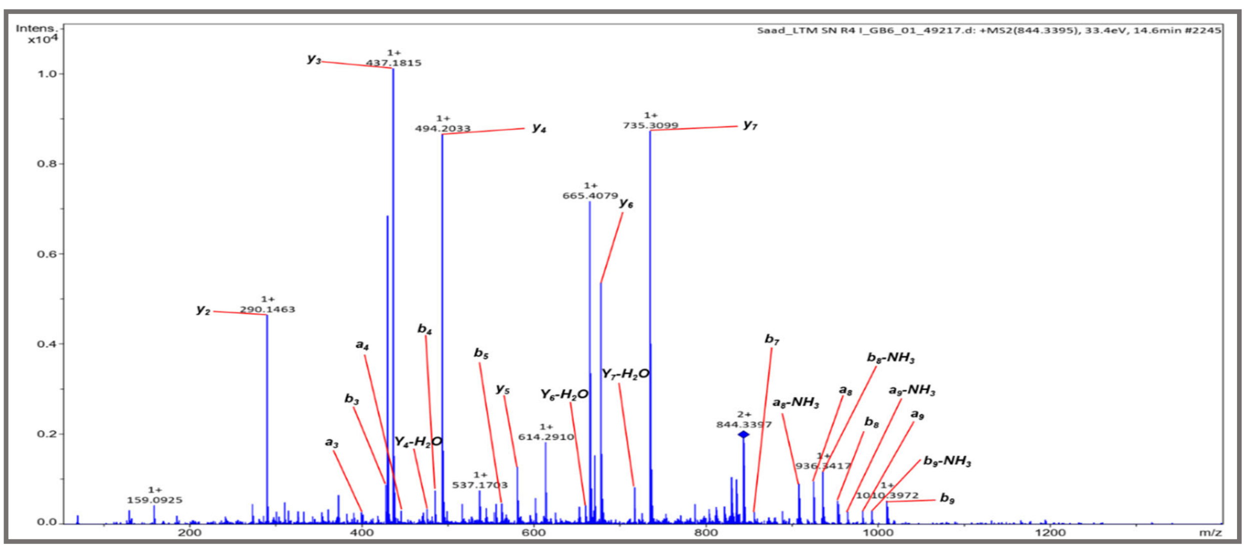

Figure 75. The annotated MS^2 spectrum of longipeptin C (**9**)

4.12 Biosynthetic Novelty and Outlook of Nocapeptin(s) and Longipeptin(s) PTMs

The bioinformatic analysis of nocapeptin BGC and its predicted scaffold facilitated to a greater extent the deorphanization and identification of the corresponding product from the large MS dataset generated upon OSMAC studies. Despite the bioinformatic disability to precisely predict the additional decoration mediated by the P450 enzyme (NopF) in the nocapeptin architecture, the current state of data, fundamentally counting on MS, served to decipher this chemical modification to be skeletally introduced as a novel oxidative inter-linkage.

The selective integration of isotopically labeled substrates within the workflow, relying on the gleaned MS^2 findings regarding a particular sequence of residues, was again a three-layered utility. The practicality covered establishing the connectivity between the BGC of interest and its expressed metabolites, probing the crosslink-contributing motifs, and assigning the stereochemistry of the supplemented substances. Yet, the recruited labeling strategy exhibited some limitations under the current study case in terms of exactly determining the second involved residue (Gly+1 or Trp +2) in the post-translational morph in nocapeptin A (**5**).

Although an epimerization reaction can still account for the same observed mass shift (+6 Da) in nocapeptin A labeling experiment, however such probability was directly excluded due to two facts. The first reason was attributed to the lack of the genetic element in the *nop* BGC that can catalyze such a specific PTM. The second justification was derived from the absence of b_2 / y_{13} ions and the presence of b_3 / y_{12} fragments in the MS data of both variants highlighting the structural ornament within this particular sequence of residues. Nevertheless, the mass shifts upon the Trp labeling experiment in nocapeptin A (**5**) did not deliver conclusive proof about the inter-linkage, it is still envisioned that the Trp+2 motif might be involved in the additional crosslink tailoring via its ring NH that cannot be inferred under the employed MS setup.

Nocapeptins, aside from being the first lasso peptides to be reported from the genus *Nocardia*, structurally feature an unprecedented oxidative linkage that has not been witnessed across the PTM space of lasso peptides regardless of the class (Table 33). Regarding the double hydroxylations in nocapeptin B (**6**), it was presumed to be catalytically induced by *npF* under the aerobic conditions used during the cultivation.

Table 33. Summary of the observed PTMs of nocapeptins

PTMs	Nocapeptin A (**5**)	Nocapeptin B (**6**)
Isopeptide PTM	Yes	Yes
Isopeptide localization	G+1**--**D+8	G+1**--**D+8
Ring crosslink PTM	Yes	Yes
Ring crosslink localization	G+1**--**W+2**--**Y+3	G+1**--**W+2**--**Y+3
Hydroxylations PTM	----	Yes
Hydroxylations localization	----	G+1**--**W+2**--**Y+3

The assembly of hydroxylated lasso entities was previously enlisted in class II exemplified by RES-701-2 and RES-701-4 where C7-hydroxylation is introduced in the C-terminal Trp residues.[175] Recently, the cloning and heterologous expression of RES-701-4 BGC proved the necessity of a conserved *resE* in the hydroxylation step to append such tailoring within similar architectures.[176] A further instance with a hydroxylated lasso skeleton was delivered by canucin

A from *Streptomyces canus* in which a hydroxyl group is installed at the β-carbon of the C-terminal aspartate residue. The biochemical characterization experiments revealed CanE, an iron/2-oxoglutarate-dependent enzyme, is in charge of introducing such PTM before the macrolactam cyclization event.[177]

Although longipeptins were disclosed via a BLASTP search using the NopA amino acid sequence with the purpose of unearthing further homologues that can encode a specific novel inter-linkage, they were post-translationally able to leverage the chemical modifications with further tailorings like hydroxylation and methylation reactions (Table 34). The study of CID-MS^2 fragments could fairly pinpoint the structural modifications of the oxidative crosslink and the hydroxylation event in contrast to the installed methylation group that remains enigmatic in terms of position. From a PTM perspective, longipeptin A represents the most tailored lasso peptide till now with one class-defining modification as a macrolactam ring, in addition to three different ancillary alterations.

Table 34. Summary of the observed PTMs of longipeptins

PTMs	Longipeptin A (**7**)	Longipeptin B (**8**)	Longipeptin C (**9**)
Isopeptide PTM	Yes	Yes	Yes
Isopeptide localization	G+1**--**D+8	G+1**--**D+8	G+1**--**D+8
Ring crosslink PTM	Yes	Yes	Yes
Ring crosslink localization	G+1**--**W+2**--**W+3	G+1**--**W+2**--**W+3 *	G+1**--**W+2**--**W+3
Hydroxylation PTM	Yes	----	Yes
Hydroxylation localization	G+1**--**W+2**--**W+3	----	M+13
Methylation PTM	Yes	Yes	----
Methylation localization	No	No	----
* deduced through b_8 / a_8 ions rather than b_3 / a_3 fragments			

Bearing in mind the genetic organization of the nocapeptin BGC, it is hypothesized that the LopF enzyme in the longipeptin BGC mediates the cross-linkage while the enzymatic installation of the hydroxyl group is catalyzed by LopG. Although *lopH* lacks putatively conserved domains to predict its catalytic function, the futuristic experiments of genetic deletion can aid in identifying its role whether it is relevant to the methylation step or is non-enzymatically controlled.

While the MS technique presented almost a complete overview about nocapeptin A (**5**) and longipeptin A (**7**) architectures, an extensive structural elucidation by NMR is still needed to close the inter-linkage gap in addition to the additional PTMs observed in longipeptin A scaffold. Currently, the isolation of longipeptin A is ongoing whereas full 2D-NMR spectra of nocapeptin A (400 and 700 MHz) were collected. Due to time constraints, the NMR datasets were not inspected.

As formerly stated, we hypothesized based on the feeding experiments of specific labeled precursors the that Trp+2 residue is the contributing motif in the oxidative linkage with either Tyr+3 unit in nocapeptins or Trp+3 residue in longipeptins via its aromatic NH. In general, the occurrence of oxidative crosslinks in RiPPs has been witnessed in a handful of instances covering different classes exmplified by streptides from *Streptococcus thermophilus*[178] and darobactin from *Photorhabdus khanii* HGB1456.[179] Structurally, such entities frame a post-translationally installed Lys– Trp and Trp-Trp crosslinks mediated by rSAM enzymes (Figure 76).

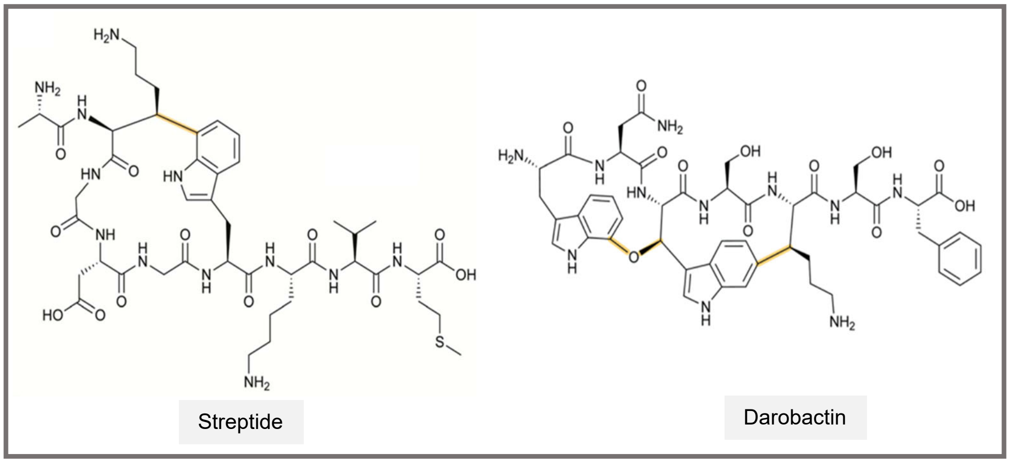

Figure 76. Exmeplary RiPPs containing oxidative crosslinks mediated by rSAM

In concert with the catalyzed macrocyclization by rSAMs, P450 cytochromes were also found to append many unusual oxidative events in numerous RiPP architectures. Corcagin A, from the myxobacterium *Chondromyces crocatus* Cm c5, depicts an exemplary morphed RiPP through an extensive posttranslationally modifying process catalyzed by a dioxygenase (Figure 77).[180] In addition, tryptorubin A, from *Streptomyces* sp. CLI2509, represnts an exquisite skeletally modified scaffold coded by a RiPP BGC in which a processing cytochrome P450 enzyme is harboured to catalyze three different oxidative crosslinks including Trp-Tyr, Trp-Trp and Trp-backbone amidic NH (Figure 77).[181]

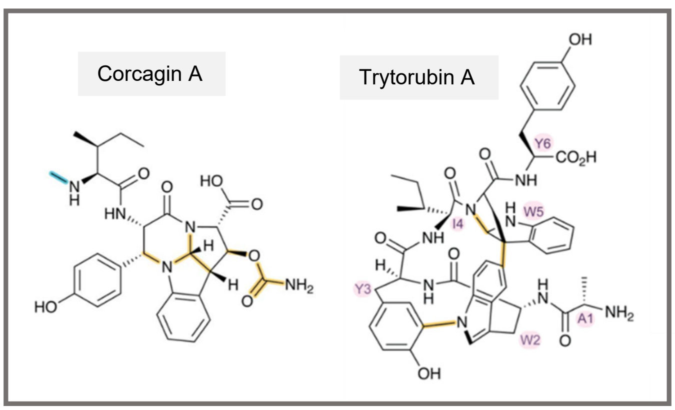

Figure 77. Selected RiPPs featuring oxidative interlinkages installed by CYP450

Aside from the interesting PTMs witnessed in nocapeptins and longipeptins frameworks, the threading property of these entities has to be also warranted through NOESY correlations to secure the lasso format and the steric plugs as well.

Since the architectures of nocapeptins and longipeptins come fully loaded with an exceptional conserved crosslink and further interesting PTMs, the genetic engineering of *nop* and *lop* BGCs in combination with the biochemical characterization will possibly be able to assign the processing enzymes to their respective biosynthetic events and hence dissecting the biogenesis order and timing.

5. Conclusion and Outlook

The latest initiatives of the genome sequencing projects of various pathogenic *Nocardia* spp. revealed untapped cryptic biosynthetic talent shared across most of the *Nocardia* genus members branding them as an underexplored source of novel secondary metabolites.

The phylogenetically related isolates *N. terpenica* IFM 0406, and IFM 0706^{T}, as representative clinical members, delivered a relatively large number of BGCs encoded within their genomes with a huge metabolic reservoir of extremely diverse biosynthetic machineries yet to be discovered.

Since major hurdles in activating this biosynthetic chemical diversity are usually encountered under laboratory conditions, a genome-mining prioritization strategy was adopted within the scope of this work, taking into account the novelty of the contributing biosynthetic enzymes in terms of occurrence and combination. While the identification of the optimal conditions that regulate the secondary metabolism of a BGC of interest remains a challenge, the application of genetics-free tactics like the variation of growth conditions (OSMAC concept) and an elicitor screening still present a simple alternative in awakening silent BGC(s) of interest.

Driven by the limited chemical space of discovered RiPP entities delivered by *Nocardia* spp. and the unusual skeletal modifications that RiPP tailoring enzymes can append, a targeted campaign of RiPP genome mining led to the prioritization of two unusual BGCs in IFM 0406, and 0706 genomes coding for novel products.

To assist and accelerate the detection of the products under investigation, a configured metabolomics strategy was recruited. The developed analytical approach mainly relied on the mass shifts observation upon using particular labeled amino acids once a candidate ion feature(s) was recognized under a defined cultivation condition. The choice of the isotopically labeled substrates was on the basis of the putative sequence of the predicted core peptide. The application of OSMAC and the tuned analytical approach enabled the retrieval of ideal growing conditions that triggered the production of secondary metabolites expressed by the two BGCs under question. Upon upscaling, enough amounts of the products were isolated and structurally characterized by NMR spectroscopy.

The deorphanization of the first RiPP-BGC, *nta*, resulted in the discovery of chimeric lanthipeptide scaffolds belonging to class I, termed nocathioamides. Their architectures represented a hyper-modified RiPP in which 11 out of 13 amino acid residues underwent specific and different tailoring reactions [(Me)Lan, thioamidation, azole formation, N-acetylation, (C and S) oxidation, dehydration, epimerization, and macroimidation]. Ultimately, nocathioamides A-C define a new class of RiPPs hovering over three different class-defining biosynthetic machineries of lanthipeptides, LAPs and rare thioamitides, additionally decorated with unprecedented macrocyclic imide tailoring.

The second prioritized RiPP-BGC, *nop*, was activated under single specific growth parameters. The genetically translated products were found to feature, besides the class-defining modification, an additional ancillary oxidative PTM(s). Nocapeptin A, isolated from IFM 0406, inaugurated the first lasso peptide entity from the genus *Nocardia* and on top of that, the scaffold delivered an elusive installation of oxidative crosslinkage (C-X). Bioinformatic leverage of nocapeptins BGC enriched this novel molecular family with further novel members, termed longipeptins from *Longimycelium tulufanense*. Structurally, longipeptin A architecture was able to posttranslationally append three further ancillary alterations [oxidative crosslink (C-X), hydroxylation, and methylation] besides the typical macrolactam tailoring.

Within the scope of this study, we demonstrated the utility and practicality of a newly optimized metabologenomic approach through its application to a set of orphan gene clusters found in the genomes of *N. terpenica* and *L. tulufanense*. This approach led to the discovery of three novel RiPP molecular families, nocathioamides, nocapeptins, and longipeptins.

Such chemical entities could have been overlooked by regular LC/MS screening due to peaks overlapping and/or the appearance as minor peaks. We achieved the isolation by the bioinformatic prediction of the resulting peptide and used this information, after a round of media optimization, to screen for specific mass drifts of some amino acid residues upon labeling besides particular NMR features after fractionation.

The practicality of the isotopic labeling experiments was multipurpose: They early connected the suspected chemotypes with the BGC of interest, narrowed down the cleavage site in nocathioamides, probed the involved residues in the oxidative crosslink (C-X) in nocapeptins and longipeptins in addition to allowing the determination of the absolute configuration of the involved amino acids. The developed hybrid MS/NMR tactic represents a valuable complement to the existing genome mining strategies, particularly for RiPPs lacking a predictable bioactivity or mass ranges as clearly found in nocathiomaides.

Albeit the adopted approach applied in this study resulted in characterizing thiazole-containing RiPPs and lasso peptides, it still could be modulated to target other rare functional groups of RiPPs. For example, the integration of ^{1}H-^{15}N HSQC and ^{1}H-^{15}N HMBC NMR screening components can enable to delve more RiPP featuring imide moieties or unusual nitrogen crosslinks. Furthermore, with a refocused ^{1}H-^{13}C-HMBC sequence that takes into account the low-relaxing quarternary atoms of thioamide carbonyl groups, it could be implemented to unearth further thioamidated RiPPs.

While the discovery of nocathioamides and nocapeptins in addition to longipeptins brings up a legion of firsts into RiPPs, the *nta*, *nop* and *lop* BGCs set the stage for studying the interplay of the involved enzymes to elucidate the currently enigmatic biosynthetic events. This will possibly enrich the biocatalytic toolbox with various tailoring RiPP enzymes that can be harnessed in synthetic biology and synthetic chemistry contexts.

For example, the futuristic in vitro reconstitution of the monooxygenases found in *nta*, *nop*, *lop* encoding clusters and their substrates tolerance represents an exquisite panel of new processing enzymes that can install specific and/or rare PTMs. In parallel, the exceptional combinations of the different biogenesis machineries with various modifying enzymes witnessed either in the *nta* chimeric BGC or in the *nop* and *lop* clusters can assist in the current combinatorial biosynthesis endeavors towards the engineering of new-to-nature hybrid RiPPs customized with rare and/or particular modifications.

6. References

1- B. G. de la Torre, F. Albericio, Molecules 2020, 25, 2293.
2- T. Dang, R. D. Süssmuth, Acc. Chem. Res. 2017, 50, 1566.
3- E. M. Nolan, C. T. Walsh, Chembiochem 2009, 10, 34.
4- C. J. Schofield, J. E. Baldwin, M. F. Byford, I. Clifton, J. Hajdu, C. Hensgens, P. Roach, Curr. Opin. Struct. Biol. 1997, 7, 857.
5- B. K. Hubbard, C. T. Walsh, Angew. Chem. Int. Ed. 2003, 42, 730.
6- a) V. Miao, M.-F. Coeffet-LeGal, P. Brian, R. Brost, J. Penn, A. Whiting, S. Martin, R. Ford, I. Parr, M. Bouchard, C. J. Silva, S. K. Wrigley, R. H. Baltz, Microbiology 2005, 151, 1507.; b) R. D. Süssmuth, A. Mainz, Angew. Chem. Int. Ed. 2017, 56, 3770.
7- A. W. Truman, Beilstein J. Org. Chem. 2016, 12, 1250.
8- a) A. D. P. van Staden, W. F. van Zyl, M. Trindade, L. M. Dicks, C. Smith, Applied and Environmental Microbiology 2021.; b) D. C. Chan, L. L. Burrows, The Journal of Antibiotics 2021, 74, 161.; c) A. A. Vinogradov, H. Suga, Cell Chemical Biology 2020, 27, 1032-1051.; d) K. E. Bird, A. A. Bowers, in Comprehensive Natural Products III, 2020, pp. 166.; e) S. Kodani, K. Unno, Journal of Industrial Microbiology; Biotechnology: Official Journal of the Society for Industrial Microbiology and Biotechnology 2020, 47, 703.; f) Y. Fu, A. H. Jaarsma, O. P. Kuipers, Cell Mol Life Sci 2021, 78, 3921.
9- F. Parenti, H. Pagani, G. Beretta, J. Antibiot. 1976, 29, 501.
10- a) N. Naruse, O. Tenmyo, K. Tomita, M. Konishi, T. Miyaki, H. Kawaguchi, K. Fukase, T. Wakamiya, T. Shiba, J. Antibiot. 1989, 42, 837.; b) M. Vestergaard, N. A. Berglund, P.-C. Hsu, C. Song, H. Koldsø, B. Schiøtt, M. S. Sansom, ACS omega 2019, 4, 18889.
11- T. E. Smith, C. D. Pond, E. Pierce, Z. P. Harmer, J. Kwan, M. M. Zachariah, M. K. Harper, T. P. Wyche, T. K. Matainaho, T. S. Bugni, L. R. Barrows, C. M. Ireland, E. W. Schmidt, Nature chemical biology 2018, 14, 179.
12- a) K. Iwamoto, T. Hayakawa, M. Murate, A. Makino, K. Ito, T. Fujisawa, T. Kobayashi, Biophysical journal, 2007, 93, 1608-1619.; b) L. Huo, A. Ökesli, M. Zhao, W. A. van der Donk, Applied and environmental microbiology, 2017, 83.
13- H. Prochnow, K. Rox, N. S. Birudukota, L. Weichert, S.-K. Hotop, P. Klahn, K. Mohr, S. Franz, D. H. Banda, S. Blockus, J.Schreiber, S. Haid, M. Oeyen, J. P. Martinez, R. D. Süssmuth, J. Wink, A. Meyerhans, C. Goffinet, M. Messerle, T. F. Schulz, A. Kröger, D. Schols, T. Pietschmann, M. Brönstrup, Journal of virology, 2020, 94.
14- F. Castiglione, A. Lazzarini, L. Carrano, E. Corti, I. Ciciliato, L. Gastaldo, P. Candiani, D. Losi, F. Marinelli, E. Selva, Chemistry; biology, 2008, 15, 22.
15- L. A. Rogers, E. O.Whittier, J. Bacteriol. 1928, 16, 211.
16- K. I. Mohr, C. Volz, R. Jansen, V. Wray, J. Hoffmann, S. Bernecker, J. Wink, K. Gerth, M. Stadler, R. Müller, Angewandte Chemie International Edition 2015, 54, 11254.
17- a) O. Potterat, H. Stephan, J. W. Metzger, V. Gnau, H. Zähner, G. Jung, Liebigs Annalen der Chemie 1994, 1994, 741.; b) M. Shao, J. Ma, Q. Li, J. Ju, Marine drugs 2019, 17, 127.
18- N. Takasaka, I. Kaweewan, M. O-. Kameyama, S. Kodani, Letters in applied microbiology 2017, 64, 150.
19- a) W. Weber, W. Fischli, E. Hochuli, E. Kupfer, E. Weibel, The Journal of antibiotics 1991, 44, 164.; b) D. Wyss, H.-W. Lahm, M. Manneberg, A. Labhardt, The Journal of antibiotics 1991, 44, 172.

20- a) O. Potterat, K. Wagner, G. Gemmecker, J. Mack, C. Puder, R. Vettermann, R. Streicher, Journal of natural products, 2004, 67, 1528.; b) T. A. Knappe, U. Linne, X. Xie, M. A. Marahiel, FEBS letters, 2010, 584, 785.

21- a) T. A. Knappe, U. Linne, S. Zirah, S. Rebuffat, X. Xie, M. A. Marahiel, Journal of the American Chemical Society, 2008, 130, 11446.; b) K. Kuznedelov, E. Semenova, T. A. Knappe, D. Mukhamedyarov, A. Srivastava, S. Chatterjee, R. H. Ebright, M. A. Marahiel, K. Severinov, Journal of molecular biology, 2011, 412, 842.

22- S. S. Elsayed, F. Trusch, H. Deng, A. Raab, I. Prokes, K. Busarakam, J. A. Asenjo, B. A. Andrews, P. Van West, A. T. Bull, The Journal of organic chemistry, 2015, 80, 10252.

23- V. Valiante, M. C. Monteiro, J. Martín, R. Altwasser, N. El Aouad, I. González, O. Kniemeyer, E. Mellado, S. Palomo, N. de Pedro, I. P.-Victoria, J. R. Tormo, F. Vicente, F. Reyes, O. Genilloud, A. A. Brakhage, Antimicrobial agents and chemotherapy, 2015, 59, 5145.

24- a) M. Iwatsuki, H. Tomoda, R. Uchida, H. Gouda, S. Hirono, S. Ōmura, Journal of the American Chemical Society, 2006, 128, 7486.; b) M. Iwatsuki, Y. Koizumi, H. Gouda, S. Hirono, H. Tomoda, S. Ōmura, Bioorganic; medicinal chemistry letters, 2009, 19, 2888.

25- E. Gavrish, C. S. Sit, S. Cao, O. Kandror, A. Spoering, A. Peoples, L. Ling, A. Fetterman, D. Hughes, A. Bissell, H. Torrey, T. Akopian, A. Mueller, S. Epstein, A. Goldberg, J. Clardy, K. Lewis, Chemistry; biology, 2014, 21, 509.

26- a) K. -i. Kimura, F. Kanou, H. Takahashi, Y. Esumi, M. Uramoto, M. Yoshihama, The Journal of antibiotics, 1997, 50, 373.; b) Y. Esumi, Y. Suzuki, Y. Itoh, M. Uramoto, K. -i. Kimura, M. Goto, M. Yoshihama, T. Ichikawa, The Journal of antibiotics, 2002, 55, 296.

27- R. Salomon, R. N. Farías, Journal of bacteriology, 1992, 174, 7428.

28- a) D. Detlefsen, S. Hill, K. Volk, S. Klohr, M. Tsunakawa, T. Furumai, P. Lin, M. Nishio, K. Kawano, T. Oki, The Journal of antibiotics, 1995, 48, 1515.; b) M. Tsunakawa, S. -L. Hu, Y. Hoshino, D. J. Detlefson, S. E. Hill, T. Furumai, R. J. White, M. Nishio, K. Kawano, S. Yamamoto, The Journal of antibiotics 1995, 48, 433.; c) P. -F. Lin, H. Samanta, C. M. Bechtold, C. A. Deminie, A. K. Patick, M. Alam, K. Riccardi, R. E. Rose, R. J. White, R. J. Colonno, Antimicrobial agents and chemotherapy, 1996, 40, 133.

29- I. Kaweewan, H. Hemmi, H. Komaki, S. Harada, S. Kodani, Bioorganic; medicinal chemistry, 2018, 26, 6050.

30- S. Um, Y.-J. Kim, H. Kwon, H. Wen, S.-H. Kim, H. C. Kwon, S. Park, J. Shin, D.-C. Oh, Journal of natural products, 2013, 76, 873.

31- S. Son, M. Jang, B. Lee, Y.-S. Hong, S.-K. Ko, J.-H. Jang, J. S. Ahn, Journal of natural products, 2018, 81, 2205.

32- a) J. M. Liesch, K. L. Rinehart Jr, Journal of the American Chemical Society, 1977, 99, 1645.; b) F. Reusser, Biochemistry, 1969, 8, 3303.; c) H. Abe, K. Kushida, Y. Shiobara, M. Kodama, Tetrahedron letters, 1988, 29, 1401.

33- a) M. Aoki, T. Ohtsuka, Y. Itezono, K. Yokose, K. Furihata, H. Seto, Tetrahedron letters, 1991, 32, 217.; b) M. Hashimoto, T. Murakami, K. Funahashi, T. Tokunaga, K. -i. Nihei, T. Okuno, T. Kimura, H. Naoki, H. Himeno, Bioorganic; medicinal chemistry, 2006, 14, 8259.; c) N. Mizuhara, M. Kuroda, A. Ogita, T. Tanaka, Y. Usuki, K. -i. Fujita, Bioorganic; medicinal chemistry, 2011, 19, 5300.

34- a) E. Selva, G. Beretta, N. Montanini, G. Saddler, L. Gastaldo, P. Ferrari, R. Lorenzetti, P. Landini, F. Ripamonti, B. Goldstein, The Journal of antibiotics, 1991, 44, 693.; b) M. J. LaMarche, J. A. Leeds, K. Amaral, J. T. Brewer, S. M. Bushell, J. M. Dewhurst, J. Dzink-Fox, E. Gangl, J. Goldovitz, A. Jain, Journal of medicinal chemistry, 2011, 54, 8099.

35- J. Martín, D. S. Sousa, G. Crespo, S. Palomo, I. González, J. R. Tormo, M. De la Cruz, M. Anderson, R. T. Hill, F. Vicente, Marine drugs, 2013, 11, 387.

36- a) B. W. Bycroft, M. S. Gowland, Journal of the Chemical Society, Chemical Communications, 1978, 256.; b) G. Degiacomi, Y. Personne, G. Mondésert, X. Ge, C. S. Mandava, R. C. Hartkoorn, F. Boldrin, P. Goel, K. Peisker, A. Benjak, Tuberculosis, 2016, 100, 95.; c) M. Lee, J. Yang, S. Park, E. Jo, H.-Y. Kim, Y.-S. Bae, M. P. Windisch, Antiviral research, 2016, 132, 287.

37- A. Mukai, T. Fukai, Y. Hoshino, K. Yazawa, K. -I. Harada, Y. Mikami, Journal of Antibiotics, 2009, 62, 613.

38- a) J. E. Leet, W. Li, H. A. Ax, J. A. Matson, S. Huang, R. Huang, J. L. Cantone, D. Drexler, R. A. Dalterio, K. S. Lam, The Journal of antibiotics, 2003, 56, 232.; b) W. Li, J. E. Leet, H. A. Ax, D. R. Gustavson, D. M. Brown, L. Turner, K. Brown, J. Clark, H. Yang, J. Fung-Tomc, The Journal of antibiotics 2003, 56, 226.; c) M. J. Pucci, J. J. Bronson, J. F. Barrett, K. L. DenBleyker, L. F. Discotto, J. C. Fung-Tomc, Y. Ueda, Antimicrobial agents and chemotherapy, 2004, 48, 3697.

39- a) F. Benazet, M. Cartier, J. Florent, C. Godard, G. Jung, J. Lunel, D. Mancy, C. Pascal, J. Renaut, P. Tarridec, Experientia, 1980, 36, 414.; b) J. M. Harms, D. N. Wilson, F. Schluenzen, S. R. Connell, T. Stachelhaus, Z. Zaborowska, C. M. T. Spahn, P.Fucini, Mol. Cell, 2008, 30, 26.; c) D. N. Wilson, Nat. Rev. Microbiol., 2014, 12, 35.; d) B. T. Porse, E. Cundliffe, R. A. Garrett, J. Mol. Biol., 1999, 287, 33.

40- a) M. Ebata, K. Miyazaki, H. Otsuka, The Journal of antibiotics, 1969, 22, 364.; b) K. Tori, K. Tokura, Y. Yoshimura, K. Okabe, H. Otsuka, F. Inagaki, T. Miyazawa, The Journal of antibiotics, 1979, 32, 1072.; c) X. Just-Baringo, F. Albericio, M. Álvarez, Mar. Drugs, 2014, 12, 317.; d) S. Baumann, S. Schoof, M. Bolten, C. Haering, M. Takagi, K. Shin-ya, H. D. Arndt, J. Am. Chem. Soc., 2010, 132, 6973.; e) J. Thompson, E. Cundliffe, M. Stark, Eur. J. Biochem., 1979, 98, 261.; f) S. Pestka, D. Weiss, R. Vince, Anal. Biochem. 1976, 71, 137.

41- a) Y. Egawa, K. Umino, Y. TAmura, M. Shimizu, K. Kaneko, M. Sakurazawa, S. Awataguchi, T. Okuda, The Journal of antibiotics, 1969, 22, 12.; b) J. Kohno, N. Kameda, M. Nishio, A. Kinumaki, S. Komatsubara, The Journal of antibiotics, 1996, 49, 1063.

42- R. P. Morris, J. A. Leeds, H. U. Naegeli, L. Oberer, K. Memmert, E. Weber, M. J. LaMarche, C. N. Parker, N. Burrer, S. Esterow, Journal of the American Chemical Society, 2009, 131, 5946.

43- a) B. Anderson, D. C. Hodgkin, M. A. Viswamitra, Nature 1970, 225, 233-235.; b) R. Donovick, J. F. Pagano, H. A. Stout, M. Weinstein, J. Antibiotics Annual, 1955, 3, 554.; c) J. D. Dutcher, J. Vandeputte, Antibiotics Annual, 1955, 3, 560.; d) Q. Zheng, Q. Wang, S. Wang, J. Wu, Q. Gao, W. Liu, Chemistry; biology 2015, 22, 1002.; e) F. Zhang, C. Li, W. L. Kelly, ACS chemical biology, 2016, 11, 415.

44- K. Engelhardt, K. F. Degnes, M. Kemmler, H. Bredholt, E. Fjærvik, G. Klinkenberg, H. Sletta, T. E. Ellingsen, S. B. Zotchev, Applied and environmental microbiology, 2010, 76, 4969.

45- C. Portmann, J. F. Blom, M. Kaiser, R. Brun, F. Jüttner, K. Gademann, Journal of natural products, 2008, 71, 1891.

46- a) G. G. Harrigan, W. Y. Yoshida, R. E. Moore, D. G. Nagle, P. U. Park, J. Biggs, V. J. Paul, S. L. Mooberry, T. H. Corbett, F. A. Valeriote, Journal of natural products, 1998, 61, 1221.; b) S. S. Mitchell, D. J. Faulkner, K. Rubins, F. D. Bushman, Journal of natural products, 2000, 63, 279.; c) H. Luesch, R. E. Moore, V. J. Paul, S. L. Mooberry, T. H. Corbett, Journal of Natural Products, 2001, 64, 907.; d) L. M. Nogle, W. H. Gerwick, Journal of natural products, 2002, 65, 21.; e) M. T. Davies-Coleman, T. M. Dzeha, C. A. Gray, S. Hess, L. K. Pannell, D. T. Hendricks, C. E. Arendse, Journal of natural products, 2003, 66, 712.

47- a) A. B. Williams, R. S. Jacobs, Cancer letters, 1993, 71, 97.; b) Y. In, M. Inoue, T. Ishida, Y. Hamada, T. Shioiri, Acta Crystallographica Section C: Crystal Structure Communications, 1994, 50, 432.; c) X. Fu, T. Do, F. J. Schmitz, V. Andrusevich, M. H. Engel, Journal of natural products, 1998, 61, 1547.; d) K. Sivonen, N. Leikoski, D. P. Fewer, J. Jokela, Applied microbiology and biotechnology, 2010, 86, 1213.; e) W. E. Houssen, M. Jaspars, ChemBioChem, 2010, 11, 1803.; e) J. Martins, V. Vasconcelos, Marine drugs, 2015, 13, 6910.

48- G. D. Garcia, B. F. Bowden, CA2252099 A1, 1997/10/23, 1997.

49- a) C. Ireland, P. J. Scheuer, Journal of the American Chemical Society, 1980, 102, 5688.; b) D. E. Williams, R. E. Moore, V. J. Paul, Journal of natural products, 1989, 52, 732.; c) K. Kohfuku, O. Yuko, Y. Yumi, K. Yutaka, K. Taketoshi, S. Yasuko, H. Yasumasa, S. Takayuki, Biochemical pharmacology, 1989, 38, 4497.

50- a) C. J. Schwalen, G. A. Hudson, B. Kille, D. A. Mitchell, J. Am. Chem. Soc., 2018, 140, 9494.; b) S. Um, E. Seibel, F. Schalk, S. Balluff, C. Beemelmanns, Journal of Natural Products, 2021, 84, 1002.

51- a) J. Santos-Aberturas, G. Chandra, L. Frattaruolo, R. Lacret, T. H. Pham, N. M. Vior, T. H. Eyles, A. W. Truman, Nucleic acids research, 2019, 47, 4624.; b) L. Frattaruolo, M. Fiorillo, M. Brindisi, R. Curcio, V. Dolce, R. Lacret, A. W. Truman, F. Sotgia, M. P. Lisanti, A. R. Cappello, Cells, 2019, 8, 1408.

52- L. Kjaerulff, A. Sikandar, N. Zaburannyi, S. Adam, J. Herrmann, J. Koehnke, R. Müller, ACS chemical biology, 2017, 12, 2837.

53- a) L. Frattaruolo, R. Lacret, A. R, Cappello, A. W. Truman, ACS Chem. Biol., 2017, 12, 2815.; b) T. Kawahara, M. Izumikawa, I. Kozone, J. Hashimoto, N. Kagaya, H. Koiwai, M. Komatsu, M. Fujie, N. Sato, H. Ikeda, K. Shin-ya, J. Nat. Prod., 2018, 81, 264.; c) Y. Li, J. Liu, H. Tang, Y. Qiu, D. Chen, W. Liu, Chinese Journal of Chemistry, 2019, 37, 1015.

54- T. Wieland, Pure Appl. Chem., 1964, 9, 145.; G. Moldenhauer, A. V. Salnikov, S. Lüttgau, I. Herr, J. Anderl, H. Faulstich, Journal of the National Cancer Institute, 2012, 104, 622.

55- a) C. C. Culvenor, P. A. Cockrum, J. A. Edgar, J. L. Frahn, C. P. Gorst-Allman, A. J. Jones, W. F. Marasas, K. E. Murray, L. W. Smith, P. S. Steyn, Journal of the Chemical Society, Chemical Communications, 1983, 1259.; b) Y. Li, H. Kobayashi, Y. Hashimoto, S. Iwasaki, Biochemical and biophysical research communications, 1992, 187, 722.; c) Y. Li, Y. Koiso, H. Kobayashi, Y. Hashimoto, S. Iwasaki, Biochemical pharmacology, 1995, 49, 1367.

56- a) Y. Koiso, Y. Li, S. Iwasaki, K. Hanaka, T. Kobayashi, R. Sonoda, Y. Fujita, H. Yaegashi, Z. Sato, The Journal of antibiotics, 1994, 47, 765.; b) Y. Li, Y. Koiso, H. Kobayashi, Y. Hashimoto, S. Iwasaki, Biochemical pharmacology, 1995, 49, 1367.; c) Y. Koiso, N. Morisaki, Y. Yamashita, Y. Mitsui, R. Shirai, Y. Hashimoto, S. Iwasaki, The Journal of antibiotics, 1998, 51, 418.

57- a) J. M. Waisvisz, M. G. van der Hoeven, J. van Peppen, W. C. M. Zwennis, J. Am. Chem. Soc., 1957, 79, 4520.; b) Y. Kobayashi, M. Ichioka, T. Hirose, K. Nagai, A. Matsumoto, H. Matsui, H. Hanaki, R. Masuma, Y. Takahashi, S. Ōmura, Bioorg. Med. Chem. Lett., 2010, 20, 6116.; c) T. Otaka, A. Kaji, J. Biol. Chem., 1976, 251, 2299.; d) T. Otaka, A. Kaji, FEBS Lett., 1981, 123, 173.; T. Otaka, A. Kaji, FEBS Lett., 1983, 153, 53.

58- a) T. Hamada, S. Matsunaga, G. Yano, N. Fusetani, Journal of the American Chemical Society, 2005, 127, 110.; b) T. Hamada, S. Matsunaga, M. Fujiwara, K. Fujita, H. Hirota, R.

Schmucki, P. Güntert, N. Fusetani, Journal of the American Chemical Society, 2010, 132, 12941.

59- a) M. O. Ishitsuka , T. Kusumi , H. Kakisawa , K. Kaya, M. M. Watanabe, J. Am. Chem. Soc., 1990, 112, 8180.; b) T. Okino, H. Matsuda, M. Murakami, K. Yamaguchi, Tetrahedron, 1995, 51, 10679.; c) H. J. Shin, M. Murakami, H. Matsuda, K. Yamaguchi, Tetrahedron, 1996, 52, 8159.; d) M. Murakami , Q. Sun , K. Ishida , H. Matsuda , T. Okino, K. Yamaguchi, Phytochemistry, 1997, 45, 1197.; e) B. Philmus, G. Christiansen, W. Y. Yoshida, T. K. Hemscheidt, ChemBioChem, 2008, 9, 3066.; f) T. Rohrlack, K. Christoffersen, M. Kaebernick, B. A. Neilan, Appl. Environ. Microbiol., 2004, 70, 5047.

60- Y. Li, S. Rebuffat, J. Biol. Chem., 2020, 295, 34.

61- D. Y. Travin, D. Bikmetov, K. Severinov, Frontiers in genetics, 2020, 11, 226.

62- a) Z. Jin, Natural product reports, 2013, 30, 869.; b) C. T. Walsh, Natural product reports, 2016, 33, 127.

63- a) J. Stubbe, J. W. Kozarich, W. Wu, D. E. Vanderwall, Accounts of chemical research 1996, 29, 322.; b) S. Puhalla, A. Brufsky, Biologics: targets; therapy 2008, 2, 505.

64- a) D. M. Citron, K. L. Tyrrell, C. V. Merriam, E. J. Goldstein, Antimicrobial agents and chemotherapy 2012, 56, 2493.; b) K. Mullane, C. Lee, A. Bressler, M. Buitrago, K. Weiss, K. Dabovic, J. Praestgaard, J. A. Leeds, J. Blais, P. Pertel, Antimicrobial agents and chemotherapy 2015, 59, 1435.; c) P. Lassalas, C. Berini, J.-B. E. Rouchet, J. Hédouin, F. Marsais, C. Schneider, C. Baudequin, C. Hoarau, Organic; biomolecular chemistry 2018, 16, 526.

65- a) NAICONS Srl. Clinical efficacy and safety of NAI-Acne gel 3% applied twice-a-day to patients with facial acne vulgaris. https://www.clinicaltrialsregister.eu/ctr search/search?query= 2014-001491-62. European Medicines Agency: EU Clinical Trials Register: Slovakia. Accessed 10 May 2021.; b) A. Fabbretti, C.-G. He, E. Gaspari, S. Maffioli, L. Brandi, R. Spurio, M. Sosio, D. Jabes, S. Donadio, Antimicrobial agents and chemotherapy 2015, 59, 4560.

66- a) M. J. LaMarche, J. A. Leeds, J. Dzink-Fox, E. Gangl, P. Krastel, G. Neckermann, D. Palestrant, M. A. Patane, E. M. Rann, S. Tiamfook, D. Yu, Journal of medicinal chemistry 2012, 55, 6934-6941.; b) M. J. LaMarche, J. A. Leeds, J. Brewer, K. Dean, J. Ding, J. Dzink-Fox, G. Gamber, A. Jain, R. Kerrigan, P. Krastel, K. Lee, F. Lombardo, D. McKenney, G. Neckermann, C. Osborne, D. Palestrant, M. A. Patane, E. M. Rann, Z. Robinson, E. Schmitt, T. Stams, S. Tiamfook, D. Yu, L. Whitehead, Journal of medicinal chemistry 2016, 59, 6920.

67- a) B. N. Naidu, M. E. Sorenson, J. J. Bronson, M. J. Pucci, J. M. Clark, Y. Ueda, Bioorganic; medicinal chemistry letters 2005, 15, 2069.; b) M. Wei, S. Wang, Y. Fang, Y. Chen, Bioresource technology 2010, 101, 3617.; c) L. Xu, A. K. Farthing, J. F. Dropinski, P. T. Meinke, C. McCallum, E. Hickey, K. Liu, Bioorganic; medicinal chemistry letters 2013, 23, 366.; d) A. Regueiro-Ren, B. N. Naidu, X. Zheng, T. W. Hudyma, T. P. Connolly, J. D. Matiskella, Y. Zhang, O. K. Kim, M. E. Sorenson, M. Pucci, Bioorganic; medicinal chemistry letters 2004, 14, 171.

68- S. Wang, Q. Zheng, J. Wang, Z. Zhao, Q. Li, Y. Yu, R. Wang, W. Liu, Organic Chemistry Frontiers 2015, 2, 106.

69- a) J. D. Hegemann, K. J. Dit-Foque, X. Xie, in Comprehensive Natural Products III, 2020, pp. 206.; b) C. Cheng, Z.-C. Hua, Frontiers in bioengineering and biotechnology 2020, 8.

70- a) J. Yuzenkova, M. Delgado, S. Nechaev, D. Savalia, V. Epshtein, I. Artsimovitch, R. A. Mooney, R. Landick, R. N. Farias, R. Salomon, Journal of Biological Chemistry 2002, 277, 50867-50875.; b) A. Bellomio, P. A. Vincent, B. F. de Arcuri, R. A. Salomón, R. D. Morero,

R. N. Farías, Biochemical and biophysical research communications 2004, 325, 1454-1458.; c) K. Adelman, J. Yuzenkova, A. La Porta, N. Zenkin, J. Lee, J. T. Lis, S. Borukhov, M. D. Wang, K. Severinov, Molecular cell 2004, 14, 753-762.; d) J. Mukhopadhyay, E. Sineva, J. Knight, R. M. Levy, R. H. Ebright, Molecular cell 2004, 14, 739-751.; e) H. Yu, X. Ding, L. Shang, X. Zeng, H. Liu, N. Li, S. Huang, Y. Wang, G. Wang, S. Cai, Frontiers in cellular and infection microbiology, 2018, 8, 242.

71- a) J. Leodolter, J. Warweg, E. Weber-Ban, PloS one, 2015, 10, e0125345.; b) I. Malik, H. Brötz-Oesterhelt, Natural product reports, 2017, 34, 815.

72- M. Sánchez-Hidalgo, J. Martín, O. Genilloud, Antibiotics, 2020, 9, 67.

73- a) T. A. Knappe, F. Manzenrieder, C. Mas-Moruno, U. Linne, F. Sasse, H. Kessler, X. Xie, M. A. Marahiel, Angewandte Chemie International Edition, 2011, 50, 8714-8717.; b) J. D. Hegemann, M. De Simone, M. Zimmermann, T. A. Knappe, X. Xie, F. S. Di Leva, L. Marinelli, E. Novellino, S. Zahler, H. Kessler, X.Xie, M. A. Marahiel, Journal of medicinal chemistry, 2014, 57, 5829-5834.

74- a) L. M. Repka, J. R. Chekan, S. K. Nair, W. A. van der Donk, Chem Rev, 2017, 117, 5457.; b) W. A. van der Donk, S. K. Nair, Current opinion in structural biology, 2014, 29, 58-66.

75- M. A. Funk, W. A. van der Donk, Acc Chem Res, 2017, 50, 1577.

76- Q. Zhang, J. R. Doroghazi, X. Zhao, M. C. Walker, W. A. van der Donk, Applied and environmental microbiology, 2015, 81, 4339.

77- M. Montalban-Lopez, T. A. Scott, S. Ramesh, I. R. Rahman, A. J. van Heel, J. H. Viel, V. Bandarian, E. Dittmann, O. Genilloud, Y. Goto, M. J. Grande Burgos, C. Hill, S. Kim, J. Koehnke, J. A. Latham, A. J. Link, B. Martinez, S. K. Nair, Y. Nicolet, S. Rebuffat, H. G. Sahl, D. Sareen, E. W. Schmidt, L. Schmitt, K. Severinov, R. D. Süssmuth, A. W. Truman, H. Wang, J. K. Weng, G. P. van Wezel, Q. Zhang, J. Zhong, J. Piel, D. A. Mitchell, O. P. Kuipers, W. A. van der Donk, Nat Prod Rep, 2021, 38, 130.

78- J. D. Hegemann, R. D. Süssmuth, RSC Chemical Biology 2020, 1, 110.

79- M. A. Ortega, Y. Hao, Q. Zhang, M. C. Walker, W. A. van der Donk, S. K. Nair, Nature 2015, 517, 509.

80- N. Garg, L. M. Salazar-Ocampo, W. A. Van Der Donk, Proceedings of the national academy of sciences 2013, 110, 7258.

81- B. Li, J. P. J. Yu, J. S. Brunzelle, G. N. Moll, W. A. Van der Donk, S. K. Nair, Science 2006, 311, 1464.

82- J. E. Velásquez, X. Zhang, W. A. Van Der Donk, Chemistry; biology 2011, 18, 857.

83- a) N. Schnell, K. -D. Entian, U. Schneider, F. Götz, H. Zähner, R. Kellner, G. Jung, Nature 1988, 333, 276.; b) N. Schnell, K. -D. Entian, F. Götz, T. Hörner, R. Kellner, G. Jung, FEMS microbiology letters 1989, 58, 263.; c) F. Majer, D. G. Schmid, K. Altena, G. Bierbaum, T. Kupke, Journal of bacteriology 2002, 184, 1234.; d) D. G. Schmid, F. Majer, T. Kupke, G. Jung, Rapid communications in mass spectrometry 2002, 16, 1779.

84- a) S. I. Maffioli, M. Iorio, M. Sosio, P. Monciardini, E. Gaspari, S. Donadio, Journal of natural products 2014, 77, 79.; b) J. o. C. Cruz, M. Iorio, P. Monciardini, M. Simone, C. Brunati, E. Gaspari, S. I. Maffioli, E. Wellington, M. Sosio, S. Donadio, Journal of natural products 2015, 78, 2642.; c) M. A. Ortega, D. P. Cogan, S. Mukherjee, N. Garg, B. Li, G. N. Thibodeaux, S. I. Maffioli, S. Donadio, M. Sosio, J. Escano, ACS chemical biology 2017, 12, 548.

85- a) L. Xie, L. M. Miller, C. Chatterjee, O. Averin, N. L. Kelleher, W. A. Van Der Donk, Science 2004, 303, 679.; b) C. Chatterjee, L. M. Miller, Y. L. Leung, L. Xie, M. Yi, N. L. Kelleher, W. A. Van Der Donk, Journal of the American Chemical Society 2005, 127, 15332.; c) Y. Goto, B. Li, J. Claesen, Y. Shi, M. J. Bibb, W. A. van der Donk, PLoS Biol 2010, 8, e1000339.

86- a) Y. O. You, W. A. Van Der Donk, Biochemistry 2007, 46, 5991.; b) M. Paul, G. C. Patton, W. A. Van Der Donk, Biochemistry 2007, 46, 6268.
87- a) M. Skaugen, J. Nissen-Meyer, G. Jung, S. StevanoVic, K. Sletten, C. Inger, M. Abildgaard, I. Nes, Journal of Biological Chemistry 1994, 269, 27183.; b) P. D. Cotter, P. M. O'Connor, L. A. Draper, E. M. Lawton, L. H. Deegan, C. Hill, R. P. Ross, Proceedings of the National Academy of Sciences 2005, 102, 18584.
88- a) A. Fredenhagen, G. Fendrich, F. Märki, W. Märki, J. Gruner, F. Raschdorf, H. H. Peter, The Journal of antibiotics 1990, 43, 1403.; b) N. Zimmermann, S. Freund, A. Fredenhagen, G. Jung, European journal of biochemistry 1993, 216, 419.
89- a) W. M. Müller, P. Ensle, B. Krawczyk, R. D. Süssmuth, Biochemistry 2011, 50, 8362.; b) Y. Goto, A. e. Ökesli, W. A. Van Der Donk, Biochemistry 2011, 50, 891.
90- W. M. Müller, T. Schmiederer, P. Ensle, R. D. Süssmuth, Angewandte Chemie International Edition 2010, 49, 2436.
91- K. Meindl, T. Schmiederer, K. Schneider, A. Reicke, D. Butz, S. Keller, H. Gühring, L. Vértesy, J. Wink, H. Hoffmann, M.Brönstrup, G. M. Sheldrick, R. D. Süssmuth, Angewandte Chemie International Edition 2010, 49, 1151.
92- a) H. Wang, W. A. Van Der Donk, ACS chemical biology 2012, 7, 1529.; b) J. M. Krawczyk, G. H. Völler, B. Krawczyk, J. Kretz, M. Brönstrup, R. D. Süssmuth, Chemistry; biology 2013, 20, 111.; c) M. Iorio, O. Sasso, S. I. Maffioli, R. Bertorelli, P. Monciardini, M. Sosio, F. Bonezzi, M. Summa, C. Brunati, R. Bordoni, ACS chemical biology 2014, 9, 398.
93- a) G. Liu, J. Zhong, J. Ni, M. Chen, H. Xiao, L. Huan, Microbiology 2009, 155, 584.; b) A. L. McClerren, L. E. Cooper, C. Quan, P. M. Thomas, N. L. Kelleher, W. A. Van Der Donk, Proceedings of the National Academy of Sciences 2006, 103, 17243.
94- J. O. Melby, N. J. Nard, D. A. Mitchell, Current opinion in chemical biology 2011, 15, 369.
95- a) R. S. Roy, P. J. Belshaw, C. T. Walsh, Biochemistry 1998, 37, 4125.; b) K. Engelhardt, K. F. Degnes, S. B. Zotchev, Applied and environmental microbiology 2010, 76, 7093.; c) M. S. Donia, J. Ravel, E. W. Schmidt, Nature chemical biology 2008, 4, 341.; d) B. J. Burkhart, C. J. Schwalen, G. Mann, J. H. Naismith, D. A. Mitchell, Chem Rev 2017, 117, 5389.
96- a) J. C. Milne, R. S. Roy, A. C. Eliot, N. L. Kelleher, A. Wokhlu, B. Nickels, C. T. Walsh, Biochemistry 1999, 38, 4768.; b) K. L. Dunbar, J. O. Melby, D. A. Mitchell, Nature chemical biology 2012, 8, 569.; c) K. L. Dunbar, J. R. Chekan, C. L. Cox, B. J. Burkhart, S. K. Nair, D. A. Mitchell, Nature chemical biology 2014, 10, 823.; d) B. J. Burkhart, G. A. Hudson, K. L. Dunbar, D. A. Mitchell, Nature chemical biology 2015, 11, 564.
97- Y. -M. Li, J. C. Milne, L. L. Madison, R. Kolter, C. T. Walsh, Science 1996, 274, 1188.; K. Li, H. L. Condurso, G. Li, Y. Ding, S. D. Bruner, Nature chemical biology 2016, 12, 973.
98- a) L. C. W. Brown, M. G. Acker, J. Clardy, C. T. Walsh, M. A. Fischbach, Proceedings of the National Academy of Sciences 2009, 106, 2549.; b) S. Hayashi, T. Ozaki, S. Asamizu, H. Ikeda, S. Ōmura, N. Oku, Y. Igarashi, H. Tomoda, H. Onaka, Chemistry; biology 2014, 21, 679.; c) G. A. Hudson, Z. Zhang, J. I. Tietz, D. A. Mitchell, W. A. Van Der Donk, Journal of the American Chemical Society 2015, 137, 16012.
99- K. L. Dunbar, D. A. Mitchell, Journal of the American Chemical Society 2013, 135, 8692-8701.
100- a) Y. Igarashi, Y. Kan, K. Fujii, T. Fujita, K.-I. Harada, H. Naoki, H. Tabata, H. Onaka, T. Furumai, The Journal of antibiotics 2001, 54, 1045.; b) T. Ozaki, Y. Kurokawa, S. Hayashi, N. Oku, S. Asamizu, Y. Igarashi, H. Onaka, ChemBioChem 2016, 17, 218.; c) W. L. Kelly, L. Pan, C. Li, Journal of the American Chemical Society 2009, 131, 4327.

101- a) D. B. Zamble, D. A. Miller, J. G. Heddle, A. Maxwell, C. T. Walsh, F. Hollfelder, Proceedings of the National Academy of Sciences 2001, 98, 7712.; b) F. J. del Castillo, I. del Castillo, F. Moreno, Journal of bacteriology 2001, 183, 2137-.; c) W. M. Parks, A. R. Bottrill, O. A. Pierrat, M. C. Durrant, A. Maxwell, Biochimie 2007, 89, 500.

102- a) F. Collin, R. E. Thompson, K. A. Jolliffe, R. J. Payne, A. Maxwell, PLoS One 2013, 8, e61459.; b) I. Shkundina, M. Serebryakova, K. Severinov, Journal of bacteriology 2014, 196, 1759.

103- N. L. Kelleher, P. J. Belshaw, C. T. Walsh, Journal of the American Chemical Society 1998, 120, 9716.

104- a) R. S. Roy, N. L. Kelleher, J. C. Milne, C. T. Walsh, Chemistry; biology 1999, 6, 305.; b) M. Metelev, M. Serebryakova, D. Ghilarov, Y. Zhao, K. Severinov, Journal of bacteriology 2013, 195, 4129.

105- a) S. W. Lee, D. A. Mitchell, A. L. Markley, M. E. Hensler, D. Gonzalez, A. Wohlrab, P. C. Dorrestein, V. Nizet, J. E. Dixon, Proceedings of the National Academy of Sciences 2008, 105, 5879.; b) K. J. Molohon, J. O. Melby, J. Lee, B. S. Evans, K. L. Dunbar, S. B. Bumpus, N. L. Kelleher, D. A. Mitchell, ACS chemical biology 2011, 6, 1307.; c) Z. Liu, A. Budiharjo, P. Wang, H. Shi, J. Fang, R. Borriss, K. Zhang, X. Huang, Applied microbiology and biotechnology 2013, 97, 10081.

106- C. D. Deane, B. J. Burkhart, P. M. Blair, J. I. Tietz, A. Lin, D. A. Mitchell, ACS chemical biology 2016, 11, 2232.

107- a) T. Romantsov, Z. Guan, J. M. Wood, Biochimica et Biophysica Acta (BBA)-Biomembranes 2009, 1788, 2092.; b) J. D. Unsay, K. Cosentino, Y. Subburaj, A. J. García-Sáez, Langmuir 2013, 29, 15878.; c) K. J. Molohon, P. M. Blair, S. Park, J. R. Doroghazi, T. Maxson, J. R. Hershfield, K. M. Flatt, N. E. Schroeder, T. Ha, D. A. Mitchell, ACS infectious diseases 2016, 2, 207.

108- C. D. Deane, J. O. Melby, K. J. Molohon, A. R. Susarrey, D. A. Mitchell, ACS chemical biology 2013, 8, 1998.

109- a) A. Sharma, P. M. Blair, D. A. Mitchell, Organic letters 2013, 15, 5076.; b) S. Banala, P. Ensle, R. D. Süssmuth, Angewandte Chemie International Edition 2013, 52, 9518.; c) H. Wada, H. E. Williams, C. J. Moody, Angewandte Chemie 2015, 127, 15362.; d) N. A. Piwowarska, S. Banala, H. S. Overkleeft, R. D. Süssmuth, Chemical Communications 2013, 49, 10703.

110- a) A. Funk, P. Divekar, Canadian journal of microbiology 1959, 5, 317.; b) B. W. Bycroft, R. Pinchin, Journal of the Chemical Society, Chemical Communications 1975, 121.; c) M. Hashimoto, T. Komori, T. Kamiya, The Journal of antibiotics 1976, 29, 890.; d) Z. J. Anderson, D. J. Fox, Organic; biomolecular chemistry 2016, 14, 1450.

111- N. Liu, L. Song, M. Liu, F. Shang, Z. Anderson, D. J. Fox, G. L. Challis, Y. Huang, Chemical science 2015, 7, 482-488.

112- a) H. Onaka, H. Tabata, Y. Igarashi, Y. Sato, T. Furumai, The Journal of antibiotics 2001, 54, 1036.; b) H. Onaka, The Journal of antibiotics 2017, 70, 865.

113- H. Onaka, M. Nakaho, K. Hayashi, Y. Igarashi, T. Furumai, Microbiology 2005, 151, 3923.

114- a) J. P. Gomez-Escribano, L. Song, M. J. Bibb, G. L. Challis, Chemical Science 2012, 3, 3522.; b) W. J. Crone, F. J. Leeper, A. W. Truman, Chemical Science 2012, 3, 3516.

115- N. Mahanta, D. M. Szantai-Kis, E. J. Petersson, D. A. Mitchell, ACS chemical biology 2019, 14, 142.

116- a) Y. Hayakawa, K. Sasaki, H. Adachi, K. Furihata, K. Nagai, K. Shin-Ya, The Journal of antibiotics 2006, 59, 1.; b) Y. Hayakawa, K. Sasaki, K. Nagai, K. Shin-Ya, K. Furihata, The Journal of antibiotics 2006, 59, 6.

117- a) M. Izawa, T. Kawasaki, Y. Hayakawa, Applied and environmental microbiology 2013, 79, 7110.; b) M. Izumikawa, I. Kozone, J. Hashimoto, N. Kagaya, M. Takagi, H. Koiwai, M. Komatsu, M. Fujie, N. Satoh, H. Ikeda, The Journal of antibiotics 2015, 68, 533.

118- T. H. Eyles, N. M. Vior, R. Lacret, A. W. Truman, Chemical Science 2021, DOI: 10.1039/D0SC06835G

119- a) M. O. Maksimov, S. J. Pan, A. J. Link, Natural product reports 2012, 29, 996.; b) J. D. Hegemann, M. Zimmermann, X. Xie, M. A. Marahiel, Accounts of chemical research 2015, 48, 1909.

120- a) M. O. Maksimov, I. Pelczer, A. J. Link, Proceedings of the National Academy of Sciences 2012, 109, 15223.; b) J. D. Hegemann, M. Zimmermann, S. Zhu, D. Klug, M. A. Marahiel, Peptide Science 2013, 100, 527.; c) J. I. Tietz, C. J. Schwalen, P. S. Patel, T. Maxson, P. M. Blair, H.-C. Tai, U. I. Zakai, D. A. Mitchell, Nature chemical biology 2017, 13, 470.

121- J. D. Hegemann, M. Zimmermann, S. Zhu, H. Steuber, K. Harms, X. Xie, M. A. Marahiel, Angewandte Chemie International Edition 2014, 53, 2230.

122- a) M. Zimmermann, J. D. Hegemann, X. Xie, M. A. Marahiel, Chemical Science 2014, 5, 4032.; b) C. Zong, M. J. Wu, J. Z. Qin, A. J. Link, Journal of the American Chemical Society 2017, 139, 10403.; c) M. Metelev, A. Arseniev, L. B. Bushin, K. Kuznedelov, T. O. Artamonova, R. Kondratenko, M. Khodorkovskii, M. R. Seyedsayamdost, K. Severinov, ACS chemical biology 2017, 12, 814.

123- a) M. Zimmermann, J. D. Hegemann, X. Xie, M. A. Marahiel, Chemistry; biology 2013, 20, 558.; b) C. D. Fage, J. D. Hegemann, A. J. Nebel, R. M. Steinbach, S. Zhu, U. Linne, K. Harms, G. Bange, M. A. Marahiel, Angewandte Chemie 2016, 128, 12909.; c) J. D. Hegemann, C. D. Fage, S. Zhu, K. Harms, F. S. Di Leva, E. Novellino, L. Marinelli, M. A. Marahiel, Molecular BioSystems 2016, 12, 1106.; d) S. Zhu, J. D. Hegemann, C. D. Fage, M. Zimmermann, X. Xie, U. Linne, M. A. Marahiel, Journal of Biological Chemistry 2016, 291, 13662.; e) M. O. Maksimov, A. J. Link, Journal of the American Chemical Society 2013, 135, 12038.

124- T. A. Knappe, U. Linne, L. Robbel, M. A. Marahiel, Chemistry; biology 2009, 16, 1290.

125- J. D. Hegemann, M. Zimmermann, X. Xie, M. A. Marahiel, Journal of the American Chemical Society 2013, 135, 210.

126- P. G. Arnison, M. J. Bibb, G. Bierbaum, A. A. Bowers, T. S. Bugni, G. Bulaj, J. A. Camarero, D. J. Campopiano, G. L. Challis, J. Clardy, P. D. Cotter, D. J. Craik, M. Dawson, E. Dittmann, S. Donadio, P. C. Dorrestein, K. D. Entian, M. A. Fischbach, J. S. Garavelli, U. Goransson, C. W. Gruber, D. H. Haft, T. K. Hemscheidt, C. Hertweck, C. Hill, A. R. Horswill, M. Jaspars, W. L. Kelly, J. P. Klinman, O. P. Kuipers, A. J. Link, W. Liu, M. A. Marahiel, D. A. Mitchell, G. N. Moll, B. S. Moore, R. Muller, S. K. Nair, I. F. Nes, G. E. Norris, B. M. Olivera, H. Onaka, M. L. Patchett, J. Piel, M. J. Reaney, S. Rebuffat, R. P. Ross, H. G. Sahl, E. W. Schmidt, M. E. Selsted, K. Severinov, B. Shen, K. Sivonen, L. Smith, T. Stein, R. D. Sussmuth, J. R. Tagg, G. L. Tang, A. W. Truman, J. C. Vederas, C. T. Walsh, J. D. Walton, S. C. Wenzel, J. M. Willey, W. A. van der Donk, Nat Prod Rep 2013, 30, 108.

127- a) C. Zong, W. L. Cheung-Lee, H. E. Elashal, M. Raj and A. J. Link, Chemical Communications 2018, 54, 1339.; b) J. Mevaere, C. Goulard, O. Schneider, O. N. Sekurova, H. Ma, S. Zirah, C. Afonso, S. Rebuffat, S. B. Zotchev, Y. Li, Scientific reports 2018, 8, 1.

128- a) S. Zhu, C. D. Fage, J. D. Hegemann, A. Mielcarek, D. Yan, U. Linne, M. A. Marahiel, Scientific reports 2016, 6, 1.; b) W. L. Cheung, M. Y. Chen, M. O. Maksimov, A. J. Link, ACS central science 2016, 2, 702.; c) C. Zong, M. O. Maksimov, A. J. Link, ACS chemical biology 2016, 11, 61.

129- a) A. J. DiCaprio, A. Firouzbakht, G. A. Hudson, D. A. Mitchell, Journal of the American Chemical Society 2019, 141, 290.; b) J. D. Hegemann, C. J. Schwalen, D. A. Mitchell, W. A. Van der Donk, Chemical Communications 2018, 54, 9007.

130- K. P. Yan, Y. Li, S. Zirah, C. Goulard, T. A. Knappe, M. A. Marahiel, S. Rebuffat, ChemBioChem 2012, 13, 1046.

131- S. J. Pan, J. Rajniak, M. O. Maksimov, A. J. Link, Chemical Communications 2012, 48, 1880.

132- a) S. Kodani, H. Hemmi, Y. Miyake, I. Kaweewan, H. Nakagawa, Journal of Industrial Microbiology and Biotechnology 2018, 45, 983.; b) M. Metelev, J. I. Tietz, J. O. Melby, P. M. Blair, L. Zhu, I. Livnat, K. Severinov, D. A. Mitchell, Chemistry; biology 2015, 22, 241.

133- H. Martin-Gómez, U. Linne, F. Albericio, J. Tulla-Puche, J. D. Hegemann, Journal of natural products 2018, 81, 2050.

134- S. Zhu, C. D. Fage, J. D. Hegemann, D. Yan, M. A. Marahiel, FEBS letters 2016, 590, 3323.

135- a) Y. Morishita, S. Chiba, E. Tsukuda, T. Tanaka, T. Ogawa, M. Yamasaki, M. Yoshida, I. Kawamoto, Y. Matsuda, J. Antibiot. (Tokyo) 1994, 47, 269.; b) T. Ogawa, K. Ochiai, T. Tanaka, E. Tsukuda, S. Chiba, K. Yano, M. Yamasaki, M. Yoshida, Y. Matsuda, J. Antibiot. (Tokyo) 1995, 48, 1213.

136- a) K. Yano, S. Toki, S. Nakanishi, K. Ochiai, K. Ando, M. Yoshida, Y. Matsuda, M. Yamasaki, Bioorganic; medicinal chemistry 1996, 4, 115.; b) Z. Feng, Y. Ogasawara, S. Nomura, T. Dairi, ChemBioChem 2018, 19, 2045.

137- Z. Feng, Y. Ogasawara, T. Dairi, Chemical Science 2021, 12, 2567.

138- L. A. Harris, P. M. Saint-Vincent, X. Guo, G. A. Hudson, A. J. DiCaprio, L. Zhu, D. A. Mitchell, ACS chemical biology 2020, 15, 3167.

139- a) Z. Zhong, B. He, J. Li, Y.-X. Li, Synthetic and Systems Biotechnology 2020, 5, 155. ; b) A. H. Russell, A. W. Truman, Computational and Structural Biotechnology Journal 2020, 1838.

140- a) K. Blin, S. Shaw, K. Steinke, R. Villebro, N. Ziemert, S. Y. Lee, M. H. Medema, T. Weber, Nucleic acids research 2019, 47, W81.; b) M. A. Skinnider, C. A. Dejong, P. N. Rees, C. W. Johnston, H. Li, A. L. Webster, M. A. Wyatt, N. A. Magarvey, Nucleic acids research 2015, 43, 9645.; c) A. J. van Heel, A. de Jong, C. Song, J. H. Viel, J. Kok, O. P. Kuipers, Nucleic acids research 2018, 46, W278.; d) P. Agrawal, S. Khater, M. Gupta, N. Sain, D. Mohanty, Nucleic acids research 2017, 45, W80.; e) N. J. Merwin, W. K. Mousa, C. A. Dejong, M. A. Skinnider, M. J. Cannon, H. Li, K. Dial, M. Gunabalasingam, C. Johnston, N. A. Magarvey, Proceedings of the National Academy of Sciences 2020, 117, 371.

141- a) J. A. Gerlt, J. T. Bouvier, D. B. Davidson, H. J. Imker, B. Sadkhin, D. R. Slater, K. L. Whalen, Biochimica Et Biophysica Acta (BBA)-Proteins and Proteomics 2015, 1854, 1019.; b) J. C. Navarro-Muñoz, N. Selem-Mojica, M. W. Mullowney, S. A. Kautsar, J. H. Tryon, E. I. Parkinson, E. L. De Los Santos, M. Yeong, P. Cruz-Morales, S. Abubucker, A. Roeters, W. Lokhorst, A. F. Guerra, L. Teresa, D. Cappelini, A. W. Goering, R. J. Thomson, W. W. Metcalf, N. L. Kelleher, F. B. Gomez, M. H. Medema, Nature chemical biology 2020, 16, 60.; c) M. H. Medema *et al.*, Nature chemical biology 2015, 11, 625.

142- a) J. I Tietz, D. A. Mitchell, Current topics in medicinal chemistry 2016, 16, 1645.; b) J. J. van Der Hooft, H. Mohimani, A. Bauermeister, P. C. Dorrestein, K. R. Duncan, M. H. Medema, Chemical Society Reviews 2020, 49, 3297.

143- a) C. L. Cox, J. I. Tietz, K. Sokolowski, J. O. Melby, J. R. Doroghazi, D. A. Mitchell, ACS chemical biology 2014, 9, 2014.; b) M. A. Georgiou, S. R. Dommaraju, X. Guo, D. H. Mast, D. A. Mitchell, ACS chemical biology 2020, 15, 2976.

144- H. Mohimani, R. D. Kersten, W.-T. Liu, M. Wang, S. O. Purvine, S. Wu, H. M. Brewer, L. Pasa-Tolic, N. Bandeira, B. S. Moore, ACS chemical biology 2014, 9, 1545.

145- H. H. Mehta, Y. Shamoo, PLoS pathogens 2020, 16, e1008280.

146- a) B. L. Beaman, L. Beaman, Clinical microbiology reviews 1994, 7, 213.; b) P. I. Lerner, Clinical infectious diseases 1996, 891.; c) J. Coussement, D. Lebeaux, C. Rouzaud, O. Lortholary, Current opinion in infectious diseases 2017, 30, 545.

147- a) T. Tamura, S. Ohji, N. Ichikawa, A. Hosoyama, A. Yamazoe, M. Hamada, H. Komaki, C. Shibata, T. Matsuzawa, T. Gonoi, The Journal of antibiotics 2018, 71, 633.; b) P. S. Conville, B. A. Brown-Elliott, T. Smith, A. M. Zelazny, Journal of clinical microbiology 2018, 56.; c) D. Männle, S. M. McKinnie, S. S. Mantri, K. Steinke, Z. Lu, B. S. Moore, N. Ziemert, L. Kaysser, Msystems 2020, 5.

148- a) H. Shigemori, H. Komaki, K. Yazawa, Y. Mikami, A. Nemoto, Y. Tanaka, T. Sasaki, Y. In, T. Ishida, J. i. Kobayashi, The Journal of organic chemistry 1998, 63, 6900.; b) S. Hideyuki, T. Yasushi, Y. Katsukiyo, M. Yuzuru, K. Jun'ichi, Tetrahedron 1996, 52, 9031.; c) F. Maglangit, Y. Yu, H. Deng, Natural Product Reports 2021, 38, 782.; d) D. Dhakal, V. Rayamajhi, R. Mishra, J. K. Sohng, J Ind Microbiol Biotechnol 2019, 46, 385.

149- a) Y. Tanaka, H. Komaki, K. Yazawa, Y. Mikami, A. Nemoto, T. Tojyo, K. Kadowaki, H. Shigemori, J. I. Kobayashi, The Journal of antibiotics 1997, 50, 1036.; b) Y. Hoshino, K. Watanabe, S. Iida, S.-i. Suzuki, T. Kudo, T. Kogure, K. Yazawa, J. Ishikawa, R. M. Kroppenstedt, Y. Mikami, International journal of systematic and evolutionary microbiology 2007, 57, 1456.; c) M. Nett, H. Ikeda, B. S. Moore, Natural product reports 2009, 26, 1362.

150- a) A. Buchmann, M. Eitel, P. Koch, P. N. Schwarz, E. Stegmann, W. Wohlleben, M. Wolański, M. Krawiec, J. Zakrzewska-Czerwińska, C. Méndez, A. Botas, L. E. Núñez, F. Morís, J. Cortés, H. Gross Genome announcements 2016, 4, e01391-01316.; b) A. Buchmann, H. Gross, Microbiology Resource Announcements 2020, 9, e00689-20.; c) H. Komaki, N. Ichikawa, A. Hosoyama, A. Takahashi-Nakaguchi, T. Matsuzawa, K. Suzuki, N. Fujita, T. Gonoi, BMC genomics 2014, 15, 1.

151- a) S. Hideyuki, T. Yasushi, Y. Katsukiyo, M. Yuzuru, K. Jun'ichi, Tetrahedron 1996, 52, 9031.; b) Y. Mikami, H. Komaki, T. Imai, K. Yazawa, A. Nemoto, Y. Tanaka, U. GRÄEFE, The Journal of Antibiotics 2000, 53, 70.; c) H. T. Chiu, C. P. Weng, Y. C. Lin, K. H. Chen, Org Biomol Chem 2016, 14, 1988.; d) H. Shigemori, H. Komaki, K. Yazawa, Y. Mikami, A. Nemoto, Y. Tanaka, T. Sasaki, Y. In, T. Ishida, J. i. Kobayashi, The Journal of organic chemistry 1998, 63, 6900.; e) Y. Hayashi, N. Matsuura, H. Toshima, N. Itoh, J. Ishikawa, Y. Mikami, T. Dairi, The Journal of antibiotics 2008, 61, 164-174.

152- V. Wiebach, A. Mainz, M. J. Siegert, N. A. Jungmann, G. Lesquame, S. Tirat, A. Dreux-Zigha, J. Aszodi, D. Le Beller, R. D. Sussmuth, Nat Chem Biol 2018, 14, 652.

153- E. C. Rosenow, Journal of Dental Research 1919, 1, 205.

154- Y. Ikeda, H. Nonaka, T. Furumai, H. Onaka, Y. Igarashi, J. Nat. Prod. 2005, 68, 1061–1065.

155- T. P. Wyche, Y. Hou, E. Vazquez-Rivera, D. Braun, T. S. Bugni. J. Nat. Prod. 2012, 75, 735.

156- K. Kumagai, K. Taya, A. Fukui, M. Fukasawa, M. Fukui, S. Nabeshima, The Journal of antibiotics 1993, 46, 972.
157- I. Perez-Victoria, D. Oves-Costales, R. Lacret, J. Martin, M. Sanchez-Hidalgo, C. Diaz, B. Cautain, F. Vicente, O. Genilloud, F. Reyes, Org Biomol Chem 2019, 17, 2954.
158- N. Garg, C. A. Kapono, Y. W. Lim, N. Koyama, M. J. A Vermeij, D. Conrad, F. Rohwer, P. C. Dorrestein, Int. J. Mass Spectrom. 2015, 377, 719.
159- J. Chen, A. Frediansyah, D. Männle, J. Straetener, H. Brötz-Oesterhelt, N. Ziemert, L. Kaysser, H. Gross, ChemBioChem 2020, 21, 2205.
160- M. Wang, J. J. Carver, V. V. Phelan, L. M. Sanchez, N. Garg, Y. Peng, D. D. Nguyen, J. Watrous, C. A. Kapono, T. Luzzatto-Knaan, C. Porto, A. Bouslimani, A. V. Melnik, M. J. Meehan, W.-T. Liu, M. Crüsemann, P. D. Boudreau, E. Esquenazi, M. Sandoval-Calderon, R. D. Kersten, L. A. Pace, R. A. Quinn, K. R. Duncan, C.-C. Hsu, D. J. Floros, R. G. Gavilan, K. Kleigrewe, T. Northen, R. J. Dutton, D. Parrot, E. E. Carlson, B. Aigle, C. F. Michelsen, L. Jelsbak, C. Sohlenkamp, P. Pevzner, A. Edlund, J. McLean, J. Piel, B. T. Murphy, L. Gerwick, C.-C. Liaw, Y.-L. Yang, H.-U. Humpf, M. Maansson, R. A. Keyzers, A. C. Sims, A. R. Johnson, A. M. Sidebottom, B. E. Sedio, A. Klitgaard, C. B. Larson, C. A. Boya P, D. Torres-Mendoza, D. J. Gonzalez, D. B. Silva, L. M. Marques, D. P. Demarque, E. Pociute, E. C. O'Neill, E. Briand, E. J. N. Helfrich, E. A. Granatosky, E. Glukhov, F. Ryffel, H. Houson, H. Mohimani, J. J. Kharbush, Y. Zeng, J. A. Vorholt, K. L. Kurita, P. Charusanti, K. L. McPhail, K. F. Nielsen, L. Vuong, M. Elfeki, M. F. Traxler, N. Engene, N. Koyama, O. B. Vining, R. Baric, R. R. Silva, S. J. Mascuch, S. Tomasi, S. Jenkins, V. Macherla, T. Hoffman, V. Agarwal, P. G. Williams, J. Dai, R. Neupane, J. Gurr, A. M. C. Rodriguez, A. Lamsa, C. Zhang, K. Dorrestein, B. M. Duggan, J. Almaliti, P.-M. Allard, P. Phapale, L.-F. Nothias, T. Alexandrov, M. Litaudon, J.-L. Wolfender, J. E. Kyle, T. O. Metz, T. Peryea, D.-T. Nguyen, D. VanLeer, P. Shinn, A. Jadhav, R. Müller, K. M. Waters, W. Shi, X. Liu, L. Zhang, R. Knight, P. R. Jensen, B. O. Palsson, K. Pogliano, R. G. Linington, M. Gutierrez, N. P. Lopes, W. H. Gerwick, B. S. Moore, P. C. Dorrestein, N. Bandeira, Nat. Biotechnol. 2016, 34, 828.
161- W. Linhuan, M. Juncai, Int. J. Syst. Evol. Microbiol. 2019, 69, 895.
162- A. M. Kloosterman, K. E. Shelton, G. P. van Wezel, M. H. Medema, D. A. Mitchell, mSystems 2020, 5, e00267.
163- M. C. Arendrup, J. Meletiadis, J. W. Mouton, K. Lagrou, P. Hamal, J. Guinea and the Subcommittee on Antifungal Susceptibility Testing (AFST) of the ESCMID European Committee for Antimicrobial Susceptibility Testing (EUCAST). Method for the determination of broth dilution minimum inhibitory concentrations of antifungal agents for yeasts. EUCAST DEFINITIVE DOCUMENT E.DEF 7.3.2. April 2020. Accessed under https://www.eucast.org/astoffungi/methodsinantifungalsusceptibilitytesting/susceptibility_testing_of_yeasts/
164- H. Saad, S. Aziz, M. Gehringer, M. Kramer, J. Straetener, A. Berscheid, H. B.-Oesterhelt, H. Gross, Angew. Chem. Int. Ed., 2021, 60, 16472.
165- A. Angelopoulou, A. K. Warda, P. M. O´Connor, S. R. Stockdale, A. N. Shkoporov, D. Field, L. A. Draper, C. Stanton, C. Hill, R. P. Ross, Front. Microbiol. 2020, 11, 788.
166- R. Kozakai, T. Ono, S. Hoshino, H. Takahashi, Y. Katsuyama, Y. Sugai, T. Ozaki, K. Teramoto, K. Teramoto, K. Tanaka, Nature Chemistry 2020, 12, 869.
167- G. C. Levy, R. L. Lichter, Nitrogen-15 Nuclear Magnetic Resonance Spectroscopy, Wiley, New York, 1979.
168- C. T. Lohans, J. C. Vederas, J. Antibiot. 2014, 67, 23.

169- H. B. Bode, D. Reimer, S. W. Fuchs, F. Kirchner, C. Dauth, C. Kegler, W. Lorenzen, A. O. Brachmann, P. Grun, Chem. Eur. J. 2012, 18, 2342.

170- L. Huo, W. A. van der Donk, J. Am. Chem. Soc. 2016, 138, 5254.

171- a) A. Bhushan, P. J. Egli, E. E. Peters, M. F. Freeman, J. Piel, Nat. Chem. 2019, 11, 931–939; b) M. Korneli, S. W. Fuchs, K. Felder, C. Ernst, L. V. Zinsli, J. Piel, ACS Synth. Biol. 2021, 10, 236.

172- a) J. Ma, H. Huang, Y. Xie, Z. Liu, J. Zhao, C. Zhang, Y. Jia, Y. Zhang, H. Zhang, T. Zhang, J. Ju, Nat. Commun. 2017, 8, 391; b) M.-C. Tang, Y. Zou, K. Watanabe, C. T. Walsh, Y. Tang, Chem. Rev. 2017, 117, 5226.

173- a) S. Somma, W. Merati, F. Parenti, Antimicrob. Agents Chemother. 1977, 11, 396; b) L. Vertesy, W. Aretz, A. Bonnefoy, E. Ehlers, M. Kurz, A. Markus, M. Schiell, M. Vogel, J. Wink, H. Kogler, J. Antibiot. 1999, 52, 730; c) M. Simone, P. Monciardini, E. Gaspari, S. Donadio, S. I. Maffiolo, J. Antibiot. 2013, 66, 73.

174- a) M. C. Walker, S. M. Eslami, K. J. Hetrick, S. E. Ackenhusen, D. A. Mitchell, W. A. van der Donk, BMC Genomics 2020, 21, 387; b) C. Wu, W. A. van der Donk, Curr. Opin. Biotechnol. 2021, 69, 221; c) B. J. Burkhart, N. Kakkar, G. A. Hudson, W. A. van der Donk, D. A. Mitchell, ACS Cent. Sci. 2017, 3, 629.

175- K. Yano, M. Yamasaki, M. Yoshida, Y. Matsuda, K. Yamaguchi, The Journal of antibiotics 1995, 48, 1368.

176- D. Oves-Costales, M. Sánchez-Hidalgo, J. Martín, O. Genilloud, Marine drugs 2020, 18, 238.

177- C. Zhang, M. R. Seyedsayamdost, ACS chemical biology 2020, 15, 890.

178- K. R. Schramma, L. B. Bushin, M.d R. Seyedsayamdost, Nat. Chem. 2015, 7, 431.

179- Y. Imai, K. J. Meyer, A. Iinishi, Q. F. Godal, R. Green, S. Manuse, M. Caboni, M. Mori, S. Niles, M. Ghiglieri, C. Honrao, X. Ma, J. J. Guo, A. Makriyannis, L. L. Otoya, N. Böhringer, Z. G. Wuisan, H. Kaur, R. Wu, A. Mateus, A. Typas, M. M. Savitski, J. L. Espinoza, A. O'Rourke, K. E. Nelson, S. Hiller, N. Noinaj, T. F. Schäberle, A. D'Onofrio, Kim Lewis, Nature 576, 459.

180- K. Viehrig, F. Surup, C. Volz, J. Herrmann, A. Abou Fayad, S. Adam, J. Köhnke, D. Trauner, R. Müller, Angew. Chem., Int. Ed., 2017, 56, 7407.

181- T. P. Wyche, A. C. Ruzzini, L. Schwab, C. R. Currie, J. Clardy, J. Am. Chem. Soc., 2017, 139, 12899.

7. Appendix

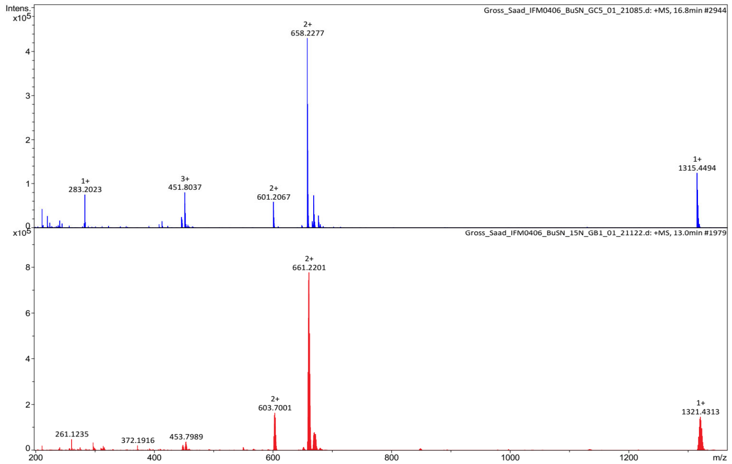

Figure A1. Comparative MS[1] of nocathioamide A (**1**) (1315 Da $[M+H]^+$, 658 Da $[M+2H]^{2+}$) and its ^{15}N-based version

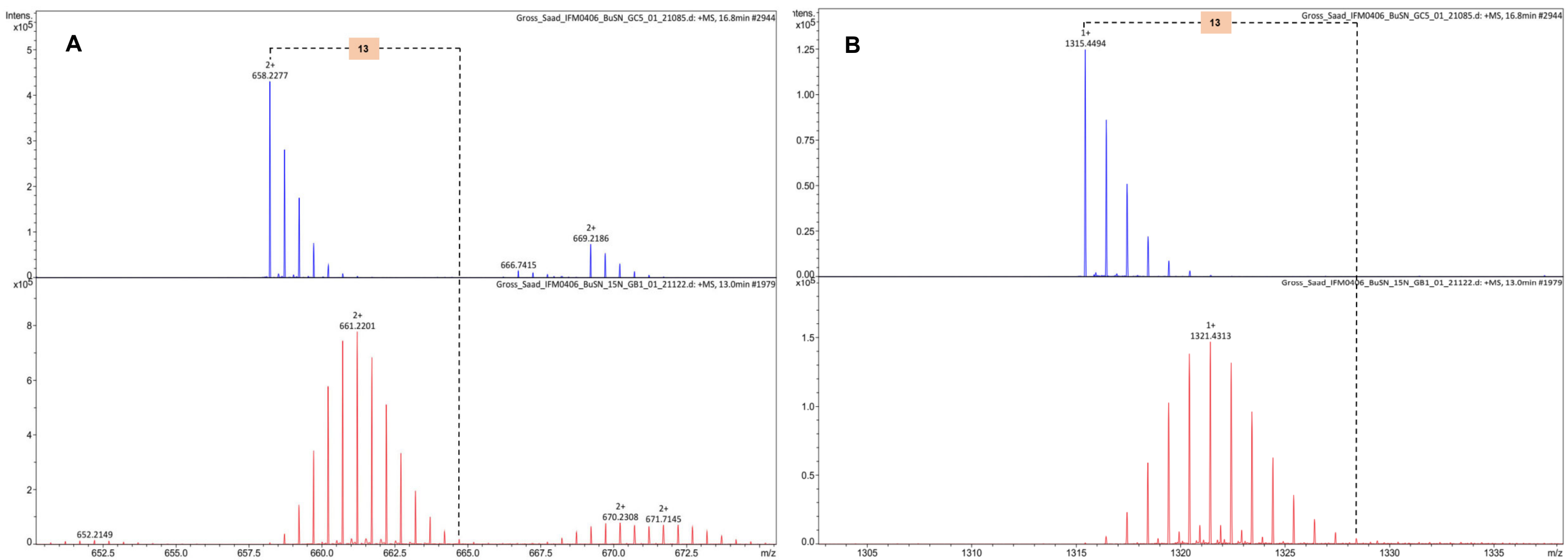

Figure A2. Magnified doubly ($[M+2H]^{2+}$, panel A) and singly ($[M+H]^+$, panel B) charged ions of nocathioamide A (**1**) and its ^{15}N-based version

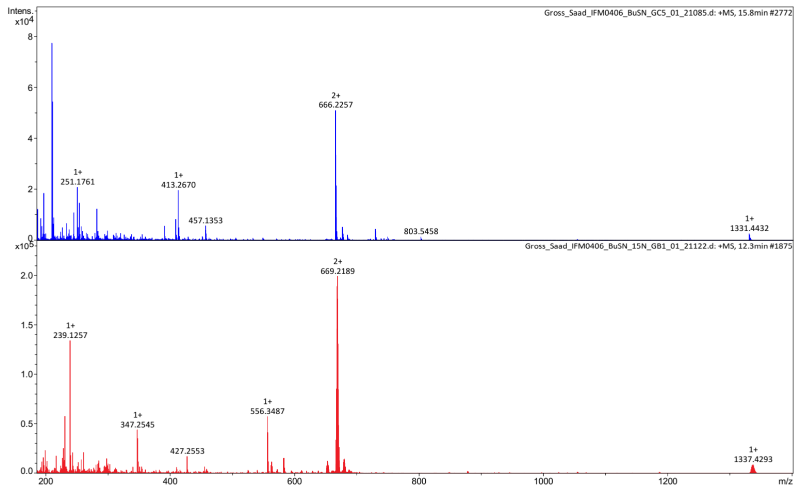

Figure A3. Comparative MS[1] of nocathioamide B (**2**) (1331 Da $[M+H]^+$, 666 Da $[M+2H]^{2+}$) and its ^{15}N-based version

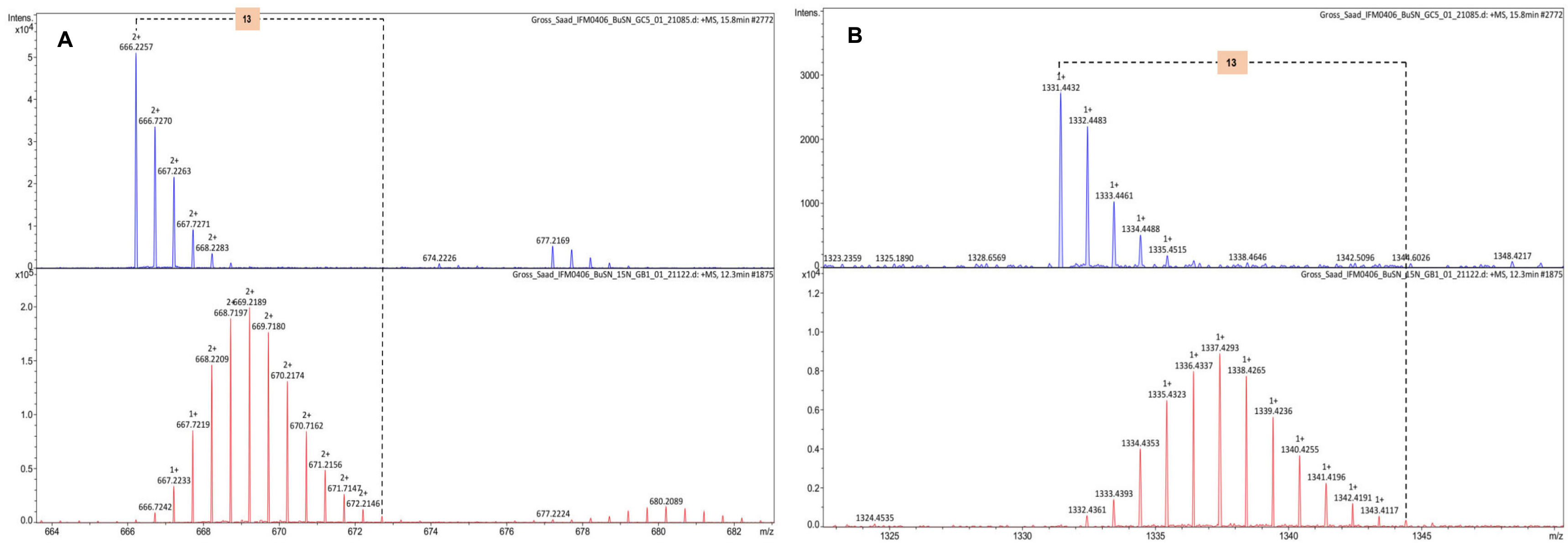

Figure A4. Magnified doubly ($[M+2H]^{2+}$, panel A) and singly ($[M+H]^+$, panel B) charged ions of nocathioamide B (**2**) and its ^{15}N-based version

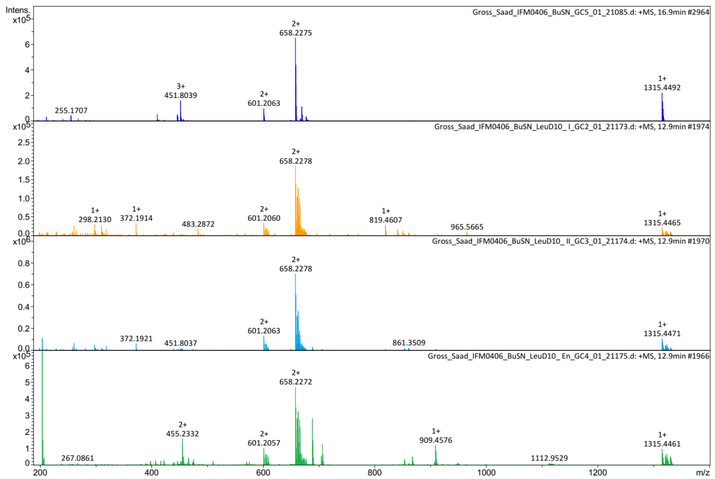

Figure A5. Comparative MS[1] of nocathioamide A (**1**) and its ([$^{2}H_{10}$] L-leucine)-based version

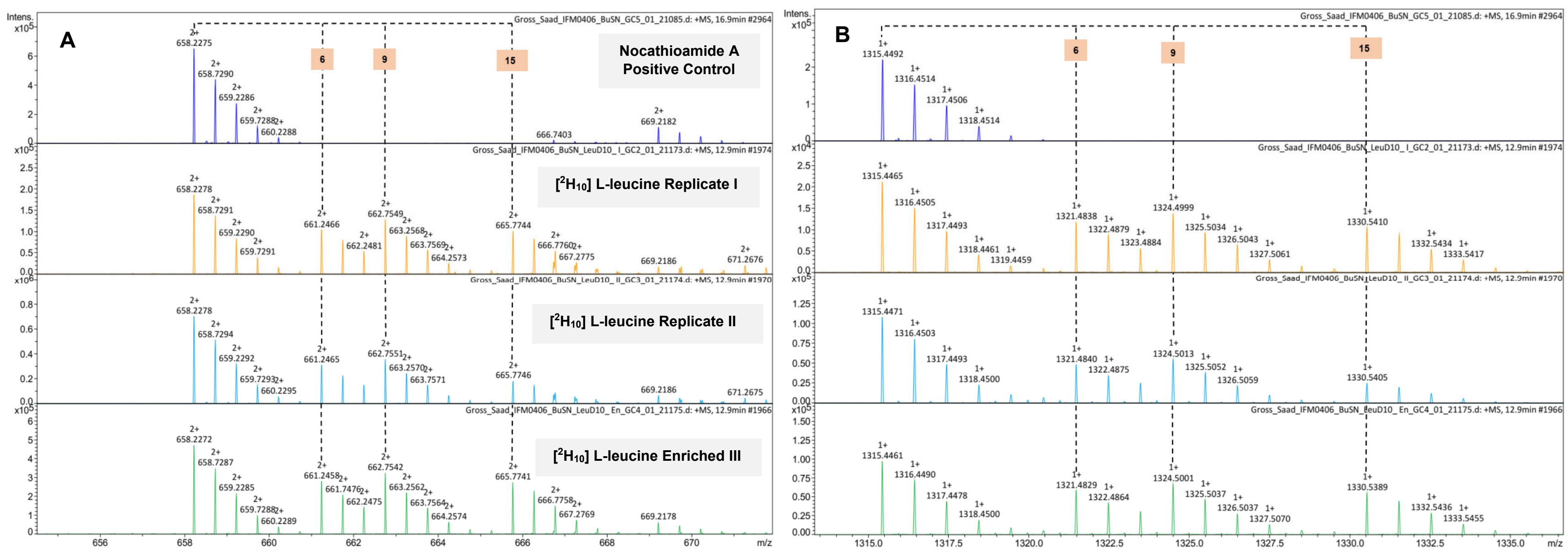

Figure A6. Enlarged doubly ($[M+2H]^{2+}$, panel A) and singly ($[M+H]^{+}$, panel B) charged ions of nocathioamide A (**1**) and its ([$^{2}H_{10}$] L-leucine)-based version

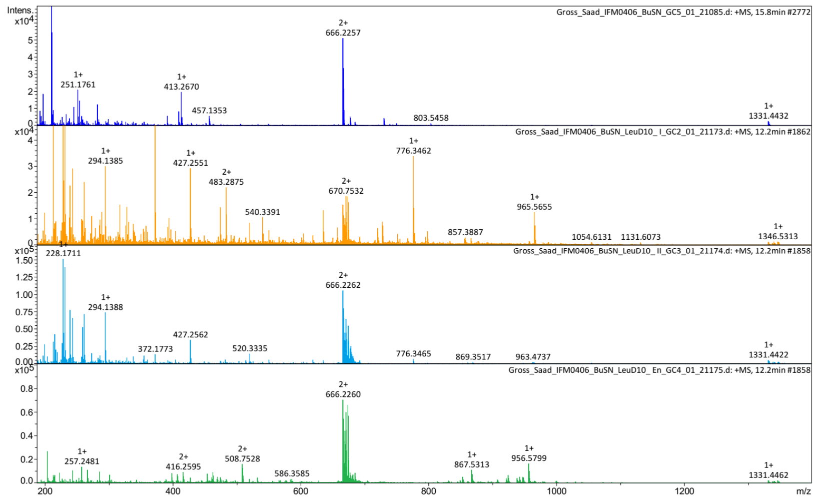

Figure A7. Comparative MS^1 of nocathioamide B (**2**) and its ([$^2H_{10}$] L-leucine)-based version

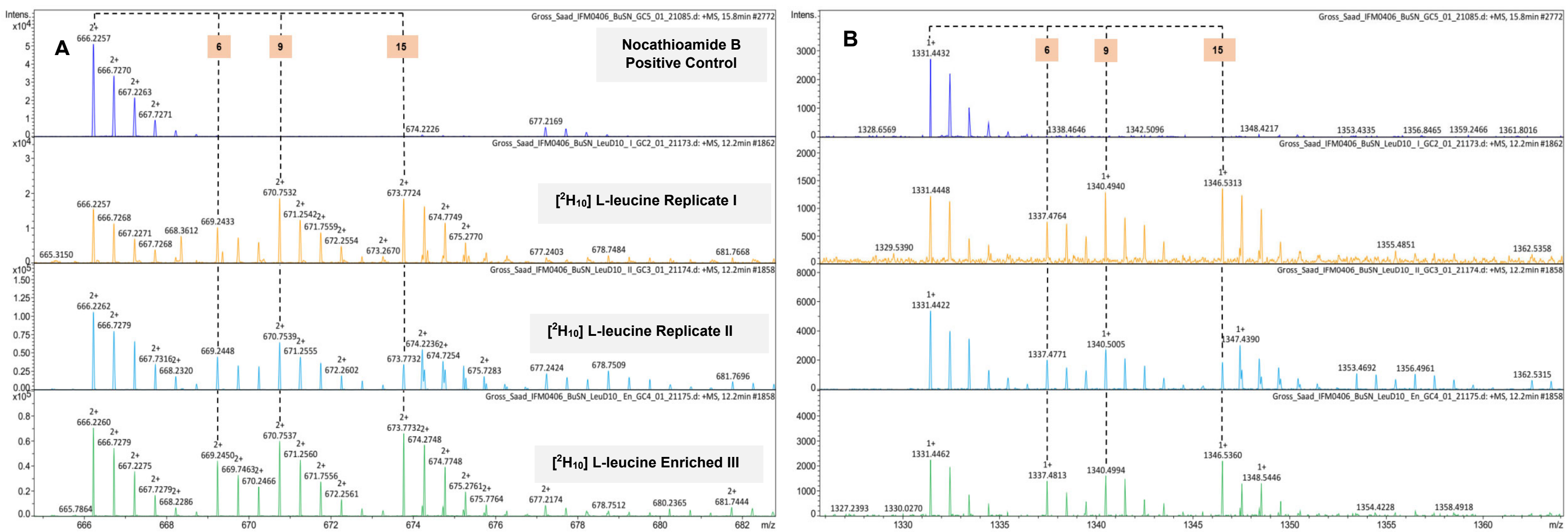

Figure A8. Enlarged doubly ($[M+2H]^{2+}$, panel A) and singly ($[M+H]^+$, panel B) charged ions of nocathioamide B (**2**) and its ([$^2H_{10}$] L-leucine)-based version

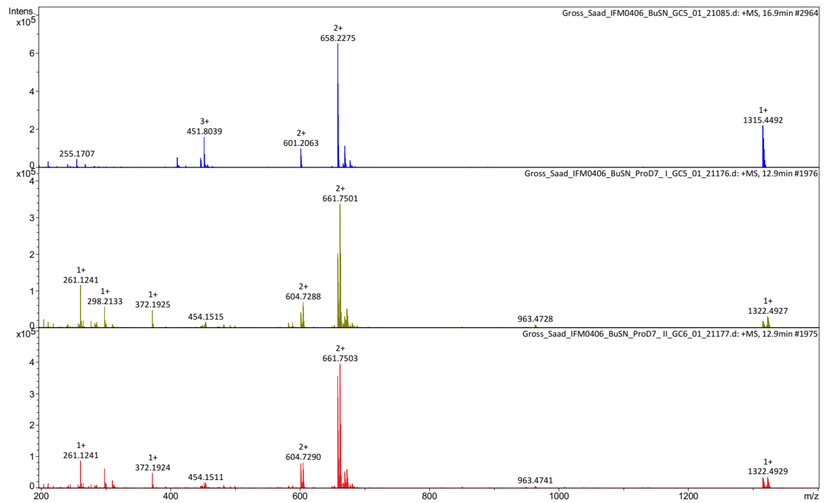

Figure A9. Comparative MS[1] of nocathioamide A (**1**) and its ([$^2H_7$] L-proline)-based version

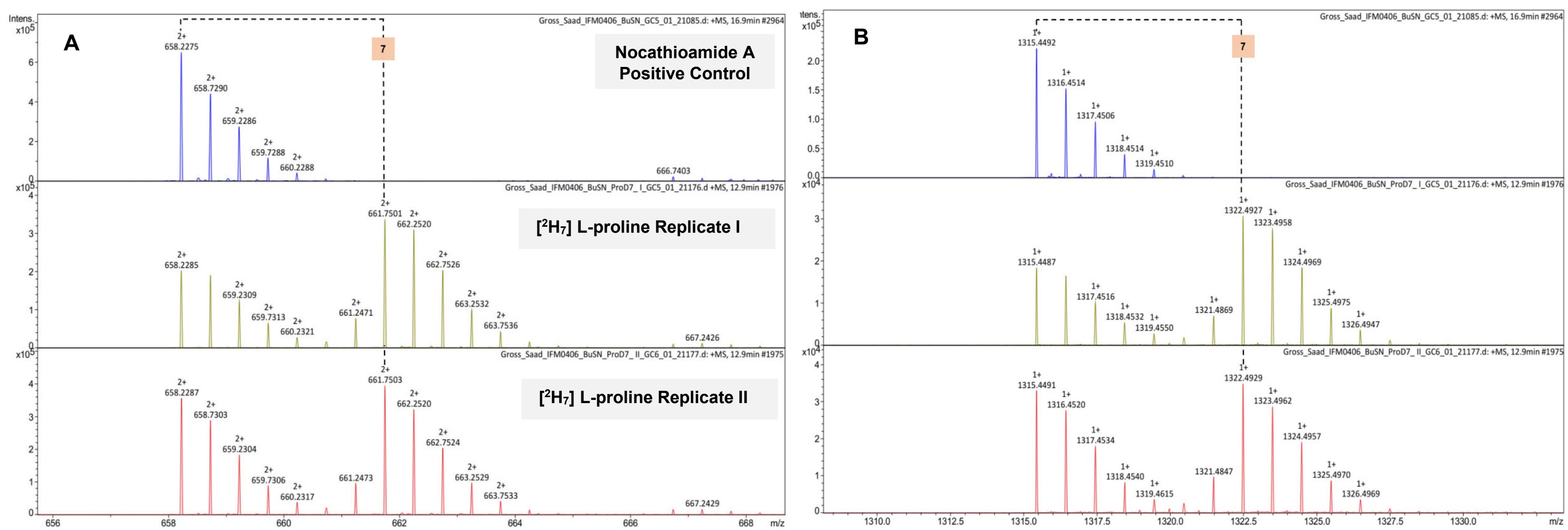

Figure A10. Enlarged doubly ([M+2H]$^{2+}$, panel A) and singly ([M+H]$^+$, panel B) charged ions of nocathioamide A (**1**) and its ([$^2H_7$] L-proline)-based version

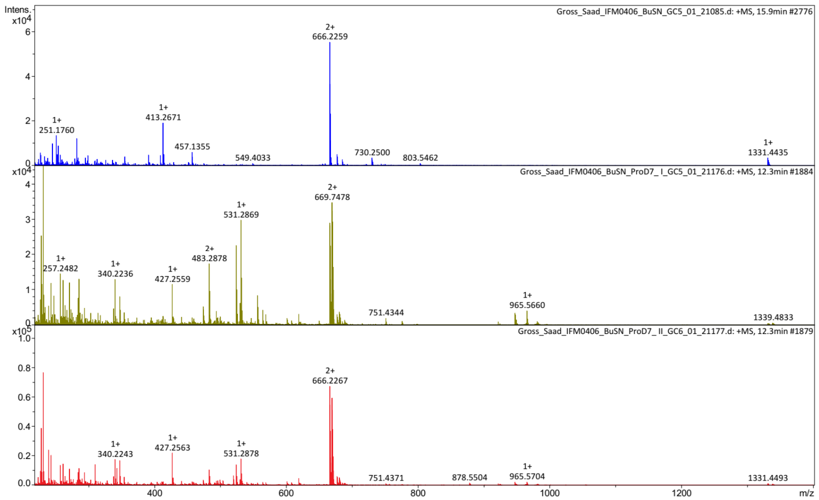

Figure A11. Comparative MS^1 of nocathioamide B (**2**) and its ([$^2H_7$] L-proline)-based version

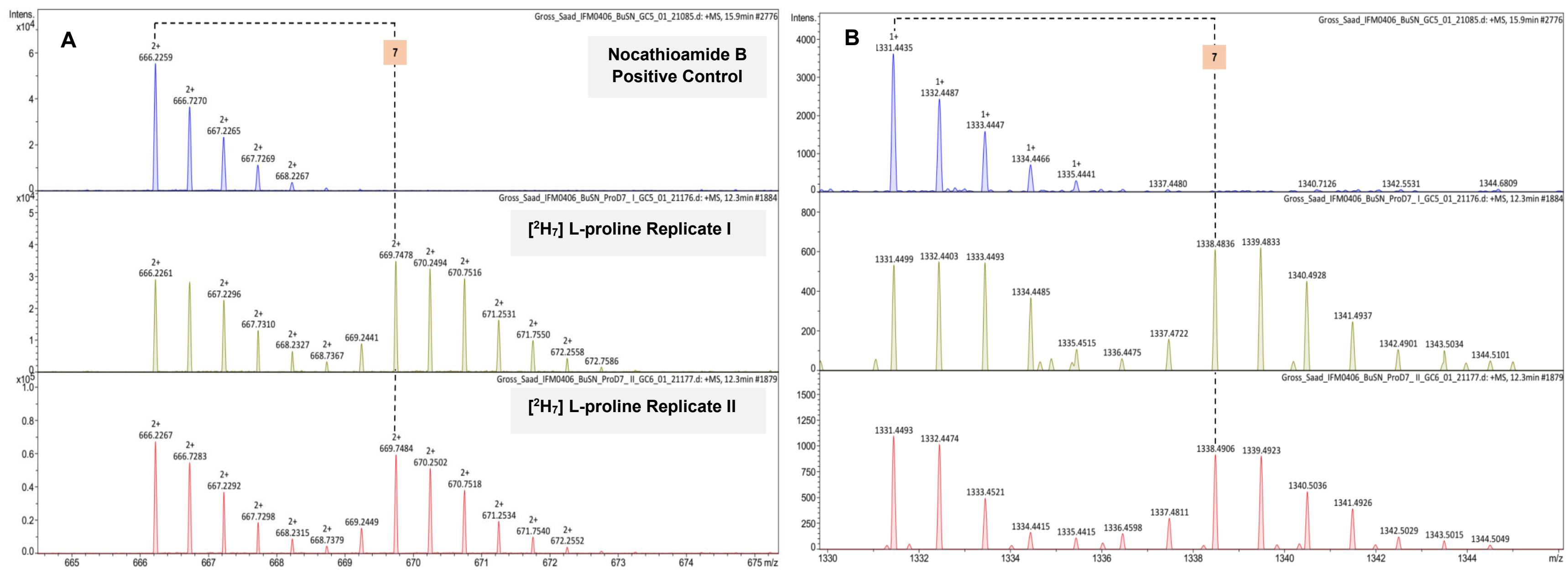

Figure A12. Enlarged doubly ($[M+2H]^{2+}$, panel A) and singly ($[M+H]^{+}$, panel B) charged ions of nocathioamide B (**2**) and its ([$^2H_7$] L-proline)-based version

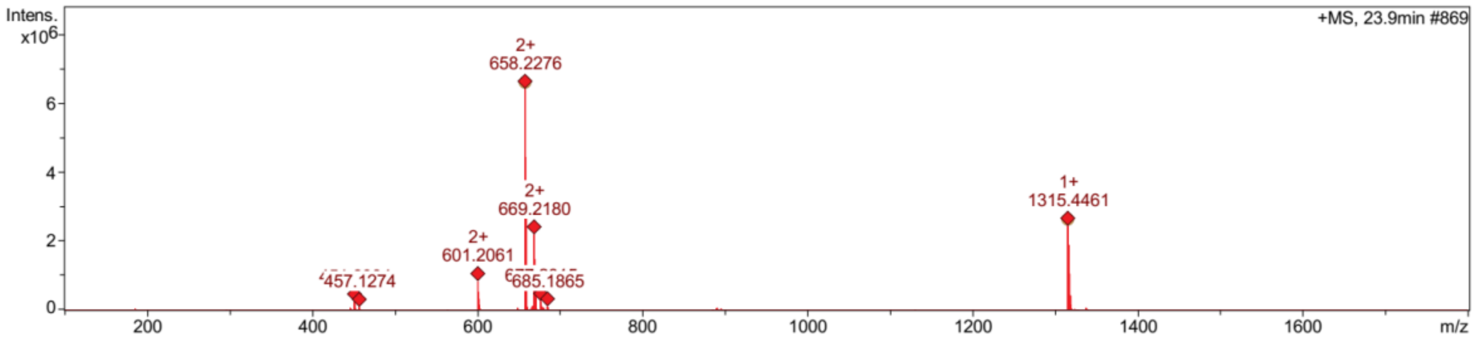

Meas. m/z	#	Ion Formula	m/z	err [ppm]	Mean err [ppm]	rdb	N-Rule	eÂ¯ Conf	mSigma	Std I
658.2276	1	C55H76N14O18S3	658.2307	4.7	5.0	26.0	ok	even	10.9	11.1
	2	C54H76N16O15S4	658.2274	-0.3	-0.5	26.0	ok	even	11.6	14.2
	3	C54H64N26O9S3	658.2250	-3.9	-4.0	37.0	ok	even	13.8	15.3
	4	C53H80N12O19S4	658.2267	-1.3	-1.4	21.0	ok	even	13.8	15.3
	5	C53H68N22O13S3	658.2244	-4.9	-4.9	32.0	ok	even	14.2	15.6
	6	C53H64N28O8S3	658.2307	4.7	4.5	37.0	ok	even	14.9	17.0
	7	C55H80N8O23S3	658.2244	-4.9	-4.4	21.0	ok	even	15.9	14.1
	8	C55H72N20O11S4	658.2281	0.7	0.5	31.0	ok	even	17.1	17.6
	9	C54H80N10O22S3	658.2300	3.7	4.1	21.0	ok	even	18.6	16.9
	10	C54H84N4O27S3	658.2237	-5.9	-5.3	16.0	ok	even	25.2	22.0
	11	C53H84N6O26S3	658.2293	2.6	3.1	16.0	ok	even	27.8	24.6
	12	C55H64N24O12S2	658.2283	1.1	1.6	37.0	ok	even	32.7	39.5
	13	C54H68N20O16S2	658.2276	0.1	0.7	32.0	ok	even	35.1	41.4
	14	C53H72N16O20S2	658.2270	-0.9	-0.2	27.0	ok	even	39.9	44.9
	15	C55H84N2O30S2	658.2270	-0.9	0.3	16.0	ok	even	41.3	42.9
1315.4461	1	C52H63N30O5S4	1315.4475	1.0	0.8	37.0	ok	even	24.7	23.8
	2	C54H63N26O9S3	1315.4428	-2.5	-2.2	37.0	ok	even	25.4	20.1
	3	C55H71N20O11S4	1315.4489	2.1	2.2	31.0	ok	even	27.8	28.9
	4	C51H67N26O9S4	1315.4462	0.0	-0.1	32.0	ok	even	33.2	29.6
	5	C54H75N16O15S4	1315.4475	1.0	1.3	26.0	ok	even	35.0	33.4
	6	C55H63N24O12S2	1315.4493	2.4	3.3	37.0	ok	even	40.2	38.7
	7	C50H71N22O13S4	1315.4448	-1.0	-1.0	27.0	ok	even	42.4	36.5
	8	C53H79N12O19S4	1315.4462	0.0	0.3	21.0	ok	even	43.4	39.3
	9	C54H67N20O16S2	1315.4480	1.4	2.4	32.0	ok	even	48.9	45.5
	10	C52H83N8O23S4	1315.4448	-1.0	-0.6	16.0	ok	even	52.5	46.2
	11	C51H59N30O10S2	1315.4466	0.4	1.0	38.0	ok	even	53.2	51.8
	12	C53H71N16O20S2	1315.4466	0.4	1.5	27.0	ok	even	58.0	53.0
	13	C50H75N16O20S3	1315.4500	3.0	3.5	22.0	ok	even	58.0	48.5
	14	C50H63N26O14S2	1315.4453	-0.6	0.1	33.0	ok	even	61.8	58.9
	15	C51H87N4O27S4	1315.4435	-2.0	-1.5	11.0	ok	even	61.9	54.0
	16	C55H83N2O30S2	1315.4467	0.4	2.0	16.0	ok	even	64.0	56.3
	17	C52H87N2O30S3	1315.4500	3.0	3.9	11.0	ok	even	66.3	55.7
	18	C52H75N12O24S2	1315.4453	-0.6	0.6	22.0	ok	even	67.2	61.1
	19	C50H91O31S4	1315.4422	-3.0	-2.4	6.0	ok	even	71.5	62.2
	20	C51H79N8O28S2	1315.4440	-1.6	-0.3	17.0	ok	even	76.5	69.7
	21	C50H83N4O32S2	1315.4426	-2.7	-1.2	12.0	ok	even	85.9	78.6

Figure A13. MS^1 and molecular formula prediction of nocathioamide A (**1**)

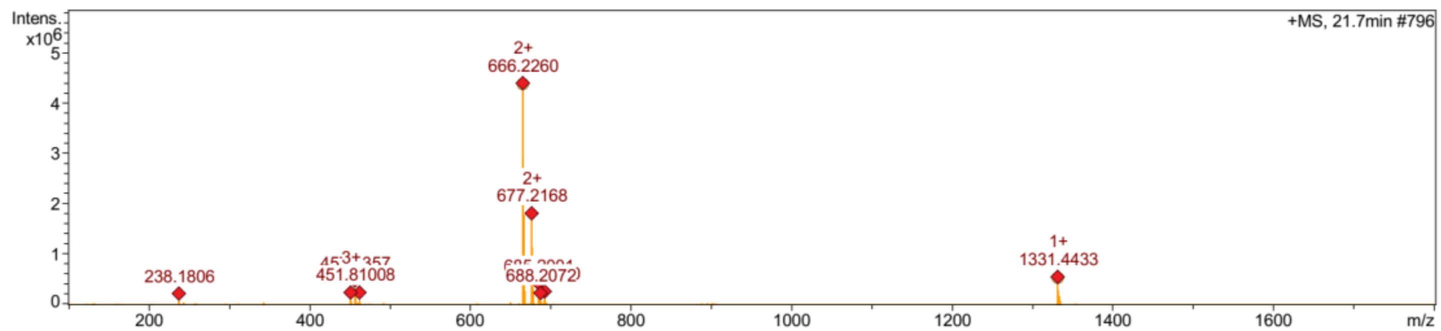

Meas. m/z	#	Ion Formula	m/z	err [ppm]	Mean err [ppm]	rdb	N-Rule	eÂ¯ Conf	mSigma	Std I
666.2260	1	C55H76N14O19S3	666.2281	3.2	3.4	26.0	ok	even	8.2	9.4
	2	C52H80N14O19S4	666.2298	5.7	5.5	21.0	ok	even	10.5	12.3
	3	C53H80N12O20S4	666.2242	-2.7	-2.9	21.0	ok	even	11.6	13.9
	4	C54H80N10O23S3	666.2274	2.2	2.5	21.0	ok	even	12.5	12.5
	5	C52H68N24O13S3	666.2274	2.1	2.0	32.0	ok	even	14.1	16.7
	6	C54H76N16O16S4	666.2249	-1.7	-2.0	26.0	ok	even	14.7	15.9
	7	C52H84N8O24S4	666.2235	-3.7	-3.8	16.0	ok	even	16.3	16.9
	8	C53H64N28O9S3	666.2281	3.2	2.9	37.0	ok	even	16.7	18.1
	9	C54H64N26O10S3	666.2225	-5.3	-5.4	37.0	ok	even	16.8	17.2
	10	C52H64N30O6S4	666.2248	-1.7	-2.4	37.0	ok	even	18.5	16.1
	11	C54H92O29S4	666.2298	5.7	5.9	10.0	ok	even	19.8	21.4
	12	C53H84N6O27S3	666.2268	1.2	1.6	16.0	ok	even	21.2	19.4
	13	C55H72N20O12S4	666.2255	-0.7	-1.1	31.0	ok	even	22.7	21.1
	14	C52H88N2O31S3	666.2261	0.1	0.7	11.0	ok	even	30.6	27.8
	15	C55H64N24O13S2	666.2258	-0.4	0.0	37.0	ok	even	32.0	39.1
	16	C54H68N20O17S2	666.2251	-1.4	-0.9	32.0	ok	even	32.4	39.8
	17	C53H72N16O21S2	666.2244	-2.4	-1.7	27.0	ok	even	35.7	42.3
	18	C55H84N2O31S2	666.2244	-2.4	-1.3	16.0	ok	even	35.8	39.1
	19	C52H72N18O20S2	666.2300	6.0	6.6	27.0	ok	even	38.2	45.1
	20	C54H84N4O30S2	666.2300	6.0	7.1	16.0	ok	even	38.5	42.1
	21	C52H76N12O25S2	666.2238	-3.4	-2.6	22.0	ok	even	41.1	46.4
	22	C53H88O34S2	666.2294	5.0	6.2	11.0	ok	even	45.8	48.2
1331.4433	1	C51H67N26O10S4	1331.4411	-1.7	-2.0	32.0	ok	even	8.5	9.2
	2	C52H63N30O6S4	1331.4424	-0.7	-1.0	37.0	ok	even	8.9	9.6
	3	C54H75N16O16S4	1331.4424	-0.7	-0.6	26.0	ok	even	13.2	15.4
	4	C55H71N20O12S4	1331.4438	0.3	0.3	31.0	ok	even	14.9	16.5
	5	C50H71N22O14S4	1331.4397	-2.7	-2.9	27.0	ok	even	16.6	14.9
	6	C53H79N12O20S4	1331.4411	-1.7	-1.5	21.0	ok	even	18.5	18.7
	7	C51H71N20O17S3	1331.4463	2.2	2.5	27.0	ok	even	26.8	25.2
	8	C52H83N8O24S4	1331.4398	-2.7	-2.4	16.0	ok	even	26.8	24.7
	9	C55H63N24O13S2	1331.4442	0.7	1.4	37.0	ok	even	32.2	38.6
	10	C53H83N6O27S3	1331.4463	2.2	3.0	16.0	ok	even	32.6	28.3
	11	C50H75N16O21S3	1331.4449	1.2	1.6	22.0	ok	even	35.8	32.7
	12	C54H67N20O17S2	1331.4429	-0.3	0.5	32.0	ok	even	36.2	41.4
	13	C51H59N30O11S2	1331.4416	-1.3	-0.9	38.0	ok	even	42.1	49.3
	14	C53H71N16O21S2	1331.4416	-1.3	-0.4	27.0	ok	even	42.2	45.9
	15	C52H87N2O31S3	1331.4449	1.2	2.1	11.0	ok	even	42.4	37.1
	16	C55H83N2O31S2	1331.4416	-1.3	0.1	16.0	ok	even	44.8	44.9
	17	C50H63N26O15S2	1331.4402	-2.4	-1.8	33.0	ok	even	47.6	53.4
	18	C52H75N12O25S2	1331.4402	-2.3	-1.3	22.0	ok	even	49.4	51.6

Figure A14. MS[1] and molecular formula prediction of nocathioamide B (**2**)

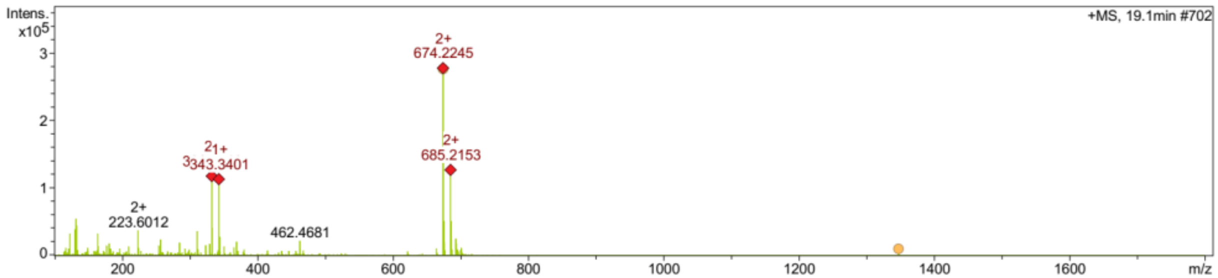

Meas. m/z	#	Ion Formula	m/z	err [ppm]	Mean err [ppm]	rdb	N-Rule	eÅ¯ Conf	mSigma	Std I
674.2245	1	C52H80N14O20S4	674.2273	4.1	3.9	21.0	ok	even	5.1	5.2
	2	C53H80N12O21S4	674.2216	-4.2	-4.4	21.0	ok	even	6.0	6.4
	3	C51H68N26O11S4	674.2216	-4.2	-4.8	32.0	ok	even	8.9	7.3
	4	C53H76N18O16S4	674.2279	5.1	4.8	26.0	ok	even	9.2	7.7
	5	C55H88N4O26S4	674.2279	5.1	5.2	15.0	ok	even	10.1	11.0
	6	C52H84N8O25S4	674.2210	-5.2	-5.3	16.0	ok	even	11.9	11.1
	7	C54H76N16O17S4	674.2223	-3.2	-3.5	26.0	ok	even	11.9	10.3
	8	C51H84N10O24S4	674.2266	3.2	3.0	16.0	ok	even	13.3	12.0
	9	C55H76N14O20S3	674.2256	1.6	1.8	26.0	ok	even	14.3	17.5
	10	C54H92O30S4	674.2273	4.2	4.3	10.0	ok	even	14.8	14.6
	11	C54H80N10O24S3	674.2249	0.7	0.9	21.0	ok	even	16.3	19.0
	12	C51H64N32O6S4	674.2279	5.1	4.3	37.0	ok	even	16.8	13.7
	13	C52H64N30O7S4	674.2223	-3.2	-3.9	37.0	ok	even	19.0	15.1
	14	C52H68N24O14S3	674.2249	0.6	0.5	32.0	ok	even	20.0	24.7
	15	C55H72N20O13S4	674.2230	-2.2	-2.6	31.0	ok	even	21.5	17.4
	16	C51H72N20O18S3	674.2242	-0.3	-0.4	27.0	ok	even	22.2	26.4
	17	C53H64N28O10S3	674.2256	1.6	1.4	37.0	ok	even	22.6	25.8
	18	C53H84N6O28S3	674.2242	-0.3	0.0	16.0	ok	even	23.0	24.0
	19	C52H88N2O32S3	674.2236	-1.3	-0.9	11.0	ok	even	31.5	30.8
	20	C55H80N8O27S2	674.2282	5.5	6.4	21.0	ok	even	36.9	44.4
	21	C54H68N20O18S2	674.2225	-2.8	-2.4	32.0	ok	even	38.0	47.5
	22	C55H64N24O14S2	674.2232	-1.9	-1.5	37.0	ok	even	38.0	47.0
	23	C55H84N2O32S2	674.2219	-3.8	-2.8	16.0	ok	even	39.4	45.3
	24	C53H68N22O17S2	674.2282	5.5	5.9	32.0	ok	even	40.0	49.9
	25	C53H72N16O22S2	674.2219	-3.8	-3.2	27.0	ok	even	40.4	49.4
	26	C54H84N4O31S2	674.2275	4.5	5.5	16.0	ok	even	41.9	48.3
	27	C52H72N18O21S2	674.2275	4.5	5.0	27.0	ok	even	42.8	52.2
	28	C51H60N30O12S2	674.2219	-3.8	-3.7	38.0	ok	even	44.0	55.4
	29	C52H76N12O26S2	674.2212	-4.8	-4.1	22.0	ok	even	44.9	52.9
	30	C51H76N14O25S2	674.2268	3.5	4.1	22.0	ok	even	47.4	55.8
	31	C53H88O35S2	674.2268	3.5	4.6	11.0	ok	even	48.4	53.5
	32	C51H80N8O30S2	674.2205	-5.8	-5.0	17.0	ok	even	50.8	57.7
1347.4373	1	C53H71N16O22S2	1347.4366	0.6	1.7	27.0	ok	even	12.6	14.6
	2	C55H83N2O32S2	1347.4365	-0.6	-1.3	16.0	ok	even	13.9	13.3
	3	C54H67N20O18S2	1347.4378	0.4	-0.9	32.0	ok	even	14.4	15.7
	4	C53H83N6O28S3	1347.4412	2.9	1.3	16.0	ok	even	16.0	20.0
	5	C52H75N12O26S2	1347.4351	-1.6	-2.5	22.0	ok	even	17.6	18.4
	6	C55H63N24O14S2	1347.4392	1.4	-0.1	37.0	ok	even	21.4	20.9
	7	C52H87N2O32S3	1347.4399	1.9	0.5	11.0	ok	even	21.8	23.8
	8	C51H79N8O30S2	1347.4338	-2.6	-3.3	17.0	ok	even	25.7	25.5
	9	C50H63N26O16S2	1347.4351	-1.6	-1.7	33.0	ok	even	54.6	67.5
	10	C51H59N30O12S2	1347.4365	-0.6	-1.1	38.0	ok	even	55.9	68.9
	11	C50H75N16O22S3	1347.4398	1.9	0.9	22.0	ok	even	64.5	83.6
	12	C51H71N20O18S3	1347.4412	2.9	1.6	27.0	ok	even	65.5	84.9
	13	C50H71N22O15S4	1347.4347	-2.0	-2.3	27.0	ok	even	79.7	103.2
	14	C51H87N4O29S4	1347.4333	-3.0	-2.8	11.0	ok	even	80.9	106.0
	15	C52H83N8O25S4	1347.4347	-2.0	-2.1	16.0	ok	even	82.0	107.1
	16	C51H67N26O11S4	1347.4360	-1.0	-1.6	32.0	ok	even	83.1	105.6
	17	C53H79N12O21S4	1347.4360	-1.0	-1.4	21.0	ok	even	84.4	108.9
	18	C52H63N30O7S4	1347.4373	0.0	-0.9	37.0	ok	even	87.7	108.6
	19	C54H75N16O17S4	1347.4373	0.0	-0.7	26.0	ok	even	87.9	111.3
	20	C55H71N20O13S4	1347.4387	1.0	0.0	31.0	ok	even	92.6	114.3

Figure A15. MS[1] and molecular formula prediction of nocathioamide C (**3**)

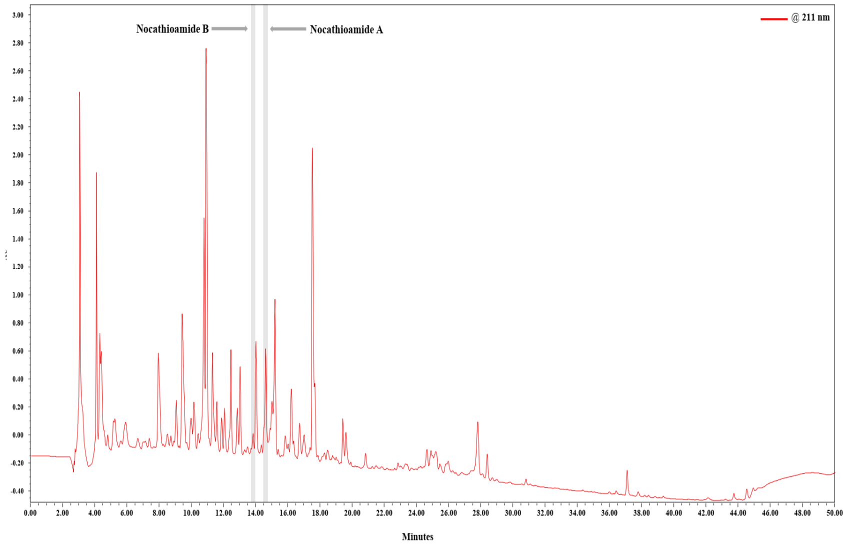

Figure A16. HPLC profile of the *n*-butanol extract of cell-free supernatant of IFM 0406

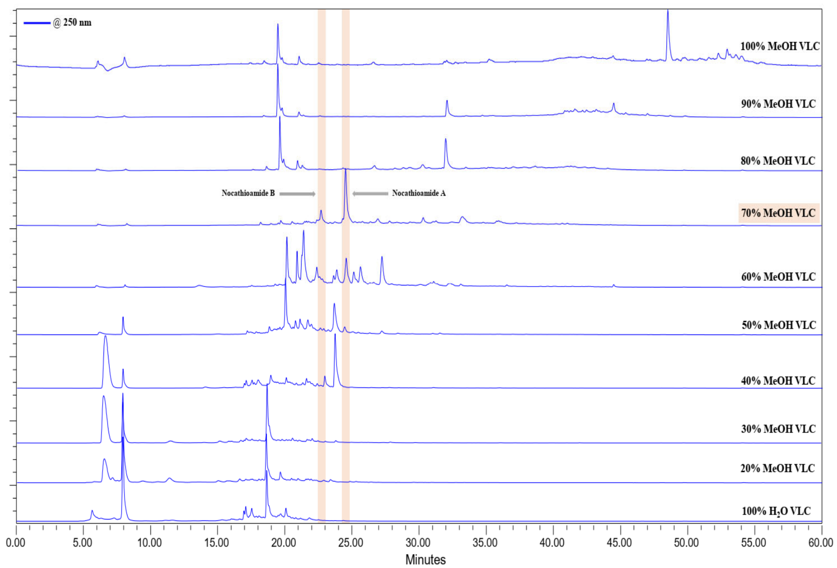

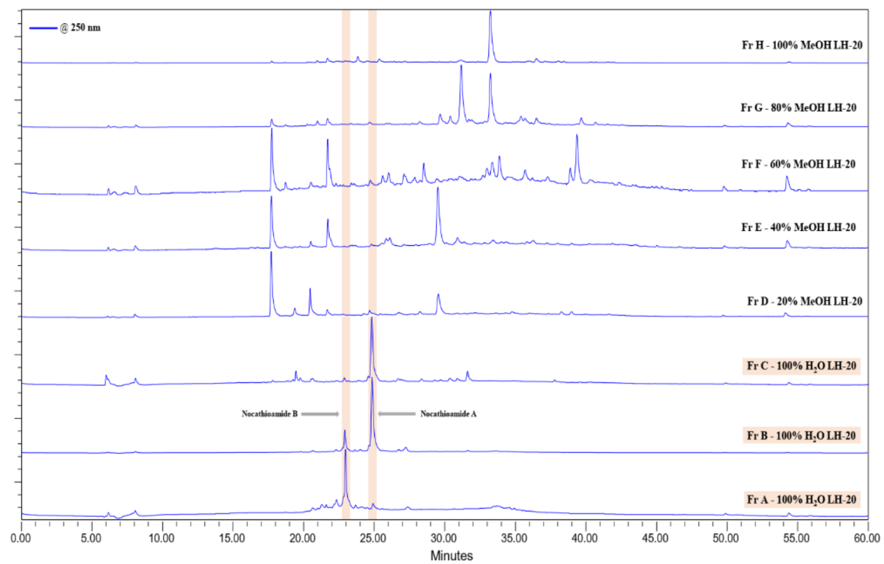

Figure A17. HPLC profiles of VLC fractions of the *n*-butanol extract (Left); HPLC profiles of Sephadex LH-20 subfractions of 70% MeOH VLC fraction (Right)

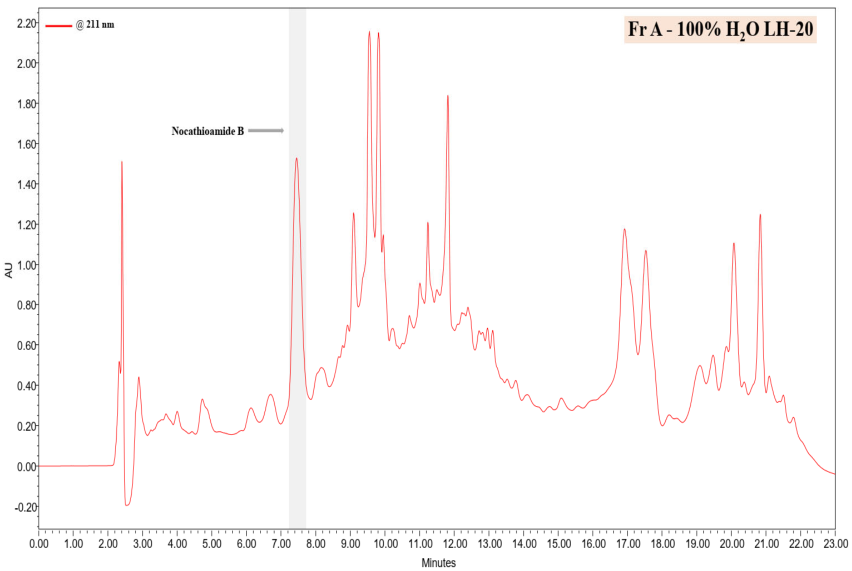

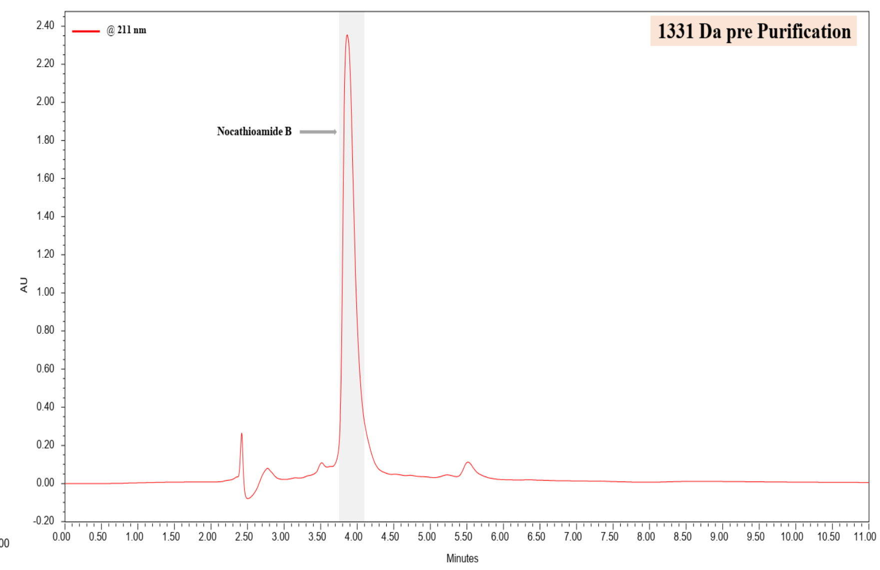

Figure A18. HPLC profile of fraction A-100% H_2O LH-20 (Left); HPLC profile of prepurified nocathioamide B (**2**) (Right)

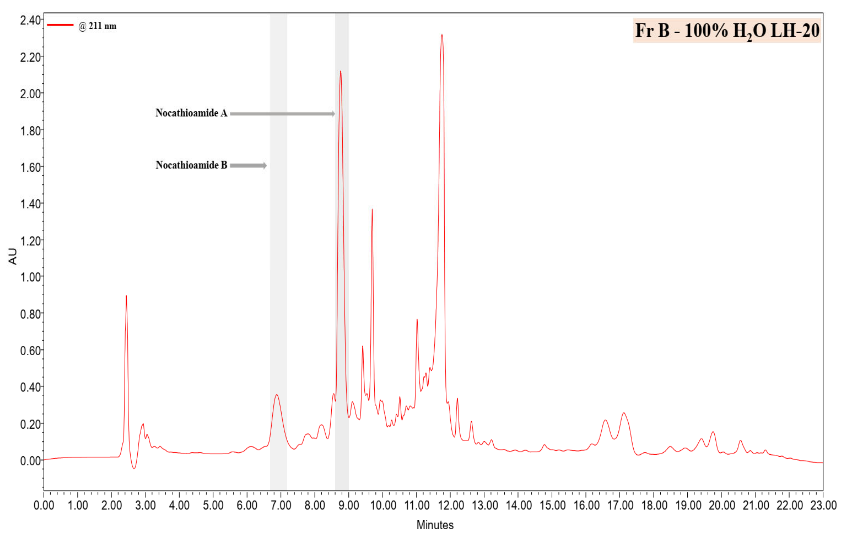

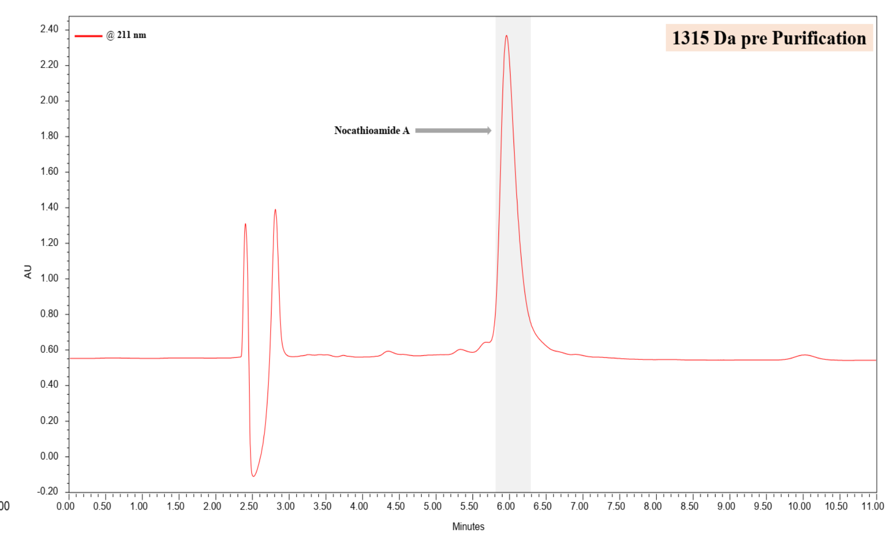

Figure A19. HPLC profile of fraction B-100% H_2O LH-20 (Left); HPLC profile of prepurified nocathioamide A (**1**) (Right)

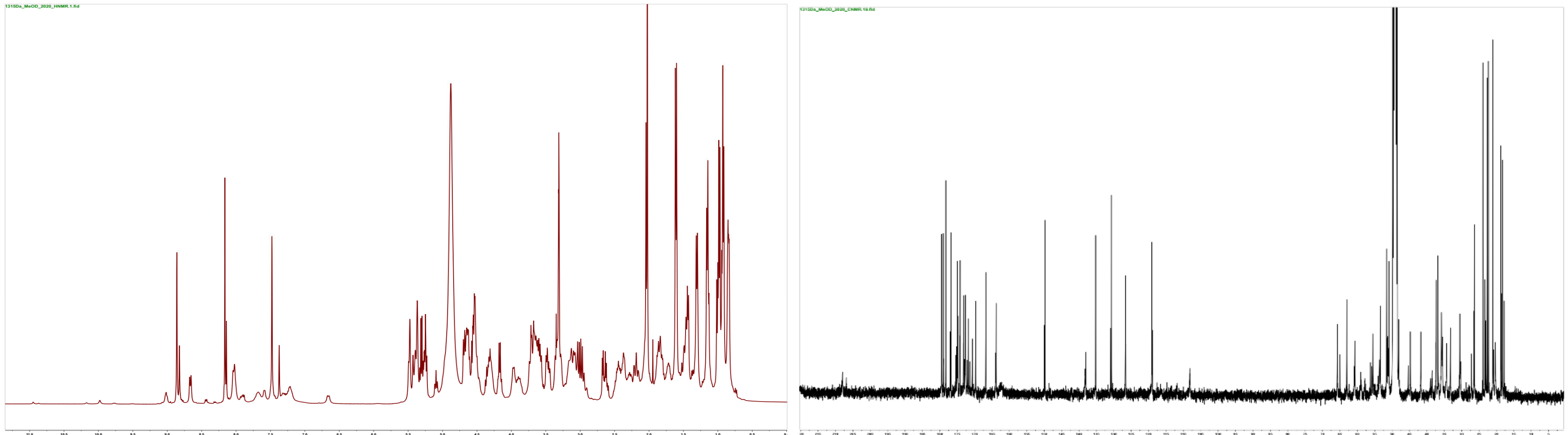

Figure A20. ^{1}H-NMR spectrum of nocathioamide A (**1**) (d_4-CH_3OH, 400 MHz, Left); ^{13}C-NMR spectrum of nocathioamide A (**1**) (d_4-CH_3OH, 100 MHz, Right)

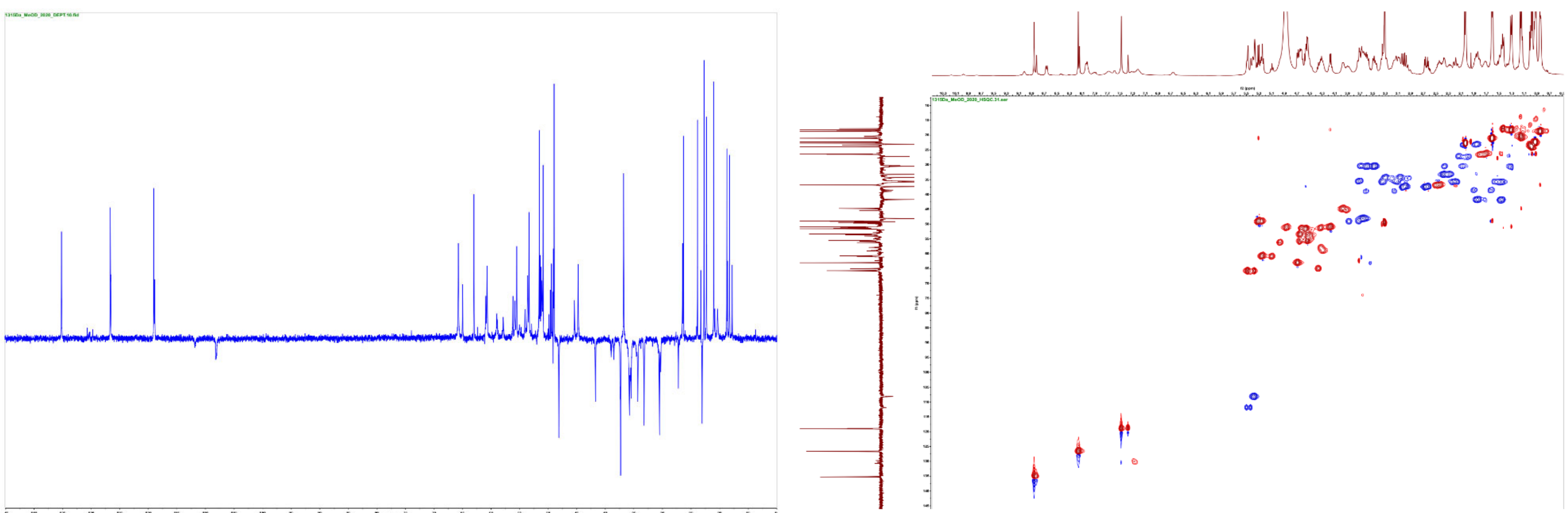

Figure A21. DEPT-135 spectrum of nocathioamide A (**1**) (d_4-CH_3OH, 100 MHz, Right); ^{1}H-^{13}C edited HSQC spectrum of nocathioamide A (**1**) (d_4-CH_3OH, 400 MHz, Left)

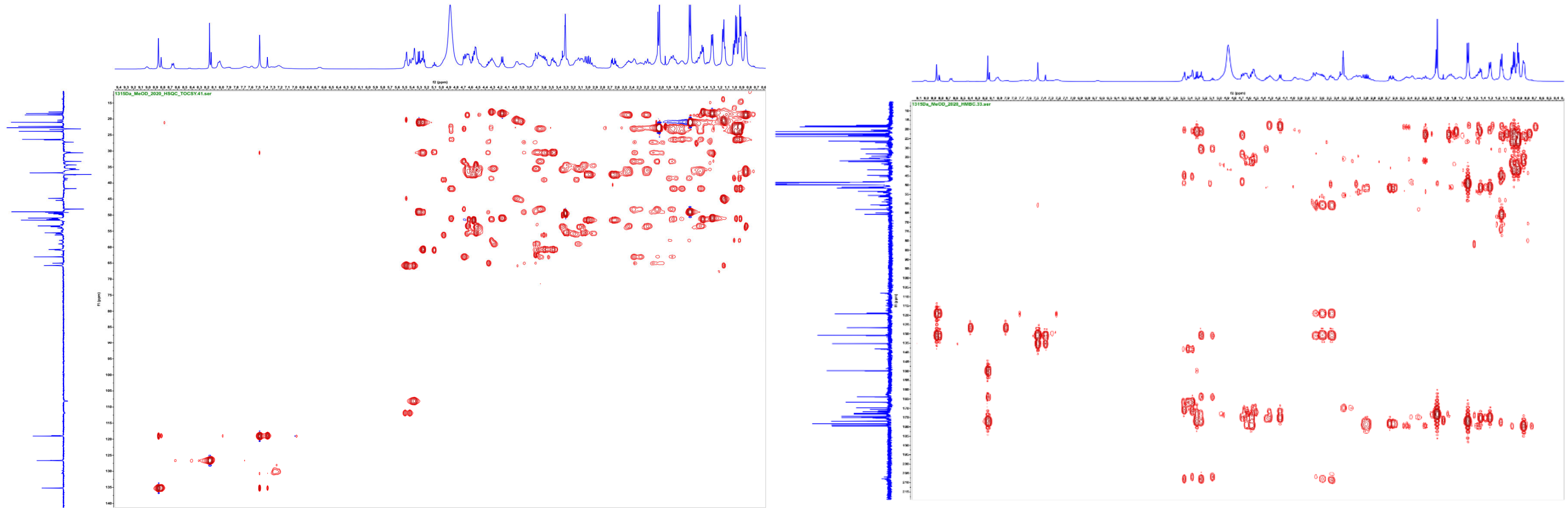

Figure A22. ^1H-^{13}C HSQC-TOCSY spectrum of nocathioamide A (**1**) (d_4-CH_3OH, 400 MHz, Left); ^1H-^{13}C HMBC spectrum of nocathioamide A (**1**) (d_4-CH_3OH, 400 MHz, Right)

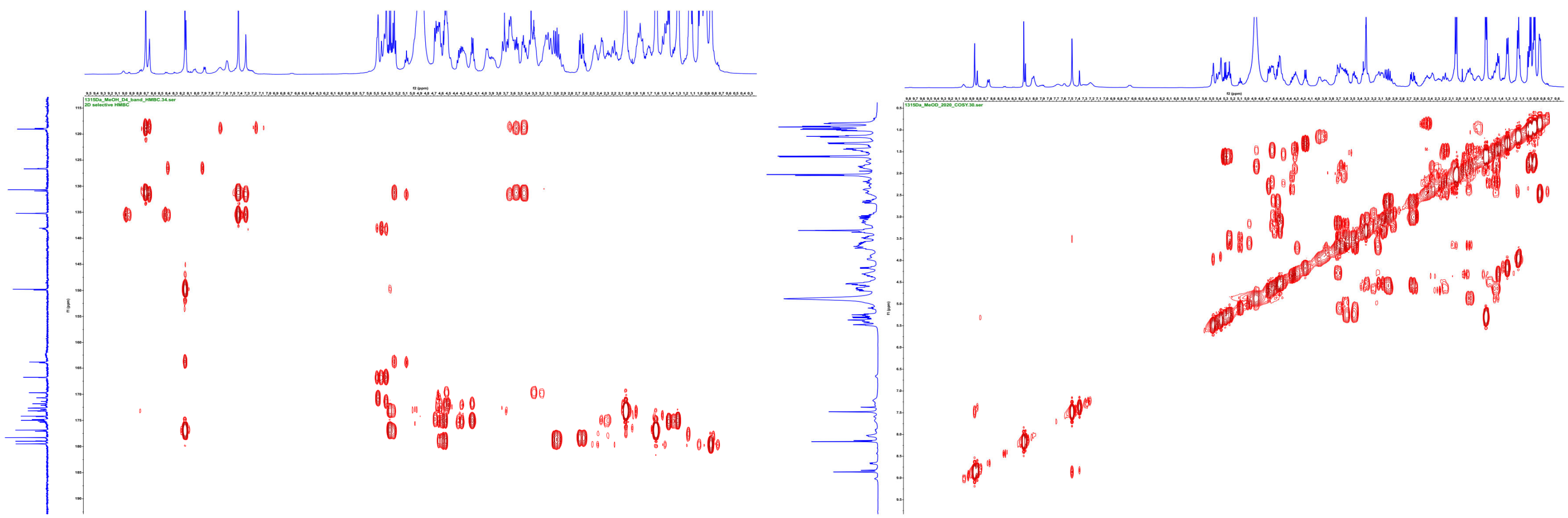

Figure A23. Band-Selective ^1H-^{13}C-HMBC spectrum of nocathioamide A (**1**) (d_4-CH_3OH, 400 MHz, Left), ^1H-^1H COSY spectrum of nocathioamide A (**1**) (d_4-CH_3OH, 400 MHz, Right)

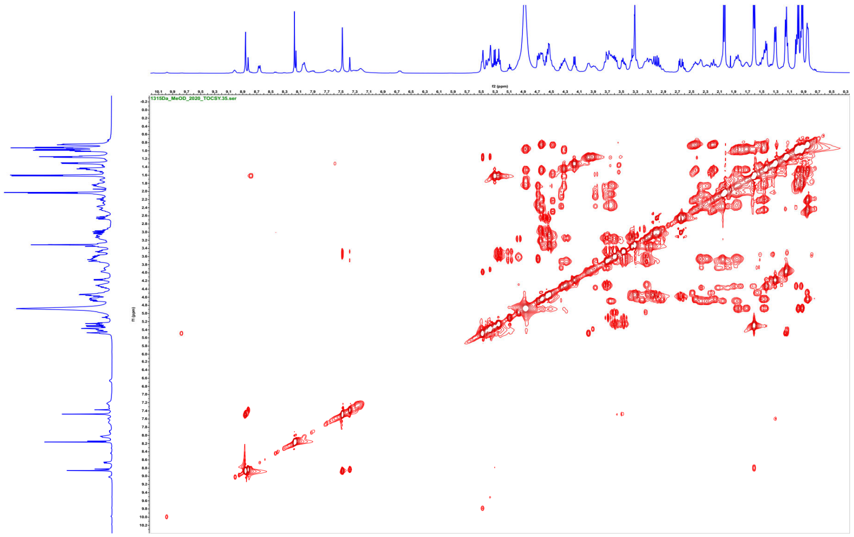

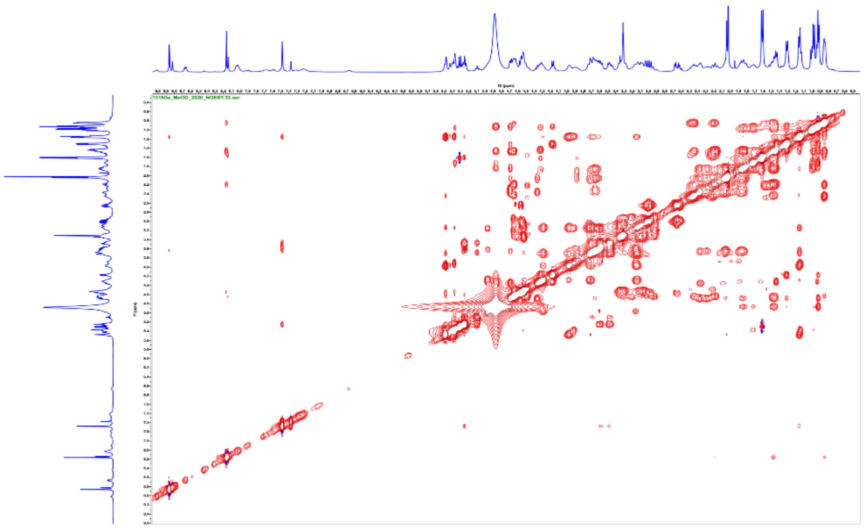

Figure A24. ^{1}H-^{1}H TOCSY spectrum of nocathioamide A (**1**) (d_4-CH_3OH, 400 MHz, left); ^{1}H-^{1}H NOESY spectrum of nocathioamide A (**1**) (d_4-CH_3OH, 400 MHz, d8 = 300 msec, Right)

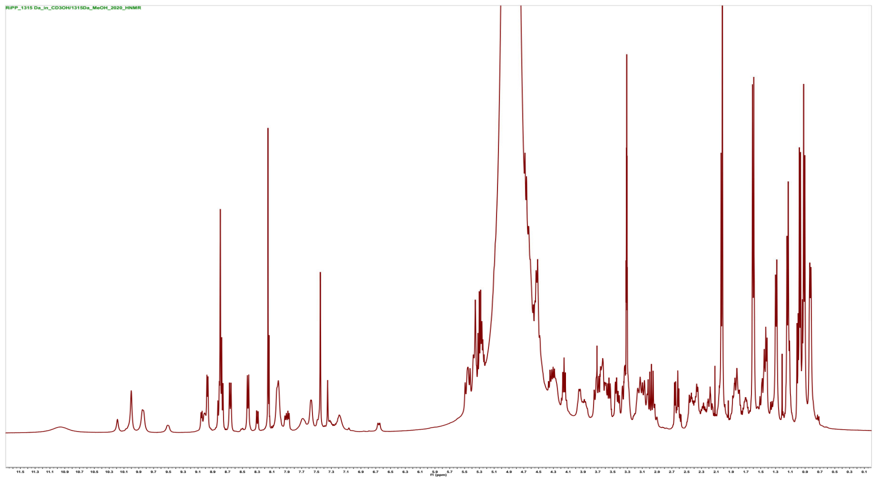

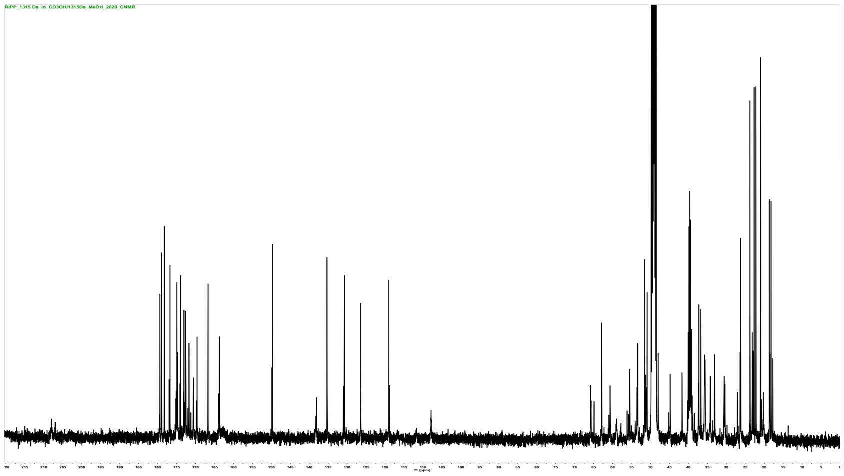

Figure A25. ^{1}H-NMR spectrum of nocathioamide A (**1**) (d_3-CH_3OH, 400 MHz, Left); ^{13}C-NMR spectrum of nocathioamide A (**1**) (d_3-CH_3OH, 100 MHz, Right)

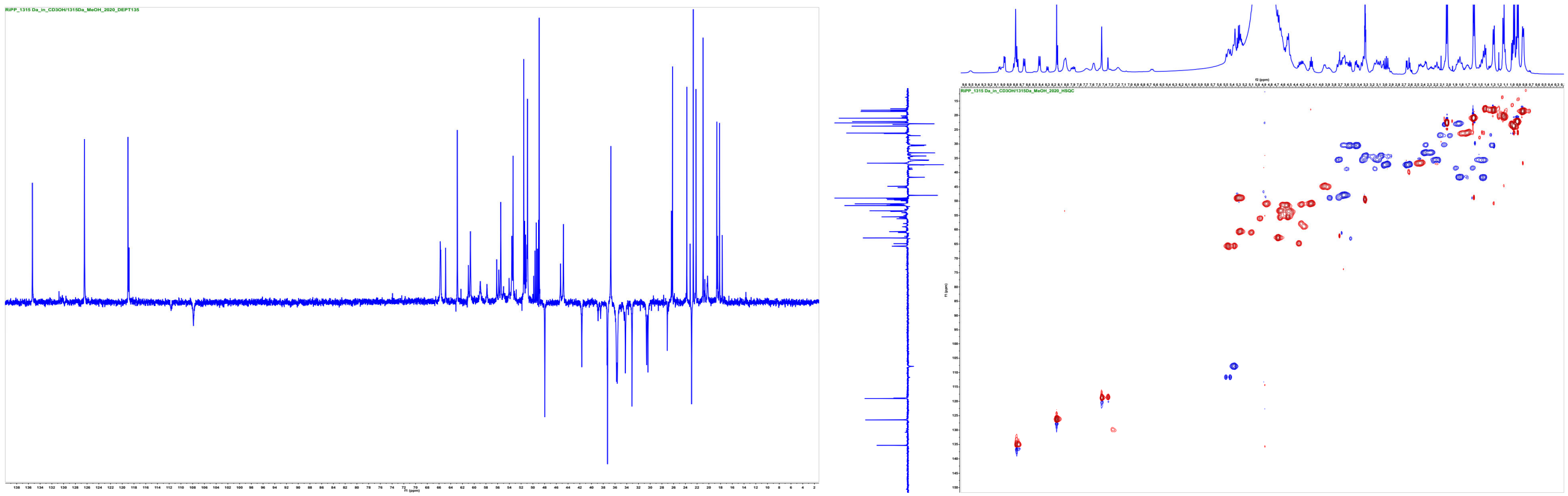

Figure A26. DEPT-135 spectrum of nocathioamide A (**1**) (d_3-CH_3OH, 100 MHz, Left); ^1H-^{13}C edited HSQC spectrum of nocathioamide A (**1**) (d_3-CH_3OH, 400 MHz, Right)

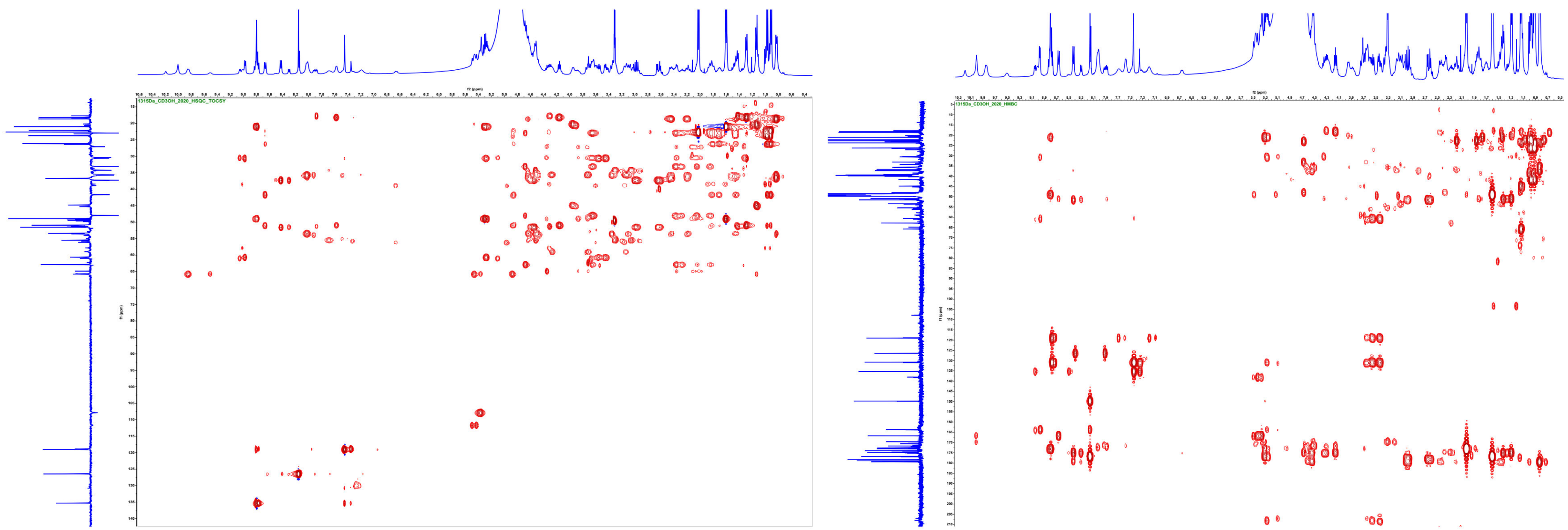

Figure A27. ^1H-^{13}C HSQC-TOCSY spectrum of nocathioamide A (**1**) (d_3-CH_3OH, 400 MHz, Left); ^1H-^{13}C HMBC spectrum of nocathioamide A (**1**) (d_3-CH_3OH, 400 MHz, Right)

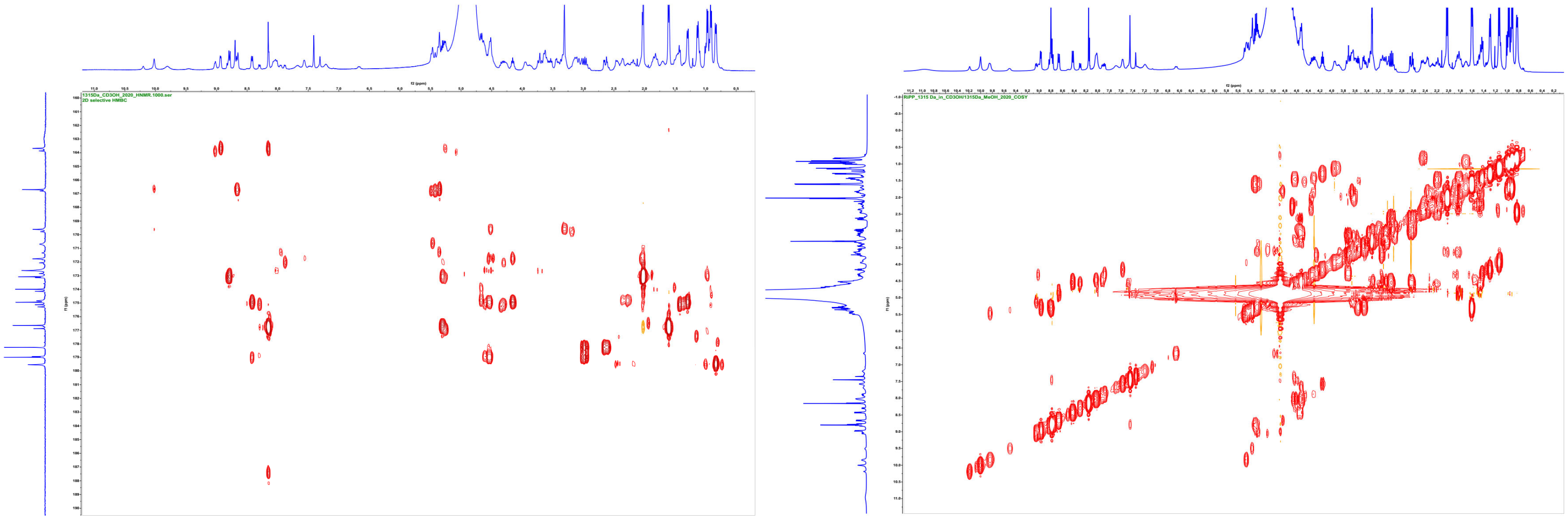

Figure A28. ^{1}H-^{13}C Band-Selective HMBC spectrum of nocathioamide A (**1**) (d_3-CH_3OH, 400 MHz, Left); ^{1}H-^{1}H COSY spectrum of nocathioamide A (**1**) (d_3-CH_3OH, 400 MHz, Right)

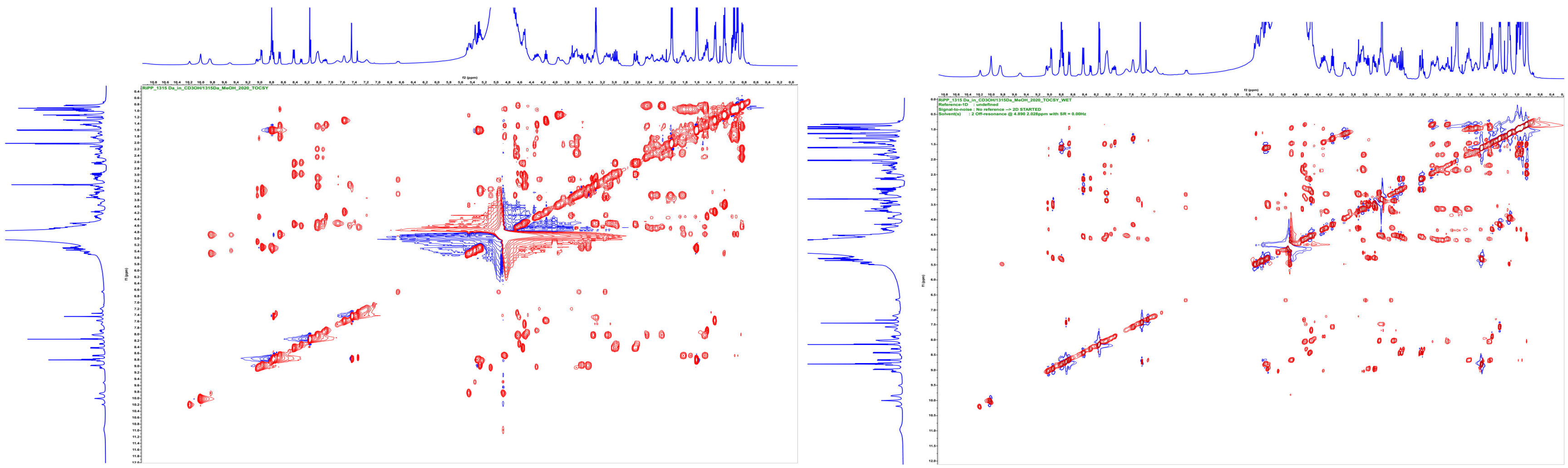

Figure A29. ^{1}H-^{1}H TOCSY spectrum of nocathioamide A (**1**) (d_3-CH_3OH, 400 MHz, Left); ^{1}H-^{1}H TOCSY WET spectrum of nocathioamide A (**1**) (d_3-CH_3OH, 400 MHz, Right)

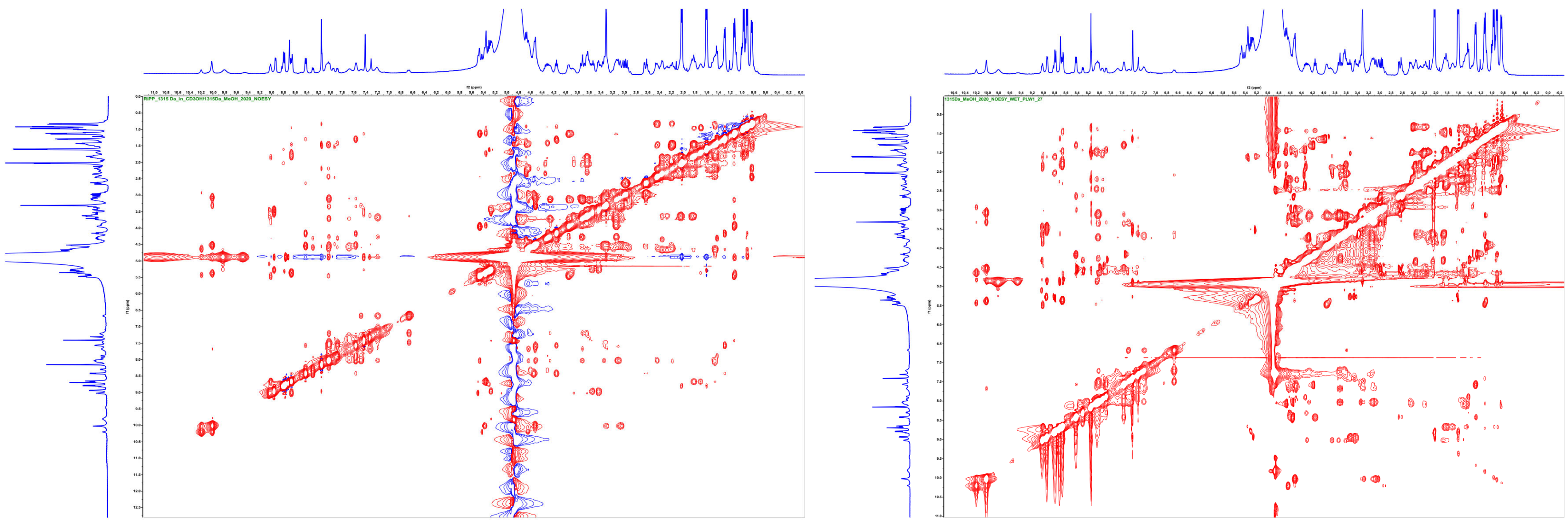

Figure A30. ^{1}H-^{1}H NOESY spectrum of nocathioamide A (**1**) (d_3-CH_3OH, 400 MHz, d8 = 300 msec, Left); ^{1}H-^{1}H NOESY WET spectrum of nocathioamide A (**1**) (d_3-CH_3OH, 400 MHz, d8 = 300 msec, PLW1 = 27, Right)

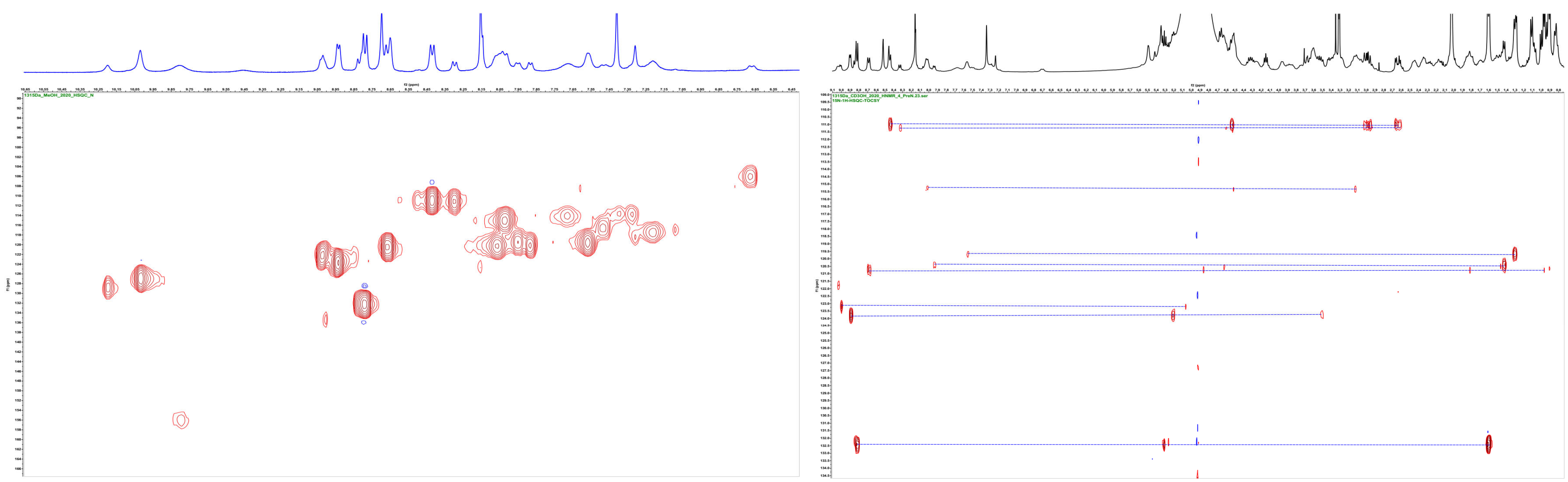

Figure A31. ^{1}H-^{15}N HSQC spectrum of nocathioamide A (**1**) (d_3-CH_3OH, 400 MHz, Left); Magnified ^{1}H-^{15}N HSQC-TOCSY spectrum of nocathioamide A (**1**) (d_3-CH_3OH, 400 MHz, Right)

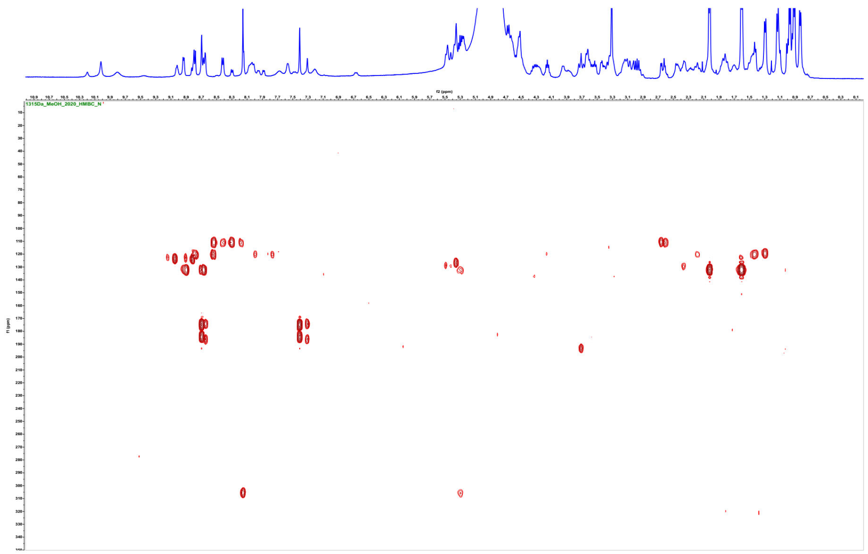

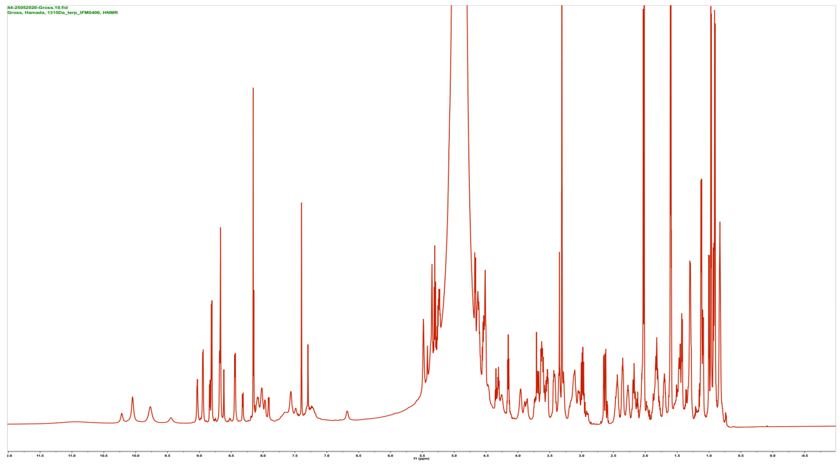

Figure A32. ^{1}H-^{15}N HMBC spectrum of nocathioamide A (**1**) (d_3-CH_3OH, 400 MHz, Left); ^{1}H-NMR spectrum of nocathioamide A (**1**) (d_3-CH_3OH, 700 MHz, Right)

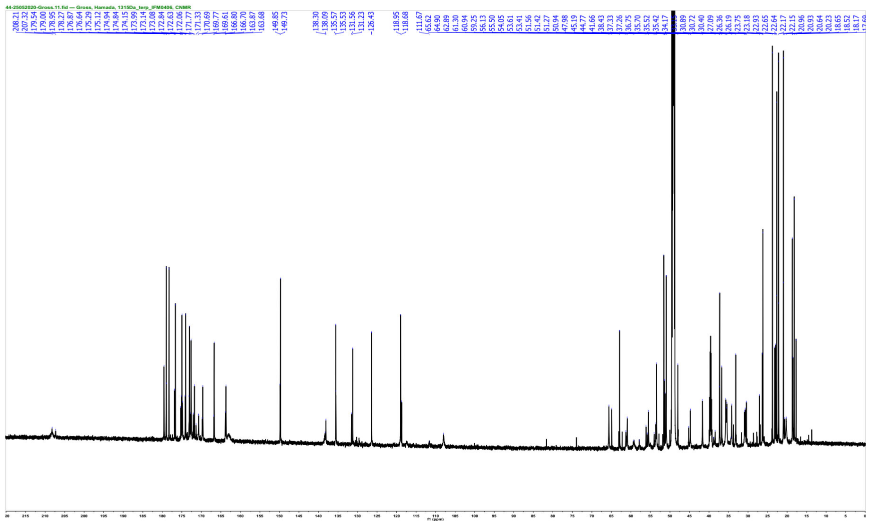

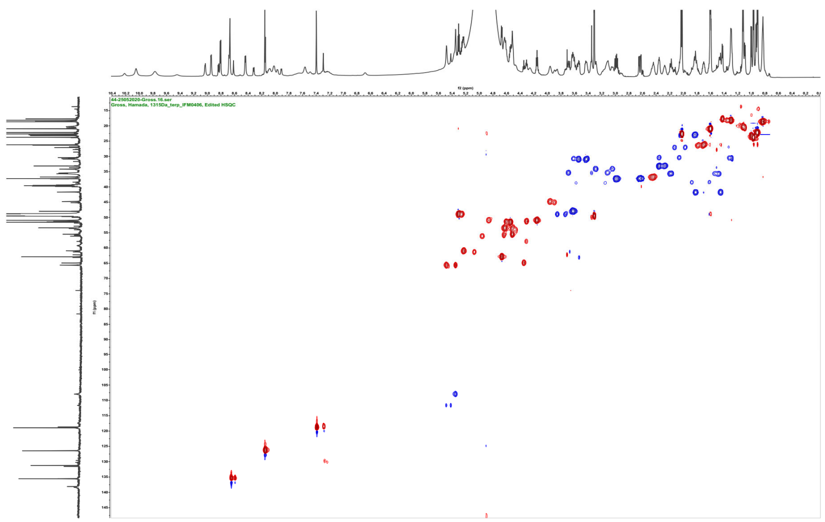

Figure A33. ^{13}C-NMR spectrum of nocathioamide A (**1**) (d_3-CH_3OH, 176 MHz, Left); ^{1}H-^{13}C HSQC spectrum of nocathioamide A (**1**) (d_3-CH_3OH, 700 MHz, Right)

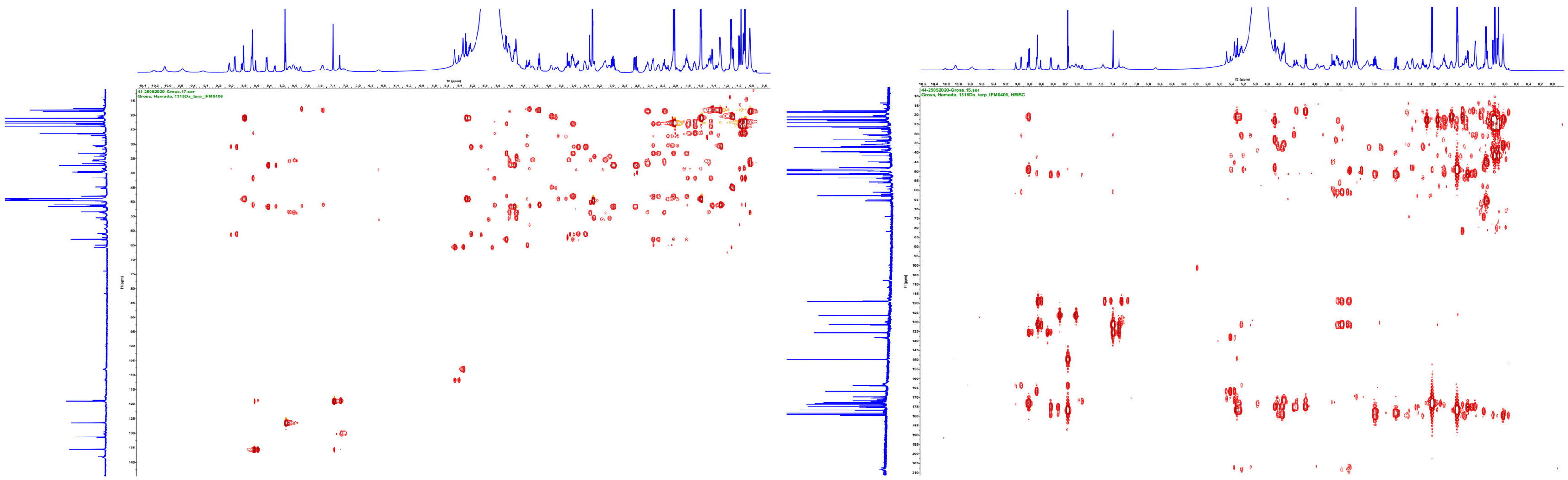

Figure A34. ^{1}H-^{13}C HSQC-TOCSY spectrum of nocathioamide A (**1**) (d_3-CH_3OH, 700 MHz, Left); ^{1}H-^{13}C HMBC spectrum of nocathioamide A (**1**) (d_3-CH_3OH, 700 MHz, Right)

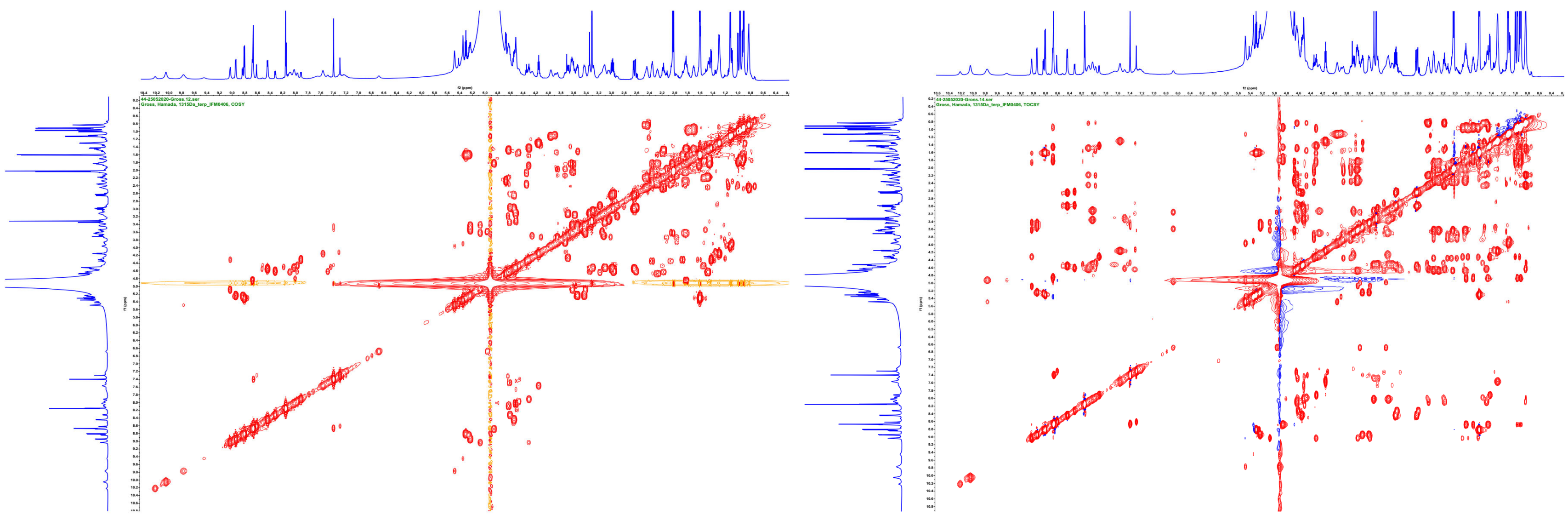

Figure A35. ^{1}H-^{1}H COSY spectrum of nocathioamide A (**1**) (d_3-CH_3OH, 700 MHz, Left); ^{1}H-^{1}H TOCSY spectrum of nocathioamide A (**1**) (d_3-CH_3OH, 700 MHz, Right)

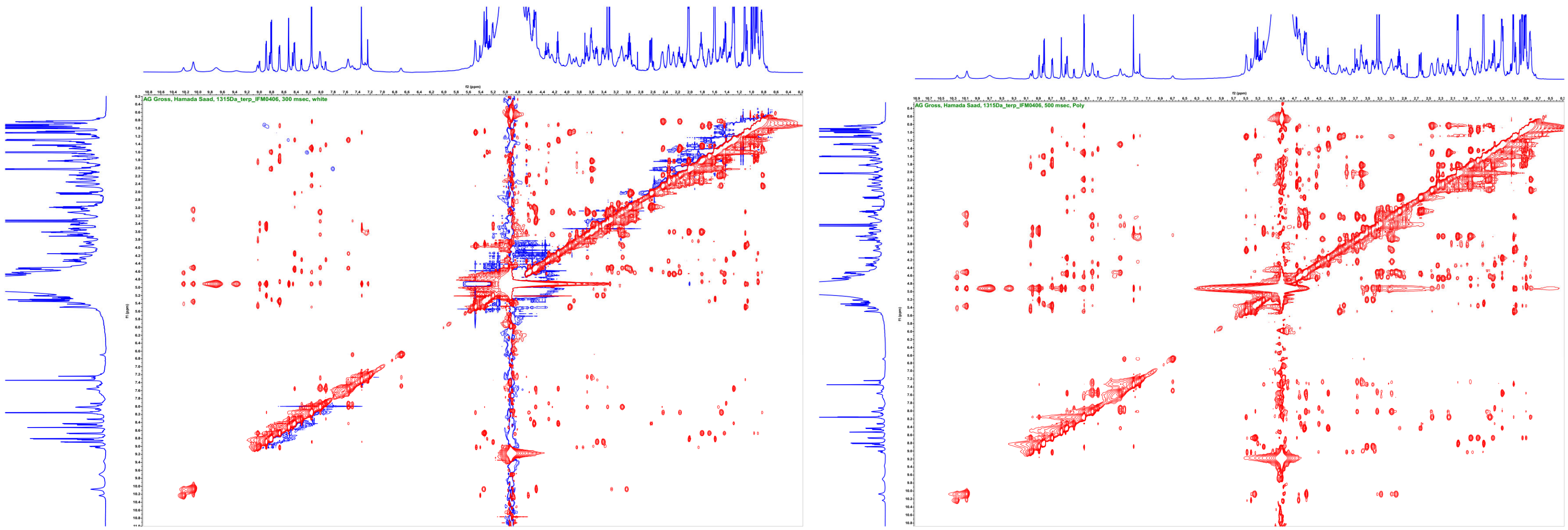

Figure A36. ^{1}H-^{1}H NOESY spectrum of nocathioamide A (**1**) (d_3-CH_3OH, 700 MHz; d8 = 300 msec, Left); ^{1}H-^{1}H NOESY spectrum of nocathioamide A (**1**) (d_3-CH_3OH, 700 MHz; d8 = 500 msec, Right)

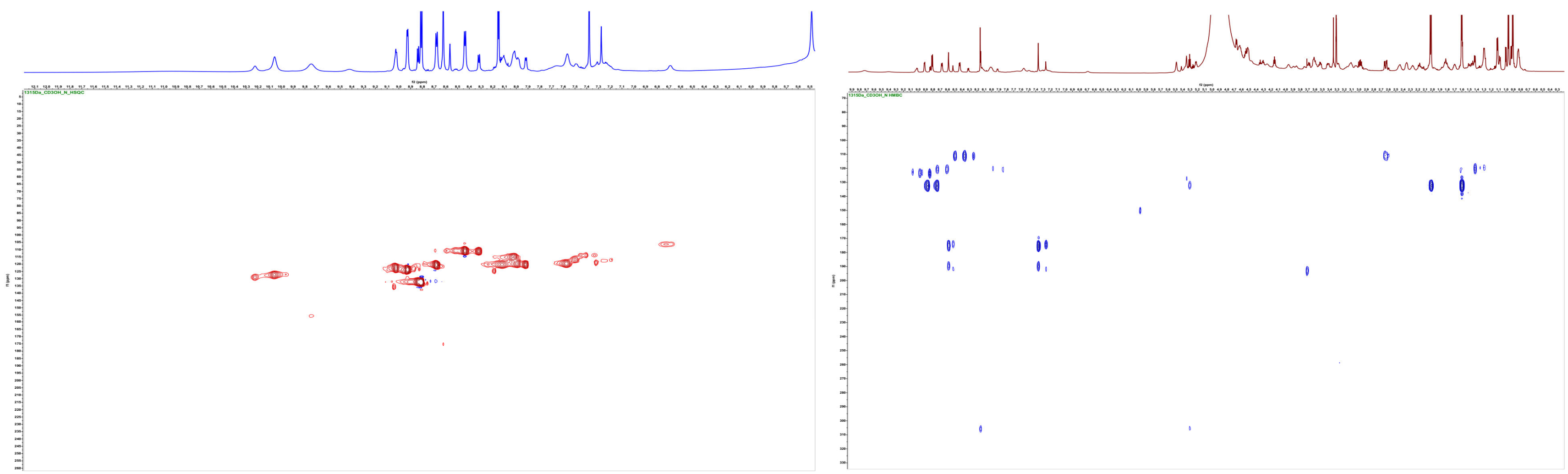

Figure A37. ^{1}H-^{15}N HSQC spectrum of nocathioamide A (**1**) (d_3-CH_3OH, 700 MHz, Left); ^{1}H-^{15}N HMBC spectrum of nocathioamide A (**1**) (d_3-CH_3OH, 700 MHz, Right)

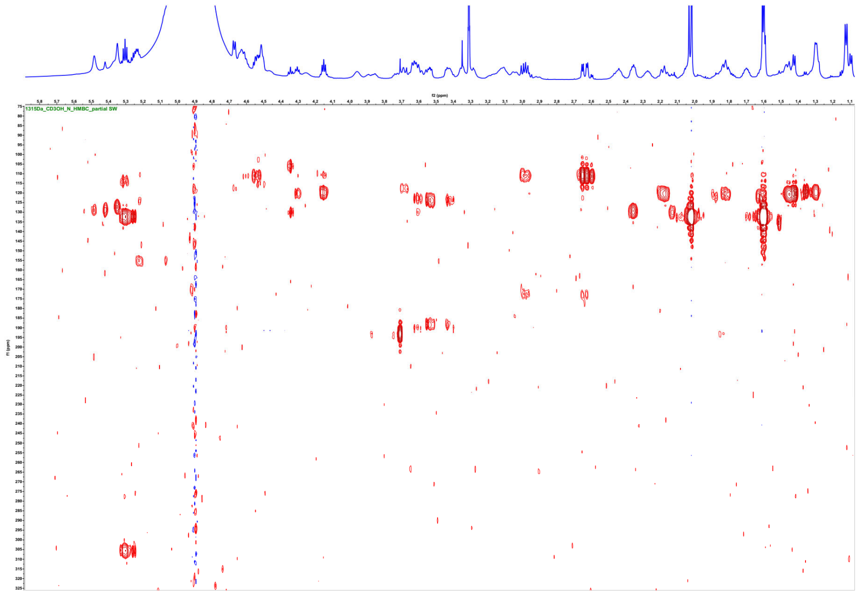

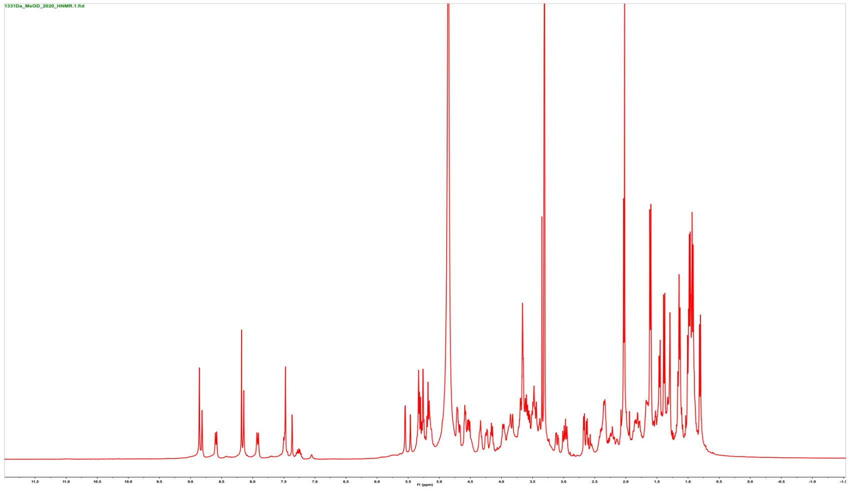

Figure A38. ^{1}H-^{15}N HMBC partial SW spectrum of nocathioamide A (**1**) (d_3-CH_3OH, 700 MHz, Left); ^{1}H-NMR spectrum of nocathioamide B (**2**) (d_4-CH_3OH, 400 MHz, Right)

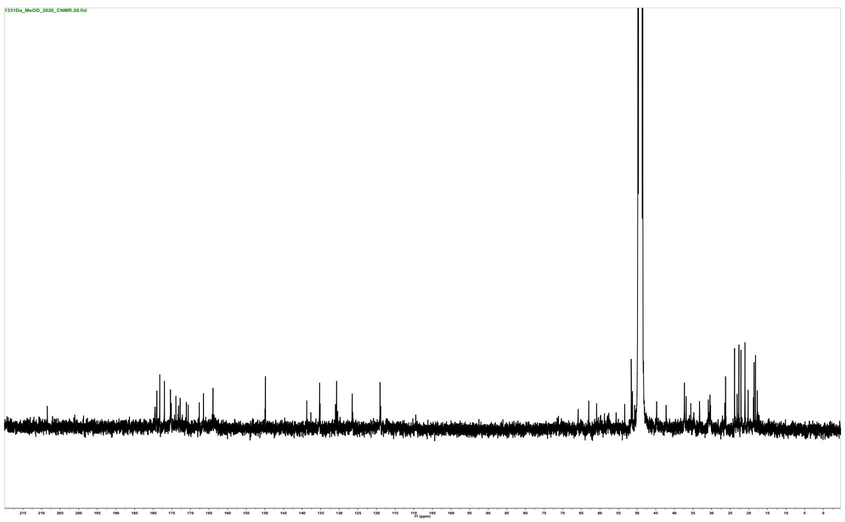

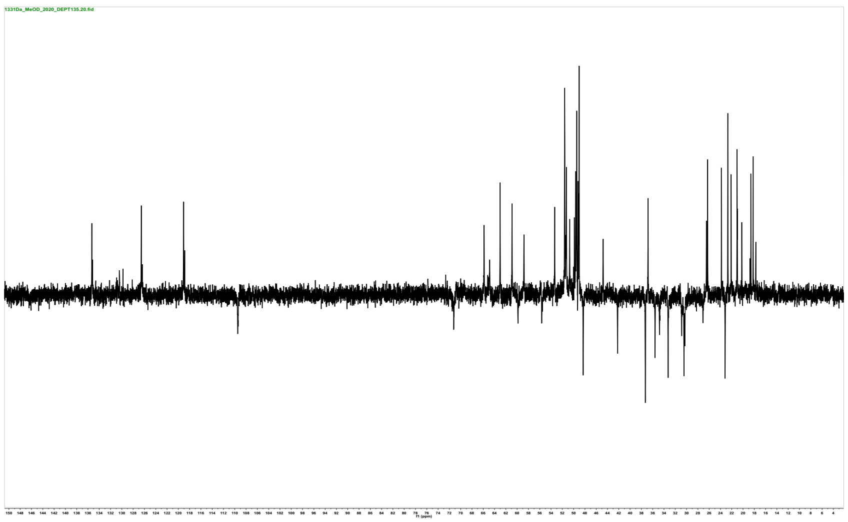

Figure A39. ^{13}C-NMR spectrum of nocathioamide B (**2**) (d_4-CH_3OH, 100 MHz, Left); DEPT-135 spectrum of nocathioamide B (**2**) (d_4-CH_3OH, 100 MHz, Right)

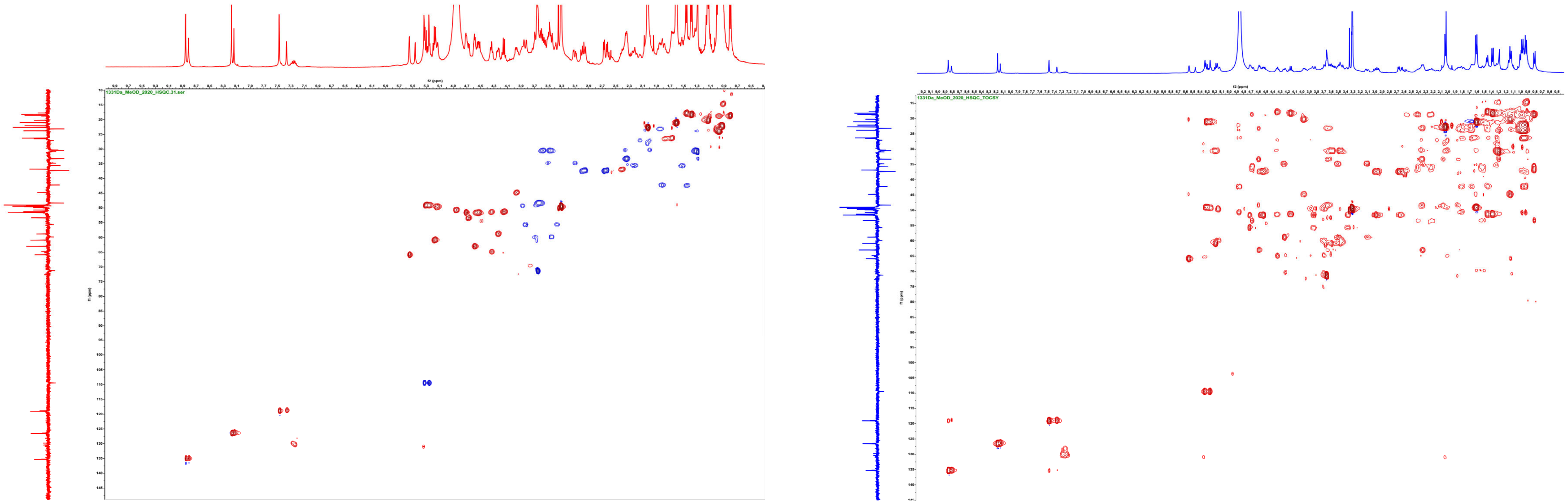

Figure A40. ^{1}H-^{13}C HSQC spectrum of nocathioamide B (**2**) (d_4-CH_3OH, 400 MHz, Left); ^{1}H-^{13}C HSQC-TOCSY spectrum of nocathioamide B (**2**) (d_4-CH_3OH, 400 MHz, Right)

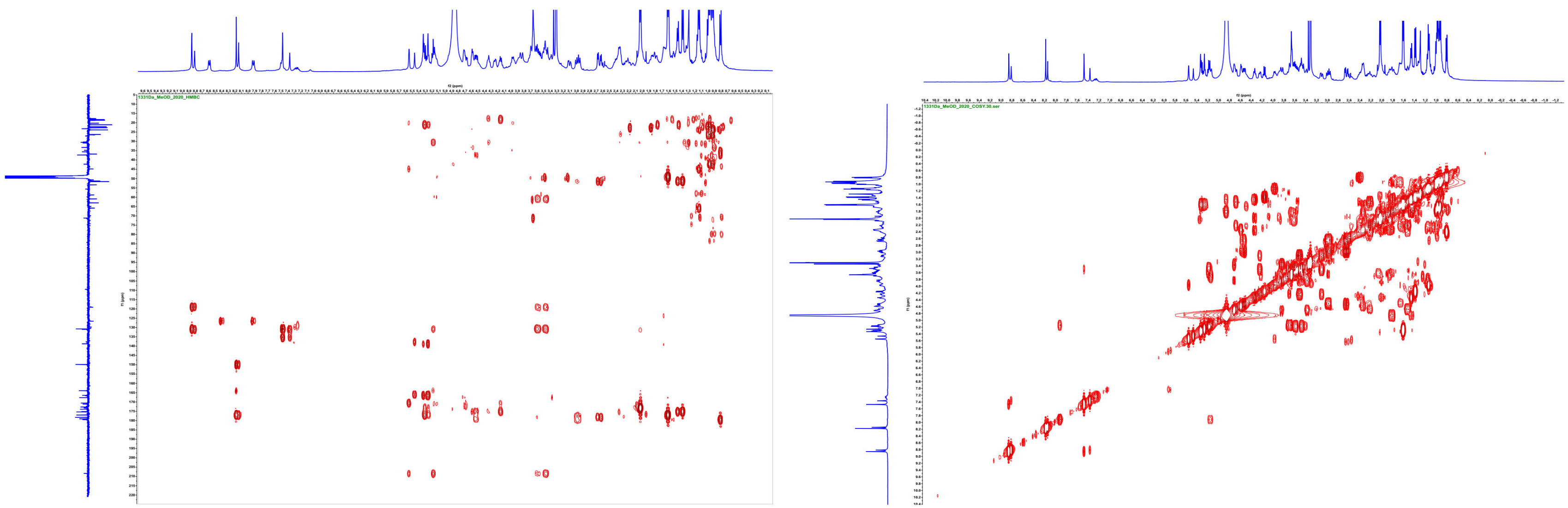

Figure A41. ^{1}H-^{13}C HMBC spectrum of nocathioamide B (**2**) (d_4-CH_3OH, 400 MHz, Left); ^{1}H-^{1}H COSY spectrum of nocathioamide B (**2**) (d_4-CH_3OH, 400 MHz, Right)

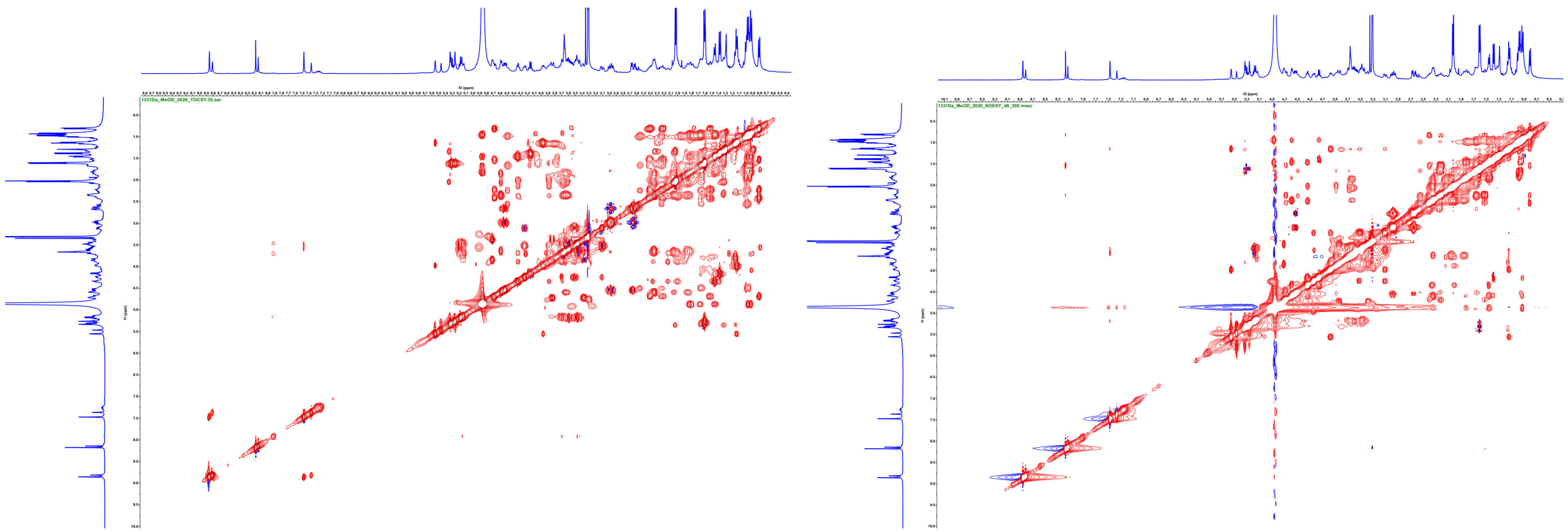

Figure A42. ^{1}H-^{1}H TOCSY spectrum of nocathioamide B (**2**) (d_4-CH_3OH, 400 MHz, Left); ^{1}H-^{1}H NOESY spectrum of nocathioamide B (**2**) (d_4-CH_3OH, 400 MHz, d8 = 300 msec, Left)

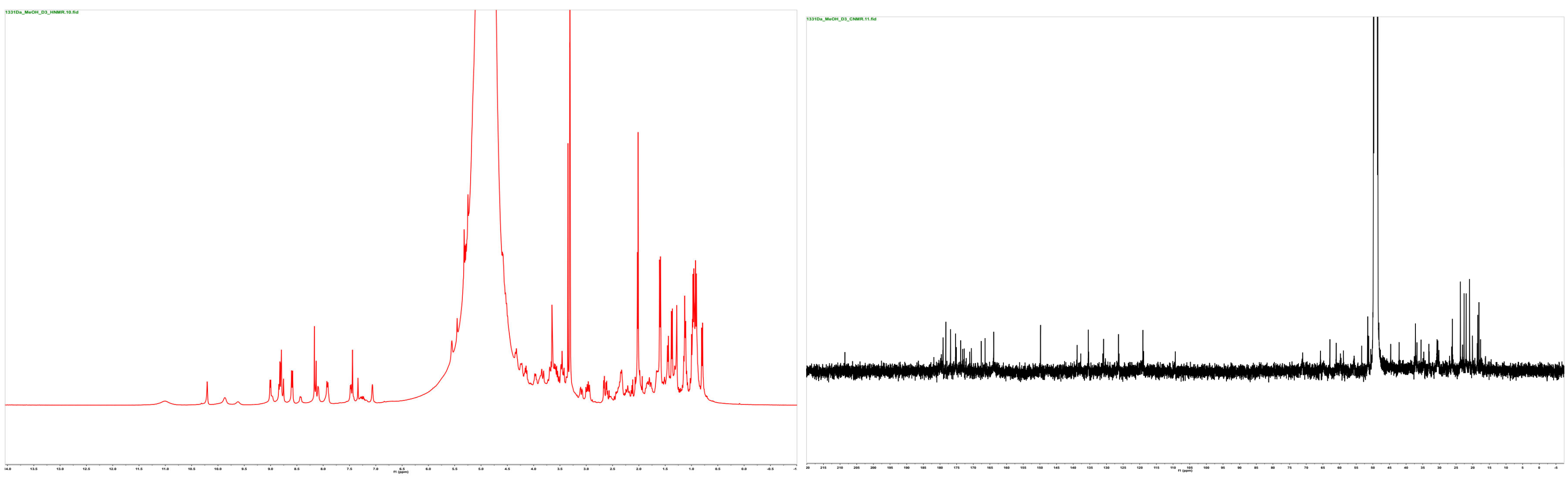

Figure A43. ^{1}H-NMR spectrum of nocathioamide B (**2**) (d_3-CH_3OH, 400 MHz, Left); ^{13}C-NMR spectrum of nocathioamide B (**2**) (d_3-CH_3OH, 100 MHz, Right)

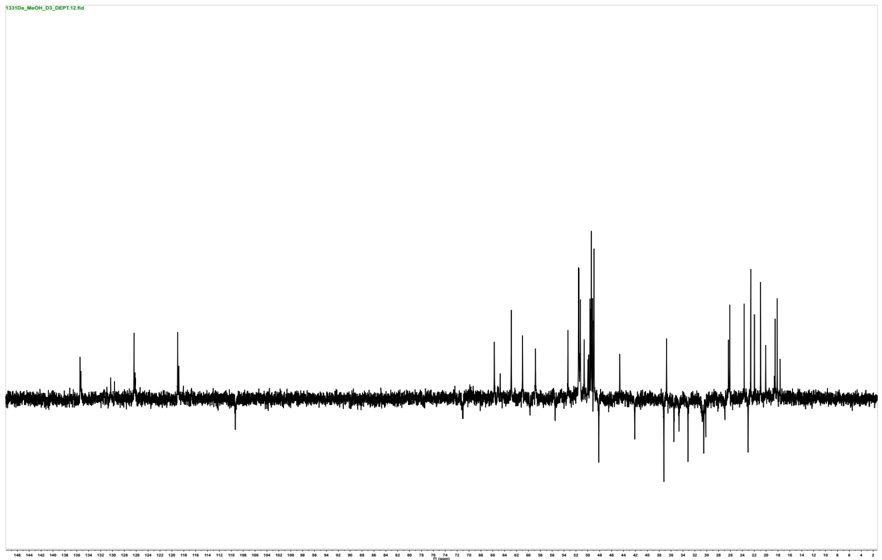

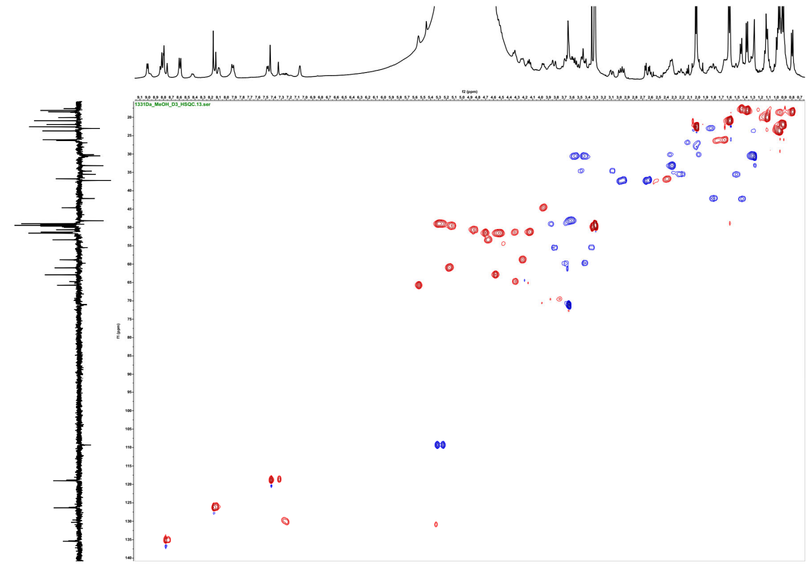

Figure A44. DEPT-135 spectrum of nocathioamide B (**2**) (d_3-CH_3OH, 100 MHz, Left); ^{1}H-^{13}C HSQC spectrum of nocathioamide B (**2**) (d_3-CH_3OH, 400 MHz, Right)

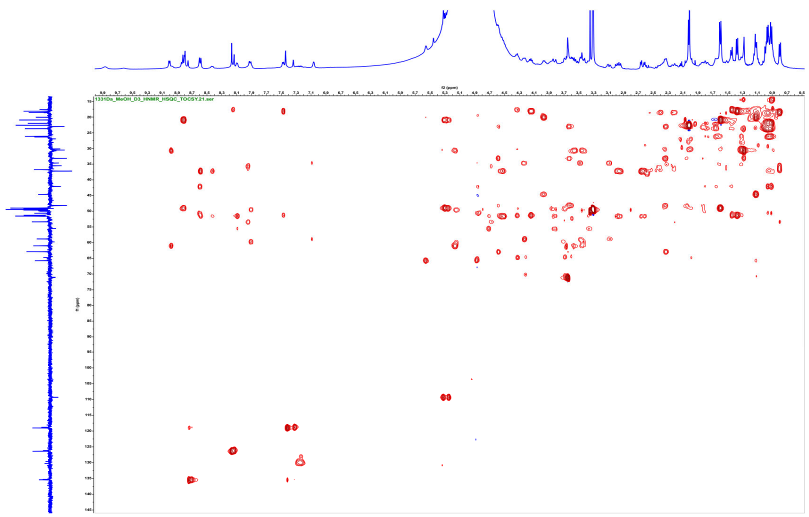

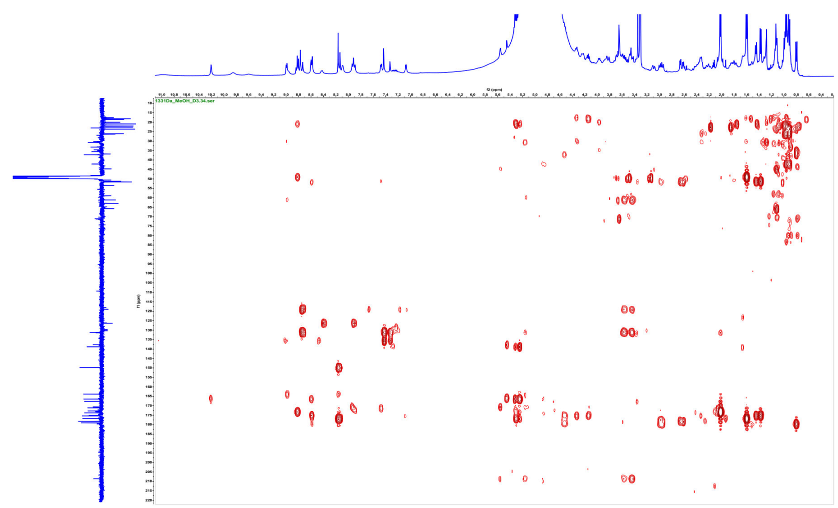

Figure A45. ^{1}H-^{13}C HSQC-TOCSY spectrum of nocathioamide B (**2**) (d_3-CH_3OH, 400 MHz, Left); ^{1}H-^{13}C HMBC spectrum of nocathioamide B (**2**) (d_3-CH_3OH, 400 MHz, Right)

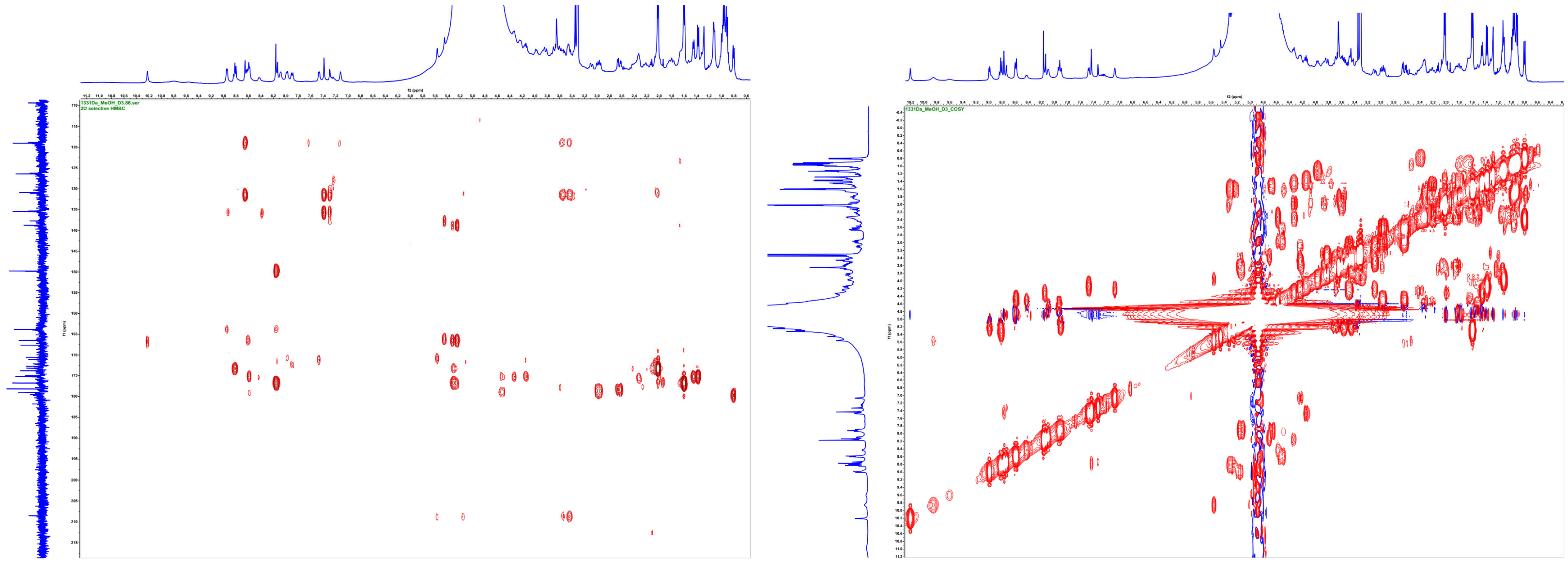

Figure A46. Band-Selective HMBC spectrum of nocathioamide B (**2**) (d_3-CH_3OH, 400 MHz, Left); ^1H-^1H COSY spectrum of nocathioamide B (**2**) (d_3-CH_3OH, 400 MHz, Right)

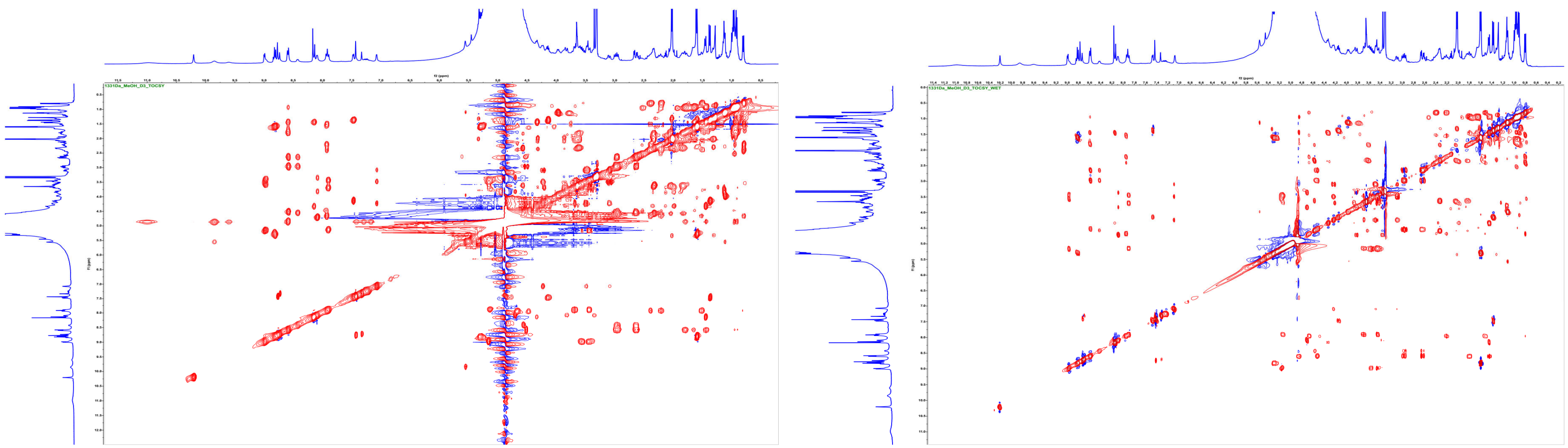

Figure A47. ^1H-^1H TOCSY spectrum of nocathioamide B (**2**) (d_3-CH_3OH, 400 MHz, Left); ^1H-^1H TOCSY WET spectrum of nocathioamide B (**2**) (d_3-CH_3OH, 400 MHz, Right)

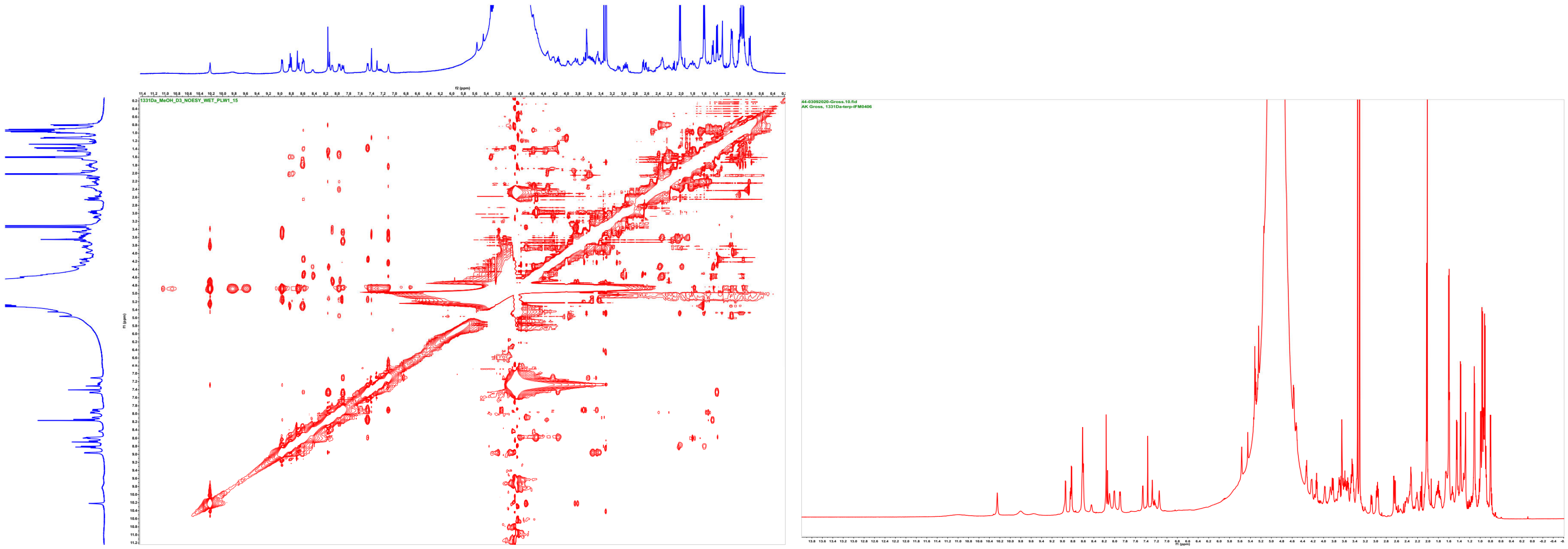

Figure A48. ^{1}H-^{1}H NOESY WET spectrum of nocathioamide B (**2**) (d_3-CH_3OH, 400 MHz, d8 = 300 msec, PLW1=15, Left); ^{1}H-NMR spectrum of nocathioamide B (**2**) (d_3-CH_3OH, 700 MHz, Right)

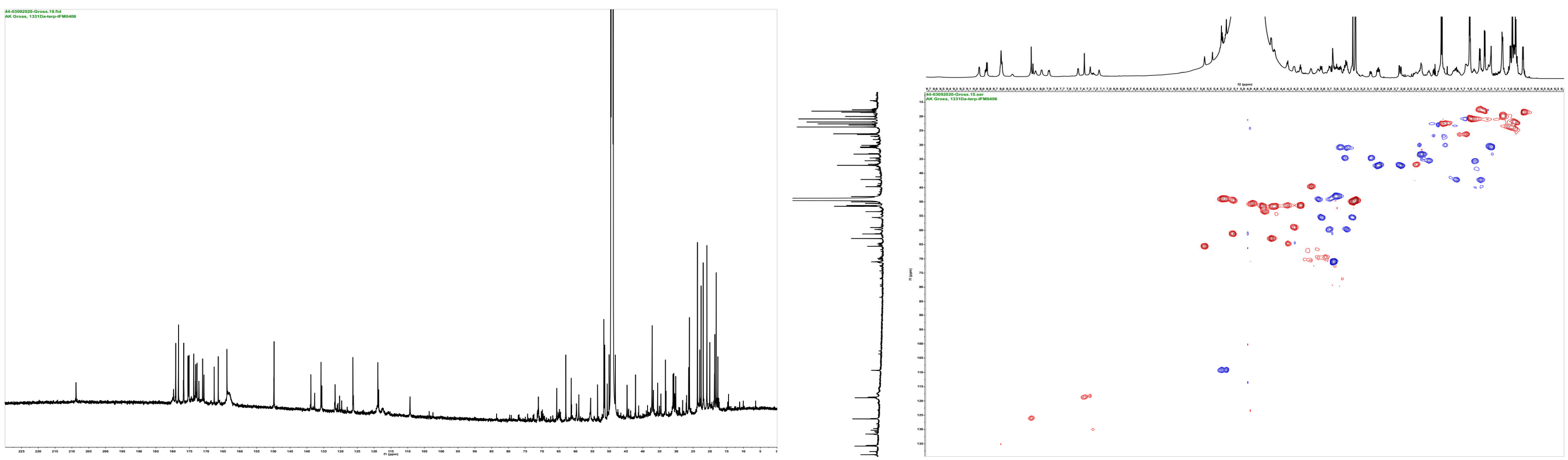

Figure A49. ^{13}C-NMR spectrum of nocathioamide B (**2**) (d_3-CH_3OH, 176 MHz, Left); ^{1}H-^{13}C edited HSQC spectrum of nocathioamide B (**2**) (d_3-CH_3OH, 700 MHz, Right)

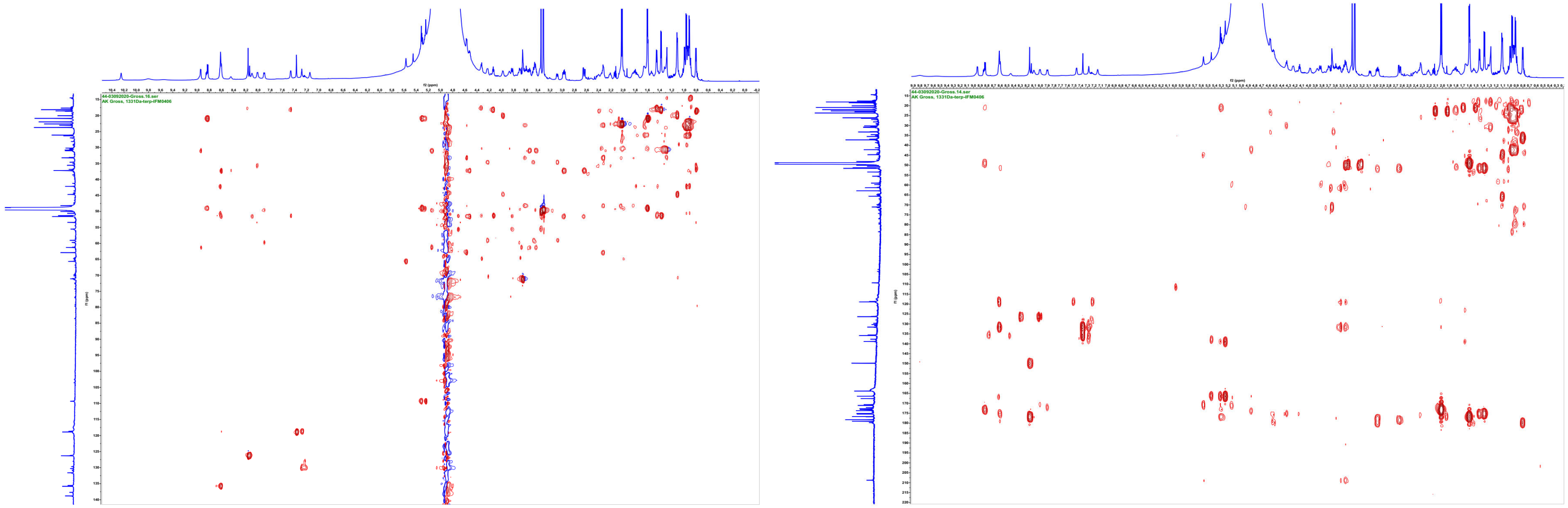

Figure A50. ^{1}H-^{13}C HSQC-TOCSY spectrum of nocathioamide B (**2**) (d_3-CH_3OH, 700 MHz, Left); ^{1}H-^{13}C HMBC spectrum of nocathioamide B (**2**) (d_3-CH_3OH, 700 MHz, Right)

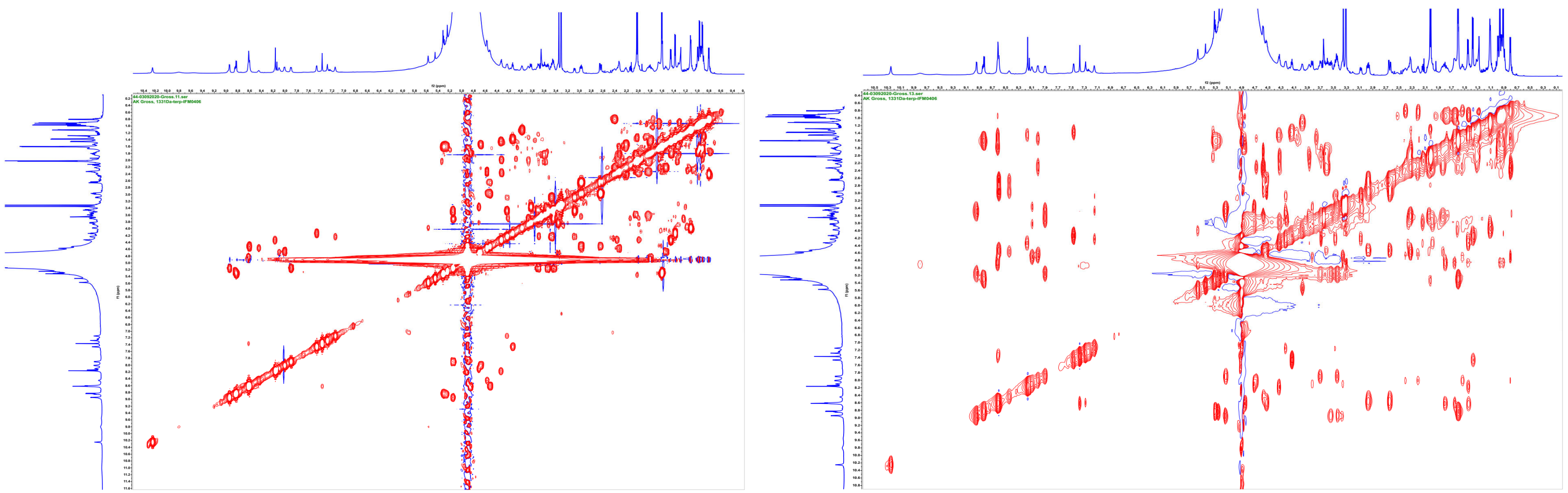

Figure A51. ^{1}H-^{1}H COSY spectrum of nocathioamide B (**2**) (d_3-CH_3OH, 700 MHz, Left); ^{1}H-^{1}H TOCSY spectrum of nocathioamide B (**2**) (d_3-CH_3OH, 700 MHz, Right)

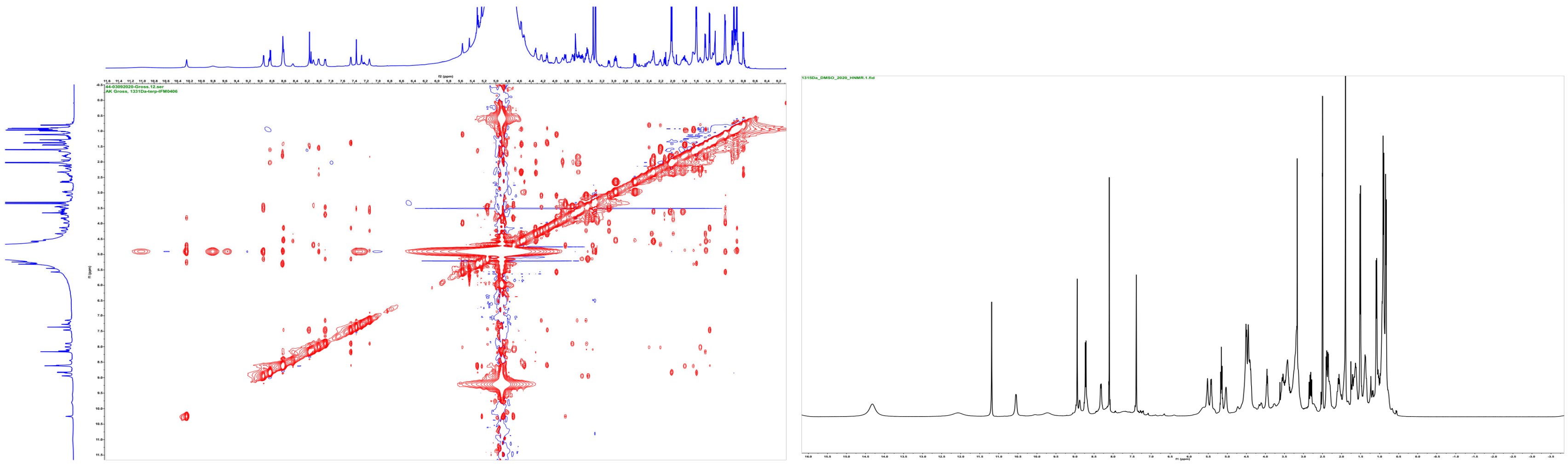

Figure A52. ^{1}H-^{1}H NOESY spectrum of nocathioamide B (**2**) (d_3-CH_3OH, 700/700 MHz, d8 = 300 msec, Left); ^{1}H-NMR spectrum of nocathioamide A (**1**) (d_6-DMSO, 400 MHz, Right)

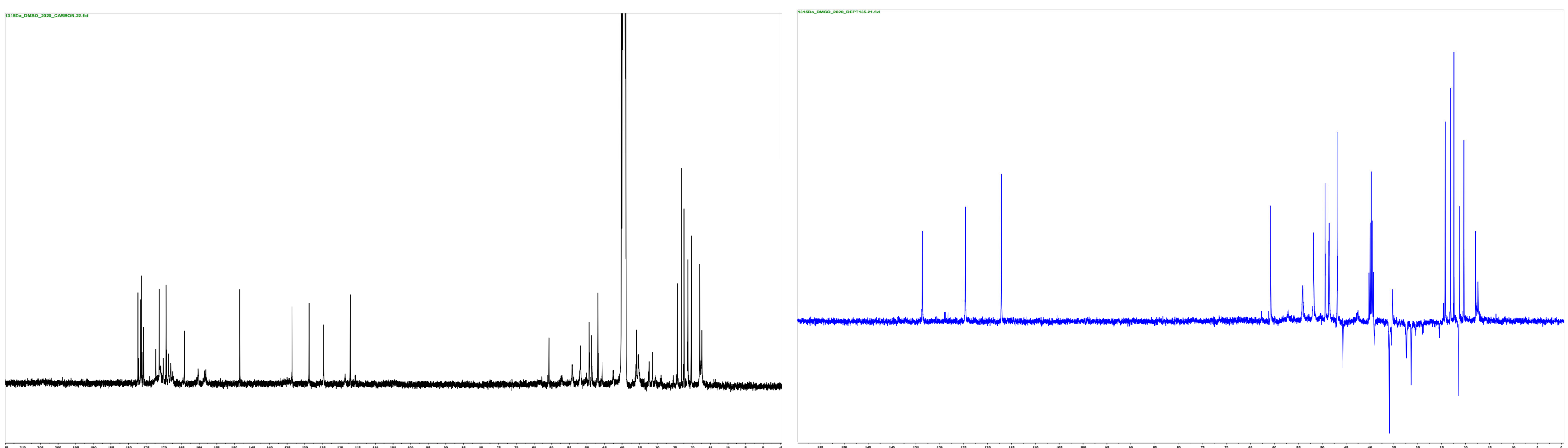

Figure A53. ^{13}C-NMR spectrum of nocathioamide A (**1**) (d_6-DMSO, 100 MHz, Left); DEPT-135 spectrum of nocathioamide A (**1**) (d_6-DMSO, 100 MHz, Right)

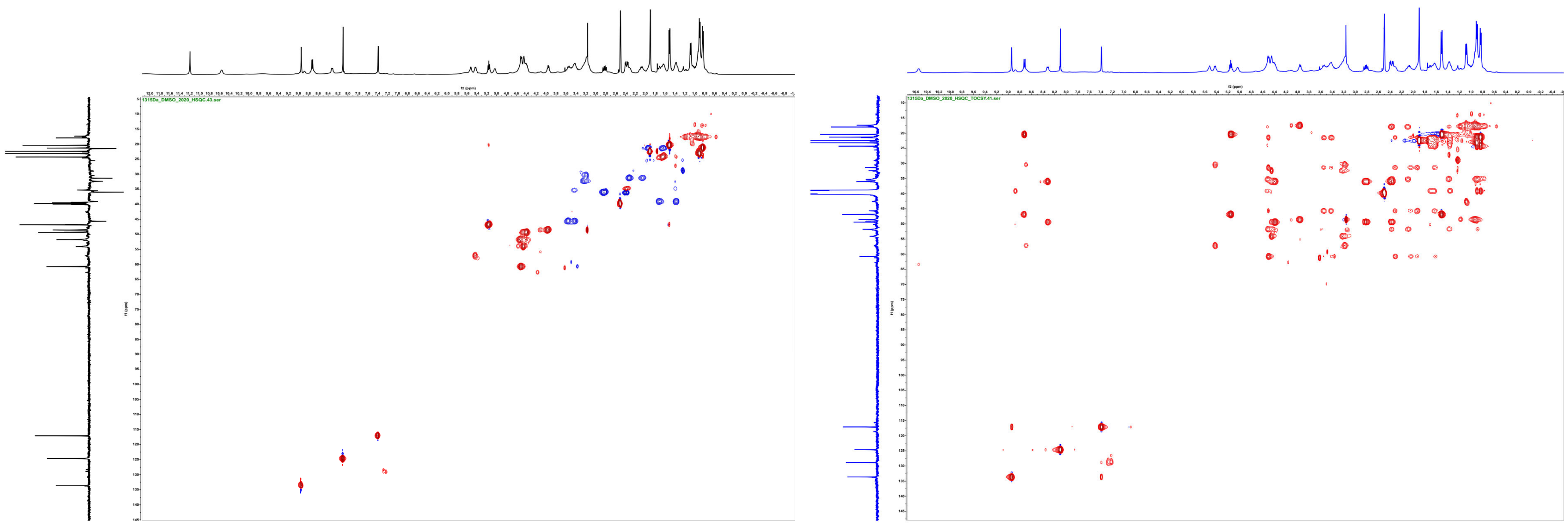

Figure A54. ^{1}H-^{13}C HSQC spectrum of nocathioamide A (**1**) (d_6-DMSO, 400 MHz, Left); ^{1}H-^{13}C HSQC-TOCSY spectrum of nocathioamide A (**1**) (d_6-DMSO, 400 MHz, Right)

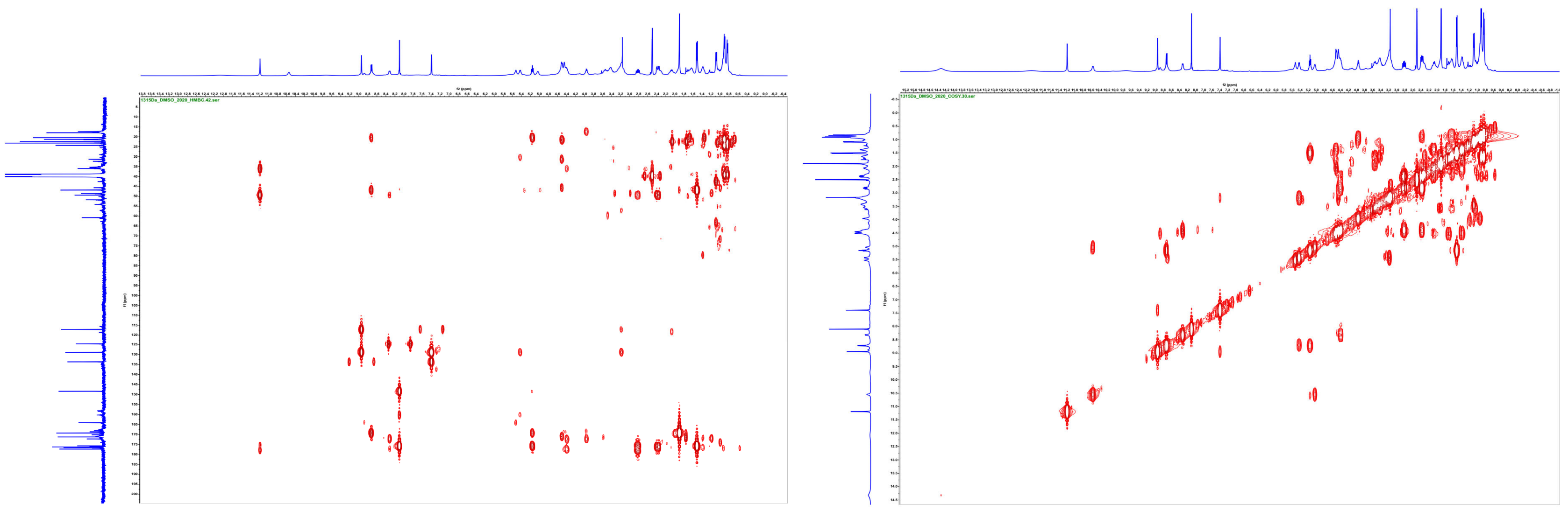

Figure A55. ^{1}H-^{13}C HMBC spectrum of nocathioamide A (**1**) (d_6-DMSO, 400 MHz, Left); ^{1}H-^{1}H COSY spectrum of nocathioamide A (**1**) (d_6-DMSO, 400 MHz, Right)

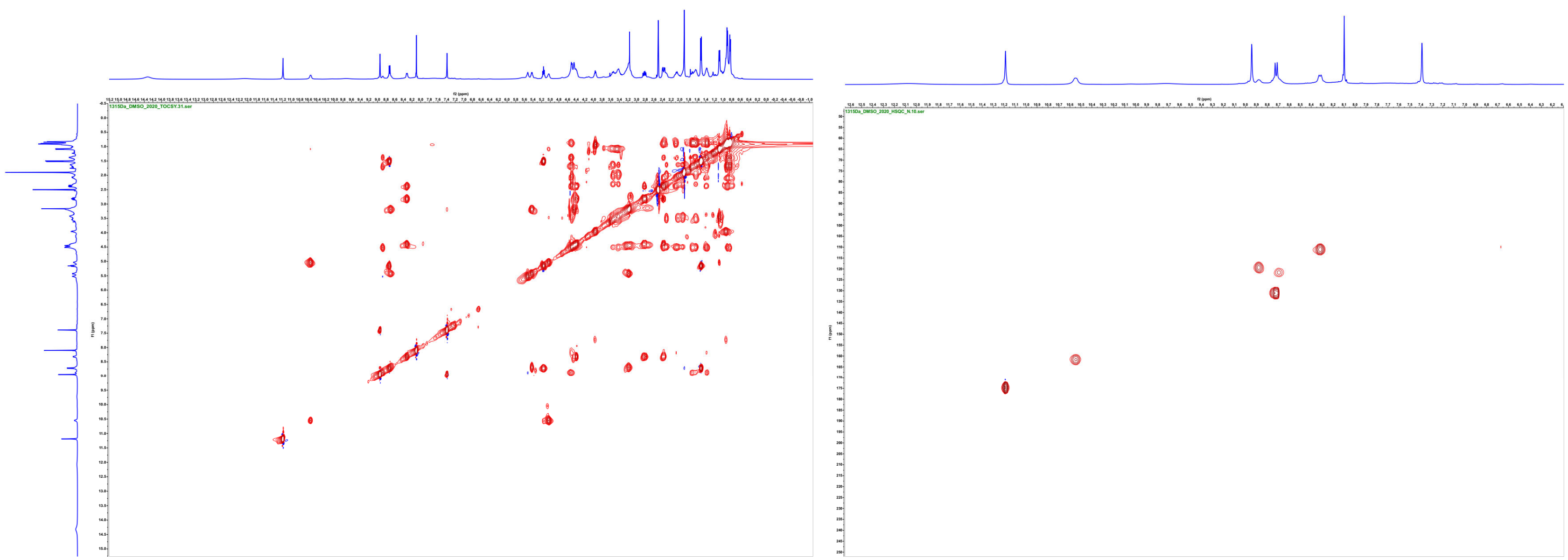

Figure A56. ^{1}H-^{1}H TOCSY spectrum of nocathioamide A (**1**) (d_6-DMSO, 400 MHz, Left); ^{1}H-^{15}N HSQC spectrum of nocathioamide A (**1**) (d_6-DMSO, 400 MHz, Right)

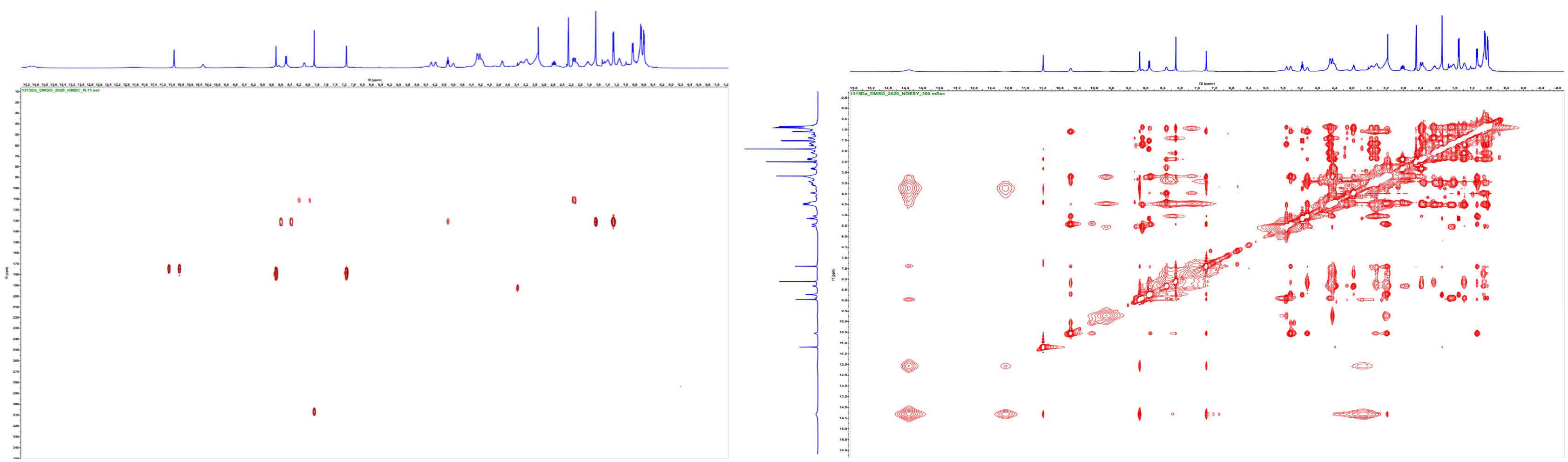

Figure A57. ^{1}H-^{15}N HMBC spectrum of nocathioamide A (**1**) (d_6-DMSO, 400 MHz, Left); ^{1}H-^{1}H NOESY spectrum of nocathioamide A (**1**) (d_6-DMSO, 400/400 MHz, d8 = 300 msec, Right)

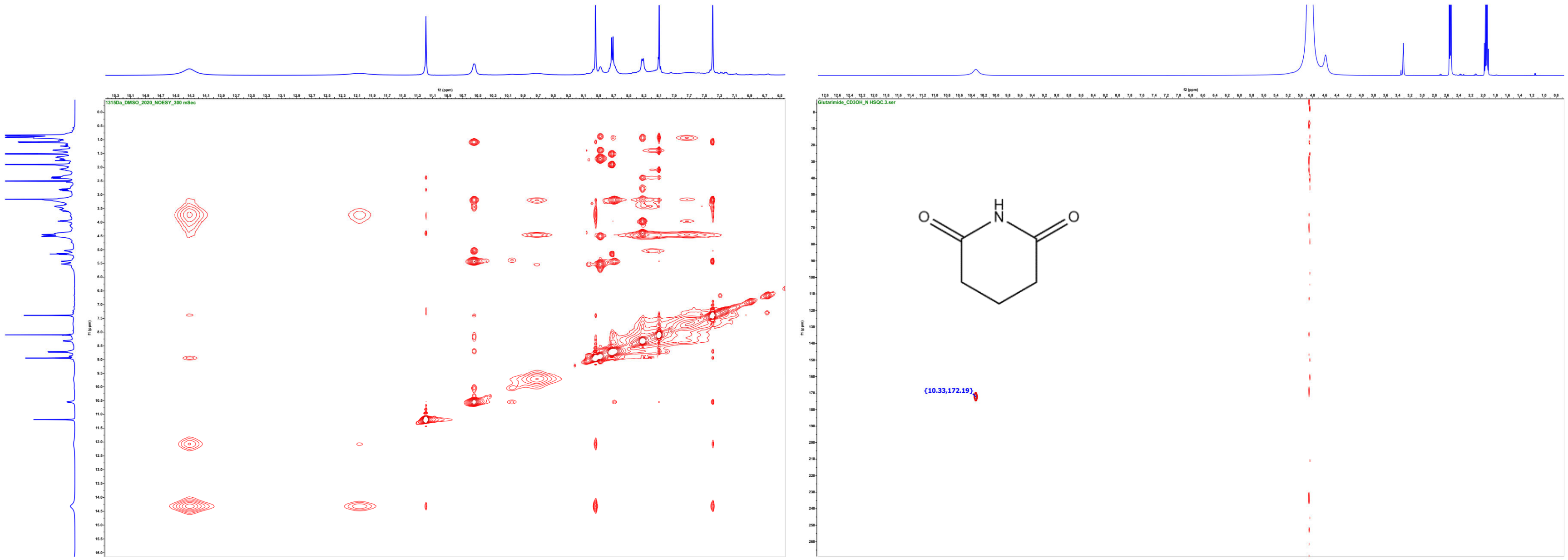

Figure A58. Magnified ^{1}H-^{1}H NOESY spectrum of nocathioamide A (**1**) (d_6-DMSO, 400 MHz, d8 = 300 msec, Left); ^{1}H-^{15}N HSQC spectrum of glutarimide (d_3-CH_3OH, 400 MHz, Right)

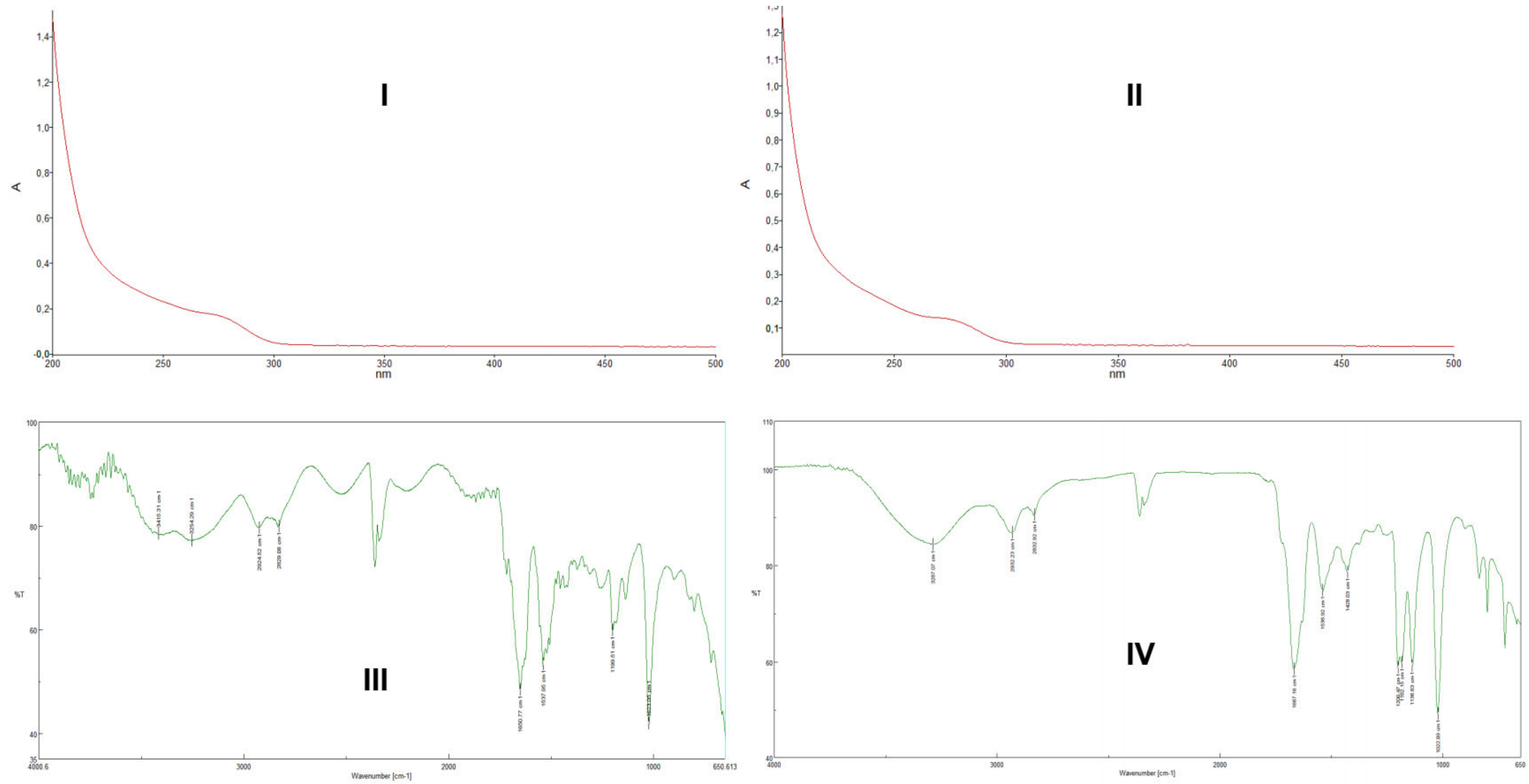

Figure A59. UV spectra of nocathioamide A (**1**) (panel I) and B (**2**) (panel II) & FT-IR spectra of nocathioamide A (**1**) (panel III) and B (**2**) (panel IV).

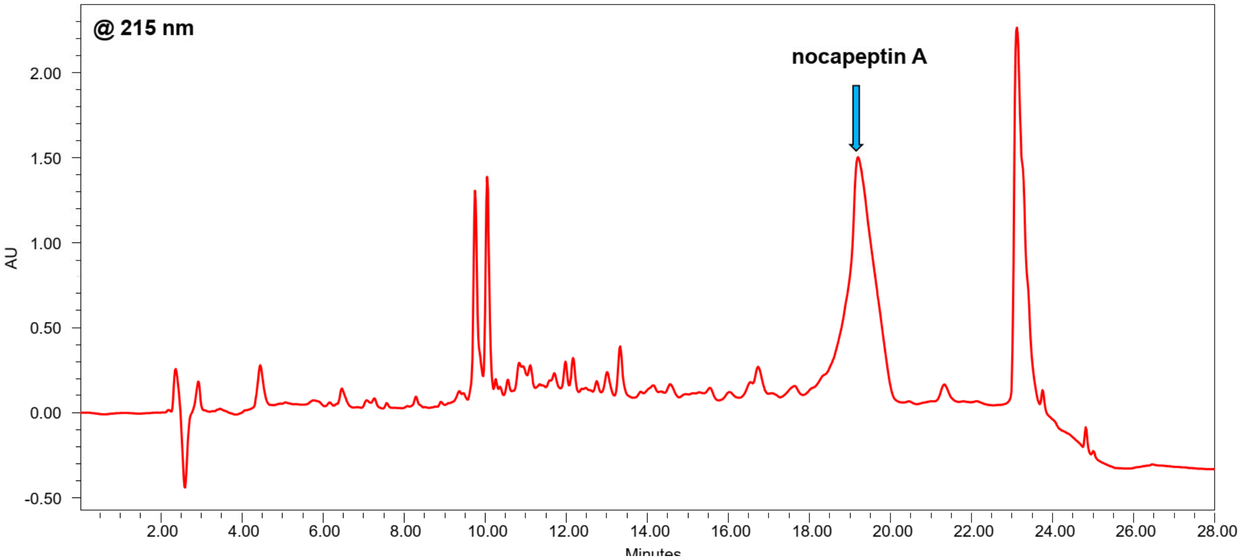

Figure A60. HPLC profile of Fr 60% MeOH VLC highlighting the isolation of nocapeptin A.

JOHN WILEY AND SONS LICENSE
TERMS AND CONDITIONS

Jul 14, 2021

This Agreement between Mr. Hamada Saad ("You") and John Wiley and Sons ("John Wiley and Sons") consists of your license details and the terms and conditions provided by John Wiley and Sons and Copyright Clearance Center.

License Number	5091790223041
License date	Jun 18, 2021
Licensed Content Publisher	John Wiley and Sons
Licensed Content Publication	Angewandte Chemie International Edition
Licensed Content Title	Nocathioamides, Uncovered by a Tunable Metabologenomic Approach, Define a Novel Class of Chimeric Lanthipeptides
Licensed Content Author	Hamada Saad, Saefuddin Aziz, Matthias Gehringer, et al
Licensed Content Date	Jun 17, 2021
Licensed Content Volume	0
Licensed Content Issue	0
Licensed Content Pages	9
Type of use	Dissertation/Thesis
Requestor type	Author of this Wiley article

Format	Electronic
Portion	Full article
Will you be translating?	No
Title	Nocathioamides, Uncovered by a Tunable Metabologenomic Approach, Define a Novel Class of Chimeric Lanthipeptides
Institution name	Department of Pharmaceutical Biology, Institute of Pharmaceutical Sciences, University of Tübingen
Expected presentation date	Jul 2021
Requestor Location	Mr. Hamada Saad Auf der Morgenstelle 8 Tübingen, Baden-Württemberg 72076 Germany Attn: Tuebingen University
Publisher Tax ID	EU826007151
Total	0.00 EUR

Terms and Conditions

TERMS AND CONDITIONS

This copyrighted material is owned by or exclusively licensed to John Wiley & Sons, Inc. or one of its group companies (each a"Wiley Company") or handled on behalf of a society with which a Wiley Company has exclusive publishing rights in relation to a particular work (collectively "WILEY"). By clicking "accept" in connection with completing this licensing transaction, you agree that the following terms and conditions apply to this transaction (along with the billing and payment terms and conditions established by the Copyright Clearance Center Inc., ("CCC's Billing and Payment terms and conditions"), at the time that you opened your RightsLink account (these are available at any time at http://myaccount.copyright.com).

Terms and Conditions

- The materials you have requested permission to reproduce or reuse (the "Wiley Materials") are protected by copyright.

- You are hereby granted a personal, non-exclusive, non-sub licensable (on a stand-alone basis), non-transferable, worldwide, limited license to reproduce the Wiley Materials for the purpose specified in the licensing process. This license, **and any CONTENT (PDF or image file) purchased as part of your order,** is for a one-time use only and limited to any maximum distribution number specified in the license. The first instance of republication or reuse granted by this license must be completed within two years of the date of the grant of this license (although copies prepared before the end date may be distributed thereafter). The Wiley Materials shall not be used in any other manner or for any other purpose, beyond what is granted in the license. Permission is granted subject to an appropriate acknowledgement given to the author, title of the material/book/journal and the publisher. You shall also duplicate the copyright notice that appears in the Wiley publication in your use of the Wiley Material. Permission is also granted on the understanding that nowhere in the text is a previously published source acknowledged for all or part of this Wiley Material. Any third party content is expressly excluded from this permission.

- With respect to the Wiley Materials, all rights are reserved. Except as expressly granted by the terms of the license, no part of the Wiley Materials may be copied, modified, adapted (except for minor reformatting required by the new Publication), translated, reproduced, transferred or distributed, in any form or by any means, and no derivative works may be made based on the Wiley Materials without the prior permission of the respective copyright owner.**For STM Signatory Publishers clearing permission under the terms of the STM Permissions Guidelines only, the terms of the license are extended to include subsequent editions and for editions in other languages, provided such editions are for the work as a whole in situ and does not involve the separate exploitation of the permitted figures or extracts,** You may not alter, remove or suppress in any manner any copyright, trademark or other notices displayed by the Wiley Materials. You may not license, rent, sell, loan, lease, pledge, offer as security, transfer or assign the Wiley Materials on a stand-alone basis, or any of the rights granted to you hereunder to any other person.

- The Wiley Materials and all of the intellectual property rights therein shall at all times remain the exclusive property of John Wiley & Sons Inc, the Wiley Companies, or their respective licensors, and your interest therein is only that of having possession of and the right to reproduce the Wiley Materials pursuant to Section 2 herein during the continuance of this Agreement. You agree that you own no right, title or interest in or to the Wiley Materials or any of the intellectual property rights therein. You shall have no rights hereunder other than the license as provided for above in Section 2. No right, license or interest to any trademark, trade name, service mark or other branding ("Marks") of WILEY or its licensors is granted hereunder, and you agree that you shall not assert any such right, license or interest with respect thereto

- NEITHER WILEY NOR ITS LICENSORS MAKES ANY WARRANTY OR REPRESENTATION OF ANY KIND TO YOU OR ANY THIRD PARTY, EXPRESS, IMPLIED OR STATUTORY, WITH RESPECT TO THE MATERIALS OR THE ACCURACY OF ANY INFORMATION CONTAINED IN THE MATERIALS, INCLUDING, WITHOUT LIMITATION, ANY IMPLIED WARRANTY OF MERCHANTABILITY, ACCURACY, SATISFACTORY QUALITY, FITNESS FOR A PARTICULAR PURPOSE, USABILITY, INTEGRATION OR NON-INFRINGEMENT AND ALL SUCH WARRANTIES ARE HEREBY EXCLUDED BY WILEY AND ITS LICENSORS AND WAIVED BY YOU.

- WILEY shall have the right to terminate this Agreement immediately upon breach of this Agreement by you.

- You shall indemnify, defend and hold harmless WILEY, its Licensors and their respective directors, officers, agents and employees, from and against any actual or threatened claims, demands, causes of action or proceedings arising from any breach of this Agreement by you.

- IN NO EVENT SHALL WILEY OR ITS LICENSORS BE LIABLE TO YOU OR ANY OTHER PARTY OR ANY OTHER PERSON OR ENTITY FOR ANY SPECIAL, CONSEQUENTIAL, INCIDENTAL, INDIRECT, EXEMPLARY OR PUNITIVE DAMAGES, HOWEVER CAUSED, ARISING OUT OF OR IN CONNECTION WITH THE DOWNLOADING, PROVISIONING, VIEWING OR USE OF THE MATERIALS REGARDLESS OF THE FORM OF ACTION, WHETHER FOR BREACH OF CONTRACT, BREACH OF WARRANTY, TORT, NEGLIGENCE, INFRINGEMENT OR OTHERWISE (INCLUDING, WITHOUT LIMITATION, DAMAGES BASED ON LOSS OF PROFITS, DATA, FILES, USE, BUSINESS OPPORTUNITY OR CLAIMS OF THIRD PARTIES), AND WHETHER OR NOT THE PARTY HAS BEEN ADVISED OF THE POSSIBILITY OF SUCH DAMAGES. THIS LIMITATION SHALL APPLY NOTWITHSTANDING ANY FAILURE OF ESSENTIAL PURPOSE OF ANY LIMITED REMEDY PROVIDED HEREIN.

- Should any provision of this Agreement be held by a court of competent jurisdiction to be illegal, invalid, or unenforceable, that provision shall be deemed amended to achieve as nearly as possible the same economic effect as the original provision, and the legality, validity and enforceability of the remaining provisions of this Agreement shall not be affected or impaired thereby.

- The failure of either party to enforce any term or condition of this Agreement shall not constitute a waiver of either party's right to enforce each and every term and condition of this Agreement. No breach under this agreement shall be deemed waived or excused by either party unless such waiver or consent is in writing signed by the party granting such waiver or consent. The waiver by or consent of a party to a breach of any provision of this Agreement shall not operate or be construed as a waiver of or consent to any other or subsequent breach by such other party.

- This Agreement may not be assigned (including by operation of law or otherwise) by you without WILEY's prior written consent.

- Any fee required for this permission shall be non-refundable after thirty (30) days from receipt by the CCC.

- These terms and conditions together with CCC's Billing and Payment terms and conditions (which are incorporated herein) form the entire agreement between you and WILEY concerning this licensing transaction and (in the absence of fraud) supersedes all prior agreements and representations of the parties, oral or written. This Agreement may not be amended except in writing signed by both parties. This Agreement shall be binding upon and inure to the benefit of the parties' successors, legal representatives, and authorized assigns.

- In the event of any conflict between your obligations established by these terms and conditions and those established by CCC's Billing and Payment terms and conditions, these terms and conditions shall prevail.

- WILEY expressly reserves all rights not specifically granted in the combination of (i) the license details provided by you and accepted in the course of this licensing transaction, (ii) these terms and conditions and (iii) CCC's Billing and Payment terms and conditions.

- This Agreement will be void if the Type of Use, Format, Circulation, or Requestor Type was misrepresented during the licensing process.

- This Agreement shall be governed by and construed in accordance with the laws of the State of New York, USA, without regards to such state's conflict of law rules. Any legal action, suit or proceeding arising out of or relating to these Terms and Conditions or the breach thereof shall be instituted in a court of competent jurisdiction in New York County in the State of New York in the United States of America and each party hereby consents and submits to the personal jurisdiction of such court, waives any objection to venue in such court and consents to service of process by registered or certified mail, return receipt requested, at the last known address of such party.

WILEY OPEN ACCESS TERMS AND CONDITIONS

Wiley Publishes Open Access Articles in fully Open Access Journals and in Subscription journals offering Online Open. Although most of the fully Open Access journals publish open access articles under the terms of the Creative Commons Attribution (CC BY) License only, the subscription journals and a few of the Open Access Journals offer a choice of Creative Commons Licenses. The license type is clearly identified on the article.

The Creative Commons Attribution License

The Creative Commons Attribution License (CC-BY) allows users to copy, distribute and transmit an article, adapt the article and make commercial use of the article. The CC-BY license permits commercial and non-

Creative Commons Attribution Non-Commercial License

The Creative Commons Attribution Non-Commercial (CC-BY-NC)License permits use, distribution and reproduction in any medium, provided the original work is properly cited and is not used for commercial purposes.(see below)

Creative Commons Attribution-Non-Commercial-NoDerivs License

The Creative Commons Attribution Non-Commercial-NoDerivs License (CC-BY-NC-ND) permits use, distribution and reproduction in any medium, provided the original work is properly cited, is not used for commercial purposes and no modifications or adaptations are made. (see below)

Use by commercial "for-profit" organizations

Use of Wiley Open Access articles for commercial, promotional, or marketing purposes requires further explicit permission from Wiley and will be subject to a fee.

Further details can be found on Wiley Online Library http://olabout.wiley.com/WileyCDA/Section/id-410895.html

Other Terms and Conditions:

v1.10 Last updated September 2015

Questions? customercare@copyright.com or +1-855-239-3415 (toll free in the US) or

Acknowledgments

First of all, I would like to acknowledge Professor Harald Gross for his continuous support throughout the whole Ph.D. journey in so many ways. He offered me the whole intellectual freedom within the scope of my assigned projects and others of my colleagues to express myself scientifically. Additionally, his entrust and encouragement of my skills regarding scientific observation and suggestion assisted me substantially during the downtimes in particular. Aside from his academic support, the setup of many costly experiments partly listed within the scope of this thesis was not possible without his sustainable financial provision.

In addition, I would also like to thank my former colleague Dr. Saefuddin Aziz for his help in the microbiology part listed in this work and many others outside the thesis scope. Furthermore, I appreciate the isolation efforts of the lasso peptides done by my colleagues Thomas Majer and Keshab Bhattarai.

I am also grateful to my colleague Irina Helme for her responsibility for the NMR instrument which contributed immensely to my research. I also acknowledge my colleague Patricia Arlt for the materials order and for assisting in the ongoing biological evaluation of lasso peptides.

I also express my appreciation for my former colleagues Dr. Lina Assad and Dr. Carolina Prieto for their willingness to help me in the S2-related work.

I would like also to thank the current and former members of the whole Pharmaceutical Biology department over the years I spent for being friendly and cheerful.

Beyond the lab, I am very indebted for my family’s support with all means, even at a distance, and their patience throughout the process of my doctorate.

Finally, I would like to tribute myself for being passionate and persistent during the entire course of the Ph.D. and keeping a high standard of perspective regarding the outputs.